Title
Polymers for the Stabilization and Delivery of Protein Therapeutics

Author
Forsythe, Neil

Publication Date
2021

Peer reviewed|Thesis/dissertation

UNIVERSITY OF CALIFORNIA

Los Angeles

Polymers for the Stabilization and Delivery of Protein Therapeutics

A dissertation submitted in partial satisfaction of

the requirements for the degree Doctor of Philosophy

in Chemistry

by

Neil Forsythe

2021

ABSTRACT OF THE DISSERTATION

Polymers for the Stabilization and Delivery of Protein Therapeutics

by

Neil Forsythe

Doctor of Philosophy in Chemistry

University of California, Los Angeles, 2021

Professor Heather D. Maynard, Chair

Proteins are an excellent therapeutic modality for the treatment of a wide range of diseases. When compared to traditional small molecule drugs, these therapies offer a number of advantages including selectivity and favorable therapeutic windows. However, proteins are inherently unstable molecules. Due to their reliance on tertiary structure for activity, proteins are often sensitive to a range of external stressors including temperature, pH change, light, and agitation which can lead to irreversible degradation or aggregation. Furthermore, after delivery, a number of *in vivo* clearance mechanisms exist such as the immune system, proteases, and renal filtration that can limit their desired effect. As a means to mitigate these challenges, polymers can be used to stabilize proteins against both external stressors and *in vivo* clearance mechanisms. In this dissertation, new polymeric methods for protein stabilization and delivery are presented.

A large and growing field in biologics development are monoclonal antibodies. These drugs can be used directly as therapies for the treatment of a large number of diseases or as means to deliver small molecule drugs (in the form of antibody drug conjugates). In chapter 1, a literature review on antibody drug conjugates (ADCs) is presented with a focus on methods to improve the stability and delivery of the modality. As a contribution to this field, a new sequence-defined and hydrophilic platform for ADCs is presented in chapter 2. This strategy involves the use of iterative poly ethylene glycol (PEG) synthesis to create solubilizing scaffolds for hydrophobic payloads. In addition to increasing the efficacy of ADCs, stabilizing polymers can be used as conjugates to stabilize monoclonal antibodies. In chapter 3, trehalose polymers are demonstrated as a stabilizing motif for both Herceptin and its Fab fragment. Both the work in chapter 2 and 3 demonstrate the applicability of polymers in increasing the stability of antibody-based drugs.

Chapter 4 outlines the work on stabilizing granulocyte colony stimulating factor (G-CSF) with trehalose polymers. Specifically, this research focuses on the optimization of the E. coli expression of G-CSF. After demonstrating an effective and scalable method for the production of the protein, a new strategy for selective conjugation is presented that utilizes a heterobifunctional benzaldehyde maleimide linker.

We also demonstrate a new method for the preparation of protein nanogels in chapter 5. By using a photocleavable monomer, we show an effective strategy to produce non-covalent and active enzyme nanogels. This strategy is employed in the encapsulation of the enzyme phenylalanine ammonia lyase (PAL) for delivery through the digestive tract.

The dissertation of Neil Forsythe is approved.

Joseph Loo

Anna Wu

Alexander Spokoyny

Heather D. Maynard, Committee Chair

University of California, Los Angeles

2021

TABLE OF CONTENTS

LIST OF FIGURES

LIST OF TABLES

LIST OF ABBREVIATIONS

ADC	antibody drug conjugates
ADMET	absorption, distribution, metabolism, excretion, and toxicity
AGET	activators generated by electron transfer
ATRP	atom transfer radical polymerization
AzMCS	azido macrocyclic sulfate
CDRs	complementarity-determining regions
DAR	drug to antibody ratio
DCM	dichloromethane
DMF	dimethyl formamide
DMSO	dimethyl sulfoxide
DSC	differential scanning calorimetry
DSF	differential scanning fluorimetry
E. coli	escherichia coli
EG	ethylene glycol
ELISA	enzyme-linked immunosorbent assay
EthOAc	ethyl acetate
G-CSF	granulocyte colony-stimulating factor

GPC	gel permeation chromatography
HIC	hydrophobic interaction chromatography
HMWS	high molecular weight species
HPLC	high performance liquid chromatography
LCMS	liquid chromatography mass spectrometry
LD	linker drug
MMAE	auristatin E
MPS	mononuclear phagocyte system
MPS	mononuclear phagocyte system
NMR	nuclear magnetic resonance
PAL	phenylalanine ammonia lyase
PD	pharmacodynamics
PEG	poly ethylene glycol
PEGMA	poly(ethylene glycol)methyl ether methacrylate)
PK	pharmacokinetics
RAFT	reversible addition−fragmentation chain-transfer
RES	reticuloendothelial system
SAR	structure-activity-relationship

SDS PAGE	sodium dodecyl sulphate–polyacrylamide gel electrophoresis
UPLC	ultra-performance liquid chromatography
UV	ultraviolet
VC	volume distribution

ACKNOWLEDGEMENTS

I would like to thank all of my friends and family for their love and support through this process. Especially, I want to recognize my wife Lexi, for whom words can only diminish my deep feelings of gratitude and love towards. Finally, I would like to thank my advisor Heather Maynard for allowing me conduct research in her lab and the freedom to pursue projects of interest to me.

VITA

Education:

University of California Los Angeles| Chemistry

MS, Chemistry **September 2018**

Ph.D., Chemistry **July 2016 – Present (Expected: Spring 2021)**

Awards: NIH Chemistry-Biology Interface Training Grant (**2017**)

Pomona College

Bachelor of Arts in Chemistry **May 2016**

Awards: Superior All-Academic Scholar Athlete (water polo), Pomona College Scholar

Experience:

UCLA Department of Chemistry & Biochemistry **July 2016-Present**

Graduate Student Researcher

Advisor: Professor Heather D. Maynard

- Expressed and purified therapeutic proteins, conducted protein/antibody conjugations, and characterized proteins/conjugates using liquid chromatography, mass spectrometry, thermal analyses, and immunoassays.
- Synthesized polymers and oligomers of varied backbones and architectures.
- Designed and synthesized nanoparticles for the delivery of proteins.
- Conducted retrosynthesis, optimized reaction conditions, and synthesized a variety of functional small molecules for protein and polymer conjugation.
- Analyzed the stability of proteins and conjugates using a variety of assays.
- Wrote and contributed to grant proposals, SOPs, and project designs.

Genentech Department of Protein Chemistry **May 2019-August 2019**

Manager: Jack Sadowsky

Genentech Graduate Internship

- Made, purified, and characterized a variety of Antibody Drug Conjugates (ADCs).
- Helped develop technologies to enhance the endosomal escape of ADC payloads.
- Characterized a library of ADCs to determine trends in hydrophobicity.

Harvey Mudd College **2015-2016**

Undergraduate Researcher

Advisor: Professor Elizabeth Orwin

- Designed synthetic and biopolymer matrices to mimic the native environment of the human cornea.

Naval Research Laboratory **June-August 2015**

Department of Homeland Security STEM Internship

Advisor: Dr. Michael Papantonakis

- Synthesized and designed polymer-wrapped carbon nanofiber composites with ballistic and energy absorbing characteristics.

Virginia Tech **June-August 2014**

Research Experience for Undergraduates (REU)

Advisor: Professor Timothy Long

- Synthesized and electrospun polyesters for gene transfection applications.

Publications

- Forsythe, N.; Maynard, H. "Synthesis of Disulfide-Bridging Trehalose Polymers for Antibody and Fab Conjugation Using a Bis-Sulfone ATRP Initiator" *Polymer Chemistry* **2021**. *Chosen as paper of the month
- Nelson, A.; Pekkanen, A.; Forsythe, N.; Herlihy, J.; Zhang, M.; Long, T., "Synthesis of Water-Soluble Imidazolium Polyesters as Potential Non-viral Gene Delivery Vehicles" *Biomacromolecules* **2016**, 18, 68–76.

Presentations

- Stabilization and Delivery of Proteins and Small Molecules. Neil L. Forsythe, Mikayla Tan, Daniele Vinciguerra, and Heather Maynard. Chemistry-Biology Interface Day, Los Angeles, California, December 2019.
- Stabilizing Therapeutic Antibodies and Antibody Fragments with Trehalose Polymers (Poster). Neil L. Forsythe and Heather D. Maynard. ACS Polymers in Medicine and Biology, Napa California, September 2018.
- Genentech Summer Intern Research Presentation (PowerPoint and Poster). Neil L. Forsythe, Pragya Adhikari, Neelie Zacharias, and Jack Sadowsky. South San Francisco, California, August 2019.
- Stabilizing Therapeutic Antibodies and Antibody Fragments with Trehalose Polymers (Poster). Neil L. Forsythe and Heather D. Maynard. Molecular Biology Institute Retreat, Ventura California, September 2018.

Service and Leadership

Historically Black College (HBCU) Summer Mentor **Summer 2018**

- Designed a summer project and provided mentorship for an HBCU student.

Graduate Student Mentor **2017-Present**

- Provide hands-on mentorship, project design, and career consultation to 3 junior graduate students.
- Lead researcher on 3 separate projects with control over project direction and scope.

Chapter 1

Strategies to Increase the Hydrophilicity of Antibody Drug Conjugates

1.1 Antibody Drug Conjugates: The *in vivo* tradeoff of higher DAR ADCs

A number of excellent reviews[1–3] have been recently written on antibody-drug conjugates (ADCs), and the purpose of this perspective is not to reiterate what has been previously written, but rather to focus on one specific challenge facing the field: hydrophobicity. Since the publication of the seminal work regarding this topic by Hamblett *et al*,[4] a fundamental dichotomy between the hydrophobicity of an ADC and it's *in vivo* performance has been at play. It has been reported in a number of publications that while achieving a higher drug-to-antibody ratio (DAR) can improve the *in vitro* performance of an ADC, the *in vivo* pharmacokinetics (PK) is often worse, leading to less effective therapies.[4,5] In addition to poorer PK outcomes, the attachment of a larger number of payloads to an antibody can further limit its solution stability, leading to aggregation, which can lead to adverse side-effects.[6] In this short perspective, we review the current understanding of hydrophobicity in the field and further present and compare a number of strategies used to address these challenges. Structurally, ADCs are broken down into three components: an antibody against the desired target, a payload to be delivered, and a linker connecting the two. Due to the disparate nature of these components, each offers a unique contribution to overall hydrophobicity of the conjugate. Therefore, for the purpose of this review, we address each of these components individually and discuss strategies employed in each area.

1.2 Hydrophobicity and its Consequences

Hydrophobicity and the hydrophobic effect are core elements of nature that allow for biological life. Protein folding and lipid membranes are but two, critically important examples of how hydrophobicity shapes our understanding of biology.[7] However, when it comes to drug design, hydrophobicity is a careful balance between binding, pharmacokinetics, and solubility. Because so many important biological reactions and interactions rely on hydrophobicity, many effective

drugs, in turn, are hydrophobic in nature. For orally formulated drugs, greater lipophilicity (LogP values above 5) are correlated with poorer absorption, distribution, metabolism, excretion, and toxicity (ADMET).[8,9] In a similar manner, many payloads used for ADCs have high lipophilicities.[10] While the antibody can help solubilize these drugs, hydrophobicity in ADCs have two distinct challenges: more rapid immune-mediated clearance and/or poorer solution stability.

In regards to the poor PK outcomes of hydrophobic ADCs, the nature of *in vivo* clearance is not fully understood, however current studies suggest that the mononuclear phagocyte system (MPS) plays a significant role.[11] The MPS, also known as the reticuloendothelial system (RES) or macrophage system, is composed of monocytes, macrophages, Kupffer cells, and dendritic cells and is part of the innate immune system.[12] Along with a wide range of other immunological functions, the MPS is responsible for the clearance of foreign substances such as bacteria, fungi, and toxins. The accumulation of ADCs in organs rich with MPS cells (principally the liver, spleen, and lung) suggest its role in the premature clearance of hydrophobic conjugates. This inference is further supported by data showing that the MPS plays a significant role in the clearance of aggregated proteins and complexes.[13] Furthermore, *in vitro* models of Kupffer cells have shown the ability to predict *in vivo* PK outcomes for highly conjugated ADCs, providing more evidence of the role of MPS cells in the clearance of conjugates.[14]

Outside of challenges with premature clearance of conjugated antibodies, there are also reports of highly variable PK and pharmacodynamics (PD) among patients. These irregular PK and PD outcomes are further thought to be a result of the MPS as the function of this system can be highly variable among different patient populations. For instance, body weight and tumor burden are two factors that can have a significant impact on the function of the MPS.[11] In an analysis of the PK of ado-trastuzumab emtansine, body weight had the largest effect on both the clearance (CL) and

central volume distribution (VC) of the ADC drug.[15] Relationships such as these have also been observed in nanoparticle PK studies and further exemplify how variable MPS behavior among patient populations can further exacerbate PK challenges when administering ADCs.[16]

Along with consequences in PK and PD, the overall hydrophobicity of an ADC can have significant impacts on the solution stability and solubility of the conjugate. Given that nearly all payloads are not water soluble (requiring cosolvents such as DMSO or DMF to perform the conjugation), it is logical to assume that the conjugation of a payload will have a negative impact on the stability of the conjugate. For antibodies, as well as many other proteins, the primary consequence of this decreased stability is aggregation and precipitation. In fact, it has been found that there can be a direct correlation between the LogP of a compound and the propensity towards aggregation after conjugation.[17] In a model study, three different fluorescent toxin surrogates of varied hydrophobicity (LogP of 1.1, 2.7, and 5.6) were conjugated to a model antibody through maleimide chemistry. The more hydrophobic compounds showed both statically lower melting temperatures for the CH_2 domain and additionally a greater propensity towards self-association. Supporting studies have also been performed with commonly used cytotoxics such as auristatin E (MMAE) and mertansine (DM-1), further showing that an increase in the DAR of an ADC results in the lowering of the melting temperatures and an increase in aggregation rate.[18,19] While these challenges with stability can be improved through formulation efforts,[6] this approach does not address the core problem of hydrophobicity.

In the following sections, we aim to review strategies that are used to ameliorate the hydrophobicity of ADCs. As we have outlined, the consequences of hydrophobicity in ADC research are largely manifested in both pharmacokinetic outcomes as well as stability. Therefore, in each section, we will demonstrate not only the technologies aimed at reducing hydrophobicity,

but additionally whether they improve outcomes in these two categories. Additionally, in chapter 3 of this thesis, the use of trehalose polymers for antibody stabilization will be presented.

1.3 Analytical Methods to Measure Hydrophobicity

Before discussing specific technologies, it is important to first review current methodologies to characterize and compare hydrophobicity. As there is no official or widely used standard for determining or comparing hydrophobicity in the protein or ADC landscape, it is important to discuss the limitations and strengths of analytical methods that are commonly used. Furthermore, it is essential to note that all analytical methods mentioned here are relative, which makes overall comparisons between publications challenging. Future work towards standardization in the field of ADCs and protein drugs will greatly aide in better cross-publication comparisons and in turn the development better technologies to address the challenge of hydrophobicity.

The most commonly employed technology for determining the hydrophobicity of ADCs is hydrophobic interaction chromatography (HIC). This technique relies on the principle that certain non-chaotropic salts such as ammonium-sulfate interact strongly with water and the hydrophilic surfaces of the protein, preferentially exposing the hydrophobic residues to the column matrix.[20] This effect is akin to the principal of "salting-out" a protein, wherein increasing concentrations of salt reduce the interactions of water with the charged protein residues, causing a decrease in solubility and eventual precipitation. By pairing this principle with a hydrophobic stationary phase, molecules can be separated based on their hydrophobicity while elution is controlled through the adjustment of the salt concentration of the mobile phase. This chromatographic technique is commonly used for protein and ADC research as it is non-denaturing and is highly tunable given everything from stationary phase, salt, and pH can be tailored to the specific biomolecule(s) one is separating.

For ADCs, HIC has proved to be versatile and powerful technique for the purification of different DARs from conjugation mixtures, calculating/determining the DAR of a heterogeneous population, or comparing the hydrophobicity of conjugates.[21] This latter approach of using HIC to compare ADCs is the most commonly employed assay to compare the hydrophobicities of conjugates and will be cited throughout future sections as a rationalization for the performance of certain ADCs over others. Despite the merits of this technique, however, it should be noted that it is a mostly qualitative technique when used in this manner. While it can be stated with a high level of certainty that ADCs with earlier HIC retention times are more hydrophilic, the magnitude of this difference is rarely discussed. For instance, it is unclear as to what degree retention time should be reduced to achieve a desired outcome. Further taking into account the differences in column matrices, salt concentrations, pH values, and other variables across research environments, it quickly becomes apparent that comparisons of HIC profiles across publications is not feasible. Until there is the development and adoption of a set of standards that can be used to calibrate columns across research environments, HIC will not be generalizable analytical tool that can be used for meta-analysis of ADCs.

While HIC remains the principal method for determining relative hydrophilicities, a number of other assays have been developed with the goal of improving throughput. One example from Estep and coworkers, termed affinity-capture self-interaction nanoparticle spectroscopy, uses plasmonic resonance at varying ammonium sulfate concentrations in order to measure the propensity of different ADCs to self-associate.[22] Other methodologies that rely on the binding of dyes to the surface of proteins can further be used in ADC research for the rapid determination of relative hydrophobicity.[23,24] In addition, rather than relying on characterization of the entire conjugate, more quantitative measurements of the hydrophobicity of the linker-drug (LD) itself

can be helpful in determining the future stability and hydrophobicity of an ADC. For instance, Pysz and coworkers developed an ultra-performance liquid chromatography (UPLC) assay to correlate the cLogP of commonly used LDs to retention time on a reversed-phase (RP) column. Methodologies such as these allow for a more quantitative analysis and can be paired along with stability data to make predictive models relating the cLogP of LDs to the stability and *in vivo* performance.

As a complement to measuring the hydrophobicity of a conjugate directly, a wide variety of analytical methods are available to measure the stability of the antibody after conjugation. These results-oriented assays give an indirect inference of the hydrophobicity by looking at the effects of conjugation and can be used to draw conclusions on the overall hydrophobicity of the conjugate. Perhaps the most widely used technique used in this type of analysis is size exclusion chromatography (SEC). As more hydrophobic ADCs tend to show a propensity towards self-association, the effect of conjugation can be visualized through the observation of dimers, trimers, or other high molecular weight species (HMWS).[25] Other techniques such as capillary isoelectric focusing, dynamic light scattering, differential scanning fluorimetry (DSF), differential scanning calorimetry (DSC), and protein conformation assays (PCA) are further examples of other assays that can give indirect insight into the hydrophobicity of conjugate by analyzing the stability and/or structure of the conjugate.[6,25,26]

While analyzing the hydrophobicity of ADCs is a non-trivial task, there exists a wide array of techniques to both directly or indirectly assay their characteristics. The nature of these current techniques, and further, our limited understanding of hydrophobicity in this field unfortunately restricts these assays to being comparative in nature. Unlike small-molecule drug development, we do not have a single number such as LogP that summarizes the hydrophobicity of a compound

and is comparable across publications and research areas. Rather, we rely on an ensemble of analytical techniques that can only give insight into the hydrophobicity of conjugates. However, in order for the field to find solutions to the consequences of hydrophobicity, there must be significant advancement in either the communication/reporting of this data or the development of methods/theories that are more absolute in determining hydrophobicity; ideally both.

1.4 The Antibody: Conjugation Chemistry to Improve Hydrophobicity

There are a number of significant, computational efforts to determine more hydrophilic complementarity-determining regions (CDRs) for antibody discovery and engineering.[27–29] By incorporating hydrophobicity considerations such as amino acid charge states into predictive, computational models, more hydrophilic antibodies can be produced. While these efforts offer promise, the work is outside of the scope of this review and instead, this section focuses on the development and optimization of conjugation chemistry to modulate the stability and hydrophilicity of ADCs.

Antibodies are large molecules with diverse topological surfaces, therefore, the impact on where and how a drug is conjugated to it can have a significant outcome on the apparent hydrophobicity of the conjugate. The advent of site-specific mutations in antibody engineering have allowed for the direct incorporation of non-native cysteine residues and noncanonical amino acids.[30] These techniques have allowed for the rapid screening and testing of a wide range of conjugation sites in order to determine optimal locations for attachment of payloads. Perhaps the most extensive and thorough study of this nature was conducted by Ohri and coworkers where 648 total sites for conjugation were screened through cysteine scanning.[31] Through this study, the team was able to identify sites for conjugation that had optimal conjugation efficiencies, linker stabilities, and were less prone to aggregation, providing an excellent example of how even small

changes in conjugation location can have significant impact on properties of the final conjugate. In a similar, site-specific manner, Benjamin and coworkers found that by conjugating a payload to glutamine 295 on the Fc domain, they could achieve more stable and hydrophilic conjugates when compared to commonly utilized conjugation sites.[32] They further rationalize the improved hydrophilicity of these conjugates to be the result of the sterically shielded topology of this conjugation site, which could help mask the hydrophobicity of the payload. Additional examples of this dependence of stability and hydrophobicity have been noted from a variety of contexts, demonstrating the importance of this optimization when designing an ADC.[33,34] However, it must be noted that other factors outside of stability and hydrophobicity are affected through alterations in the conjugation site. For instance, it has been demonstrated that the susceptibility of maleimides to deconjugation *in vivo* can largely be impacted by site where the payload is attached.[35] Furthermore, certain linker-drugs can undergo proteolytic degradation in mouse plasma when conjugated to certain locations on an antibody, and thus can have a large effect on the efficacy and toxicity of the ADC.[36] Taking into consideration these multitude of factors when considering a conjugation strategy, there is unfortunately no rule-of-thumb that can be followed. Instead, like many aspects of designing ADCs, conjugation site must be considered along with other factors in order to tailor the final conjugate for its specific application.

In addition to careful selection of conjugation site, the chemistry that is used to form the conjugate can have an effect on the overall hydrophobicity of an ADC. For instance, through a number of studies, there has been a clear link between the tolerability/PK of an antibody and the specificity of the conjugation chemistry.[37–40] Generally, it is reported that site-specific conjugations (through enzymatic or maleimide chemistry), have more favorable PK outcomes than those that heterogeneously target lysine residues. However, it is important to note that there are

examples of heterogeneous, lysine conjugates outperforming site-specific conjugates.[41] In addition to *in vivo* performance, conjugation chemistry can have a significant effect on the stability and hydrophobicity of the conjugate. Lysine conjugation methods typically remove the positive charge of native antibody, as the ammonium is converted into an amide. Cysteine modification through the use of maleimides or iodoacetamides, however, do not affect the overall charge of the protein, likely conferring a more hydrophilic conjugate. Furthermore, advances in new conjugation chemistries, such as self-hydrolyzing maleimides,[42] ethynylphosphonamidates,[43] 2-(maleimidomethyl)-1,3-Dioxanes,[44] and non-covalent methodologies[45] offer promise in their ability to modulate the hydrophobicity of conjugates. While there is no single conjugation chemistry or conjugation site that is ideal for all conditions, it has been demonstrated repeatedly these factors play an important role in the development of effective ADCs. As with many other topics discussed herein, it is an important optimization parameter that should be considered when designing an ADC.

1.5 The Payload: Medicinal Chemistry Approaches to Improve Hydrophilicity

The discovery of novel payloads for ADCs is likely the least fruitful endeavor in the pursuit of more hydrophilic conjugates. Often, hydrophobic interactions are the core forces that drive binding and activity in ADC payloads. For instance, a strong, positive correlation between the cLogP of DNA-alkylating agents and their potency has been demonstrated.[46] Since the current principal behind ADCs is the use of highly potent drugs, this fundamental dichotomy between hydrophobicity and activity proves a significant hurdle. One innovative method to overcome this challenge is through reversible modification of payloads with solubilizing agents. King and coworkers demonstrated a ten-fold decrease in aggregation when attaching a triethylene glycol moiety to the ketone of doxorubicin.[47] Since the attachment of triethylene glycol was done through

a hydrazone linker that would hydrolyze in endosomal compartments, this strategy allows for the stabilization of the ADC during production and administration while not effecting the overall binding activity of the drug. Outside of reversible modifications, there have been some noted success in the improvement of certain existing payloads through structure-activity-relationship (SAR) efforts[48,49] as well as the discovery of new classes of more hydrophilic payloads.[50] Furthermore, in addition to direct payload modification, one notable innovation has arisen regarding new methods to attach drugs to linkers. An important technology for payload attachment was pioneered by Genentech wherein tertiary amines could be directly attached to protease or reductively cleavable linkers.[51] The resulting quarternized amine from this chemistry could be released, not only providing new handles for the attachment of payloads, but further demonstrating a novel strategy for lowering the hydrophobicity of linker-drugs. Studies of the LogD of drugs attached in this manner resulted a 2,000-fold decrease in hydrophobicity, demonstrating the applicability of this chemistry in the preparation of ADCs. In a similar manner, Seattle Genetics developed quaternary ammonium linkers that expand the scope of available drugs for linker attachment.[52] Novel approaches such as these that rely on hydrophilic chemistries to attach drugs to linkers or reversible methods to attach solubilizing agents are the most promising routes in payload chemistry as they do not directly alter the drug itself.

1.6 The Linker: Solubilizing Motifs to Improve Hydrophilicity

The most investigated and promising method to increase the hydrophilicity of ADCs is through the use of solubilizing linkers. As discussed previously, both the antibody itself as well as the payload have limitations in what modifications can be done without impacting affinity or activity. The linker, on the other hand, offers greater flexibility in the types modifications that can be made as its only purpose is to provide a direct linkage between the antibody and the payload, often

through a self-immolative, cleavable linker. A large variety of different strategies have been employed in linker chemistry with varied effects on either the pharmacokinetics of an ADC and/or its stability. To summarize some of these modifications, we have outlined a diverse set of hydrophilic functionalities that have been utilized in **Table 1.1**. In these comparisons, we carefully selected linker chemistries from the literature where only a single variable was altered, allowing for a direct understanding of the how each solubilizing group affects both the hydrophilicity of the linker (through cLogP/cLogD (7.4) calculations) as well as the overall impact on the ADC.

From the outlined examples of linker chemistries, a number of interesting conclusions can be drawn. For one, poly (ethylene glycol) (PEG) spacers, which are the most commonly employed solubilizing group, can have marked improvement on the hydrophilicity, stability, and performance of the resulting conjugate. Repeat units as small as two and up to 24 show reduced cLogP values and further demonstrate improvements in solubility, conjugation efficiency, pharmacokinetics, and stability (**Table 1.1**). The most thorough investigation of PEG spacers was done by Seattle Genetics wherein a large range of PEG linkers were investigated in their ability to reduce hydrophobicity and improve pharmacokinetics.[53] The researchers reported a marked improvement in therapeutic indices, pharmacokinetics, and efficacies as a function of the size of PEG spacer used. Interestingly, no further improvement in PK was observed beyond a PEG size of 8, suggesting sufficient shielding of the MMAE payload. Furthermore, in xenograft models, the PEG_8 and PEG_{12} conjugates outperformed the PEG_{24} conjugate, demonstrating that larger PEGs can inhibit *in vivo* activity and therefore reinforces the importance of careful optimization and tuning necessary to develop effective ADCs. In addition to considering the length of the PEG spacers utilized for conjugates, an important parameter that has been noted is the architecture of the linker. Lyon and coworkers demonstrated that branching structures can have improved

hydrophilicity over linear structures as measured both by hydrophobic interaction chromatography as well as PK perfromance.[54] This study, along with those previously cited, demonstrates the sensitivity of ADC performance and stability to slight alterations in PEG spacer size and makeup, reinforcing the need to strategic and rigorous optimization in linker design.

Outside of the addition of PEG spacers to linkers, a variety of other strategies have been investigated in order to modulate the hydrophobicity of ADCs. Traditional linker structures often rely on cleavable valine-citrulline-p-aminobenzyl (VC-PAB) linkers that selectively release payloads in the endosomal compartment after protease cleavage. However, while these motifs are robust in terms of their selectivity for endosomal proteases, they are hydrophobic in nature. Therefore, a number of new technologies have been developed and explored as more hydrophilic alternatives. In terms of improving the hydrophilicity of VC-PAB linkers, a number of alternative peptide sequences and peptidomimetic mimics have been explored to either confer grater circulation stability, hydrophilicity, or both.[55–58] Outside of peptidyl linkers, a variety of other cleavable linkers have been developed that rely on more hydrophilic recognition motifs. One strategy that avoids hydrophobic peptide sequences is the use of direct disulfide conjugates to cysteine residues that can be released by free glutathione in the cystol.[59] This strategy pioneered by Genentech reduces the overall size and hydrophobicity of the linker and, due to careful selection of conjugation site, shows remarkable stability *in vivo*. Disulfide conjugates can be further enhanced in their hydrophilicity through the addition of sulfonate groups as demonstrated by Zhao and coworkers.[60] Additional linkers with hydrophilic, cleavable linkers have been demonstrated with pyrophosphate diesters,[61,62] glucuronides,[63] and arylsulfates,[64] which further expands the diversity of chemistries that can be utilized in the design of hydrophilic ADC linkers.

As ADCs have advanced, there has been a recent push to increase the DARs of conjugates. Higher loadings of payload allow for greater efficacy against lower-antigen presenting cells and additionally higher DARs expand the breadth of cytotoxics available for delivery as lower potency drugs can be employed.[65] A natural outgrowth of this development has been the use of polymeric linkers for ADCs, which, unlike traditional linkers, offer higher valency. Furthermore, through selection of hydrophilic backbones and side-chains, polymers can offer an excellent platform for masking the hydrophobicity of payloads. An example that embodies this concept is the work from Yurkovetskiy and coworkers, wherein polyacetal polymers are used to create DAR 20 ADCs that maintain physiochemical stability and favorable pharmacokinetic profiles.[66] This polymeric platform, also known as Fleximers, offers the additional advantage of being degradable, as they are composed of polyacetals that degrade in the acidic, endosomal compartment. Additional examples of polymers based on dextran[67] and acrylamides[68,69] have been reported with similar advantages in valency and hydrophilicity. One challenge, however, with polymeric scaffolds is the inherent dispersity that is a result of most polymerization techniques. Since these linkers are not chemically-defined, the resulting conjugates are heterogenous, making characterization and precise drug loading challenging. To overcome these difficulties, sequence-defined oligomers are currently being investigated as they can offer similar advantages in hydrophilicity and valency while additionally being chemically-defined. Methodologies to prepare such oligomers have been reported using allyl acrylamides[70] and sarcosines[71] which have been employed successfully in creating multivalent, hydrophilic ADC linkers. While these strategies of pursuing chemically-defined oligomers for ADCs is in its early stages, we believe the continued development and application of these types of linkers can make a significant contribution to the field of ADCs by further enabling the production of stable, higher DAR conjugates.

Linker-Drug 1 cLog P/cLog D (7.4)	Linker-Drug 2 cLog P/cLog D (7.4)	Improvement	Reference
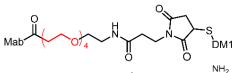 1.795/1.8	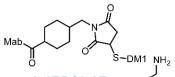 4.473/4.47	Improved retention in MDR expressing cells and efficacy in xenograft models	72
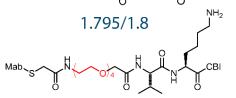 3.108/0.5	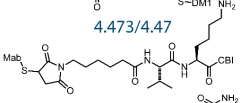 4.613/2.04	95% reduction in aggregation at Dar 8	73
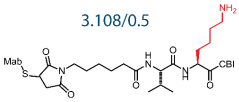 3.654/3.65	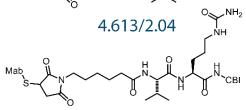 4.613/2.01	22% reduction in aggregation at Dar 4	73
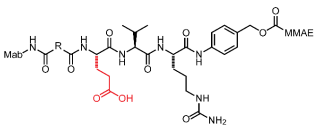 6.123/-6.44	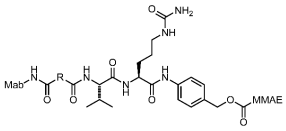 8.283/1.87	Improved pharmacokinetic outcome	56
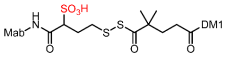 3.039/1.74	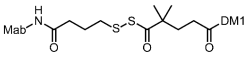 5.05/5.05	Improved or equivalent efficacy in vitro	74
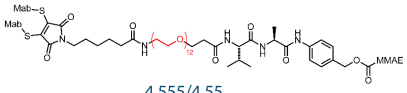 4.555/4.55	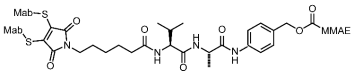 5.987/5.99	Improved conjugation efficiency	75
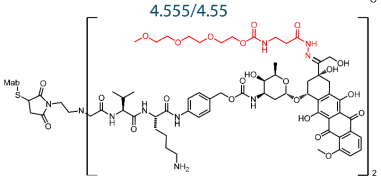 0.779/-0.72	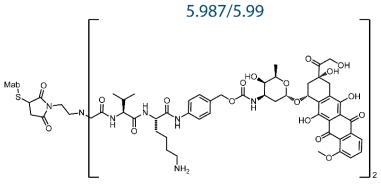 2.691/1.53	10-fold decrease in aggregation	47
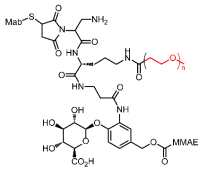 n=2, -4.254/-3.3 n=8, -3.535/-3.61 n=24, -4.287/-4.36 n=4, -3.347/-3.43 n=12, -3.723/-3.80	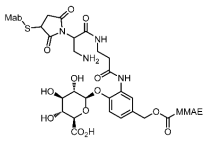 -1.975/-2.05	Reduced PK clearance as a function of PEG length and improved tolerability. Reduced nonspecific uptake in organs	53, 76

Table 1.1. Head-to-head comparisons of linker chemistries with and the resulting effect on ADC stability/pharmacokinetics. cLogP and cLogD(7.4) were calculated using Chemicalize® and are provided as a reference to compare the effect of these chemistries on the overall hydrophobicity.[47,53,56,72–76]

1.7 Summary and Future Directions for the Field

Current generation ADCs rely on the formula of attaching hydrophobic, potent payloads through self-immolative linkers. While this strategy has led to the development and approval of 9 ADCs (with many promising drugs in clinical trials), a number of challenges still exist in the field. Largely, instability and poor pharmacokinetic outcomes are challenges that are largely the result

of hydrophobicity. Aspects of conjugation chemistry, payload, antibody primary sequence, and linker design all offer unique contributions to the overall hydrophobicity of the conjugate, creating a host of variables that must be considered when designing ADCs. With the goal of mitigating the impact of hydrophobicity on the conjugate, each of these components have been optimized and investigated, and the most promising and successful strategies have involved the design of new linker chemistries. Unlike altering the payload or antibody sequence, hydrophilic linkers can be used in a modular fashion as they often do not impact the affinity or potency of the conjugate. Additionally, with recent interests in increasing the DAR of ADCs, new linker designs offer the ability to attach more drugs per conjugation site, and, depending on the chemistry used, can provide a method to mask the hydrophobicity of payloads.

It is this focus on new linker technologies and targeting higher DAR conjugates that marks the transition of the field to the second-generation technologies. Polymeric and oligomeric scaffolds broaden the scope of cytotoxics that can employed as payloads and further open the possibility of co-delivering a combination of different drugs. Furthermore, many of the linker chemistries outlined offer the ability to prolong half-life and improve pharmacokinetic outcomes by solubilizing hydrophobic payloads. As the field progresses in this direction, a number of questions remain to be investigated: the effect of linker architecture on ADC performance, the most effective backbones for payload solubilization, and efficient methods to synthesize polymeric/oligomeric linkers that satisfy the requirements outlined previously. While hydrophobicity remains a persistent challenge in the development of effective ADCs with favorable therapeutic windows, recent developments and technologies offer significant promise in the continued growth and expansion of the field. As an addition to this body of work, chapter 2 of this thesis will provide a

new methodology for the synthesis of sequence-defined, hydrophilic scaffolds for antibody drug conjugates.

1.8 References

(1) Kim, E. G.; Kim, K. M. Strategies and Advancement in Antibody-Drug Conjugate Optimization for Targeted Cancer Therapeutics. *Biomol Ther (Seoul)* **2015**, *23*, 493–509.

(2) Beck, A.; Goetsch, L.; Dumontet, C.; Corvaïa, N. Strategies and Challenges for the next Generation of Antibody–Drug Conjugates. *Nature Reviews Drug Discovery* **2017**, *16*, 315–337.

(3) Tsuchikama, K.; An, Z. Antibody-Drug Conjugates: Recent Advances in Conjugation and Linker Chemistries. *Protein Cell* **2018**, *9*, 33–46.

(4) Hamblett, K. J.; Senter, P. D.; Chace, D. F.; Sun, M. M. C.; Lenox, J.; Cerveny, C. G.; Kissler, K. M.; Bernhardt, S. X.; Kopcha, A. K.; Zabinski, R. F.; Meyer, D. L.; Francisco, J. A. Effects of Drug Loading on the Antitumor Activity of a Monoclonal Antibody Drug Conjugate. *Clin. Cancer Res.* **2004**, *10*, 7063–7070.

(5) Sun, X.; Ponte, J. F.; Yoder, N. C.; Laleau, R.; Coccia, J.; Lanieri, L.; Qiu, Q.; Wu, R.; Hong, E.; Bogalhas, M.; Wang, L.; Dong, L.; Setiady, Y.; Maloney, E. K.; Ab, O.; Zhang, X.; Pinkas, J.; Keating, T. A.; Chari, R.; Erickson, H. K.; Lambert, J. M. Effects of Drug-Antibody Ratio on Pharmacokinetics, Biodistribution, Efficacy, and Tolerability of Antibody-Maytansinoid Conjugates. *Bioconjug. Chem.* **2017**, *28*, 1371–1381.

(6) Duerr, C.; Friess, W. Antibody-Drug Conjugates- Stability and Formulation. *European Journal of Pharmaceutics and Biopharmaceutics* **2019**, *139*, 168–176.

(7) Sarkar, A.; Kellogg, G. E. Hydrophobicity – Shake Flasks, Protein Folding and Drug Discovery. *Curr Top Med Chem* **2010**, *10*, 67–83.

(8) Lobo, S. Is There Enough Focus on Lipophilicity in Drug Discovery? *Expert Opinion on Drug Discovery* **2020**, *15*, 261–263.

(9) Arnott, J. A.; Planey, S. L. The Influence of Lipophilicity in Drug Discovery and Design. *Expert Opinion on Drug Discovery* **2012**, *7*, 863–875.

(10) Tumey, L. N. Next Generation Payloads for ADCs. In *Innovations for Next-Generation Antibody-Drug Conjugates*; Damelin, M., Ed.; Cancer Drug Discovery and Development; Springer International Publishing: Cham, 2018; pp 187–214.

(11) Lucas, A. T.; Price, L. S. L.; Schorzman, A. N.; Storrie, M.; Piscitelli, J. A.; Razo, J.; Zamboni, W. C. Factors Affecting the Pharmacology of Antibody–Drug Conjugates. *Antibodies* **2018**, *7*, 10.

(12) Chow, A.; Brown, B. D.; Merad, M. Studying the Mononuclear Phagocyte System in the Molecular Age. *Nature Reviews Immunology* **2011**, *11*, 788–798.

(13) Finbloom, D. S.; Abeles, D.; Rifai, A.; Plotz, P. H. The Specificity of Uptake of Model Immune Complexes and Other Protein Aggregates by the Murine Reticuloendothelial System. *J. Immunol.* **1980**, *125*, 1060–1065.

(14) Meyer, D. W.; Bou, L. B.; Shum, S.; Jonas, M.; Anderson, M. E.; Hamilton, J. Z.; Hunter, J. H.; Wo, S. W.; Wong, A. O.; Okeley, N. M.; Lyon, R. P. An in Vitro Assay Using Cultured Kupffer Cells Can Predict the Impact of Drug Conjugation on in Vivo Antibody Pharmacokinetics. *Mol. Pharmaceutics* **2020**, *17*, 802–809.

(15) Lu, D.; Girish, S.; Gao, Y.; Wang, B.; Yi, J.-H.; Guardino, E.; Samant, M.; Cobleigh, M.; Rimawi, M.; Conte, P.; Jin, J. Y. Population Pharmacokinetics of Trastuzumab Emtansine (T-DM1), a HER2-Targeted Antibody–Drug Conjugate, in Patients with HER2-Positive Metastatic Breast Cancer: Clinical Implications of the Effect of Covariates. *Cancer Chemother Pharmacol* **2014**, *74*, 399–410.

(16) Zamboni, W. C.; Strychor, S.; Maruca, L.; Ramalingam, S.; Zamboni, B. A.; Wu, H.; Friedland, D. M.; Edwards, R. P.; Stoller, R. G.; Belani, C. P.; Ramanathan, R. K. Pharmacokinetic Study of Pegylated Liposomal CKD-602 (S-CKD602) in Patients With Advanced Malignancies. *Clinical Pharmacology & Therapeutics* **2009**, *86*, 519–526.

(17) Buecheler, J. W.; Winzer, M.; Tonillo, J.; Weber, C.; Gieseler, H. Impact of Payload Hydrophobicity on the Stability of Antibody–Drug Conjugates. *Mol. Pharmaceutics* **2018**, *15*, 2656–2664.

(18) Adem, Y. T.; Schwarz, K. A.; Duenas, E.; Patapoff, T. W.; Galush, W. J.; Esue, O. Auristatin Antibody Drug Conjugate Physical Instability and the Role of Drug Payload. *Bioconjugate Chem.* **2014**, *25*, 656–664.

(19) Gandhi, A. V.; Arlotta, K. J.; Chen, H.-N.; Owen, S. C.; Carpenter, J. F. Biophysical Properties and Heating-Induced Aggregation of Lysine-Conjugated Antibody-Drug Conjugates. *J Pharm Sci* **2018**, *107*, 1858–1869.

(20) Fekete, S.; Veuthey, J.-L.; Beck, A.; Guillarme, D. Hydrophobic Interaction Chromatography for the Characterization of Monoclonal Antibodies and Related Products. *J Pharm Biomed Anal* **2016**, *130*, 3–18.

(21) Fleming, R. ADC Analysis by Hydrophobic Interaction Chromatography. *Antibody-Drug Conjugates* **2020**, 147–161.

(22) Estep, P.; Caffry, I.; Yu, Y.; Sun, T.; Cao, Y.; Lynaugh, H.; Jain, T.; Vásquez, M.; Tessier, P. M.; Xu, Y. An Alternative Assay to Hydrophobic Interaction Chromatography for High-Throughput Characterization of Monoclonal Antibodies. *MAbs* **2015**, *7*, 553–561.

(23) Kato, A.; Nakai, S. Hydrophobicity Determined by a Fluorescence Probe Method and Its Correlation with Surface Properties of Proteins. *Biochimica et Biophysica Acta (BBA) - Protein Structure* **1980**, *624*, 13–20.

(24) Kato, A.; Matsuda, T.; Matsudomi, N.; Kobayashi, K. Determination of Protein Hydrophobicity Using Sodium Dodecyl Sulfate Binding Method. *J. Agric. Food Chem.* **1984**, *32*, 284–288.

(25) Chen, T.; Chen, Y.; Stella, C.; Medley, C. D.; Gruenhagen, J. A.; Zhang, K. Antibody-Drug Conjugate Characterization by Chromatographic and Electrophoretic Techniques. *Journal of Chromatography B* **2016**, *1032*, 39–50.

(26) Fu, C.; Zhang, Z.; Zhou, S.; Pritts, W. A.; Zhang, Q. Assessing Localized Conformational Stability of Antibody-Drug Conjugate by Protein Conformation Assay. *Journal of Pharmaceutical and Biomedical Analysis* **2020**, *179*, 113020.

(27) Raybould, M. I. J.; Marks, C.; Krawczyk, K.; Taddese, B.; Nowak, J.; Lewis, A. P.; Bujotzek, A.; Shi, J.; Deane, C. M. Five Computational Developability Guidelines for Therapeutic Antibody Profiling. *PNAS* **2019**, *116*, 4025–4030.

(28) Li, W.; Prabakaran, P.; Chen, W.; Zhu, Z.; Feng, Y.; Dimitrov, D. S. Antibody Aggregation: Insights from Sequence and Structure. *Antibodies* **2016**, *5*, 19.

(29) Hebditch, M.; Warwicker, J. Charge and Hydrophobicity Are Key Features in Sequence-Trained Machine Learning Models for Predicting the Biophysical Properties of Clinical-Stage Antibodies. *PeerJ* **2019**, *7*.

(30) Walsh, S. J.; Bargh, J. D.; Dannheim, F. M.; Hanby, A. R.; Seki, H.; Counsell, A. J.; Ou, X.; Fowler, E.; Ashman, N.; Takada, Y.; Isidro-Llobet, A.; Parker, J. S.; Carroll, J. S.; Spring, D. R. Site-Selective Modification Strategies in Antibody–Drug Conjugates. *Chem. Soc. Rev.* **2020**.

(31) Ohri, R.; Bhakta, S.; Fourie-O'Donohue, A.; dela Cruz-Chuh, J.; Tsai, S. P.; Cook, R.; Wei, B.; Ng, C.; Wong, A. W.; Bos, A. B.; Farahi, F.; Bhakta, J.; Pillow, T. H.; Raab, H.; Vandlen, R.; Polakis, P.; Liu, Y.; Erickson, H.; Junutula, J. R.; Kozak, K. R. High-Throughput Cysteine Scanning To Identify Stable Antibody Conjugation Sites for Maleimide- and Disulfide-Based Linkers. *Bioconjugate Chem.* **2018**, *29*, 473–485.

(32) Benjamin, S. R.; Jackson, C. P.; Fang, S.; Carlson, D. P.; Guo, Z.; Tumey, L. N. Thiolation of Q295: Site-Specific Conjugation of Hydrophobic Payloads without the Need for Genetic Engineering. *Mol. Pharmaceutics* **2019**, *16*, 2795–2807.

(33) Mills, B. J.; Kruger, T.; Bruncko, M.; Zhang, X.; Jameel, F. Effect of Linker-Drug Properties and Conjugation Site on the Physical Stability of ADCs. *Journal of Pharmaceutical Sciences* **2020**.

(34) Strop, P.; Liu, S.-H.; Dorywalska, M.; Delaria, K.; Dushin, R. G.; Tran, T.-T.; Ho, W.-H.; Farias, S.; Casas, M. G.; Abdiche, Y.; Zhou, D.; Chandrasekaran, R.; Samain, C.; Loo, C.; Rossi, A.; Rickert, M.; Krimm, S.; Wong, T.; Chin, S. M.; Yu, J.; Dilley, J.; Chaparro-Riggers, J.; Filzen, G. F.; O'Donnell, C. J.; Wang, F.; Myers, J. S.; Pons, J.; Shelton, D. L.; Rajpal, A. Location Matters: Site of Conjugation Modulates Stability and Pharmacokinetics of Antibody Drug Conjugates. *Chemistry & Biology* **2013**, *20*, 161–167.

(35) Shen, B.-Q.; Xu, K.; Liu, L.; Raab, H.; Bhakta, S.; Kenrick, M.; Parsons-Reponte, K. L.; Tien, J.; Yu, S.-F.; Mai, E.; Li, D.; Tibbitts, J.; Baudys, J.; Saad, O. M.; Scales, S. J.; McDonald, P. J.; Hass, P. E.; Eigenbrot, C.; Nguyen, T.; Solis, W. A.; Fuji, R. N.; Flagella, K. M.; Patel, D.; Spencer, S. D.; Khawli, L. A.; Ebens, A.; Wong, W. L.; Vandlen, R.; Kaur, S.; Sliwkowski, M. X.; Scheller, R. H.; Polakis, P.; Junutula, J. R. Conjugation Site Modulates the in Vivo Stability and Therapeutic Activity of Antibody-Drug Conjugates. *Nat Biotech* **2012**, *30*, 184–189.

(36) Dorywalska, M.; Strop, P.; Melton-Witt, J. A.; Hasa-Moreno, A.; Farias, S. E.; Galindo Casas, M.; Delaria, K.; Lui, V.; Poulsen, K.; Loo, C.; Krimm, S.; Bolton, G.; Moine, L.; Dushin, R.; Tran, T.-T.; Liu, S.-H.; Rickert, M.; Foletti, D.; Shelton, D. L.; Pons, J.; Rajpal, A. Effect of Attachment Site on Stability of Cleavable Antibody Drug Conjugates. *Bioconjugate Chem.* **2015**, *26*, 650–659.

(37) Junutula, J. R.; Raab, H.; Clark, S.; Bhakta, S.; Leipold, D. D.; Weir, S.; Chen, Y.; Simpson, M.; Tsai, S. P.; Dennis, M. S.; Lu, Y.; Meng, Y. G.; Ng, C.; Yang, J.; Lee, C. C.; Duenas, E.; Gorrell, J.; Katta, V.; Kim, A.; McDorman, K.; Flagella, K.; Venook, R.; Ross, S.; Spencer, S. D.; Lee Wong, W.; Lowman, H. B.; Vandlen, R.; Sliwkowski, M. X.; Scheller,

R. H.; Polakis, P.; Mallet, W. Site-Specific Conjugation of a Cytotoxic Drug to an Antibody Improves the Therapeutic Index. *Nature Biotechnology* **2008**, *26*, 925–932.

(38) Lhospice, F.; Brégeon, D.; Belmant, C.; Dennler, P.; Chiotellis, A.; Fischer, E.; Gauthier, L.; Boëdec, A.; Rispaud, H.; Savard-Chambard, S.; Represa, A.; Schneider, N.; Paturel, C.; Sapet, M.; Delcambre, C.; Ingoure, S.; Viaud, N.; Bonnafous, C.; Schibli, R.; Romagné, F. Site-Specific Conjugation of Monomethyl Auristatin E to Anti-CD30 Antibodies Improves Their Pharmacokinetics and Therapeutic Index in Rodent Models. *Mol. Pharmaceutics* **2015**, *12*, 1863–1871.

(39) Strop, P.; Delaria, K.; Foletti, D.; Witt, J. M.; Hasa-Moreno, A.; Poulsen, K.; Casas, M. G.; Dorywalska, M.; Farias, S.; Pios, A.; Lui, V.; Dushin, R.; Zhou, D.; Navaratnam, T.; Tran, T.-T.; Sutton, J.; Lindquist, K. C.; Han, B.; Liu, S.-H.; Shelton, D. L.; Pons, J.; Rajpal, A. Site-Specific Conjugation Improves Therapeutic Index of Antibody Drug Conjugates with High Drug Loading. *Nature Biotechnology* **2015**, *33*, 694–696.

(40) Bai, C.; Reid, E. E.; Wilhelm, A.; Shizuka, M.; Maloney, E. K.; Laleau, R.; Harvey, L.; Archer, K. E.; Vitharana, D.; Adams, S.; Kovtun, Y.; Miller, M. L.; Chari, R.; Keating, T. A.; Yoder, N. C. Site-Specific Conjugation of the Indolinobenzodiazepine DGN549 to Antibodies Affords Antibody–Drug Conjugates with an Improved Therapeutic Index as Compared with Lysine Conjugation. *Bioconjugate Chem.* **2020**, *31*, 93–103.

(41) Yoder, N. C.; Bai, C.; Tavares, D.; Widdison, W. C.; Whiteman, K. R.; Wilhelm, A.; Wilhelm, S. D.; McShea, M. A.; Maloney, E. K.; Ab, O.; Wang, L.; Jin, S.; Erickson, H. K.; Keating, T. A.; Lambert, J. M. A Case Study Comparing Heterogeneous Lysine- and Site-Specific

Cysteine-Conjugated Maytansinoid Antibody-Drug Conjugates (ADCs) Illustrates the Benefits of Lysine Conjugation. *Mol. Pharmaceutics* **2019**, *16*, 3926–3937.

(42) Lyon, R. P.; Setter, J. R.; Bovee, T. D.; Doronina, S. O.; Hunter, J. H.; Anderson, M. E.; Balasubramanian, C. L.; Duniho, S. M.; Leiske, C. I.; Li, F.; Senter, P. D. Self-Hydrolyzing Maleimides Improve the Stability and Pharmacological Properties of Antibody-Drug Conjugates. *Nature Biotechnology* **2014**, *32*, 1059–1062.

(43) Kasper, M.-A.; Stengl, A.; Ochtrop, P.; Gerlach, M.; Stoschek, T.; Schumacher, D.; Helma, J.; Penkert, M.; Krause, E.; Leonhardt, H.; Hackenberger, C. P. R. Ethynylphosphonamidates for the Rapid and Cysteine-Selective Generation of Efficacious Antibody–Drug Conjugates. *Angewandte Chemie International Edition* **2019**, *58*, 11631–11636.

(44) Dovgan, I.; Kolodych, S.; Koniev, O.; Wagner, A. 2-(Maleimidomethyl)-1,3-Dioxanes (MD): A Serum-Stable Self-Hydrolysable Hydrophilic Alternative to Classical Maleimide Conjugation. *Scientific Reports* **2016**, *6*, 1–6.

(45) Muguruma, K.; Yakushiji, F.; Kawamata, R.; Akiyama, D.; Arima, R.; Shirasaka, T.; Kikkawa, Y.; Taguchi, A.; Takayama, K.; Fukuhara, T.; Watabe, T.; Ito, Y.; Hayashi, Y. Novel Hybrid Compound of a Plinabulin Prodrug with an IgG Binding Peptide for Generating a Tumor Selective Noncovalent-Type Antibody–Drug Conjugate. *Bioconjugate Chem.* **2016**, *27*, 1606–1613.

(46) Wolfe, A. L.; Duncan, K. K.; Lajiness, J. P.; Zhu, K.; Duerfeldt, A. S.; Boger, D. L. A Fundamental Relationship between Hydrophobic Properties and Biological Activity for the Duocarmycin Class of DNA-Alkylating Antitumor Drugs: Hydrophobic-Binding-Driven Bonding. *J. Med. Chem.* **2013**, *56*, 6845–6857.

(47) King, H. D.; Dubowchik, G. M.; Mastalerz, H.; Willner, D.; Hofstead, S. J.; Firestone, R. A.; Lasch, S. J.; Trail, P. A. Monoclonal Antibody Conjugates of Doxorubicin Prepared with Branched Peptide Linkers: Inhibition of Aggregation by Methoxytriethyleneglycol Chains. *J. Med. Chem.* **2002**, *45*, 4336–4343.

(48) Akaiwa, M.; Dugal-Tessier, J.; Mendelsohn, B. A. Antibody–Drug Conjugate Payloads; Study of Auristatin Derivatives. *Chemical and Pharmaceutical Bulletin* **2020**, *68*, 201–211.

(49) Satomaa, T.; Pynnönen, H.; Vilkman, A.; Kotiranta, T.; Pitkänen, V.; Heiskanen, A.; Herpers, B.; Price, L. S.; Helin, J.; Saarinen, J. Hydrophilic Auristatin Glycoside Payload Enables Improved Antibody-Drug Conjugate Efficacy and Biocompatibility. *Antibodies* **2018**, *7*, 15.

(50) Verma, V. A.; Pillow, T. H.; DePalatis, L.; Li, G.; Phillips, G. L.; Polson, A. G.; Raab, H. E.; Spencer, S.; Zheng, B. The Cryptophycins as Potent Payloads for Antibody Drug Conjugates. *Bioorganic & Medicinal Chemistry Letters* **2015**, *25*, 864–868.

(51) Staben, L. R.; Koenig, S. G.; Lehar, S. M.; Vandlen, R.; Zhang, D.; Chuh, J.; Yu, S.-F.; Ng, C.; Guo, J.; Liu, Y.; Fourie-O'Donohue, A.; Go, M.; Linghu, X.; Segraves, N. L.; Wang, T.; Chen, J.; Wei, B.; Phillips, G. D. L.; Xu, K.; Kozak, K. R.; Mariathasan, S.; Flygare, J. A.; Pillow, T. H. Targeted Drug Delivery through the Traceless Release of Tertiary and Heteroaryl Amines from Antibody–Drug Conjugates. *Nature Chemistry* **2016**, *8*, 1112–1119.

(52) Burke, P. J.; Hamilton, J. Z.; Pires, T. A.; Setter, J. R.; Hunter, J. H.; Cochran, J. H.; Waight, A. B.; Gordon, K. A.; Toki, B. E.; Emmerton, K. K.; Zeng, W.; Stone, I. J.; Senter, P. D.; Lyon, R. P.; Jeffrey, S. C. Development of Novel Quaternary Ammonium Linkers for Antibody–Drug Conjugates. *Mol Cancer Ther* **2016**, *15*, 938–945.

(53) Burke, P. J.; Hamilton, J. Z.; Jeffrey, S. C.; Hunter, J. H.; Doronina, S. O.; Okeley, N. M.; Miyamoto, J. B.; Anderson, M. E.; Stone, I. J.; Ulrich, M. L.; Simmons, J. K.; McKinney, E. E.; Senter, P. D.; Lyon, R. P. Optimization of a PEGylated Glucuronide-Monomethylauristatin E Linker for Antibody–Drug Conjugates. *Mol Cancer Ther* **2017**, *16*, 116–123.

(54) Lyon, R. P.; Bovee, T. D.; Doronina, S. O.; Burke, P. J.; Hunter, J. H.; Neff-LaFord, H. D.; Jonas, M.; Anderson, M. E.; Setter, J. R.; Senter, P. D. Reducing Hydrophobicity of Homogeneous Antibody-Drug Conjugates Improves Pharmacokinetics and Therapeutic Index. *Nature Biotechnology* **2015**, *33*, 733–735.

(55) Wei, B.; Gunzner-Toste, J.; Yao, H.; Wang, T.; Wang, J.; Xu, Z.; Chen, J.; Wai, J.; Nonomiya, J.; Tsai, S. P.; Chuh, J.; Kozak, K. R.; Liu, Y.; Yu, S.-F.; Lau, J.; Li, G.; Phillips, G. D.; Leipold, D.; Kamath, A.; Su, D.; Xu, K.; Eigenbrot, C.; Steinbacher, S.; Ohri, R.; Raab, H.; Staben, L. R.; Zhao, G.; Flygare, J. A.; Pillow, T. H.; Verma, V.; Masterson, L. A.; Howard, P. W.; Safina, B. Discovery of Peptidomimetic Antibody–Drug Conjugate Linkers with Enhanced Protease Specificity. *J. Med. Chem.* **2018**, *61*, 989–1000.

(56) Anami, Y.; Yamazaki, C. M.; Xiong, W.; Gui, X.; Zhang, N.; An, Z.; Tsuchikama, K. Glutamic Acid–Valine–Citrulline Linkers Ensure Stability and Efficacy of Antibody–Drug Conjugates in Mice. *Nature Communications* **2018**, *9*, 1–9.

(57) Wang, Y.; Fan, S.; Zhong, W.; Zhou, X.; Li, S. Development and Properties of Valine-Alanine Based Antibody-Drug Conjugates with Monomethyl Auristatin E as the Potent Payload. *International Journal of Molecular Sciences* **2017**, *18*, 1860.

(58) Dorywalska, M.; Dushin, R.; Moine, L.; Farias, S. E.; Zhou, D.; Navaratnam, T.; Lui, V.; Hasa-Moreno, A.; Casas, M. G.; Tran, T.-T.; Delaria, K.; Liu, S.-H.; Foletti, D.; O'Donnell, C. J.; Pons, J.; Shelton, D. L.; Rajpal, A.; Strop, P. Molecular Basis of Valine-Citrulline-PABC Linker Instability in Site-Specific ADCs and Its Mitigation by Linker Design. *Mol Cancer Ther* **2016**, *15*, 958–970.

(59) Blanchette, C. D.; Woo, Y.-H.; Thomas, C.; Shen, N.; Sulchek, T. A.; Hiddessen, A. L. Decoupling Internalization, Acidification and Phagosomal-Endosomal/Lysosomal Fusion during Phagocytosis of InlA Coated Beads in Epithelial Cells. *PLOS ONE* **2009**, *4*, e6056.

(60) Zhao, R. Y.; Wilhelm, S. D.; Audette, C.; Jones, G.; Leece, B. A.; Lazar, A. C.; Goldmacher, V. S.; Singh, R.; Kovtun, Y.; Widdison, W. C.; Lambert, J. M.; Chari, R. V. J. Synthesis and Evaluation of Hydrophilic Linkers for Antibody–Maytansinoid Conjugates. *J. Med. Chem.* **2011**, *54*, 3606–3623.

(61) Kern, J. C.; Cancilla, M.; Dooney, D.; Kwasnjuk, K.; Zhang, R.; Beaumont, M.; Figueroa, I.; Hsieh, S.; Liang, L.; Tomazela, D.; Zhang, J.; Brandish, P. E.; Palmieri, A.; Stivers, P.; Cheng, M.; Feng, G.; Geda, P.; Shah, S.; Beck, A.; Bresson, D.; Firdos, J.; Gately, D.; Knudsen, N.; Manibusan, A.; Schultz, P. G.; Sun, Y.; Garbaccio, R. M. Discovery of Pyrophosphate Diesters as Tunable, Soluble, and Bioorthogonal Linkers for Site-Specific Antibody–Drug Conjugates. *J. Am. Chem. Soc.* **2016**, *138*, 1430–1445.

(62) Hydrophilic Linkers and Their Uses for Conjugation of Drugs to a Cell Binding Molecules, November 24, 2012.

(63) Jeffrey, S. C.; Andreyka, J. B.; Bernhardt, S. X.; Kissler, K. M.; Kline, T.; Lenox, J. S.; Moser, R. F.; Nguyen, M. T.; Okeley, N. M.; Stone, I. J.; Zhang, X.; Senter, P. D. Development and

Properties of β-Glucuronide Linkers for Monoclonal Antibody−Drug Conjugates. *Bioconjugate Chem.* **2006**, *17*, 831–840.

(64) Bargh, J. D.; Walsh, S. J.; Isidro-Llobet, A.; Omarjee, S.; Carroll, J. S.; Spring, D. R. Sulfatase-Cleavable Linkers for Antibody-Drug Conjugates. *Chem. Sci.* **2020**, *11*, 2375–2380.

(65) Bodyak, N.; Yurkovetskiy, A. V. Delivering More Payload (High DAR ADCs). In *Innovations for Next-Generation Antibody-Drug Conjugates*; Damelin, M., Ed.; Cancer Drug Discovery and Development; Springer International Publishing: Cham, 2018; pp 215–240.

(66) Yurkovetskiy, A. V.; Yin, M.; Bodyak, N.; Stevenson, C. A.; Thomas, J. D.; Hammond, C. E.; Qin, L.; Zhu, B.; Gumerov, D. R.; Ter-Ovanesyan, E.; Uttard, A.; Lowinger, T. B. A Polymer-Based Antibody–Vinca Drug Conjugate Platform: Characterization and Preclinical Efficacy. *Cancer Res* **2015**, *75*, 3365–3372.

(67) Schneider, H.; Deweid, L.; Pirzer, T.; Yanakieva, D.; Englert, S.; Becker, B.; Avrutina, O.; Kolmar, H. Dextramabs: A Novel Format of Antibody-Drug Conjugates Featuring a Multivalent Polysaccharide Scaffold. *ChemistryOpen* **2019**, *8*, 354–357.

(68) Zhang, L.; Fang, Y.; Kopeček, J.; Yang, J. A New Construct of Antibody-Drug Conjugates for Treatment of B-Cell Non-Hodgkin's Lymphomas. *European Journal of Pharmaceutical Sciences* **2017**, *103*, 36–46.

(69) Etrych, T.; Strohalm, J.; Kovár, L.; Kabesová, M.; Ríhová, B.; Ulbrich, K. HPMA Copolymer Conjugates with Reduced Anti-CD20 Antibody for Cell-Specific Drug Targeting. I.

Synthesis and in Vitro Evaluation of Binding Efficacy and Cytostatic Activity. *J Control Release* **2009**, *140*, 18–26.

(70) Walker, J. A.; Sorkin, M. R.; Ledesma, F.; Kabaria, S. R.; Barfield, R. M.; Rabuka, D.; Alabi, C. A. Hydrophilic Sequence-Defined Cross-Linkers for Antibody–Drug Conjugates. *Bioconjugate Chem.* **2019**, *30*, 2982–2988.

(71) Viricel, W.; Fournet, G.; Beaumel, S.; Perrial, E.; Papot, S.; Dumontet, C.; Joseph, B. Monodisperse Polysarcosine-Based Highly-Loaded Antibody-Drug Conjugates. *Chem. Sci.* **2019**, *10*, 4048–4053.

(72) Kovtun, Y. V.; Audette, C. A.; Mayo, M. F.; Jones, G. E.; Doherty, H.; Maloney, E. K.; Erickson, H. K.; Sun, X.; Wilhelm, S.; Ab, O.; Lai, K. C.; Widdison, W. C.; Kellogg, B.; Johnson, H.; Pinkas, J.; Lutz, R. J.; Singh, R.; Goldmacher, V. S.; Chari, R. V. J. Antibody-Maytansinoid Conjugates Designed to Bypass Multidrug Resistance. *Cancer Res* **2010**, *70*, 2528–2537.

(73) Jeffrey, S. C.; Torgov, M. Y.; Andreyka, J. B.; Boddington, L.; Cerveny, C. G.; Denny, W. A.; Gordon, K. A.; Gustin, D.; Haugen, J.; Kline, T.; Nguyen, M. T.; Senter, P. D. Design, Synthesis, and in Vitro Evaluation of Dipeptide-Based Antibody Minor Groove Binder Conjugates. *J. Med. Chem.* **2005**, *48*, 1344–1358.

(74) Ab, O.; Whiteman, K. R.; Bartle, L. M.; Sun, X.; Singh, R.; Tavares, D.; LaBelle, A.; Payne, G.; Lutz, R. J.; Pinkas, J.; Goldmacher, V. S.; Chittenden, T.; Lambert, J. M. IMGN853, a Folate Receptor-α (FRα)–Targeting Antibody–Drug Conjugate, Exhibits Potent Targeted Antitumor Activity against FRα-Expressing Tumors. *Mol Cancer Ther* **2015**, *14*, 1605–1613.

(75) Bryden, F.; Martin, C.; Letast, S.; Lles, E.; Viéitez-Villemin, I.; Rousseau, A.; Colas, C.; Brachet-Botineau, M.; Allard-Vannier, E.; Larbouret, C.; Viaud-Massuard, M.-C.; Joubert, N. Impact of Cathepsin B-Sensitive Triggers and Hydrophilic Linkers on in Vitro Efficacy of Novel Site-Specific Antibody–Drug Conjugates. *Organic & Biomolecular Chemistry* **2018**, *16*, 1882–1889.

(76) Simmons, J. K.; Burke, P. J.; Cochran, J. H.; Pittman, P. G.; Lyon, R. P. Reducing the Antigen-Independent Toxicity of Antibody-Drug Conjugates by Minimizing Their Non-Specific Clearance through PEGylation. *Toxicology and Applied Pharmacology* **2020**, *392*, 114932.

(77) Joubert, N.; Beck, A.; Dumontet, C.; Denevault-Sabourin, C. Antibody–Drug Conjugates: The Last Decade. *Pharmaceuticals* **2020**, *13*, 245.

(78) Khongorzul, P.; Ling, C. J.; Khan, F. U.; Ihsan, A. U.; Zhang, J. Antibody–Drug Conjugates: A Comprehensive Review. *Mol Cancer Res* **2020**, *18*, 3–19.

Chapter 2

Diazido Macrocyclic Sulfates as a Platform for the Synthesis of Sequence-Defined Polymers for Antibody Drug Conjugates

2.1 Introduction

Antibody drug conjugates (ADCs) are an increasingly important therapeutic modality for the treatment of cancer. The attachment of a cytotoxic agent to an antibody against antigen-presenting cancer cells is a proven formula that has yielded the approval of 9 drugs with many more promising candidates in clinical development.[1,2] This strategy of targeted delivery of potent, apoptotic agents such a tubulin binders, DNA-damaging molecules, spliceosome inhibitors, and RNA polymerase inhibitors typically offers larger therapeutic windows over traditional chemotherapy due to reduced toxicity towards healthy cells.[3] To further expand on the success of this platform, a variety of strategies have been employed to improve the therapeutic index of ADCs. For one, improvements in antigen selection and discovery are important in order to successfully target cancer cells over healthy tissue. Considerations such as antigen overexpression, cell surface availability, and internalization pathways are considered when engineering antibodies for more effective ADCs .[2,4]

In addition to these antigen discovery and antibody engineering efforts, new conjugation and linker chemistries are under development for next-generation ADCs to further improve the therapeutic indices of the modality. One method that has been pursued in order to reduce the minimum effective dose (MED) is to increase the drug to antibody ratio (DAR) of the final conjugate. In theory, higher drug loadings would allow for increased delivery of cytotoxics, being especially effective in cancer cells with lower antigen presentation or when using lower potency payloads.[5] However, it has been demonstrated that while higher DAR ADCs do often show increased potency *in vitro*, they often show lower tolerability and have poorer pharmacokinetic (PK) outcomes.[6,7] This observed discrepancy is thought to be the result of rapid, immune-mediated clearance of the more hydrophobic, highly-loaded conjugates. In addition to poor *in vivo*

performance, highly loaded ADCs can suffer from decreased stability as the hydrophobic payloads can cause aggregation and precipitation.[8] While previous attempts to mitigate these challenges have focused on targeting DARs between 2-4, new polymeric linkers have the potential to both provide increased DARs, while masking the hydrophobicity of payloads.[9]

Hydrophilic polymers can confer significant advantages over traditional ADC linkers given their multivalency for drug attachment as well solubilizing characteristics. Indeed, polymeric linkers based on poly(ethylene glycol),[9,10] dextran,[11,12] and acrylamides[13,14] demonstrate the ability to achieve a higher DAR while maintaining hydrophilicity. However, when using these scaffolds, the inherent dispersity of the polymer can lead to challenges in obtaining precise drug loading per linker and are more difficult to characterize. Sequence-defined polymers offer the unique advantage of being chemically defined, allowing for more facile characterization and consistent drug loading. Strategies utilizing step-growth polysarcosines[15] or allyl acrylamide building blocks[16,17] have demonstrated the added benefit and utility of sequence-defined hydrophilic polymers as ADC linkers.

In this work, we offer a new strategy for the synthesis of chemically-defined polymers based on the step growth polymerization of azide-functionalized, macrocyclic sulfate monomers. Inspired by the work of Jiang and coworkers,[18] we envisioned that incorporation of an azide functional handle into an ethylene glycol (EG) macrocycle (**Figure 2.1.1**) would allow for the efficient synthesis of sequence-defined oligo-ethylene glycols that could be functionalized with a desired payload. We believe this strategy offers the unique advantage over other step-growth polymerization processes in that each ring opening step can be purified rapidly via flash chromatography. This feature of the synthesis could therefore accommodate a larger scale and could be more economical in both time and cost when compared to methods that rely on

preparatory HPLC purification. Furthermore, this method results in polymers with poly (ethylene glycol) backbones, which is a proven scaffold for the solubilization of hydrophobic, organic molecules.

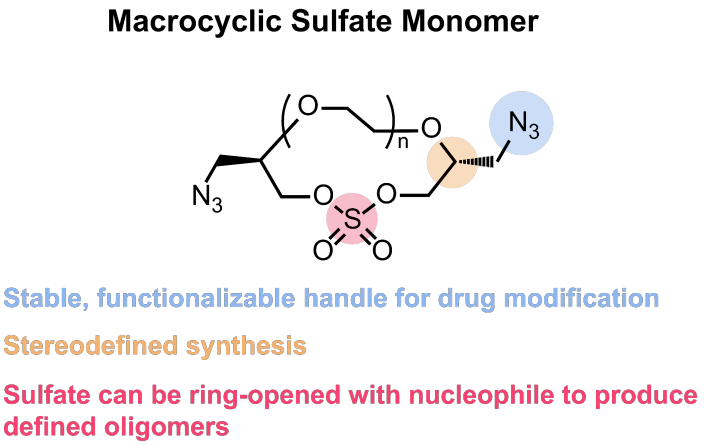

Figure 2.1.1. Advantages of the macrocyclic sulfate monomer in the research.

2.2 Results and Discussion

2.2.1 Synthesis of Macrocyclic Monomers

When considering the synthesis of these azido macrocyclic sulfates (AzMCS) monomers, we determined two criteria to be essential. First, the incorporation of the azide functionality needed be accomplished in a stereodefined manner to avoid diastereomeric mixtures during the polymerization process. Second, the synthesis needed to be amenable to the production of a diverse set of macrocycles such that the platform is tunable in terms of the size of the macrocycles, spacing of azides in the polymer, and eventual spacing of drugs in the well-defined polymers. To address the first requirement, we started with (R)-epichlorohydrin starting material, which could be purchased cheaply at $0.50 per gram (**Figure 2.2.1**). Installation of benzyl alcohol and ring opening with sodium azide then proceeds in high yields to produce a secondary alcohol that can be diversified with ditosylated EGs. The resulting di-benzylated products could be deprotected non-reductively using $NaBrO_3$ and sodium dithionite to yield the diazido ethylene glycols.[19,20]

While good yields were obtained in the preparation of the di-azido ethylene glycols, we observed a pattern of decreasing yield for larger EGs during the macrocyclization reaction. While it may be expected that this reaction would be less efficient for larger EGs, we further noticed that the larger macrocycles, particularly the heptaethylene glycol (n=5 in **Figure 2.2.1**), are less stable and can degrade during flash chromatography. While a one-pot macrocyclization and oxidation could help avoid exposure of the less stable macrocyclic sulfite to silica, we found that such methods resulted in an unacceptable amount of impurities that proved difficult to remove. Despite the lower yield of the di-azido heptaethylene glycol, we were pleased that macrocyclization for the smaller (n=2 through n=4 in **Figure 2.2.1**) diazido EGs could be achieved in good yields (53-72%). Final oxidation of the sulfite intermediates to the more stable sulfate additionally proceeded in high yields to provide the AzMCS monomers.

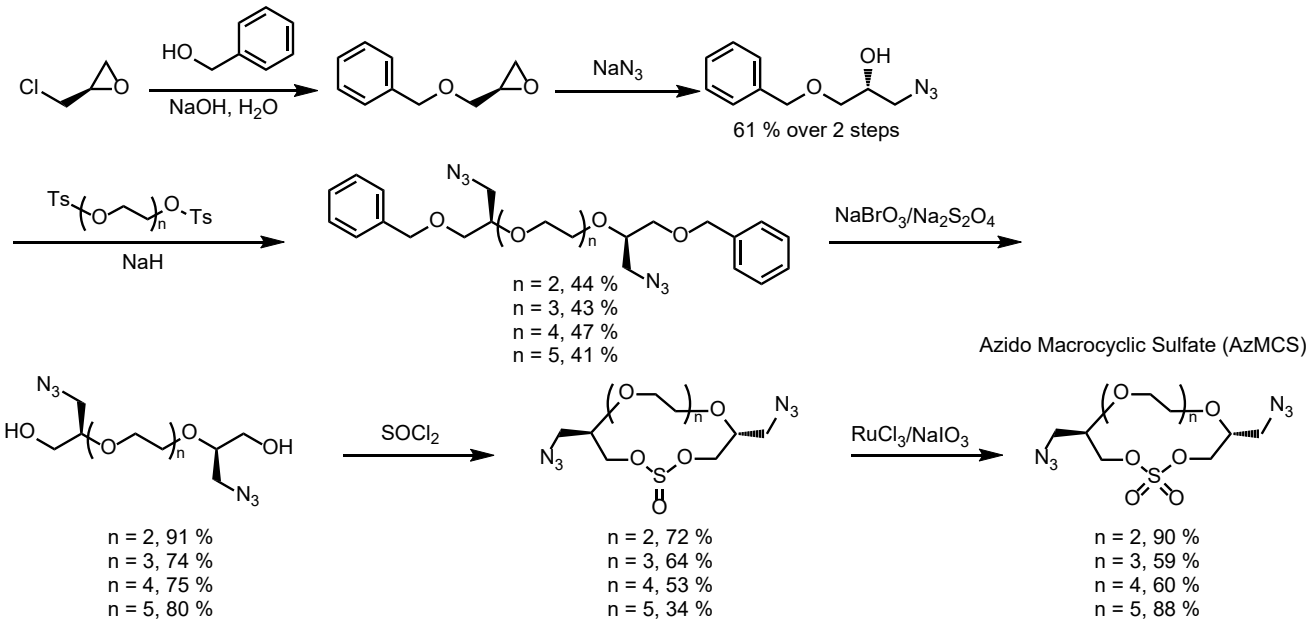

Figure 2.2.1. Scheme for the synthesis of di-azido macrocyclic sulfate monomers of varid size.

2.2.2 Preparation of Polymer and Conjugation to Trastuzumab

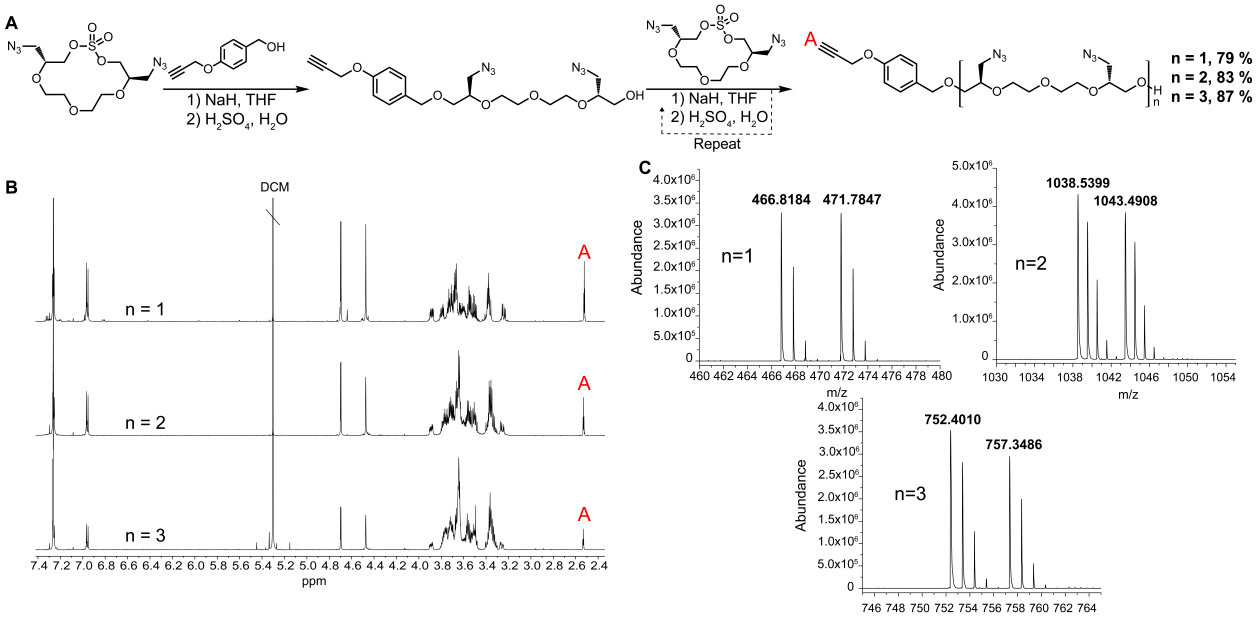

Figure 2.2.2. Polymerization of AzMCS monomers. A) Synthesis of propargyl hexaazide polymer, B) purified NMR of each ring-opening step, and C) mass spec of each chain extension.

For the polymerization reactions, we decided to demonstrate the methodology by proceeding with the highest yielding tetraethylene glycol (n=2 in **Figure 2.2.1**) AzMCS. We chose to use 1,4 propargyloxy benzyl alcohol in the first ring opening step as it would provide a future handle for modification through a 1,3 dipolar cycloaddition and is UV active, allowing for more facile purification during flash chromatography. While this benzyl alcohol suites our applications well, it should be noted that a wide range of nucleophiles are compatible with this ring opening procedure.[18] Flexibility in type of nucleophile is an additional advantageous feature of this synthesis as it could allow for the installation of wide range of functionalities at the beginning of the polymerization process. We were pleased to see that ring opening of the AzMCS monomer using 1,4 propargyloxy benzyl alcohol proceeds with a high yield of 79% and the pure product could be rapidly obtained via flash chromatography (**Figure 2.2.2 A**). Two additional cycles of

ring opening and chain extension were performed with similarly high yields and purity to yield the 3rd generation hexa-azide dodeca-ethyleneglycol polymer.

One advantage of iterative, step-growth polymerization is the ability to tailor the sequence and composition of the polymer exactly. To demonstrate this in our system, we performed the same procedure of successive ring-opening polymerization reactions alternating AzMCS monomers with unfunctionalized macrocyclic sulfates to make a tetraazide hexadeca-ethylene glycol polymer (**Figure 2.2.2**). Alternating monomers allows for greater spacing between the azide functionalities and illustrates how these molecules can be tailored in terms of azide composition, spacing, and overall size.

We next explored a proof-of-concept application for these polymers. Given the previously noted challenges with obtaining high-DAR ADCs, we envisioned this as a useful scaffold in achieving highly-conjugated antibodies. Using a coumarin derivative as a model, we first reduced the tetrazide hexadeca-ethylene glycol polymer using a Staudinger reduction to form the tetra-amine product (**Figure 2.2.2**). In one pot, we then alkylated the amines with N-hydroxysuccinimide (NHS)-activated coumarin to form the tetra-coumarin product. Finally, we installed a maleimide for thiol conjugation through a copper catalyzed 1,3 dipolar cycloaddition in order to yield the final product for antibody conjugation in 53 % yield.

The polymer was then conjugated to Trastuzumab, which is a commonly employed antibody in ADCs for the treatment of Her_2 positive breast cancer. By first reducing the interchain disulfide bonds of the antibody using TCEP, we were able to successfully conjugate the maleimide-containing tetracoumarin to the antibody using Michael addition. By liquid chromatography mass-spectrometry (LCMS), the polymer-to-antibody ratio was 6.6, which translates to approximately 25 coumarin molecules per antibody (**Figure 2.2.3 B**). Additionally,

in order to ensure that the conjugate maintained activity towards the Her2 antigen, we analyzed affinity via indirect ELISA. In this experiment, we observed no significant difference in binding between our conjugate and unmodified Trastuzmab (**Figure 2.2.3 C**), which reinforces that these polymers do not have a significant impact on the affinity of the antibody due to their monodisperse size and location.

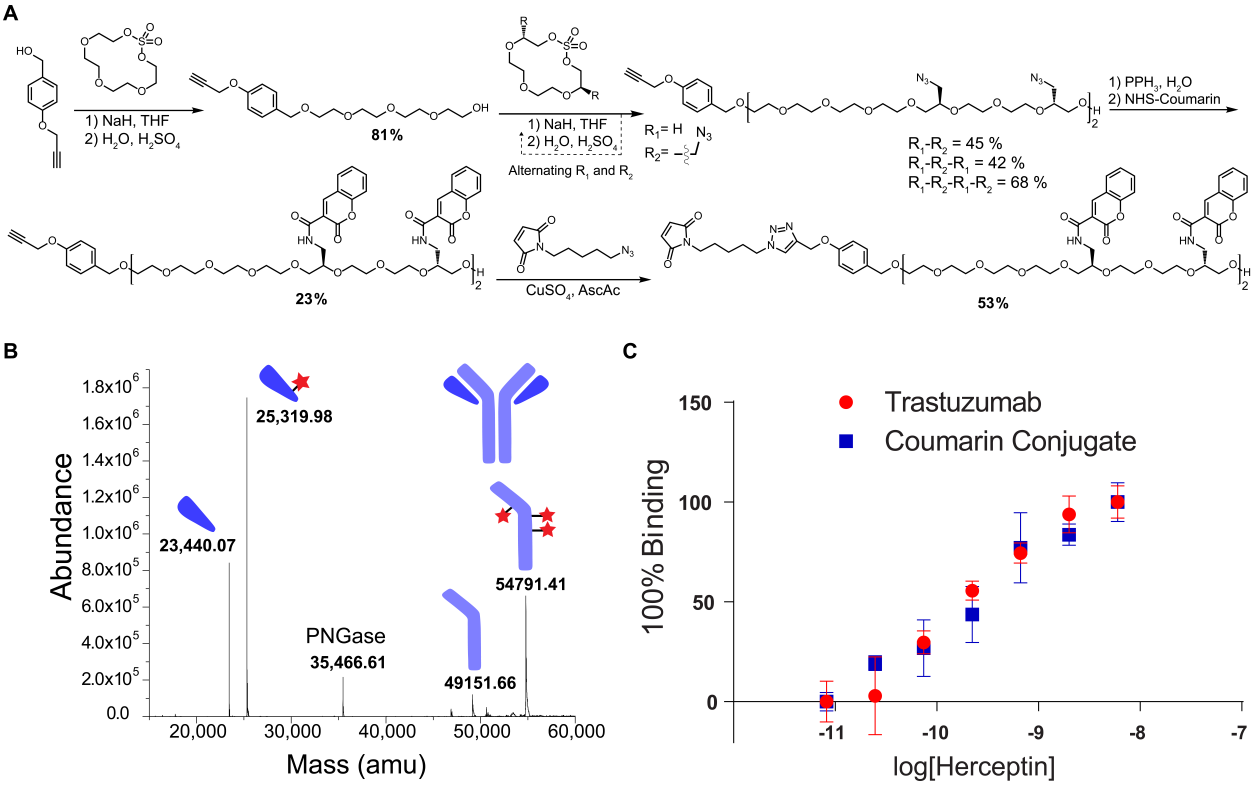

Figure 2.2.3. A) Scheme for the synthesis of tetraazide poly (ethylene glycol) along with coumarin functionalization and maleimide installation. B) Mass spectrometry of digested and reduced antibody-coumarin conjugate. Red stars represent the number of polymers modifying each antibody subunit. C) Activity of Trastuzumab and coumarin conjugate towards Her2 antigen as measured by ELISA.

The success of this model system indicates the applicability of these chemically-defined polymers as scaffolds for ADCs. The advantage of this approach is the facile characterization of the conjugate via LCMS and the large total number of coumarins that could be conjugated through

the multivalent, hydrophilic linker without reduction in binding activity. Future work includes investigation of these scaffolds for ADCs by incorporating cytotoxic payloads, which are more hydrophobic than coumarin, and comparing the performance of these monodisperse scaffolds to current linker technology.

2.3. Conclusions

In summary, we present a new method for the preparation of sequence-defined polymers based on diazido macrocyclic sulfate building blocks. This strategy offers a number of benefits over other methodologies, primarily that each successive chain-growth step can be purified rapidly via flash chromatography. Additionally, due to the makeup of the macrocycles, the final polymer contains a backbone solely composed of hydrophilic, non-ionic ethylene glycol units. We hypothesize that these unique characteristics are ideally suited for ADC linkers and look forward to continued investigation of this application. Additionally, due to the tunable and modular nature of this platform, we envision it to be useful in a variety of polymer and drug-delivery settings.

2.4 References

(1) Joubert, N.; Beck, A.; Dumontet, C.; Denevault-Sabourin, C. Antibody–Drug Conjugates: The Last Decade. *Pharmaceuticals* **2020**, *13*, 245.

(2) Khongorzul, P.; Ling, C. J.; Khan, F. U.; Ihsan, A. U.; Zhang, J. Antibody–Drug Conjugates: A Comprehensive Review. *Mol Cancer Res* **2020**, *18*, 3–19.

(3) Tumey, L. N. Next Generation Payloads for ADCs. In *Innovations for Next-Generation Antibody-Drug Conjugates*; Damelin, M., Ed.; Cancer Drug Discovery and Development; Springer International Publishing: Cham, 2018; pp 187–214.

(4) Strohl, W. R. Current Progress in Innovative Engineered Antibodies. *Protein Cell* **2018**, *9*, 86–120.

(5) Bodyak, N.; Yurkovetskiy, A. V. Delivering More Payload (High DAR ADCs). In *Innovations for Next-Generation Antibody-Drug Conjugates*; Damelin, M., Ed.; Cancer Drug Discovery and Development; Springer International Publishing: Cham, 2018; pp 215–240.

(6) Sun, X.; Ponte, J. F.; Yoder, N. C.; Laleau, R.; Coccia, J.; Lanieri, L.; Qiu, Q.; Wu, R.; Hong, E.; Bogalhas, M.; Wang, L.; Dong, L.; Setiady, Y.; Maloney, E. K.; Ab, O.; Zhang, X.; Pinkas, J.; Keating, T. A.; Chari, R.; Erickson, H. K.; Lambert, J. M. Effects of Drug–Antibody Ratio on Pharmacokinetics, Biodistribution, Efficacy, and Tolerability of Antibody–Maytansinoid Conjugates. *Bioconjugate Chem.* **2017**, *28*, 1371–1381.

(7) Hamblett, K. J.; Senter, P. D.; Chace, D. F.; Sun, M. M. C.; Lenox, J.; Cerveny, C. G.; Kissler, K. M.; Bernhardt, S. X.; Kopcha, A. K.; Zabinski, R. F.; Meyer, D. L.; Francisco, J. A. Effects of Drug Loading on the Antitumor Activity of a Monoclonal Antibody Drug Conjugate. *Clin. Cancer Res.* **2004**, *10*, 7063–7070.

(8) Buecheler, J. W.; Winzer, M.; Tonillo, J.; Weber, C.; Gieseler, H. Impact of Payload Hydrophobicity on the Stability of Antibody–Drug Conjugates. *Mol. Pharmaceutics* **2018**, *15*, 2656–2664.

(9) Lyon, R. P.; Bovee, T. D.; Doronina, S. O.; Burke, P. J.; Hunter, J. H.; Neff-LaFord, H. D.; Jonas, M.; Anderson, M. E.; Setter, J. R.; Senter, P. D. Reducing Hydrophobicity of Homogeneous Antibody-Drug Conjugates Improves Pharmacokinetics and Therapeutic Index. *Nature Biotechnology* **2015**, *33*, 733–735.

(10) Burke, P. J.; Hamilton, J. Z.; Jeffrey, S. C.; Hunter, J. H.; Doronina, S. O.; Okeley, N. M.; Miyamoto, J. B.; Anderson, M. E.; Stone, I. J.; Ulrich, M. L.; Simmons, J. K.; McKinney, E. E.; Senter, P. D.; Lyon, R. P. Optimization of a PEGylated Glucuronide-

Monomethylauristatin E Linker for Antibody–Drug Conjugates. *Mol Cancer Ther* **2017**, *16*, 116–123.

(11) Schneider, H.; Deweid, L.; Pirzer, T.; Yanakieva, D.; Englert, S.; Becker, B.; Avrutina, O.; Kolmar, H. Dextramabs: A Novel Format of Antibody-Drug Conjugates Featuring a Multivalent Polysaccharide Scaffold. *ChemistryOpen* **2019**, *8*, 354–357.

(12) Yurkovetskiy, A. V.; Yin, M.; Bodyak, N.; Stevenson, C. A.; Thomas, J. D.; Hammond, C. E.; Qin, L.; Zhu, B.; Gumerov, D. R.; Ter-Ovanesyan, E.; Uttard, A.; Lowinger, T. B. A Polymer-Based Antibody–Vinca Drug Conjugate Platform: Characterization and Preclinical Efficacy. *Cancer Res* **2015**, *75*, 3365–3372.

(13) Etrych, T.; Strohalm, J.; Kovár, L.; Kabesová, M.; Ríhová, B.; Ulbrich, K. HPMA Copolymer Conjugates with Reduced Anti-CD20 Antibody for Cell-Specific Drug Targeting. I. Synthesis and in Vitro Evaluation of Binding Efficacy and Cytostatic Activity. *J Control Release* **2009**, *140*, 18–26.

(14) Zhang, L.; Fang, Y.; Kopeček, J.; Yang, J. A New Construct of Antibody-Drug Conjugates for Treatment of B-Cell Non-Hodgkin's Lymphomas. *European Journal of Pharmaceutical Sciences* **2017**, *103*, 36–46.

(15) Viricel, W.; Fournet, G.; Beaumel, S.; Perrial, E.; Papot, S.; Dumontet, C.; Joseph, B. Monodisperse Polysarcosine-Based Highly-Loaded Antibody-Drug Conjugates. *Chem. Sci.* **2019**, *10*, 4048–4053.

(16) Porel, M.; Alabi, C. A. Sequence-Defined Polymers via Orthogonal Allyl Acrylamide Building Blocks. *J. Am. Chem. Soc.* **2014**, *136*, 13162–13165.

(17) Walker, J. A.; Sorkin, M. R.; Ledesma, F.; Kabaria, S. R.; Barfield, R. M.; Rabuka, D.; Alabi, C. A. Hydrophilic Sequence-Defined Cross-Linkers for Antibody–Drug Conjugates. *Bioconjugate Chem.* **2019**, *30*, 2982–2988.

(18) Zhang, H.; Li, X.; Shi, Q.; Li, Y.; Xia, G.; Chen, L.; Yang, Z.; Jiang, Z.-X. Highly Efficient Synthesis of Monodisperse Poly(Ethylene Glycols) and Derivatives through Macrocyclization of Oligo(Ethylene Glycols). *Angewandte Chemie* **2015**, *127*, 3834–3838.

(19) Adinolfi, M.; Barone, G.; Guariniello, L.; Iadonisi, A. Facile Cleavage of Carbohydrate Benzyl Ethers and Benzylidene Acetals Using the NaBrO3Na2S2O4 Reagent under Two-Phase Conditions. *Tetrahedron Letters* **1999**, *40*, 8439–8441.

(20) Niemietz, M.; Perkams, L.; Hoffman, J.; Eller, S.; Unverzagt, C. Selective Oxidative Debenzylation of Mono- and Oligosaccharides in the Presence of Azides. *Chem. Commun.* **2011**, *47*, 10485–10487.

2.5 Materials and Methods

R-(-)-Epichlorohydrin was purchased from Oakwood Chemicals. All other chemicals were purchased from Fisher Scientific and were used without purification unless otherwise noted. Herceptin® was purchased from the UCLA pharmacy. Whole molecule (Anti-Human IgG (whole molecule)−Peroxidase antibody produced in rabbit) imaging antibodies were purchased from Sigma-Aldrich.

Analytical Techniques. Nuclear Magnetic Resonance (NMR) spectra were recorded on a Bruker DRX 500 MHz, Bruker AV 500 MHz, and Bruker AV 600 MHz spectrometer. Mass spectrometry for both proteins and small molecules was obtained on an Agilent Q-TOF 6530 LC/MS.

Preparatory reverse phase high performance liquid chromatography (RP-HPLC) was performed on an Agilent 1290 Infinity II system with an open bed sampler/fraction collector equipped with a UV detector using a Luna 5 µm C18 100A column (5 µm, 250 x 21.2 mm). Small molecule purification was done via flash chromatography on a Biotage Isolera One auto-column system. As a safety precaution, all azides were handled behind the protection of a blast shield.

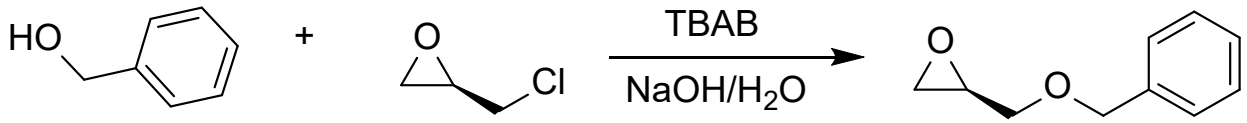

(R)-2-((benzyloxy)methyl)oxirane.[1] To a round-bottom flask, NaOH (110 g, 2.9 mol, 13 equivalents) and tetrabutylammonium bromide (3.9 g, 12 mmol, 0.055 equivalents) were dissolved in 180 mL of water and cooled to 0 °C. Next, (R)-(-)-epichlorohydrin (26 mL, 0.33 mol, 1.5 equivalents) was added to the vigorously stirring solution. Benzyl alcohol (23 mL, 0.22 mol, 1.0 equivalents) was then added dropwise to the solution and the reaction was allowed to proceed for 3 hours. The reaction mixture was then added to a separatory funnel and extracted three times with ether and dried with $MgSO_4$. The crude was then purified via biotage with an 8:2 hexanes:ethyl acetate (EthOAc) isocratic mobile phase to yield the product as a clear oil (25.9 g, 71%). ^{1}H NMR (600 MHz, Chloroform-*d*) δ 7.35 (m, *J* = 4.4 Hz, 5H), 4.64 – 4.53 (m, 2H), 3.78 (dd, *J* = 11.4, 3.0 Hz, 1H), 3.44 (dd, *J* = 11.4, 5.9 Hz, 1H), 3.20 (m, 1H), 2.81 (m, 1H), 2.63 (dd, *J* = 5.0, 2.7 Hz, 1H). ^{13}C NMR (101 MHz, Chloroform-*d*) δ 137.92, 128.46, 127.79, 73.35, 70.84, 50.89, 44.32. IR: ν = 3031, 2999, 2860, 1736, 1453, 1244, 1092, 845, 736.

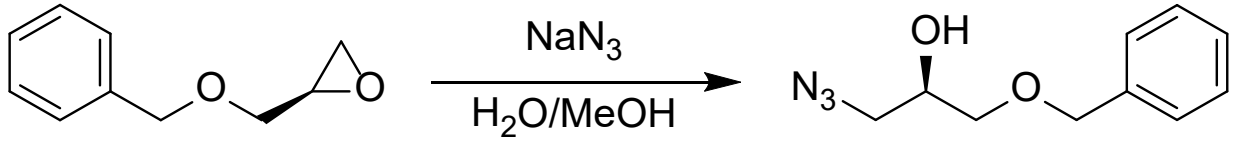

(R)-1-azido-3-(benzyloxy)propan-2-ol.[2] In a round-bottom flask, (R)-Benzyl Oxirane (36 g, 0.22 mol, 1 equivalent), ammonium chloride (23 g, 0.44 mol, 2 equivalents), and sodium azide (43 g, 0.66 mol, 3 equivalents) were suspended in 200 mL of methanol and 50 mL of H_2O. The reaction was heated to 65 °C and allowed to proceed for 12 h. Methanol was then removed via rotary evaporation and the product was then extracted three times with diethyl ether. The organic layers were dried with $MgSO_4$ and concentrated to yield the product as a clear oil (32.95g, 73%). ^{1}H NMR (600 MHz, Chloroform-*d*) δ 7.39 – 7.31 (m, 5H), 4.57 (s, 2H), 3.97 (m, 1H), 3.57 – 3.48 (m, 2H), 3.43 – 3.35 (m, 2H), 2.45 (broad s, 1H). ^{13}C NMR (101 MHz, Chloroform-*d*) δ 137.59, 128.57, 128.01, 127.88, 73.59, 71.36, 69.71, 53.51. IR: ν = 3424, 2866, 2095, 1453, 1275, 1088, 1074, 737, 697.

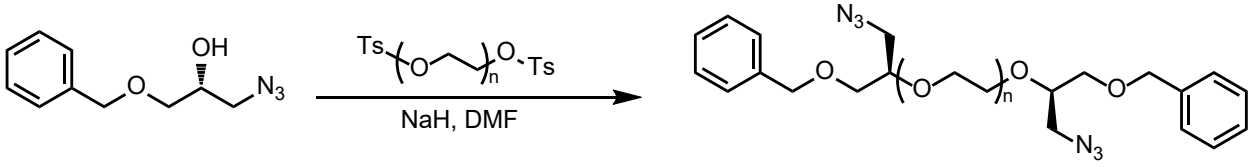

General Procedure of Dibenzylated Azido PEGs (using dibenzyl-azido tetraethyleneglycol as example). (R)-1-azido-3-(benzyloxy)propan-2-ol (5.03 g, 24.3 mmol, 2.05 equivalents) was dissolved in dry DMF (0.5 M) and cooled to 0 °C. Sodium hydride (60% dispersion, 2.37 g, 59.2 mmol, 5 equivalents) was added portion wise and reaction was allowed to stir for 5 minutes. Diethyleneglycol ditosylate (4.91 g, 11.8 mmol, 1 equivalents) was then added and reaction was allowed to proceed for 8 h at room temperature. Methanol was then added slowly to reaction to quench remaining sodium hydride and the solution was added to a separatory funnel. 100 mL of water was then added to the separatory funnel and the crude was extracted from DMF/H_2O three times with hexanes. The pooled hexanes layers were then dried with $MgSO_4$ and evaporated. The crude was then purified via flash chromatography with a hexanes:ether gradient (0% ether to 100%

ether) to yield the product as a clear oil (2.51 g, 44%). ^{1}H NMR (600 MHz, Chloroform-*d*) δ 7.38 – 7.27 (m, 10H), 4.53 (s, 4H), 3.79 – 3.75 (m, 2H), 3.74 – 3.63 (m, 8H), 3.56 (dd, *J* = 9.9, 4.9 Hz, 2H), 3.51 (dd, *J* = 10.0, 5.9 Hz, 2H), 3.37 (d, *J* = 5.1 Hz, 4H). ^{13}C NMR (126 MHz, Chloroform-*d*) δ 137.92, 128.44, 127.78, 127.69, 78.53, 73.49, 70.85, 69.91, 69.53, 51.97. IR: ν = 2867, 2094, 1738, 1453, 1365, 1277, 1092, 736. HRMS (ESI) calculated for $C_{24}H_{32}N_6O_5$ $[M+NH_4]^+$ = 502.2777, observed = 502.2832.

Dibenzyl-Azido pentaethyleneglycol. Product isolated as a clear oil (43%). ^{1}H NMR (400 MHz, Chloroform-*d*) δ 7.40 – 7.27 (m, 10H), 4.53 (s, 4H), 3.82 – 3.62 (m, 14H), 3.59 – 3.48 (m, 4H), 3.37 (d, *J* = 5.1 Hz, 4H). ^{13}C NMR (126 MHz, Chloroform-*d*) δ 137.92, 128.44, 127.78, 127.69, 78.54, 73.50, 70.79, 70.66, 69.92, 69.52, 51.98. IR: ν = 2866, 2094, 1453, 1277, 1092, 736, 697. HRMS (ESI) calculated for $C_{10}H_{18}N_6O_7S$ $[M+NH_4]$ = 546.3040, observed = 546.3168.

Dibenzyl-Azido hexaethylenegylcol. Product isolated as a clear oil (47%). ^{1}H NMR (400 MHz, Chloroform-*d*) δ 7.39 – 7.26 (m, 10H), 4.53 (s, 4H), 3.82 – 3.60 (m, 18H), 3.59 – 3.48 (m, 4H), 3.37 (d, *J* = 5.2 Hz, 4H). ^{13}C NMR (126 MHz, Chloroform-*d*) δ ^{13}C NMR (126 MHz, Chloroform-*d*) δ 137.92, 128.44, 127.78, 127.69, 78.54, 73.50, 70.78, 70.65, 70.59, 69.92, 69.52, 51.98. IR: ν = 2865, 2095, 1738, 1453, 1278, 1094, 736. HRMS (ESI) calculated for $C_{28}H_{40}N_6O_7$ $[M+NH_4]^+$ = 590.3302, observed = 590.3405.

Dibenzyl-Azido heptaethyleneglycol. Product isolated as a clear oil (41%). ^{1}H NMR (500 MHz, Chloroform-*d*) δ 7.38 – 7.26 (m, 10H), 4.53 (s, 4H), 3.78 (m, 2H), 3.74 – 3.61 (m, 20H), 3.58 – 3.49 (m, 4H), 3.37 (d, *J* = 5.2 Hz, 4H).^{13}C NMR (126 MHz, Chloroform-*d*) δ 137.92, 128.44, 127.77, 127.69, 78.54, 73.49, 70.79, 70.65, 70.59, 69.92, 69.53, 51.98. IR: ν = 2866, 2095, 1738,

1614, 1453, 1278, 1097, 737. HRMS (ESI) calculated for $C_{30}H_{44}N_6O_8$ $[M+NH_4]^+$ = 634.3564, observed = 634.3706.

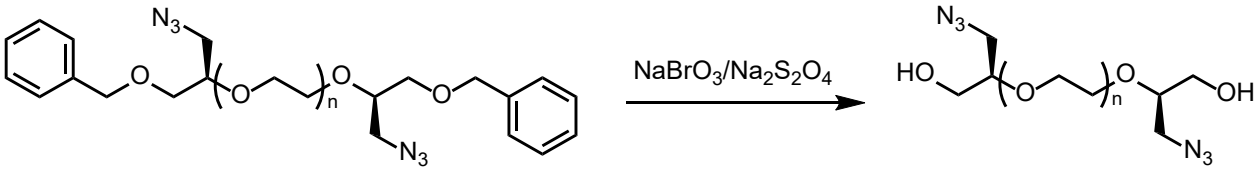

General Debenzylation Procedure (using tetraethyleneglycol diazide as an example). Dibenzylazide tetraethyleneglycol (21.79 g, 44.97 mmol, 1 equivalent) was dissolved in 50 mL of ethyl acetate in a round-bottom flask. Sodium bromate (20.36 g, 134.9 mmol, 3 equivalents) was dissolved in 100 mL of water and added to the vigorously stirring solution. Sodium dithionite (23.49 g, 134.9 mmol, 3 equivalents) was dissolved in water and added to an addition funnel. The dithionite solution was added slowly over the course of 2 h (caution: reaction auto-heats rapidly if solution is added too quickly). After addition, the reaction was allowed to stir at 23 °C for 1 hr. The biphasic solution was then transferred to a separatory funnel and the organic layer was collected. The aqueous layer was the extracted three times with ethyl acetate and the pooled organic layers were dried with $MgSO_4$ and concentrated to yield the crude. The resulting oil was then purified via flash chromatography with a first isocratic 100% ethyl acetate mobile phase over 5 column volumes to elute the UV active byproducts followed by an isocratic dichloromethane (DCM)+5% MeOH mobile phase to elute the product as a clear oil (12.51 g, 91 %). ^{1}H NMR (600 MHz, Chloroform-*d*) δ 3.91 – 3.86 (m, 2H), 3.83 – 3.70 (m, 6H), 3.63 – 3.52 (m, 6H), 3.41 (dd, *J* = 12.9, 7.4 Hz, 2H), 3.22 (dd, *J* = 12.9, 4.2 Hz, 2H). ^{13}C NMR (126 MHz, Chloroform-*d*) δ 80.76, 70.61, 69.39, 62.42, 51.67. IR: ν = 3408, 2921, 2092, 1447, 1343, 1274, 1104, 1069, 954, 833. HRMS (ESI) calculated for $C_{10}H_{20}N_6O_5$ $[M + Na]^+$ = 327.1392, observed: 327.1417.

Pentaethyleneglycol diazide. Product isolated as a clear oil (74%). ^{1}H NMR (600 MHz, Chloroform-*d*) δ 3.84 (m, 2H), 3.78 (m, 2H), 3.74 – 3.51 (m, 16H), 3.41 (dd, *J* = 12.9, 7.3 Hz, 2H), 3.23 (dd, *J* = 12.9, 4.1 Hz, 2H). ^{13}C NMR (126 MHz, Chloroform-*d*) δ 80.50, 70.82, 70.27, 69.59, 62.18, 51.75. IR: ν = 3433, 2873, 2093, 1739, 1447, 1346, 1275, 1100, 1071, 947, 837. HRMS (ESI) calculated for $C_{12}H_{24}N_6O_6$ [M+NH_4] = 366.2101, observed = 366.2139.

Hexaethylenegylcol diazide. Product isolated as a clear oil (75%). ^{1}H NMR (600 MHz, Chloroform-*d*) δ 3.87 (m, 2H), 3.76 (m, 2H), 3.72 – 3.55 (m, 18H), 3.39 (dd, *J* = 12.9, 6.9 Hz, 2H), 3.26 (dd, *J* = 12.8, 4.0 Hz, 2H). ^{13}C NMR (126 MHz, Chloroform-*d*) δ 80.49, 70.93, 70.49, 70.38, 69.68, 62.24, 51.74. IR: ν = 3433, 2872, 2094, 1738, 1450, 1347, 1275, 1096, 1074, 947, 837. HRMS (ESI) calculated for $C_{14}H_{28}N_6O_7$ $[M+H]^+$ = 393.2097, observed = 393.2175.

Heptaethylenegylcol diazide. Product isolated as a clear oil (80%). ^{1}H NMR (600 MHz, Chloroform-*d*) δ 3.88 (ddd, *J* = 11.3, 4.3, 2.6 Hz, 2H), 3.79 – 3.54 (m, 24H), 3.39 (dd, *J* = 12.9, 7.0 Hz, 2H), 3.33 (s, 2H), 3.26 (dd, *J* = 12.9, 4.1 Hz, 2H). ^{13}C NMR (126 MHz, Chloroform-*d*) δ 80.45, 70.89, 70.48, 70.45, 70.40, 69.71, 62.27, 51.76. IR: ν = 3421, 2873, 2094, 1450, 1346, 1277, 1094, 947. HRMS (ESI) calculated for HRMS (ESI) calculated for $C_{16}H_{32}N_6O_8$ $[M+H]^+$ = 437.2359, observed = 437.2495.

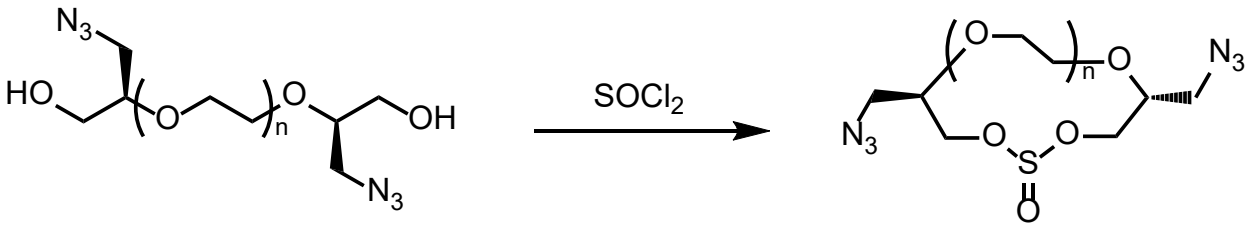

General Procedure for Macrocyclic Sulfite Synthesis (Using tetraethyleneglycol diazide macrocyclic sulfite as an example).[3] To a round-bottom flask, tetraethyleneglycol diazide sulfite (2.85 g, 9.37 mmol, 1 equivalent) and DIPEA (7.9 mL, 45 mmol, 4.8 equivalents) was dissolved in DCM (60 mM) under argon. The reaction was cooled to 0 °C and thionyl chloride (1 molar solution in DCM, 18.7 mL, 18.7 mmol, 2 equivalents) was added dropwise over the course of 1 hr. The reaction was then allowed to stir for 1 hr at 23 °C before the addition of cold brine. The solution was then transferred to a separatory funnel and the organic layer was collected. The aqueous layer was then extracted three times with DCM and the pooled organic layers were dried with $MgSO_4$. The crude was then concentrated and purified via flash chromatography with a hexanes:ethyl acetate gradient (0-100% ethyl acetate) to yield the product as black oil (2.35 g, 72%). Note: macrocyclic sulfites show some degradation on silica, therefore dry loading can lead to decreased yields. ^{1}H NMR (400 MHz, Chloroform-*d*) δ 4.30 (dd, *J* = 10.7, 5.9 Hz, 1H), 4.21 (dd, *J* = 10.5, 4.7 Hz, 1H), 4.13 (dd, *J* = 10.5, 4.6 Hz, 1H), 3.97 – 3.68 (m, 9H), 3.63 – 3.54 (m, 2H), 3.47 – 3.31 (m, 4H). ^{13}C NMR (101 MHz, Chloroform-*d*) δ 77.90, 77.60, 70.72, 70.62, 70.53, 70.47, 62.47, 61.05, 51.74, 51.65. IR: ν = 2924, 2871, 2093, 1448, 1293, 1275, 1202, 1116, 956, 738. HRMS (ESI) calculated for $C_{10}H_{18}N_6O_6S$ $[M+NH_4]^+$ = 368.1352, observed: 368.1417.

Pentaethyleneglycol diazide macrocyclic sulfite. Product isolated as a black oil (64%). ^{1}H NMR (400 MHz, Acetonitrile-d_3) δ 4.15 (dd, *J* = 11.5, 4.7 Hz, 1H), 4.11 – 3.98 (m, 3H), 3.82 – 3.66 (m, 6H), 3.55 (m, 8H), 3.43 – 3.28 (m, 4H). ^{13}C NMR (101 MHz, Acetonitrile-d_3) δ 77.35, 77.07, 70.55, 70.44, 70.32, 70.29, 70.20, 70.07, 62.49, 61.32, 51.22, 51.10. IR: ν = 2875, 2094, 1735, 1450, 1347, 1277, 1203, 1106, 949, 731. HRMS (ESI) calculated for $C_{12}H_{22}N_6O_7S$ $[M + Na]^+$ = 417.1168, observed 417.1124.

Hexaethyleneglycol diazide macrocyclic sulfite. Product isolated as a black oil (53%). ^{1}H NMR (400 MHz, Acetonitrile-d_3) δ 4.15 – 3.99 (m, 4H), 3.86 – 3.79 (m, 2H), 3.77 – 3.67 (m, 4H), 3.61 – 3.51 (m, 12H), 3.45 – 3.30 (m, 4H). ^{13}C NMR (101 MHz, Acetonitrile-d_3) δ 77.02, 76.82, 70.74, 70.64, 70.32, 70.30, 70.27, 70.23, 69.56, 69.52, 62.29, 61.08, 50.96, 50.90. IR: ν = 2872, 2100, 1738, 1452, 1350, 1296, 1206, 1114, 955, 832, 746. HRMS (ESI) calculated for $C_{14}H_{26}N_6O_8S$ [M + Na]$^+$ = 461.1430, observed = 461.1364.

Heptaethyleneglycol diazide macrocyclic sulfite. Product isolated as a black oil (34%). ^{1}H NMR (500 MHz, Acetonitrile-d_3) δ 4.12 – 3.97 (m, 4H), 3.80 (m, 2H), 3.74 (m, 4H), 3.62 – 3.54 (m, 16H), 3.48 – 3.33 (m, 4H). ^{13}C NMR (126 MHz, Acetonitrile-d_3) δ 77.20, 77.13, 70.62, 70.58, 70.39, 70.37, 70.25, 69.68, 69.66, 61.68, 61.36, 50.91. IR: ν = 2870, 2098, 1755, 1450, 1348, 1295, 1204, 1112, 955, 743. HRMS (ESI) calculated for $C_{16}H_{30}N_6O_9S$ [M+NH$_4$]$^+$ = 500.2138, observed = 500.2230.

Tetraethyleneglycol macrocyclic sulfite.[3] Product isolated as a black oil (82 %). ^{1}H NMR (300 MHz, Chloroform-*d*) δ 4.39 (m, *J* = 2H), 4.21 – 4.08 (m, 2H), 3.91 – 3.65 (m, 12H). ^{13}C NMR (126 MHz, Acetonitrile-d_3) δ 70.35, 70.14, 69.25, 62.04. IR: ν = 2868, 1638, 1449, 1200, 1113, 1013, 929, 875, 710.

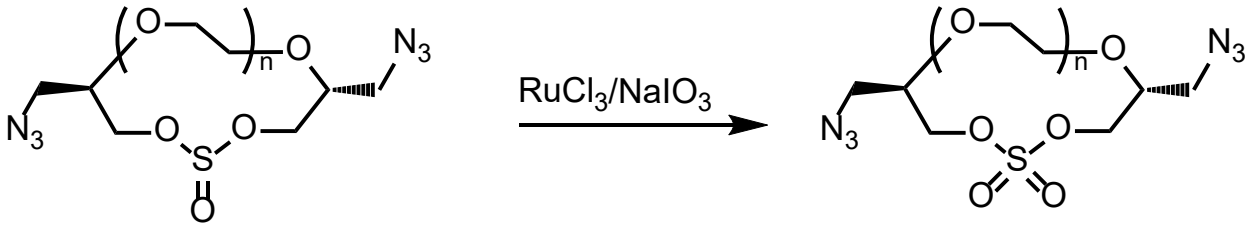

General Procedure for Macrocyclic Sulfite Oxidation (Using tetraethyleneglycol diazide macrocyclic sulfate as an example), adapted from Zhang *et al*.[3] To a round-bottom flask,

tetraethyleneglycol diazide macrocyclic sulfite (2.35 g, 6.71 mmol, 1 equivalent) was dissolved in 1:1:2 acetonitrile:DCM:water (70 mM) and stirred vigorously. Next, ruthenium chloride (70 mg, 335 μmol, 0.05 equivalents) and sodium periodate (14.3 g, 67.1 mmol, 10 equivalents) were added sequentially and the reaction was allowed to proceed at 23 °C for 4 h. The solution was then transferred to separatory funnel and the organic layer was collected. The aqueous layer was then extracted with DCM three times and the pooled organic layers were then dried with $MgSO_4$ and the solution was filtered through celite. The resulting filtrate was concentrated and purified via flash chromatography with a hexanes:ethyl acetate gradient (0 to 100% ethyl acetate) to yield the product as a white solid (2.22g, 90%). ^{1}H NMR (400 MHz, Chloroform-*d*) δ 4.45 (dd, *J* = 10.1, 5.3 Hz, 2H), 4.33 (dd, *J* = 10.1, 4.7 Hz, 2H), 3.96 – 3.89 (m, 2H), 3.88 – 3.70 (m, 6H), 3.61 – 3.52 (m, 2H), 3.46 – 3.34 (m, 4H). ^{13}C NMR (101 MHz, Acetonitrile-d_3) δ 76.47, 72.36, 70.15, 70.07, 50.73. IR: ν = 2941, 2879, 2095, 1737, 1448, 1400, 1192, 1014, 924, 861, 831. HRMS (ESI) calculated for $C_{10}H_{18}N_6O_7S$ $[M+NH_4]^+$ = 389.0855, observed = 389.0879.

Pentaethyleneglycol diazide macrocyclic sulfate. Product isolated as a clear oil (59%). ^{1}H NMR (600 MHz, Chloroform-*d*) δ 4.39 (dd, *J* = 5.0, 0.9 Hz, 4H), 3.92 – 3.76 (m, 6H), 3.72 – 3.57 (m, 8H), 3.49 – 3.35 (m, 4H). ^{13}C NMR (101 MHz, Chloroform-*d*) δ 81.55, 77.62, 75.74, 75.68, 75.65, 56.01. IR: ν = 2874, 2097, 1738, 1451, 1393, 1277, 1193, 1106, 960, 929, 858. HRMS (ESI) calculated for $C_{12}H_{22}N_6O_8S$ $[M + Na]^+$ = 433.1117, observed = 433.1057.

Hexaethyleneglycol diazide macrocyclic sulfate. Product isolated as a clear oil (60%). ^{1}H NMR (600 MHz, Chloroform-*d*) δ 4.45 – 4.35 (m, 4H), 3.96 (m, 2H), 3.90 – 3.77 (m, 4H), 3.75 – 3.60 (m, 12H), 3.42 (d, *J* = 5.4 Hz, 4H). ^{13}C NMR (101 MHz, Chloroform-*d*) δ 76.33, 72.11, 71.34,

70.69, 70.62, 70.02, 51.00. IR: ν = 2872, 2098, 1737, 1713, 1450, 1392, 1194, 1104, 997, 980, 862. HRMS (ESI) calculated for $C_{14}H_{26}N_6O_9S$ $[M + Na]^+$ = 477.1379, observed = 477.1254.

Heptaethyleneglycol diazide macrocyclic sulfate. Product isolated as a clear oil (88%). ^{1}H NMR (600 MHz, Chloroform-*d*) δ 4.44 – 4.34 (m, 4H), 3.91 (m,2H), 3.87 – 3.78 (m, 4H), 3.70 – 3.61 (m, 16H), 3.51 – 3.38 (m, 4H). ^{13}C NMR (101 MHz, Acetonitrile-d_3) δ 76.23, 72.42, 70.58, 70.26, 70.25, 70.15, 69.74, 50.49. IR: ν = 2873, 2098, 1738, 1451, 1394, 1194, 1105, 994, 926, 861. HRMS (ESI) calculated for $C_{16}H_{30}N_6O_{10}S$ $[M+NH_4]^+$ = 516.2087, observed = 516.2138.

Tetraethyleneglycol macrocyclic sulfate.[3] Product isolated as a clear oil (61%). ^{1}H NMR (400 MHz, Chloroform-*d*) δ 4.51 – 4.44 (m, 4H), 3.88 – 3.81 (m, 4H), 3.72 – 3.61 (m, 8H). ^{13}C NMR (126 MHz, Acetonitrile-d_3) δ 72.90, 70.33, 70.13, 68.09. IR: ν = 2871, 1729, 1287, 1191, 1124, 1004, 920.

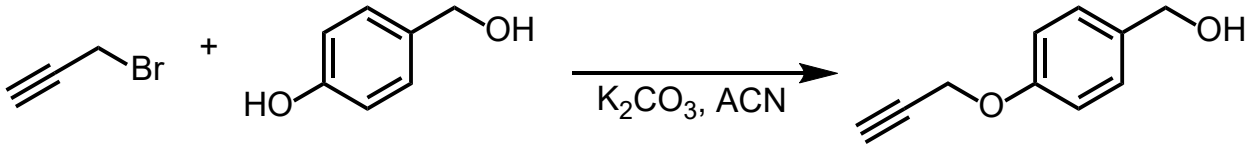

(4-(prop-2-yn-1-yloxy)phenyl)methanol Synthesis.[4] To a round-bottom flask with a stir-bar, K_2CO_3 (14 g, 100 mmol, 5 equivalents) and 4-(hydroxymethyl)phenol (2.5 g, 20 mmol, 1 equivalent) were added and suspended in 30 mL of acetonitrile. Propargyl bromide (80% in toluene, 2.7 mL, 24 mmol, 1.2 equivalents) was then added dropwise and the reaction was stirred at 70 °C for 5 hrs. The reaction was then cooled, filtered through celite, concentrated, and dissolved in dichloromethane. The remaining insoluble precipitate was then filtered through a 0.45 μM filter and concentrated to yield the pure product as an orange oil (1.47 g, 45%). ^{1}H NMR (600 MHz,

Chloroform-*d*) δ 7.32 (d, *J* = 8.7 Hz, 2H), 6.98 (d, *J* = 8.7 Hz, 2H), 4.70 (d, *J* = 2.4 Hz, 2H), 4.64 (s, 2H), 2.52 (t, *J* = 2.4 Hz, 1H). ^{13}C NMR (101 MHz, Chloroform-*d*) δ 157.16, 134.09, 128.61, 115.03, 78.52, 75.56, 65.01, 55.87. IR: ν = 3283, 2922, 2871, 1739, 1609, 1509, 1212, 1022, 1008, 811. HRMS (ESI) calculated for $C_{10}H_{10}O_2$ $[M+H]^+$ = 163.0759, observed = 163.0717.

General Ditosylation Procedure (Using diethyleneglycol ditosylate as an example). Diethyleneglycol (7.0 mL, 73 mmol, 1 equivalent), triethylamine (30 mL, 0.22 mol, 3 equivalents), and tosyl chloride (31 g, 0.16 mol, 2.2 equivalents) were dissolved in 150 mL of dichloromethane in a round-bottom flask. The reaction was allowed to proceed for 4 hours and the crude was transferred to a separatory funnel. The organic layer was then washed with water once followed by one wash with 1 M HCl. The organic layer was dried over $MgSO_4$ and dried to yield the crude solid. The product was then recrystallized by first dissolving in hot toluene followed by a slow addition of 14 mL of petroleum ether. The crystalized product was then collected via filtration and washed with cold toluene (20.54 g, 68%). ^{1}H NMR (600 MHz, Chloroform-*d*) δ 7.79 (d, *J* = 8.3 Hz, 2H), 7.35 (d, *J* = 7.9 Hz, 2H), 4.13 – 4.06 (m, 2H), 3.64 – 3.59 (m, 2H), 2.45 (s, 3H). ^{13}C NMR (101 MHz, Chloroform-*d*) δ 144.98, 132.87, 129.92, 127.97, 69.01, 68.77, 21.68. IR: ν = 2900, 1597, 1351, 1170, 1017, 916, 814. HRMS (ESI) calculated for $C_{18}H_{22}O_7S_2$ $[M+H]^+$ = 415.0885, observed = 415.0992.

Triethyleneglycol ditosylate. Product purified via flash chromatography with a 7:3 hexanes:ethyl acetate isocratic mobile phase to yield the product was a white solid (56%). ^{1}H NMR (400 MHz, Chloroform-*d*) δ 7.79 (d, *J* = 8.3 Hz, 4H), 7.34 (d, *J* = 7.9 Hz, 4H), 4.17 – 4.09 (m, 4H), 3.68 –

3.62 (m, 4H), 3.52 (s, 4H), 2.44 (s, 6H). ^{13}C NMR (101 MHz, Chloroform-*d*) δ 144.86, 132.97, 129.85, 127.97, 70.70, 69.21, 68.76, 21.66. IR: ν = 2876, 1597, 1451, 1351, 1173, 914, 814, 772, 661. HRMS (ESI) calculated for $C_{20}H_{26}O_8S_2$ $[M+H]^+$ = 459.1147, observed = 459.1175.

Tetraethyleneglycol ditosylate. Product purified via flash chromatography with a 7:3 hexanes:ethyl acetate isocratic mobile phase to yield the product as a clear oil (56%). ^{1}H NMR (400 MHz, Chloroform-*d*) δ 7.79 (d, *J* = 8.3 Hz, 4H), 7.33 (d, *J* = 8.0 Hz, 4H), 4.18 – 4.13 (m, 4H), 3.71 – 3.66 (m, 4H), 3.60 – 3.52 (m, 8H), 2.44 (s, 6H). ^{13}C NMR (101 MHz, Chloroform-*d*) δ 144.82, 132.99, 129.84, 127.98, 70.75, 70.56, 69.27, 68.70, 21.66. IR: ν = 2873, 1737, 1597, 1451, 1351, 1173, 913, 814, 771. HRMS (ESI) calculated for $C_{22}H_{30}O_9S_2$ $[M+H]^+$ = 503.1409, observed = 503.1497.

Pentaethyleneglycol ditosylate. Product purified via flash chromatography with a 0-100% hexanes:ethyl gradient (0% ethyl acetate to 100%) to yield the product was a clear oil. ^{1}H NMR (300 MHz, Chloroform-*d*) δ 7.79 (d, *J* = 8.3 Hz, 4H), 7.34 (d, *J* = 7.9 Hz, 4H), 4.17 – 4.13 (m, 4H), 3.70 – 3.64 (m, 4H), 3.59 (d, *J* = 6.4 Hz, 12H), 2.44 (s, 6H). ^{13}C NMR (101 MHz, Chloroform-*d*) δ 144.83, 133.01, 129.85, 127.99, 70.76, 70.61, 70.52, 69.28, 68.68, 21.65. IR: ν = 2871, 1734, 1597, 1352, 1174, 1095, 1012, 915, 815, 772, 661. HRMS (ESI) calculated for $C_{24}H_{34}O_{10}S_2$ $[M+H]^+$ = 547.1671, observed = 547.1776.

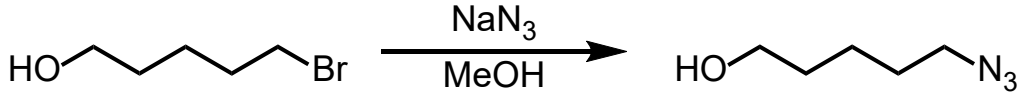

5-azido-pentan-1-ol.[5] To a scintillation vial with a stirbar, sodium azide (1.41 g, 21.7 mmol, 3 equivalents) and 5-bromopentan-1-ol (1.21 g, 7.24 mmol, 1 equivalent) was added. The reagents were dissolved in 10 mL of methanol and the reaction was heated to 80 °C for 10 hrs. The reaction

was then cooled and the crude was dry-loaded onto silica. The product was then purified via flash chromatography with a hexanes:ethyl acetate gradient (0% ethyl acetate to 100% ethyl acetate) to yield the product as a clear oil (574 mg, 61%). ^{1}H NMR (400 MHz, Chloroform-*d*) δ 3.65 (t, *J* = 6.4 Hz, 2H), 3.28 (t, *J* = 6.9 Hz, 2H), 1.69 – 1.55 (m, 4H), 1.49 – 1.39 (m, 2H). ^{13}C NMR (101 MHz, Chloroform-*d*) δ 62.60, 51.40, 32.17, 28.66, 23.01. IR: ν = 3325, 2936, 2865, 2090, 1455, 1348, 1259, 1052.

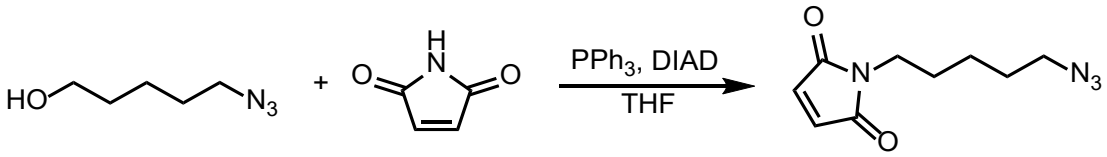

5-azidopentyl-1-maleimide. Triphenylphosphine (305 mg, 1.16 mmol, 1 equivalent) was dissolved in dry THF (5 mL) and cooled to 0 °C. DIAD (226 μL, 1.16 mmol, 1 equivalent) was added then dropwise and reaction was allowed to stir for 15 min at 0 °C. 5-azido-pentan-1-ol (150 mg, 1.16 mmol, 1 equivalent) was then added and reaction was allowed to stir for an additional 15 min at 0 °C. Finally, maleimide (135 mg, 1.39 mmol, 1.2 equivalents) was added and reaction was allowed to stir at 23 °C for 2 hrs. The product was then concentrated and purified via flash chromatography with a hexanes:ethyl acetate gradient (0% ethyl acetate to 50% ethyl acetate) to yield the product as an oil (119 mg, 49 %). Note: the final product degrades if stored under concentrated conditions. Therefore, after purification, the final material was only concentrated to 10 mg/mL in the hexanes/ethyl acetate mixture and dried immediately before use by blowing a stream of air over aliquoted solution. ^{1}H NMR (600 MHz, Chloroform-*d*) δ 6.70 (s, 2H), 3.53 (t, *J* = 7.2 Hz, 2H), 3.26 (t, *J* = 6.9 Hz, 2H), 1.66 – 1.58 (m, 4H), 1.41 – 1.32 (m, 2H).^{13}C NMR (126 MHz, Chloroform-*d*) δ 170.82, 134.09, 51.18, 37.53, 28.33, 28.06, 23.86. IR: ν = 2942, 2095,

1703, 1409, 1147, 828, 695. HRMS (ESI) calculated for $C_9H_{12}N_4O_2$ $[M + Na]^+$ = 231.0857, observed = 231.0855.

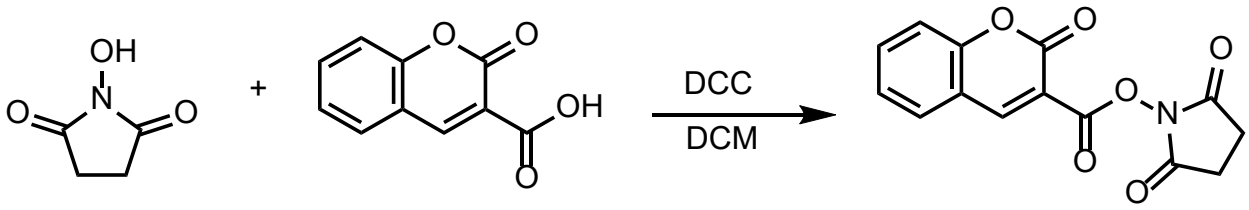

Coumarin-3-carboxylic acid N-succinimidyl ester.[6] Coumarin-3-carboxylic acid (1.0 g, 5.3 mmol, 1 equivalents), DCC (1.6 g, 7.9 mmol, 1.5 equivalents), and N-hydroxysuccinimide (0.91 g, 7.9 mmol, 1.5 equivalents) was dissolved in 10 mL of DCM in a scintillation vial. The reaction was allowed proceed at 23 °C for 12 h. The reaction was then filtered, concentrated, and purified via flash chromatography with a DCM:ethyl acetate gradient (0% to 50% ethyl acetate). ^{1}H NMR (300 MHz, Acetonitrile-*d*$_3$) δ 8.94 (s, 1H), 7.90 – 7.79 (m, 2H), 7.52 – 7.41 (m, 2H), 2.88 (s, 4H). ^{13}C NMR (101 MHz, Chloroform-*d*) δ 168.84, 151.94, 136.06, 130.25, 125.36, 117.36, 117.19, 25.68. HRMS (ESI) calculated for $C_{14}H_9NO_6$ $[M+H]^+$ = 288.0508, observed = 288.0549.

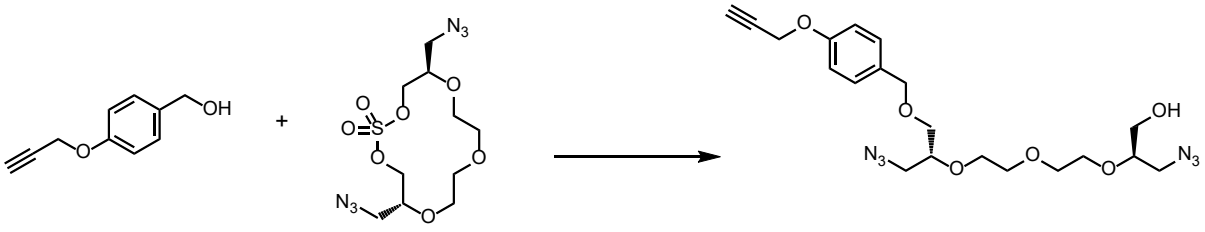

General macrocyclic sulfate ring opening procedure (Using tetraethyleneglycol diazide macrocyclic sulfate as an example). (4-(prop-2-yn-1-yloxy)phenyl)methanol (184 mg, 1.14 mmol, 1 equivalent) was dissolved in dry THF (0.3 M) and cooled to 0 °C. Sodium hydride (60 % dispersion in mineral oil, 136 mg, 3.41 mmol, 3 equivalents) was then added and reaction was

stirred for 5 minutes at 0 °C. Tetraethyleneglycol diazide macrocyclic sulfate (625 mg, 1.71 mmol, 1.5 equivalents) was then added and reaction was allowed to proceed for 12 h at 23 °C. Water (72 µL, 3.98 mmol, 3.5 equivalents) was then added to the stirring mixture dropwise followed by sulfuric acid (90.9 µL, 1.71 mmol, 1.5 equivalents). The reaction was stirred for a further 4 h at 23 °C. The contents were then transferred to a separatory funnel along with 25 mL of DCM and 15 mL of H_2O. The organic layer was collected and the aqueous layer was further extracted 3 times with DCM. The pooled organic layers were dried with $MgSO_4$ and concentrated to yield the crude. The product was then purified via flash chromatography with a DCM:MeOH gradient (0% MeOH to 5% MeOH) to yield the product as an orange oil (402 mg, 79%). ^{1}H NMR (600 MHz, Chloroform-*d*) δ 6.96 (d, *J* = 8.7 Hz, 2H), 4.70 (d, *J* = 2.4 Hz, 2H), 4.47 (s, 2H), 3.92 – 3.82 (m, 1H), 3.81 – 3.50 (m, 13H), 3.41 – 3.34 (m, 3H), 3.25 (dd, *J* = 12.9, 4.2 Hz, 1H), 2.53 (t, *J* = 2.4 Hz, 1H). HRMS (ESI) calculated for $C_{20}H_{28}N_6O_6$ $[M+NH_4]^+$ = 466.2414, observed = 466.2540.

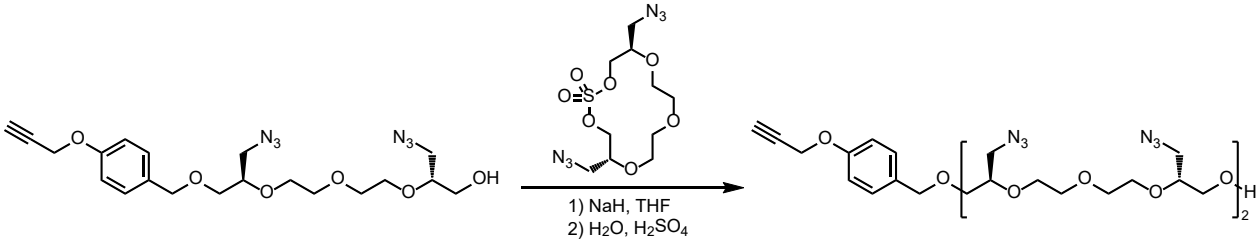

Propargylbenzyl (tetra-azide octaethyleneglycol). Product made following general macrocyclic sulfate ring opening procedure. Purified product was isolated as a brown oil (83%). ^{1}H NMR (600 MHz, Chloroform-*d*) δ 6.96 (d, *J* = 8.7 Hz, 2H), 4.70 (d, *J* = 2.4 Hz, 2H), 4.47 (s, 2H), 3.89 (m, 2H), 3.82 – 3.47 (m, 41H), 3.42 – 3.30 (m, 10H), 3.26 (dd, *J* = 12.8, 4.3 Hz, 2H), 2.53 (t, *J* = 2.4 Hz, 1H). HRMS (ESI) calculated for $C_{30}H_{46}N_{12}O_{10}$ $[M+NH_4]^+$ = 752.3803, observed = 752.3873.

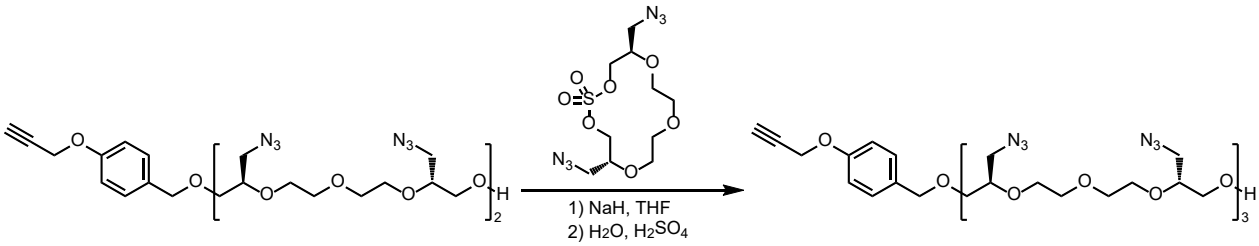

Propargylbenzyl (Hexa-azide dodecaethyleneglycol). Product was made following general macrocyclic sulfate ring opening procedure. Purified product was isolated as a brown oil (87%). ^{1}H NMR (600 MHz, Chloroform-*d*) δ 6.96 (d, *J* = 8.6 Hz, 2H), 4.70 (d, *J* = 2.4 Hz, 2H), 4.47 (s, 2H), 3.89 (m, 2H), 3.83 – 3.46 (m, 67H), 3.42 – 3.24 (m, 18H), 2.53 (t, *J* = 2.4 Hz, 1H). HRMS (ESI) calculated for $C_{40}H_{64}N_{18}O_{14}$ $[M+NH_4]^+$ = 1038.5193, observed = 1038.5292.

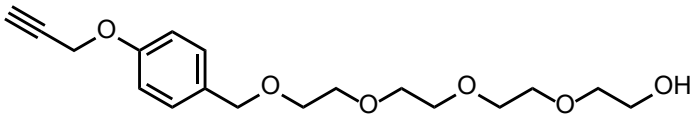

Propargylbenzyl (tetraethyleneglycol). Product was made following the general macrocyclic sulfate ring opening procedure. Purified product was isolated as a brown oil (80%). ^{1}H NMR (600 MHz, Chloroform-*d*) δ 7.29 (d, *J* = 8.8 Hz, 2H), 6.95 (d, *J* = 8.7 Hz, 2H), 4.69 (d, *J* = 2.4 Hz, 2H), 4.50 (s, 2H), 3.74 – 3.70 (m, 2H), 3.67 (m, 10H), 3.63 – 3.60 (m, 4H), 2.52 (t, *J* = 2.4 Hz, 1H). HRMS (ESI) calculated for $C_{18}H_{26}O_6$ $[M+NH_4]^+$ = 356.2073, observed = 356.2057.

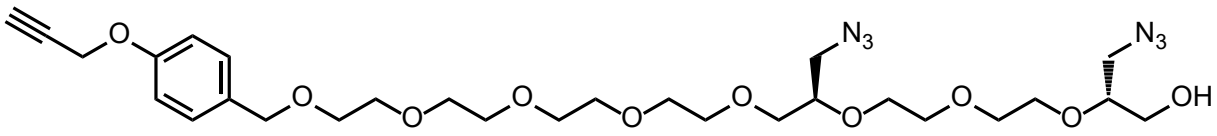

Propargylbenzyl (diazide octaethyleneglycol). Product was made following the general macrocyclic sulfate ring opening procedure. Purified product was isolated as a brown oil (45%). ^{1}H NMR (600 MHz, Chloroform-*d*) δ 7.28 (d, *J* = 8.6 Hz, 2H), 6.95 (d, *J* = 8.6 Hz, 2H), 4.69 (d, *J* = 2.4 Hz, 2H), 4.50 (s, 2H), 3.88 (m, 1H), 3.83 – 3.47 (m, 37H), 3.42 – 3.35 (m, 3H), 3.27 – 3.23

(m, 1H), 2.52 (t, J = 2.4 Hz, 1H). HRMS (ESI) calculated for $C_{28}H_{44}N_6O_{10}$ $[M+NH_4]^+$ = 642.3462, observed = 642.3544.

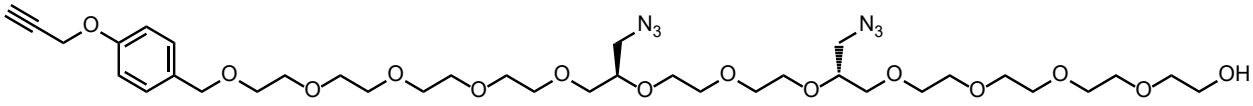

Propargylbenzyl (diazide dodeca-ethyleneglycol). Product was made following the general macrocyclic sulfate ring opening procedure. Purified product was isolated as a brown oil (42%). ^{1}H NMR (500 MHz, Chloroform-*d*) δ 6.94 (d, J = 8.6 Hz, 2H), 4.68 (d, J = 2.4 Hz, 2H), 4.50 (s, 2H), 3.81 – 3.47 (m, 48H), 3.42 – 3.31 (m, 4H), 2.52 (t, J = 2.4 Hz, 1H). HRMS (ESI) calculated for $C_{36}H_{60}N_6O_{14}$ $[M+NH_4]^+$ = 818.4511, observed = 818.4574.

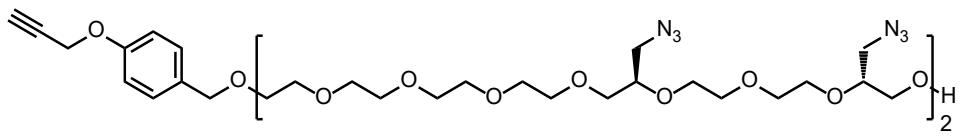

Propargylbenzyl (tetra-azide hexadeca-ethyleneglycol). Product was made following the general macrocyclic sulfate ring opening procedure. Purified product was isolated as a brown oil (68%). ^{1}H NMR (600 MHz, Chloroform-*d*) δ 7.28 (d, J = 8.5 Hz, 2H), 6.95 (d, J = 8.6 Hz, 2H), 4.69 (d, J = 2.4 Hz, 2H), 4.50 (s, 2H), 3.92 – 3.87 (m, 1H), 3.83 – 3.48 (m, 89H), 3.43 – 3.32 (m, 9H), 3.26 (dd, J = 12.8, 4.2 Hz, 1H), 2.53 (t, J = 2.4 Hz, 1H). HRMS (ESI) calculated for $C_{46}H_{78}N_{12}O_{18}$ $[M+NH_4]^+$ = 1104.5900, observed = 1104.3670.

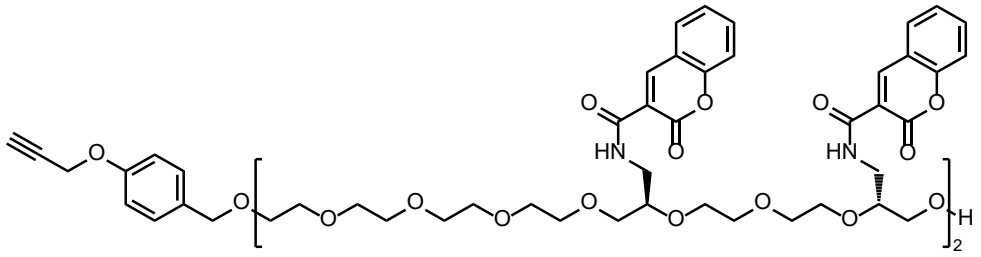

Propargylbenzyl (tetra-azide hexadeca-ethyleneglycol) reduction and coumarin addition. Propargylbenzyl (tetra-azide hexadeca-ethyleneglycol) (17 mg, 16 µmol, 1 equivalent) and triphenylphosphine (41 mg, 160 µmol, 10 equivalents) were dissolved in 700 µL of THF and 200 µL of water in a dram vial. The reduction was allowed to proceed for 12 hrs at 23 °C. Solvent was then removed under vacuum. To the solid, coumarin-3-carboxylic acid N-succinimidyl ester (44 mg, 150 µmol, 10 equivalents) and N,N-diisopropylethylamine (16 µL, 92 µmol, 6 equivalents) were added. The reagents were then dissolved in 0.5 mL of DMSO and the alkylation was allowed to proceed for 4 h at 23 °C. The crude reaction was then diluted with acetonitrile, filtered, and purified via preparatory high-performance liquid chromatography (HPLC) with a 50-100% acetonitrile gradient and lyophilized to yield the product as a clear oil (6.6 mg, 26%). ^{1}H NMR (500 MHz, Chloroform-*d*) δ 9.08 (s, 4H), 8.86 (d, *J* = 11.1 Hz, 4H), 7.71 – 7.59 (m, 9H), 6.92 (d, *J* = 8.2 Hz, 2H), 4.67 (d, *J* = 2.4 Hz, 2H), 4.48 (s, 2H), 3.88 – 3.48 (m, 79H), 2.52 (t, *J* = 2.4 Hz, 1H). HRMS (ESI) calculated for $C_{86}H_{102}N_4O_{30}$ $[M+H]^+$ = 1671.6657, observed = 1671.6698.

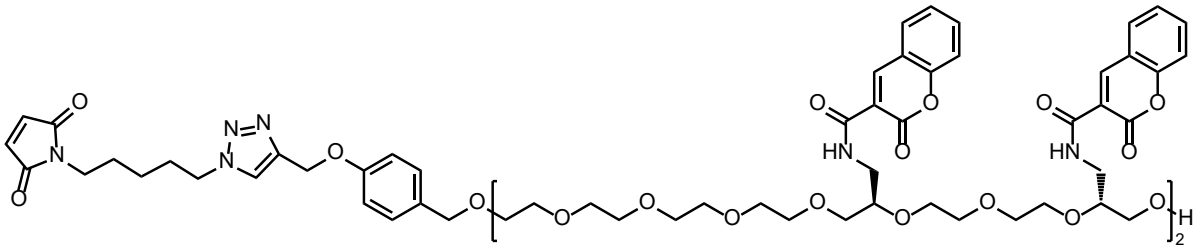

Maleimide (tetra-coumarin hexadeca-ethyleneglycol). An aliquoted stock solution of the 5-azidopentyl-1-maleimide (2.27 mg, 10.9 µmol, 5 equivalents) was added to a dram vial and dried with a stream of air. A stock solution (18.2 mg/mL in DMF) of propargylbenzyl (tetra-coumarin hexadeca-ethyleneglycol) was then added (3.64 mg, 2.18 µmol, 1 equivalents) and the reaction was diluted to a total volume of 400 µL. Stock solutions of copper(II)sulfate (3.5 mg/mL) and sodium ascorbate (4.3 mg/mL) were prepared in water. Aliquots of both copper(II)sulfate (174 µg,

1.09 μmol, 0.5 equivalents) and ascorbic acid (216 μg, 1.09 μmol, 0.5 equivalents) were then added and reaction was allowed to stir for 15 minutes at 23 °C. An additional 0.5 equivalents of copper(II)sulfate and ascorbic acid were added every 15 minutes until a total of 2 equivalents of each was added. The reaction was allowed to stir at 23 °C for 4 h. The reaction was then diluted with acetonitrile and product was purified via preparatory HPLC with a 50-100% acetonitrile gradient and lyophilized to yield the product as white residue (2.3 mg, 56%). ^{1}H NMR (500 MHz, Acetonitrile-d_3) δ 8.89 (t, J = 5.6 Hz, 4H), 8.78 (dd, J = 10.2, 5.5 Hz, 4H), 7.84 – 7.71 (m, 5H), 7.71 – 7.62 (m, 4H), 7.41 – 7.31 (m, 9H), 7.21 (d, J = 8.3 Hz, 2H), 6.92 (d, J = 8.4 Hz, 2H), 6.71 (s, 2H), 5.07 (s, 2H), 4.41 (s, 2H), 4.31 (t, J = 7.1 Hz, 2H), 3.79 – 3.68 (m, 12H), 3.67 – 3.44 (m, 67H). HRMS (ESI) calculated for $C_{95}H_{114}N_8O_{32}$ $[M+H]^+$ = 1879.7617, observed = 1879.7776.

Trastuzumab Conjugation Protocol. Trastuzumab (1 mg, 0.0068 μmol, 1 equivalent) was buffer exchanged into DPBS + 10 mM EDTA via 5 cycles of centrifugal (100 MW cutoff) filtration. The Trastuzumab solution was then concentrated to 10 mg/mL and TCEP (19 μg, 0.068 μmol, 10 equivalents) was then added via a freshly prepared stock solution and reduction was allowed to proceed at 37 °C for 1 hr. Excess TCEP was then removed with a desalting ZEBA® column (7 MWCO cutoff). A stock solution of the maleimide (tetra-coumarin hexadeca-ethyleneglycol) was prepared in DMF and added (0.25 mg, 0.14 μmol, 20 equivalents, 20% final DMF concentration). The conjugation was allowed to proceed for 12 hrs. Precipitate was removed via centrifugation and the supernatant was run through a ZEBA® column. Remaining small molecule reagents were then removed via centrifugal filtration (10 total washes) with PBS.

Indirect ELISA Protocol.[7] To the wells of a high-binding 96 well plate, 100 μL of a 1 μg/mL solution (diluted in 0.1 M carbonate buffer, pH 9.6) of recombinant Her2 was added. The plate was covered with foil and incubated at 4 °C for 12 h. The following day, the solution was aspirated

and the plate was washed four times with ELISA wash buffer (PBS + 0.3% Tween 20). To the wells, 200 µL of blocking buffer (1% BSA in PBS, filtered with 0.22 µM filter) was added and incubated at 22 °C for 2 h. Again, 4 washes were performed with wash buffer before adding 100 µL of antibody or conjugate samples at appropriate dilution (dilution buffer = 1% BSA in PBS). The plate was incubated at 22 °C for 1 h before repeating the aspiration and wash procedure. Whole molecule anti-Human IgG (whole molecule)−Peroxidase antibody produced in rabbit (diluted 1:40,000 in dilution buffer) was then added (100 µL per well) and the plate was incubated at 37 °C for 45 min. After aspirating and washing the plate a final time, 100 µL of TMB (3,3',5,5'-Tetramethylbenzidine) substrate solution was added to the wells via a multichannel pipette and the plate was incubated in the dark for ~5 min. After sufficient development of blue color, 50 µL of 1 M sulfuric acid was added and absorbance of each well was measured at 450.

2.6. Appendix with Supplementary Figures

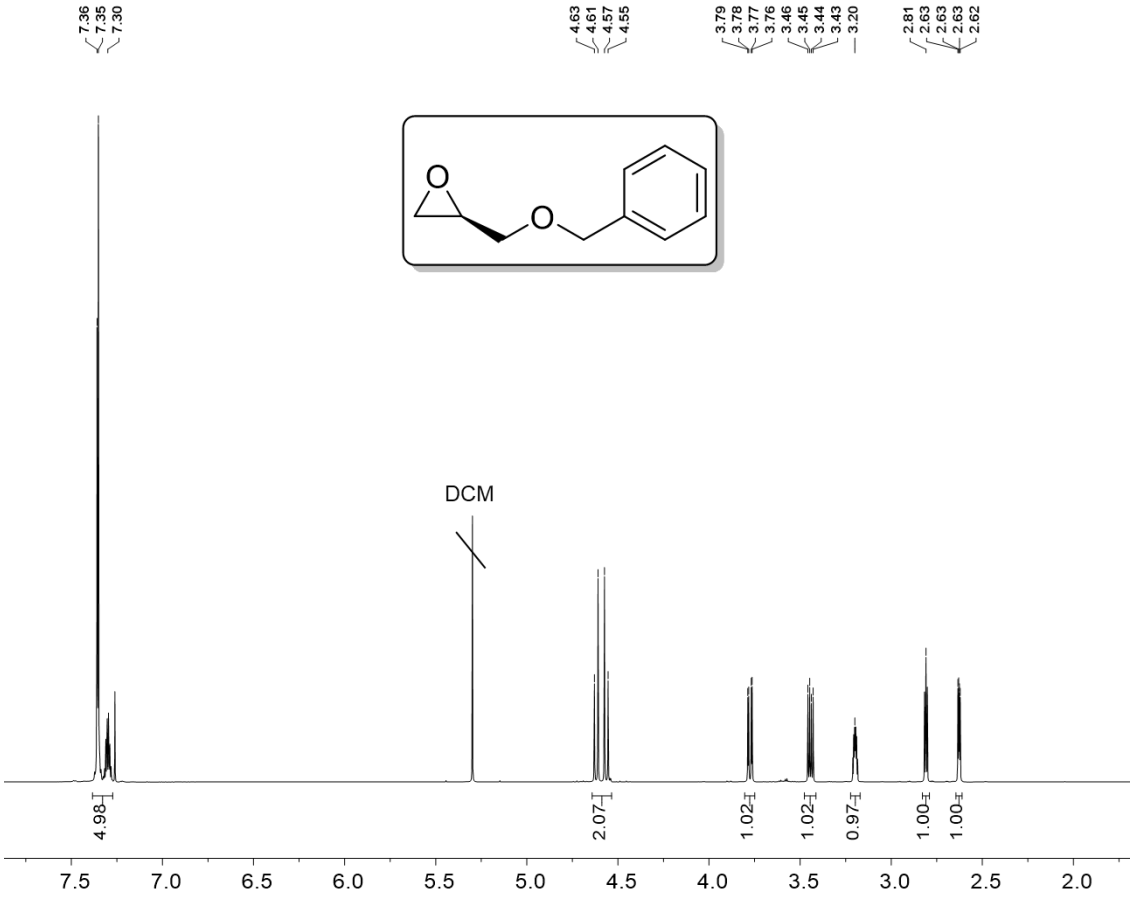

Figure 2.6.1. (R)-2-((benzyloxy)methyl)oxirane ^{1}H NMR.

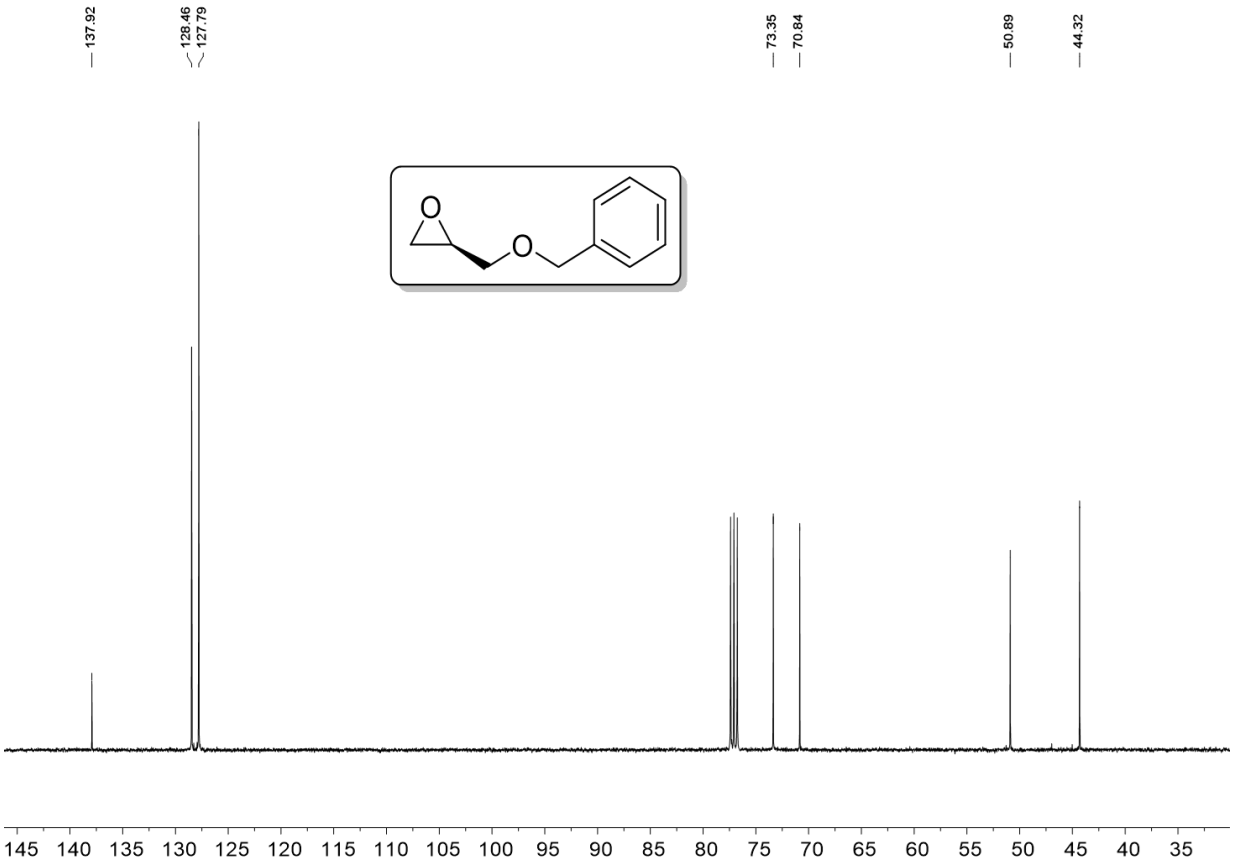

Figure 2.6.2. (R)-2-((benzyloxy)methyl)oxirane ^{13}C NMR.

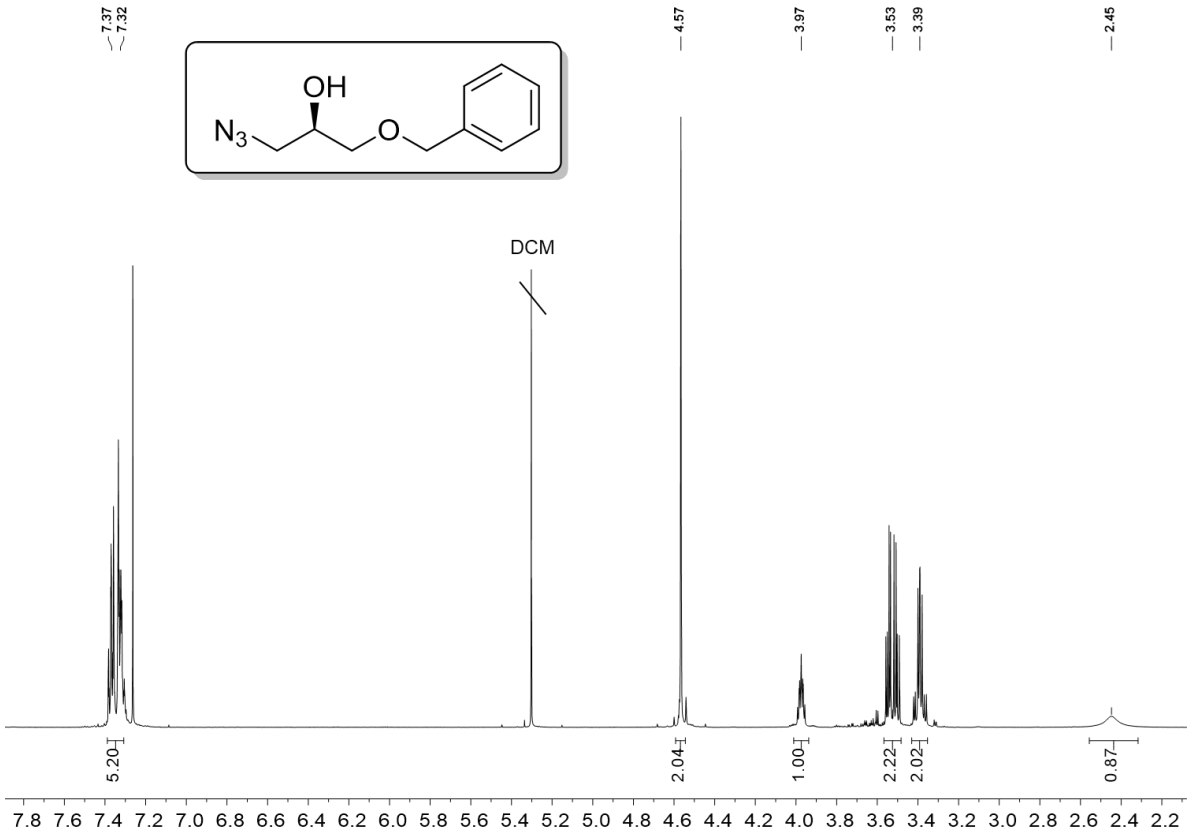

Figure 2.6.3. (R)-1-azido-3-(benzyloxy)propan-2-ol ^{1}H NMR.

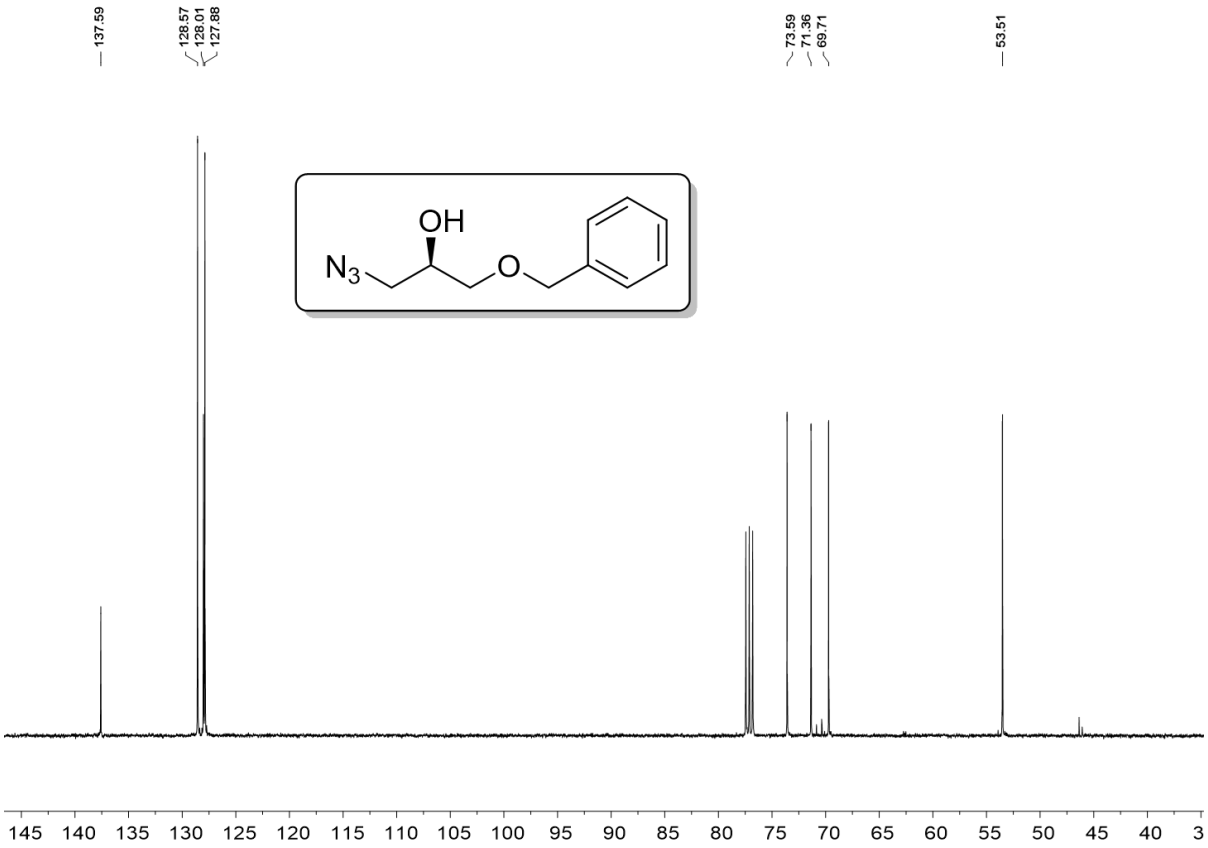

Figure 2.6.4. (R)-1-azido-3-(benzyloxy)propan-2-ol ^{13}C NMR.

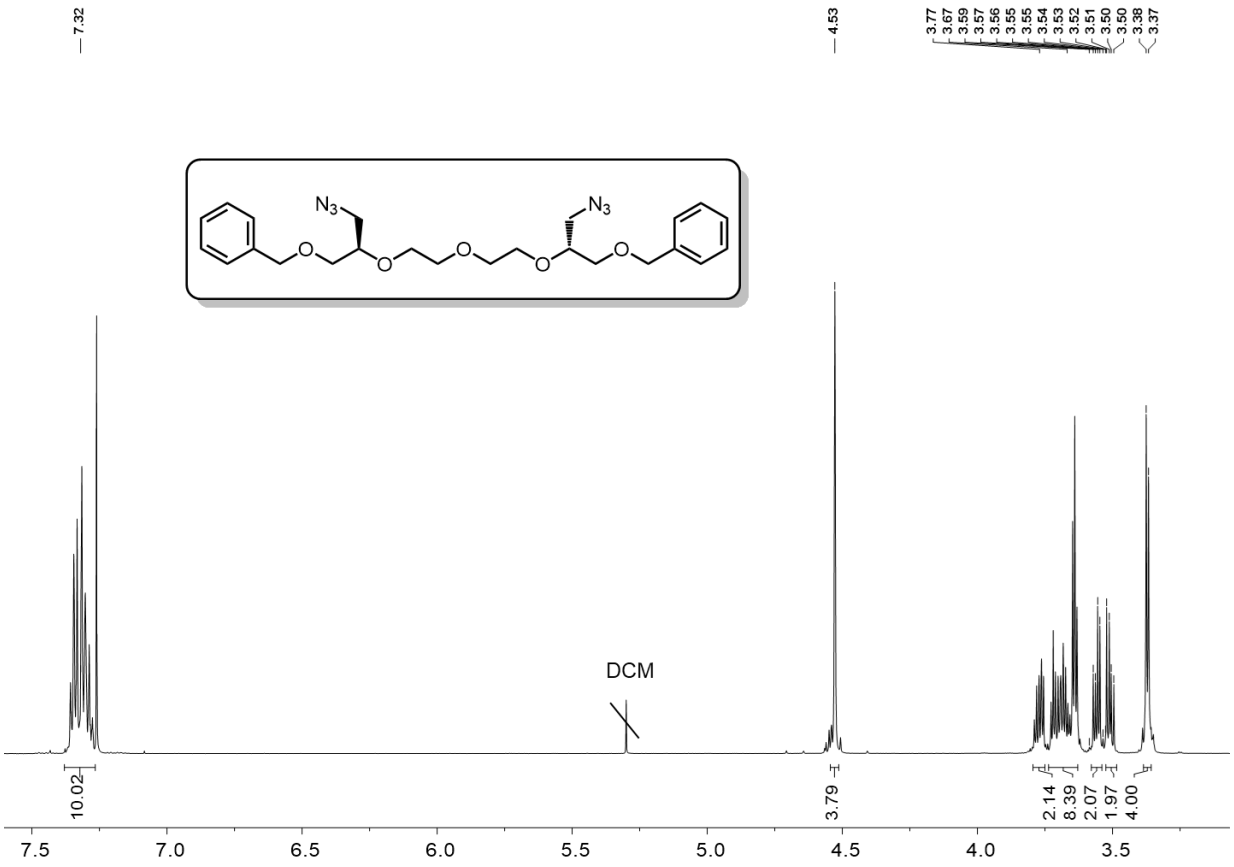

Figure 2.6.5. Dibenzyl-azido tetraethyleneglycol ^{1}H NMR.

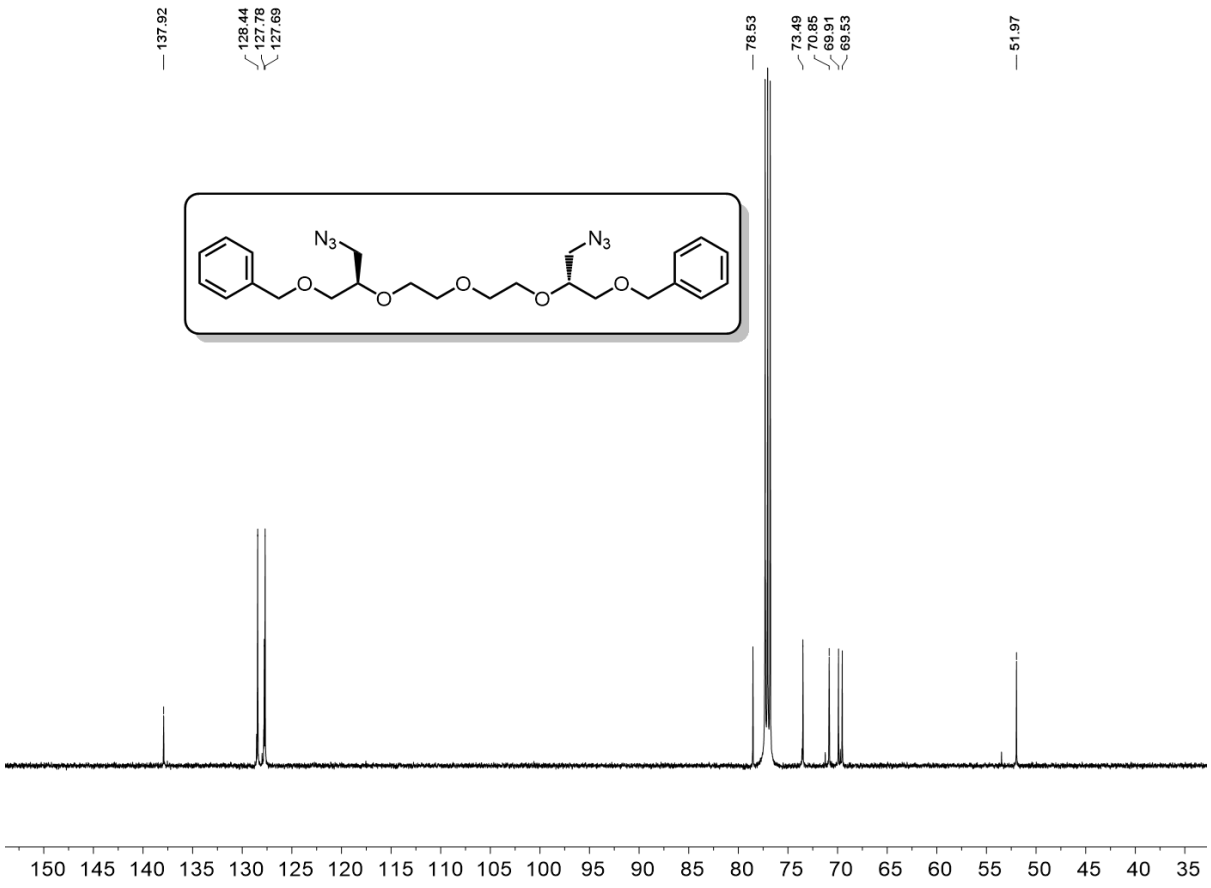

Figure 2.6.6. Dibenzyl-azido tetraethyleneglycol ^{13}C NMR.

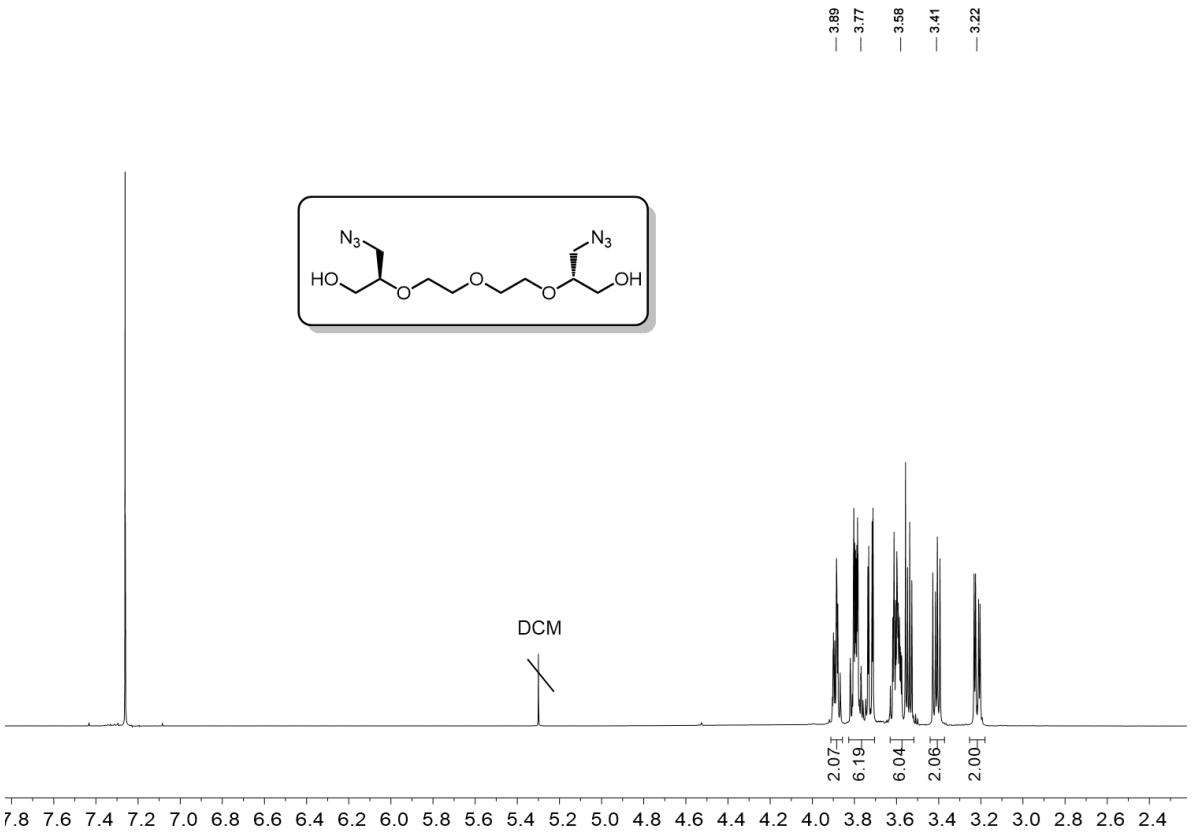

Figure 2.6.7. Tetraethyleneglycol diazide ^{1}H NMR.

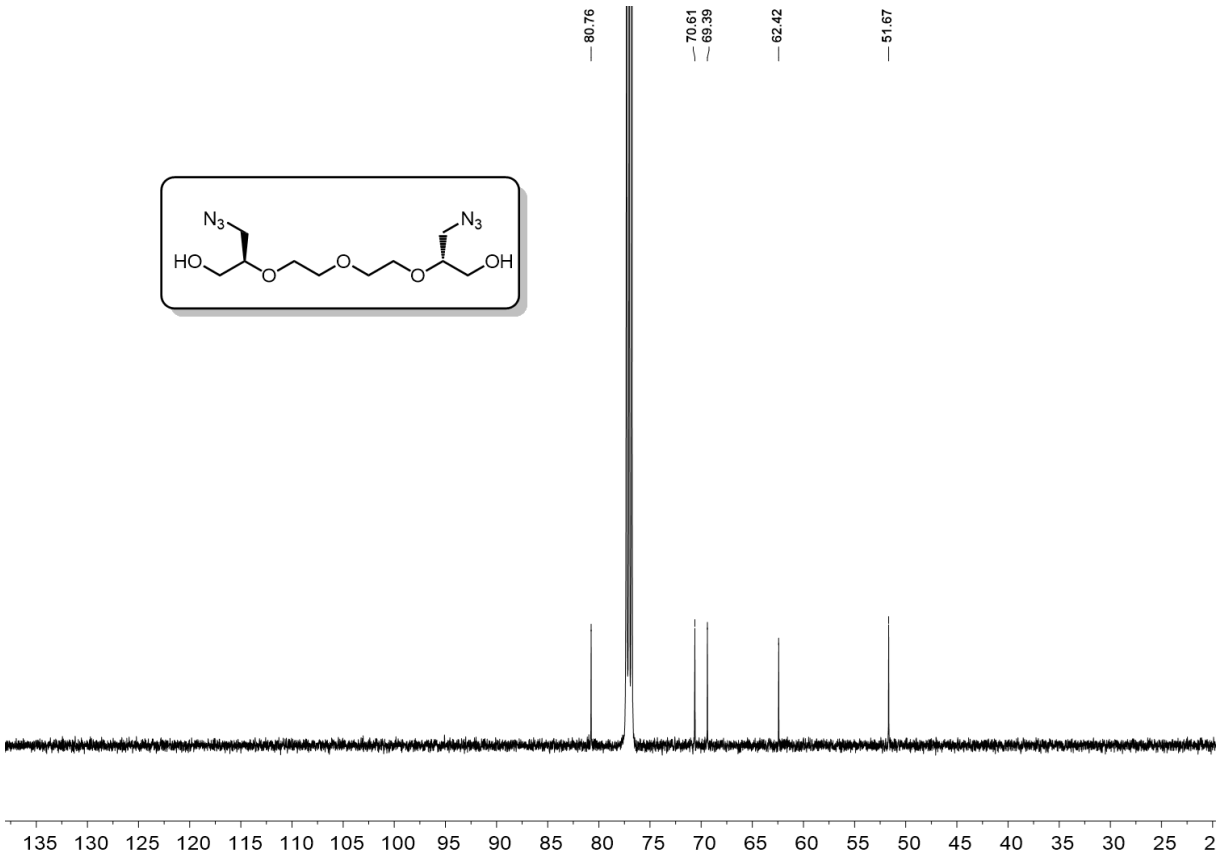

Figure 2.6.8. Tetraethyleneglycol diazide ^{13}C NMR.

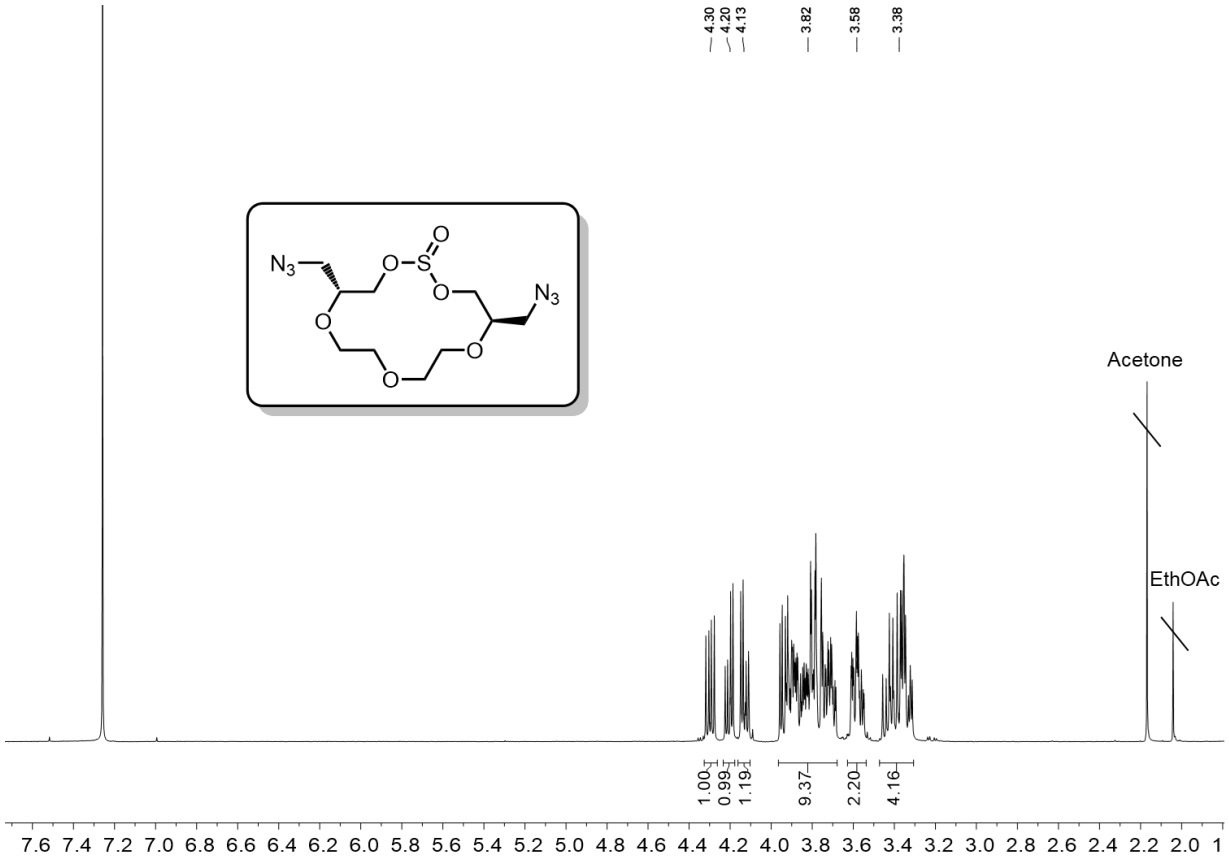

Figure 2.6.9. Tetraethyleneglycol diazide macrocyclic sulfite ^{1}H NMR.

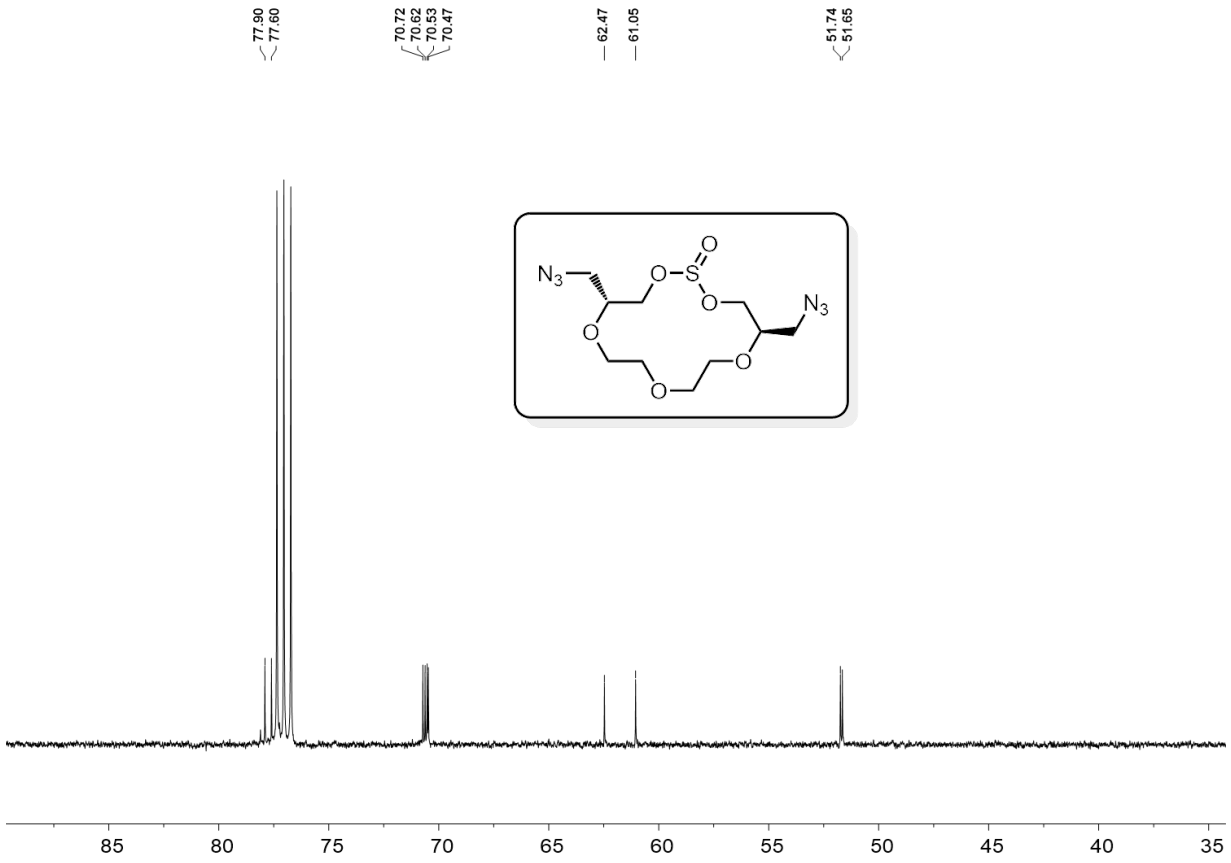

Figure 2.6.10. Tetraethyleneglycol diazide macrocyclic sulfite ^{13}C NMR.

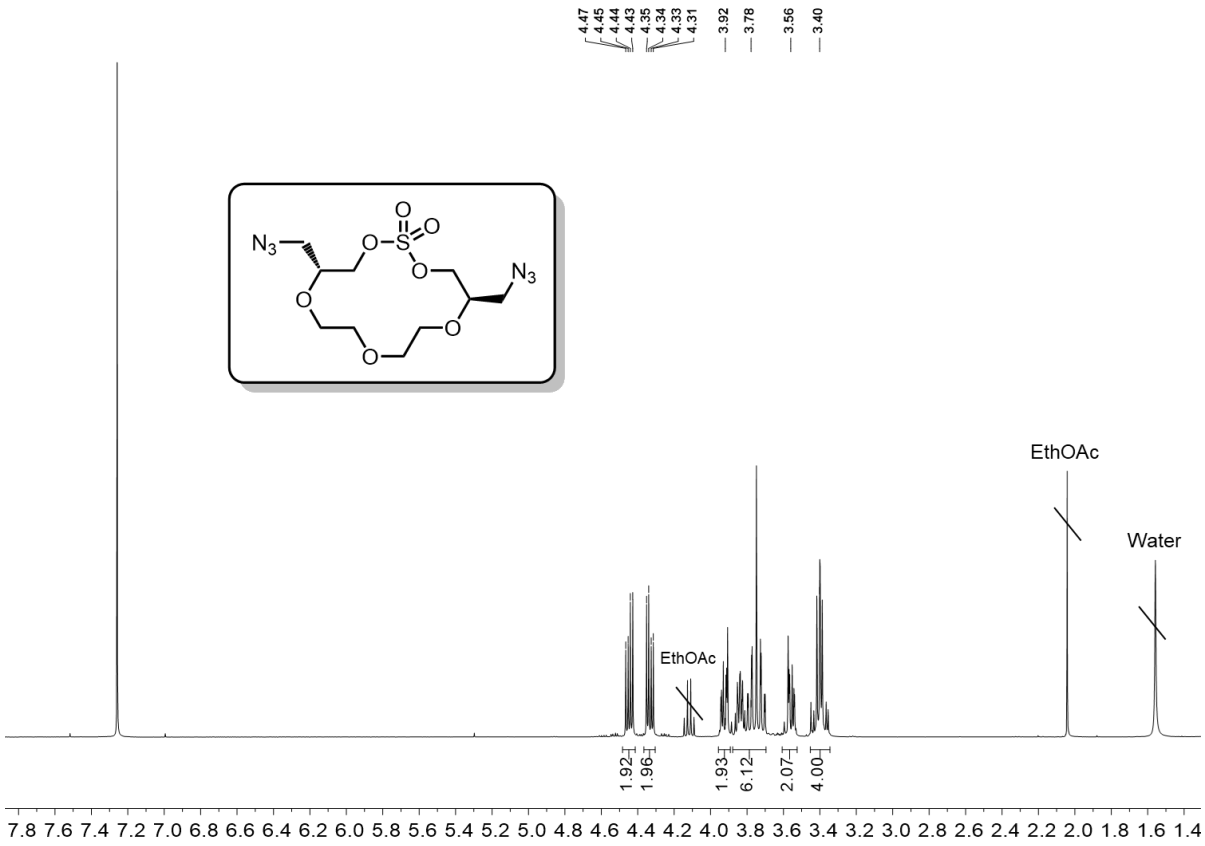

Figure 2.6.11. Tetraethyleneglycol diazide macrocyclic sulfate ^{1}H NMR.

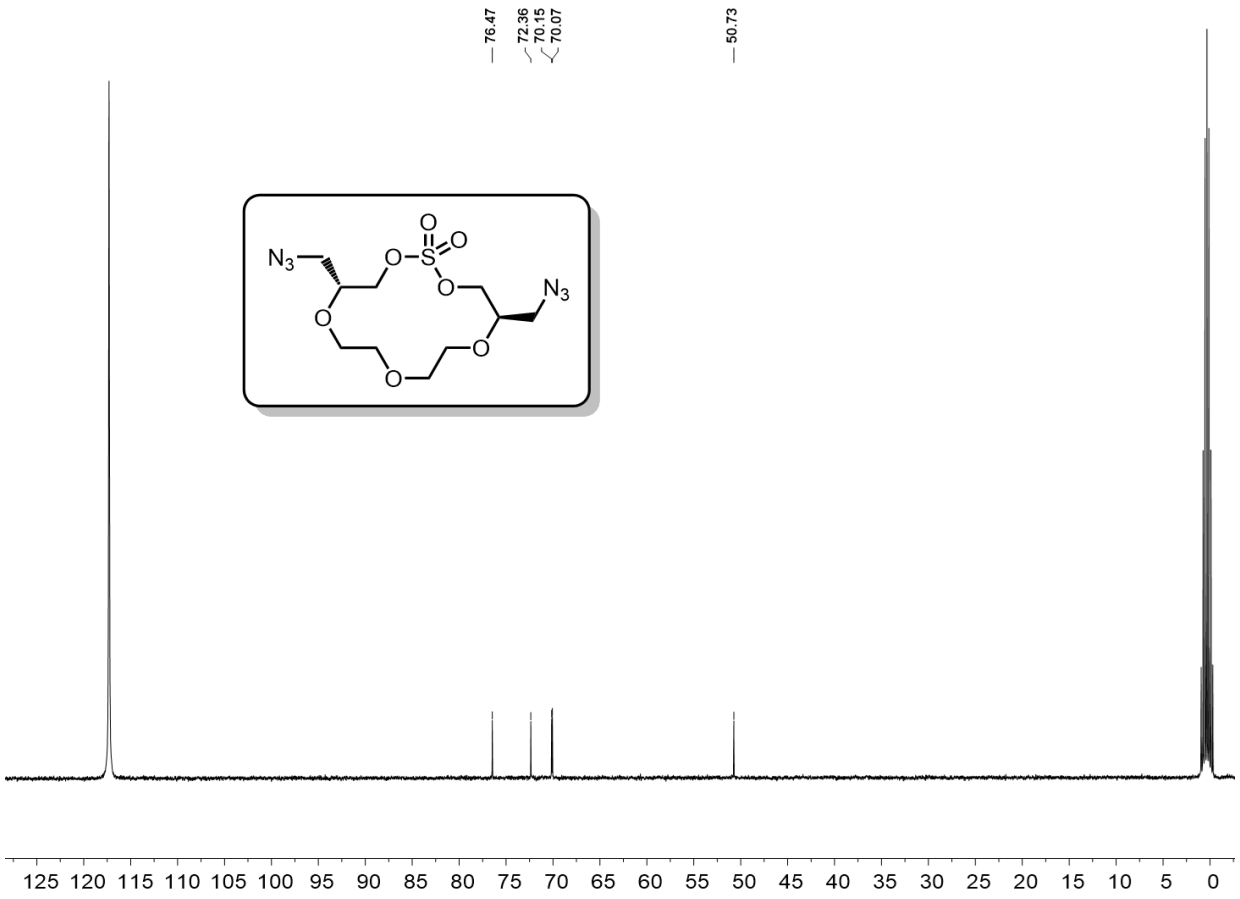

Figure 2.6.12. Tetraethyleneglycol diazide macrocyclic sulfate ^{13}C NMR.

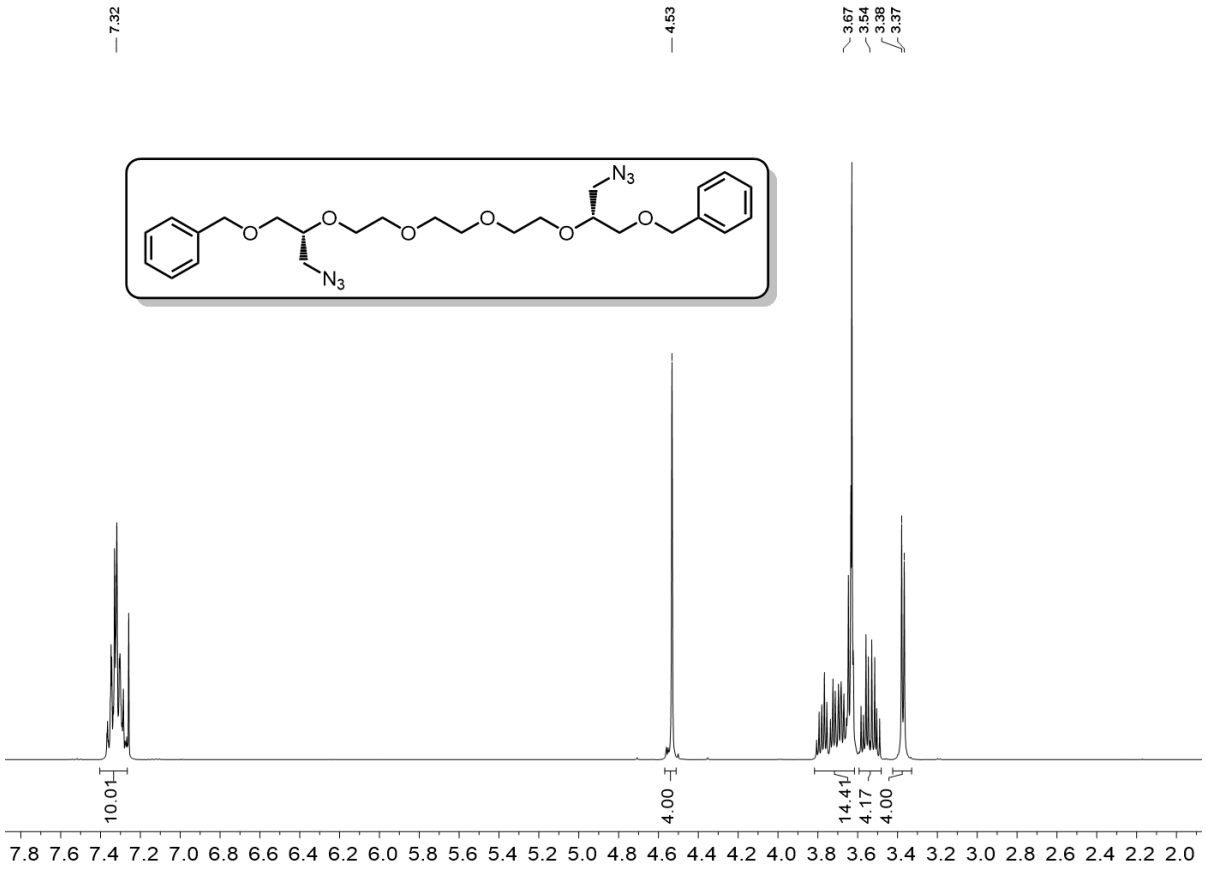

Figure 2.6.13. Dibenzyl-azido pentaethyleneglycol ^{1}H NMR.

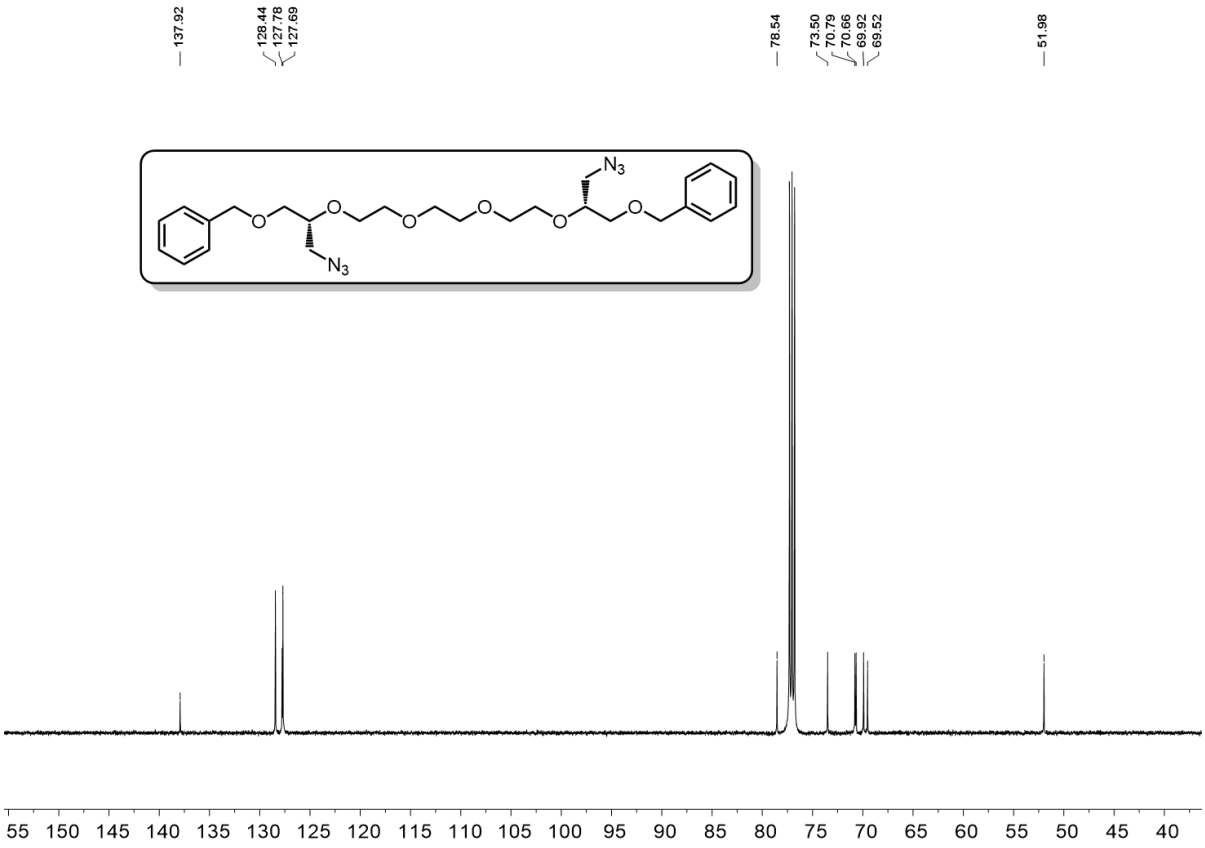

Figure 2.6.14. Dibenzyl-azido pentaethyleneglycol ^{13}C NMR.

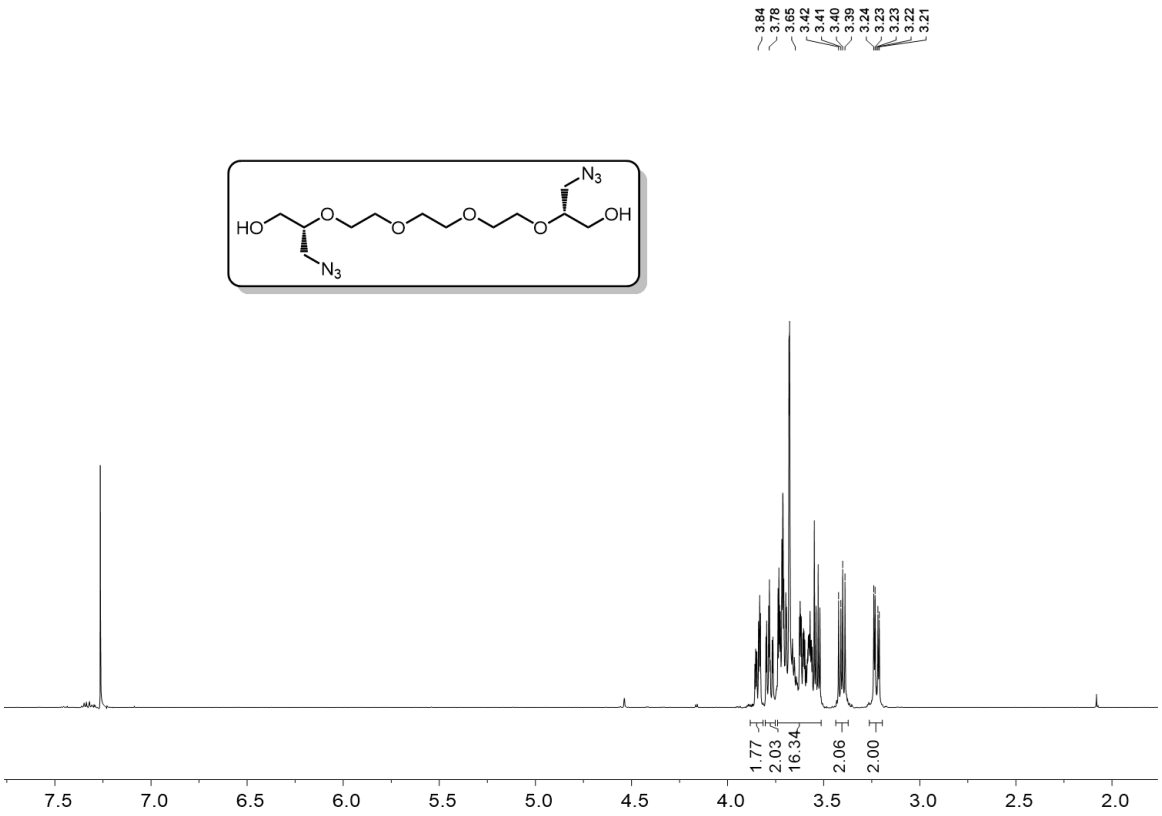

Figure 2.6.15. Pentaethyleneglycol diazide ^{1}H NMR.

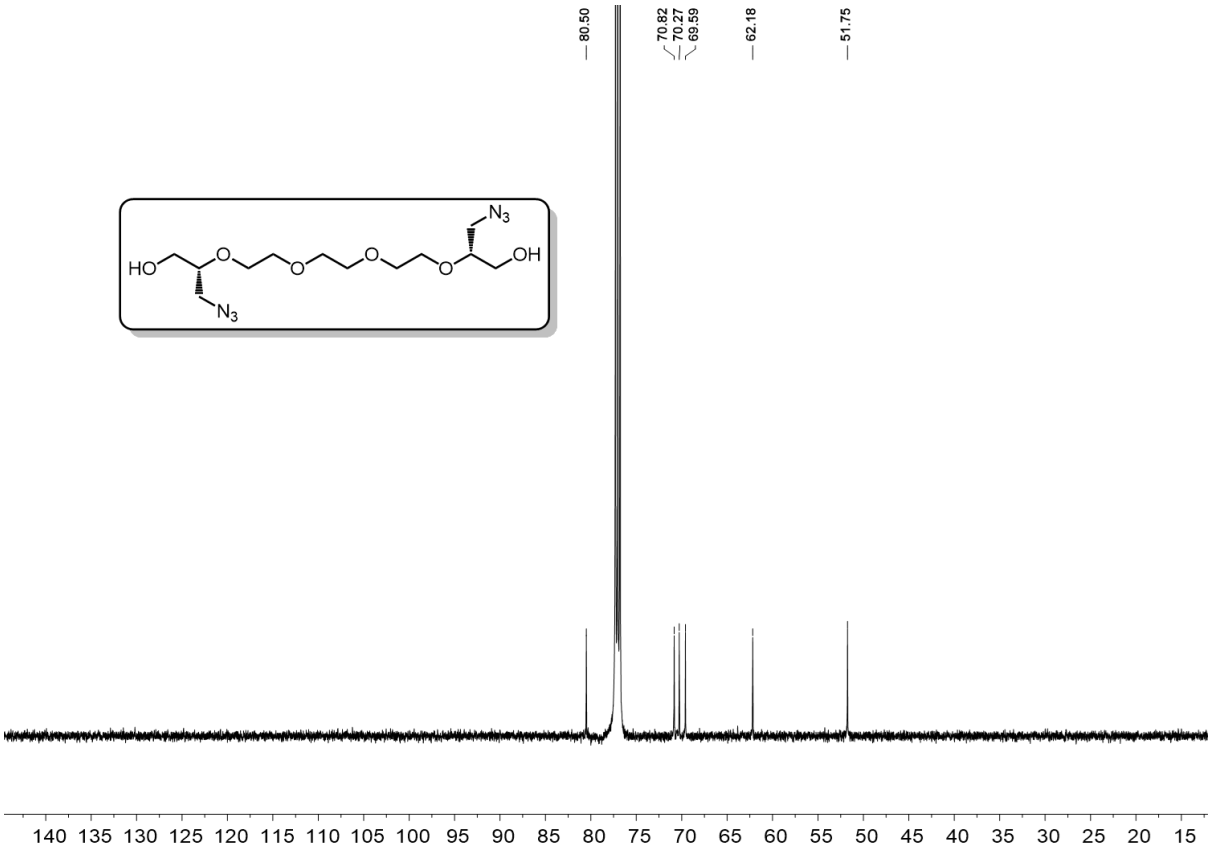

Figure 2.6.16. Pentaethyleneglycol diazide ^{13}C NMR.

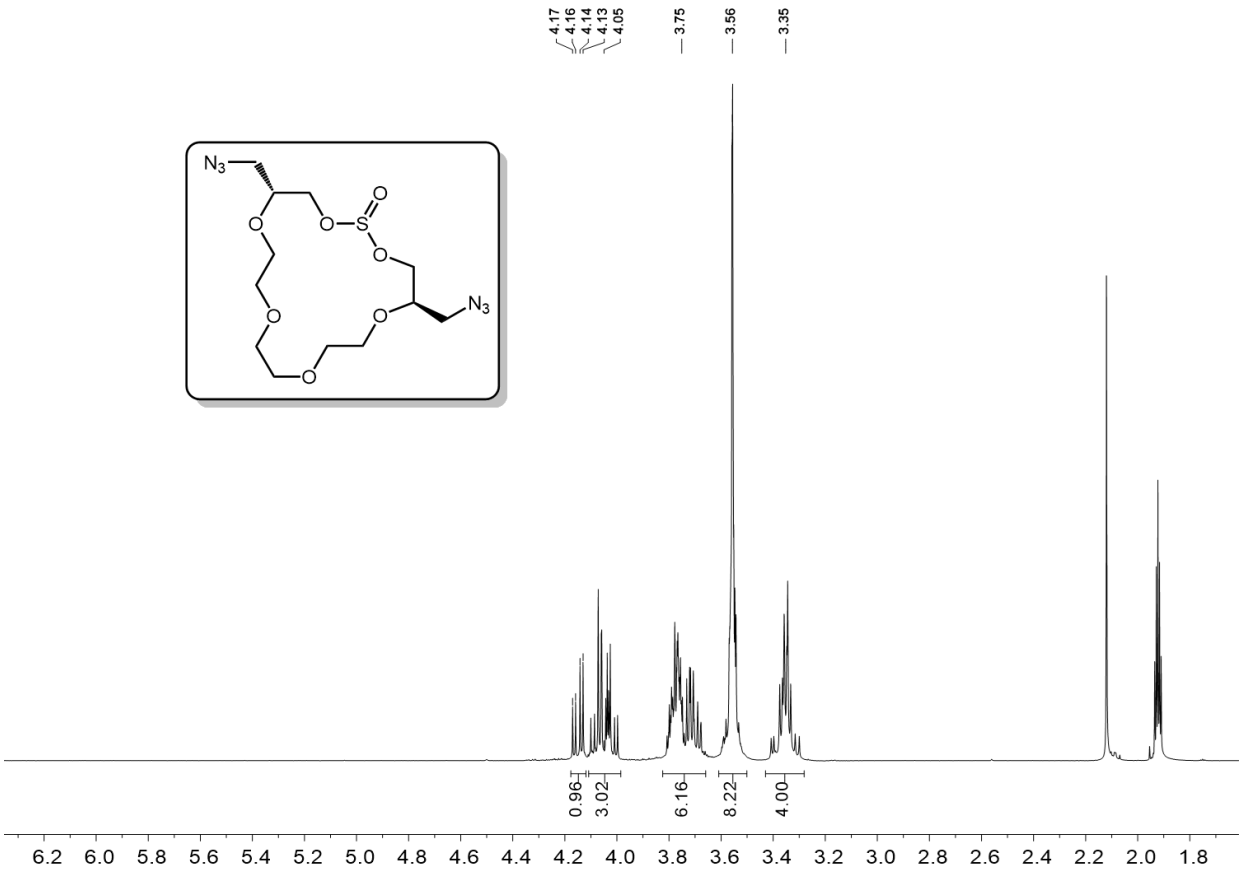

Figure 2.6.17. Pentaethyleneglycol macrocyclic sulfite ^{1}H NMR.

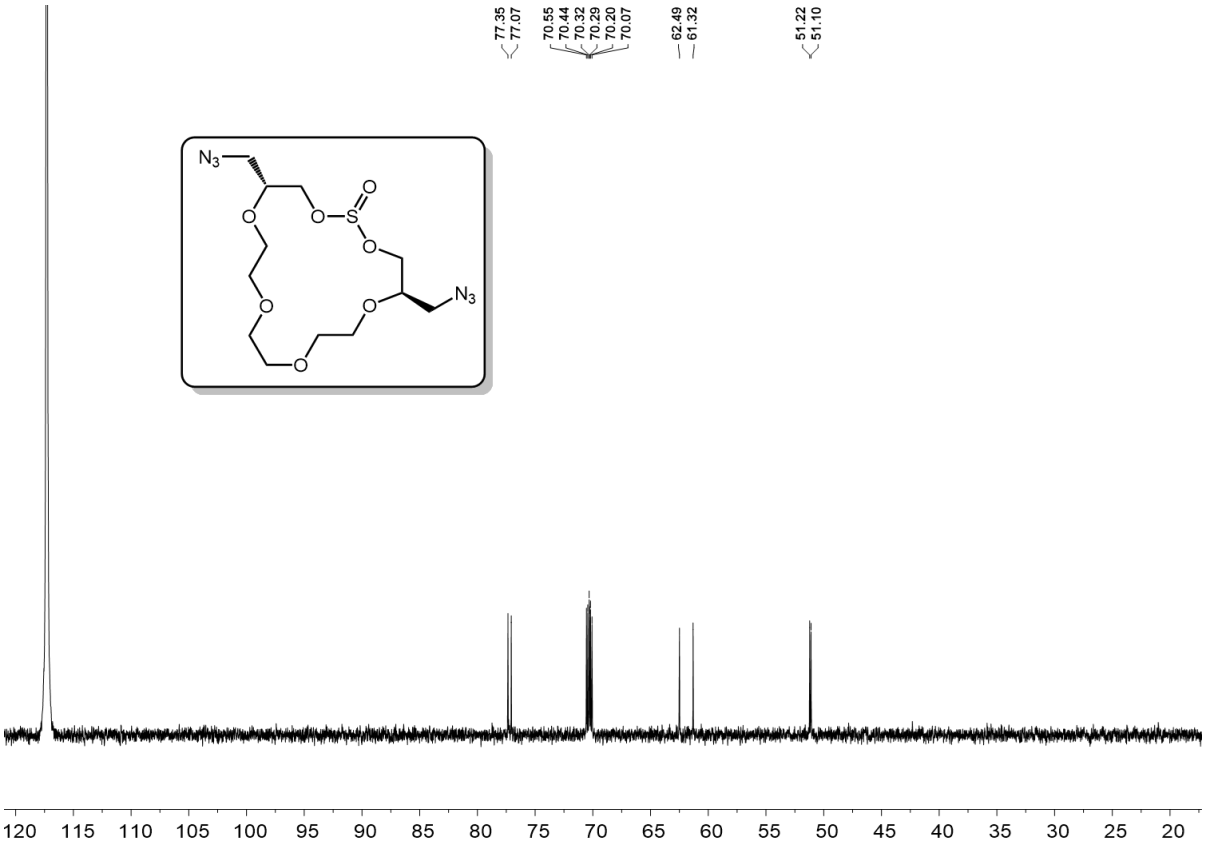

Figure 2.6.18. Pentaethyleneglycol macrocyclic sulfite ^{13}C NMR.

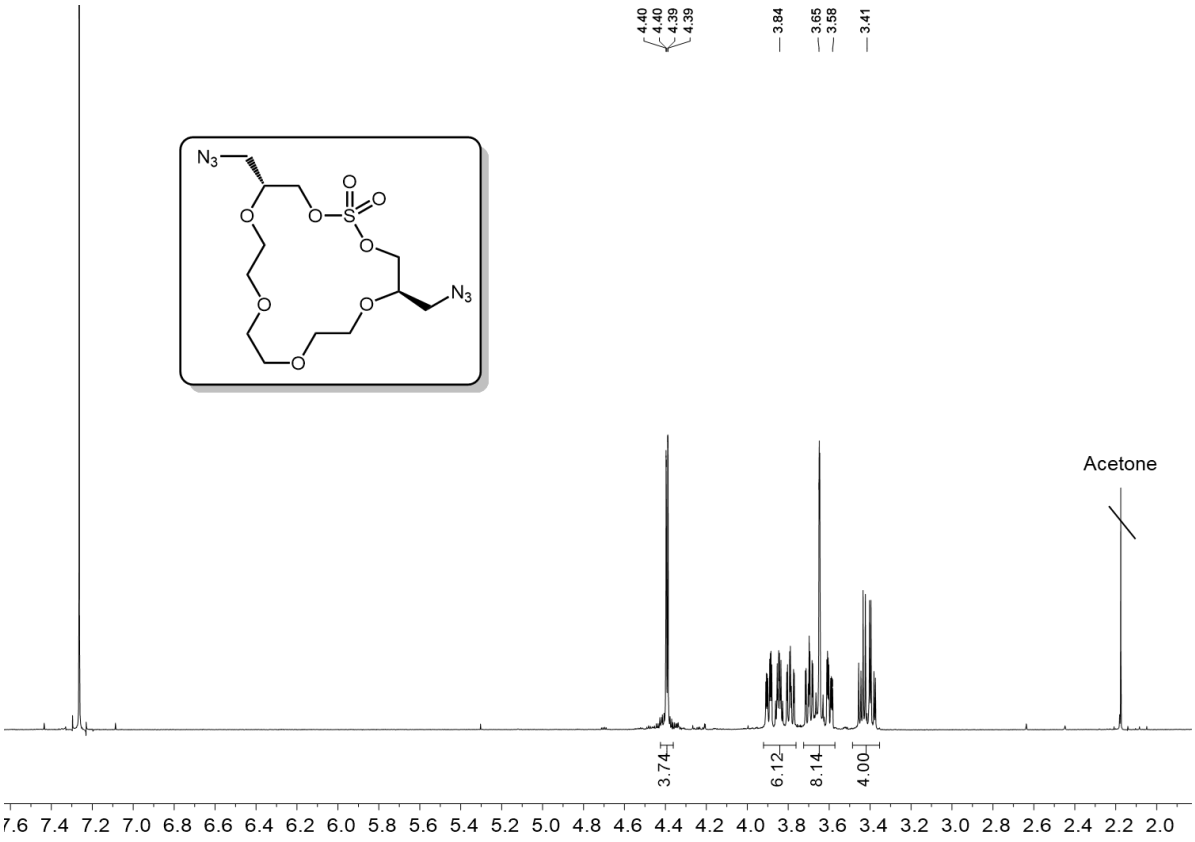

Figure 2.6.19. Pentaethyleneglycol macrocyclic sulfate ^{1}H NMR.

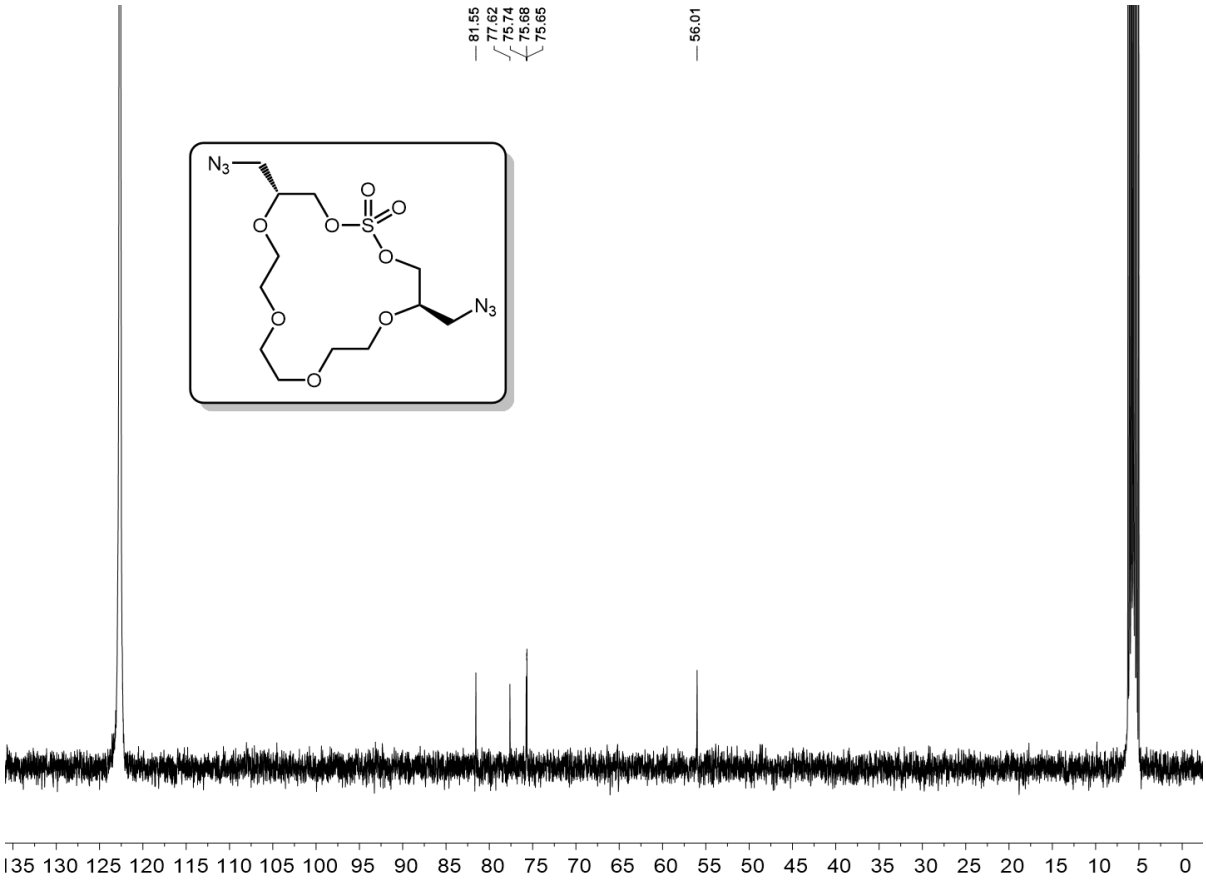

Figure 2.6.20. Pentaethyleneglycol macrocyclic sulfate ^{13}C NMR.

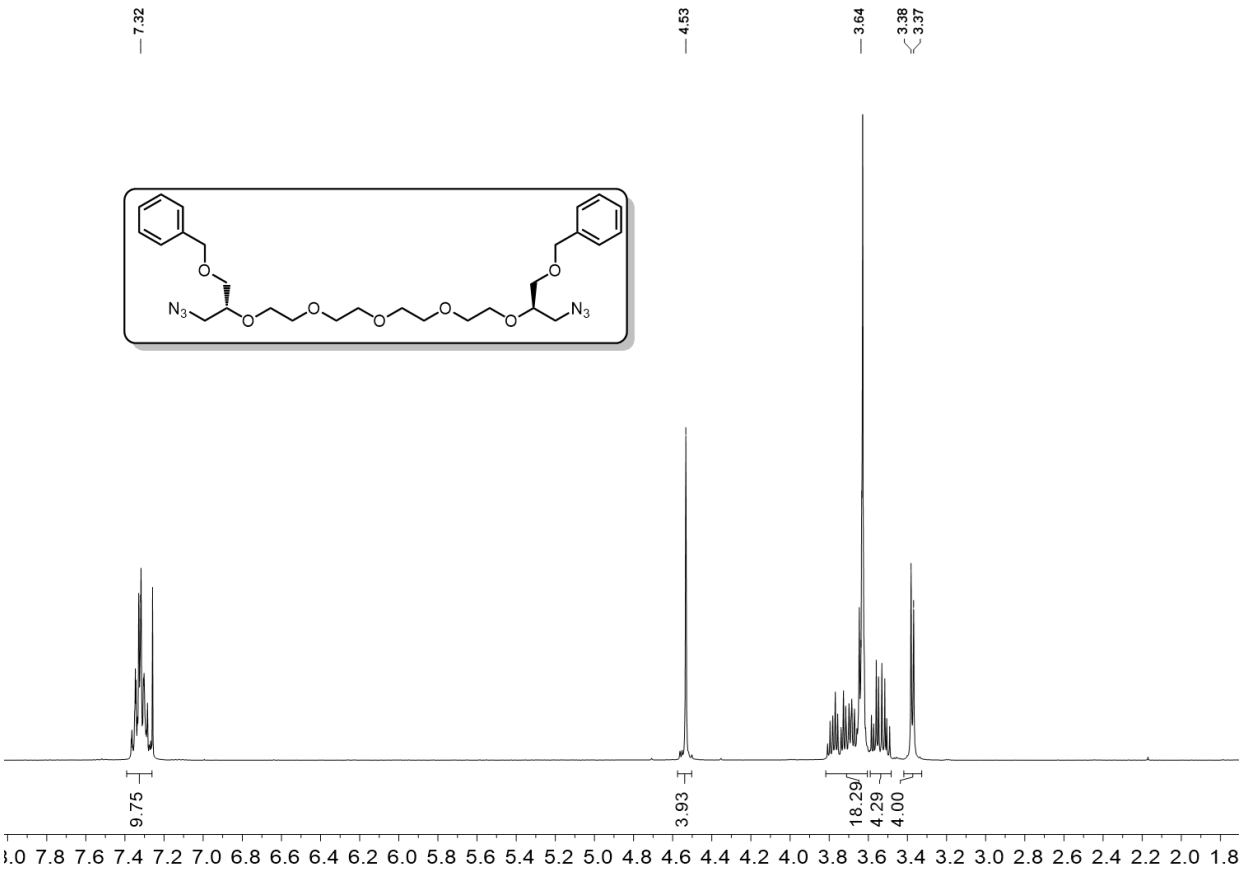

Figure 2.6.21. Dibenzylazide hexaethyleneglycol ^{1}H NMR.

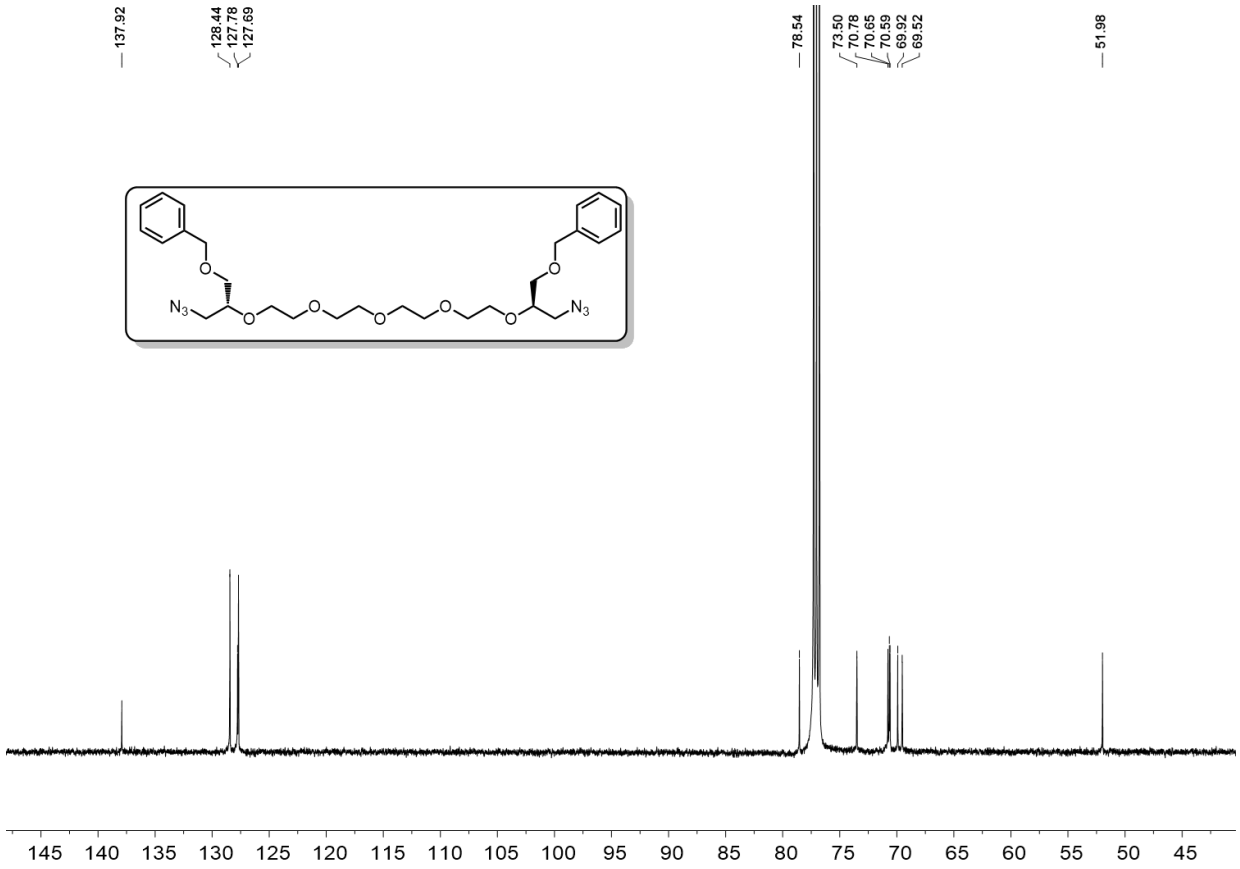

Figure 2.6.22. Dibenzylazide hexaethyleneglycol ^{13}C NMR.

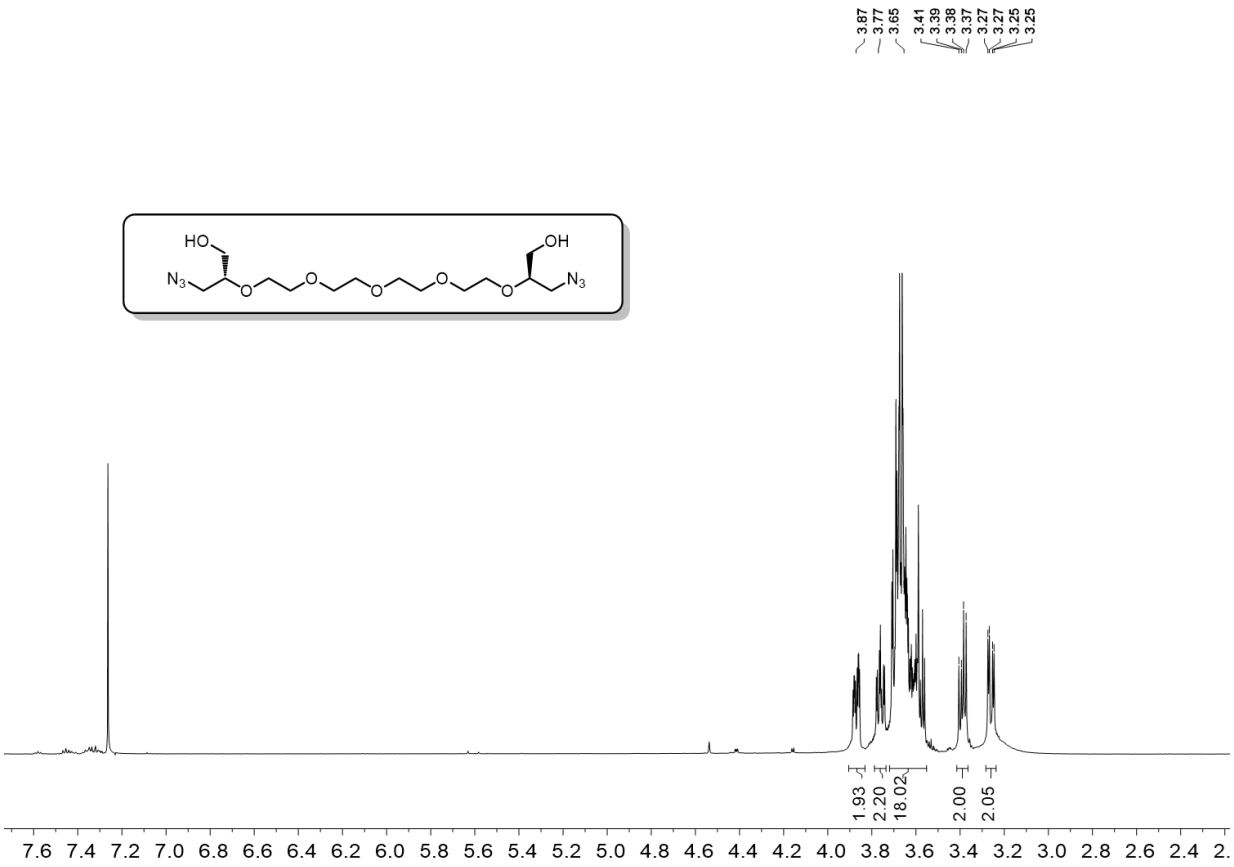

Figure 2.6.23. Hexaethyleneglycol diazide ^{1}H NMR.

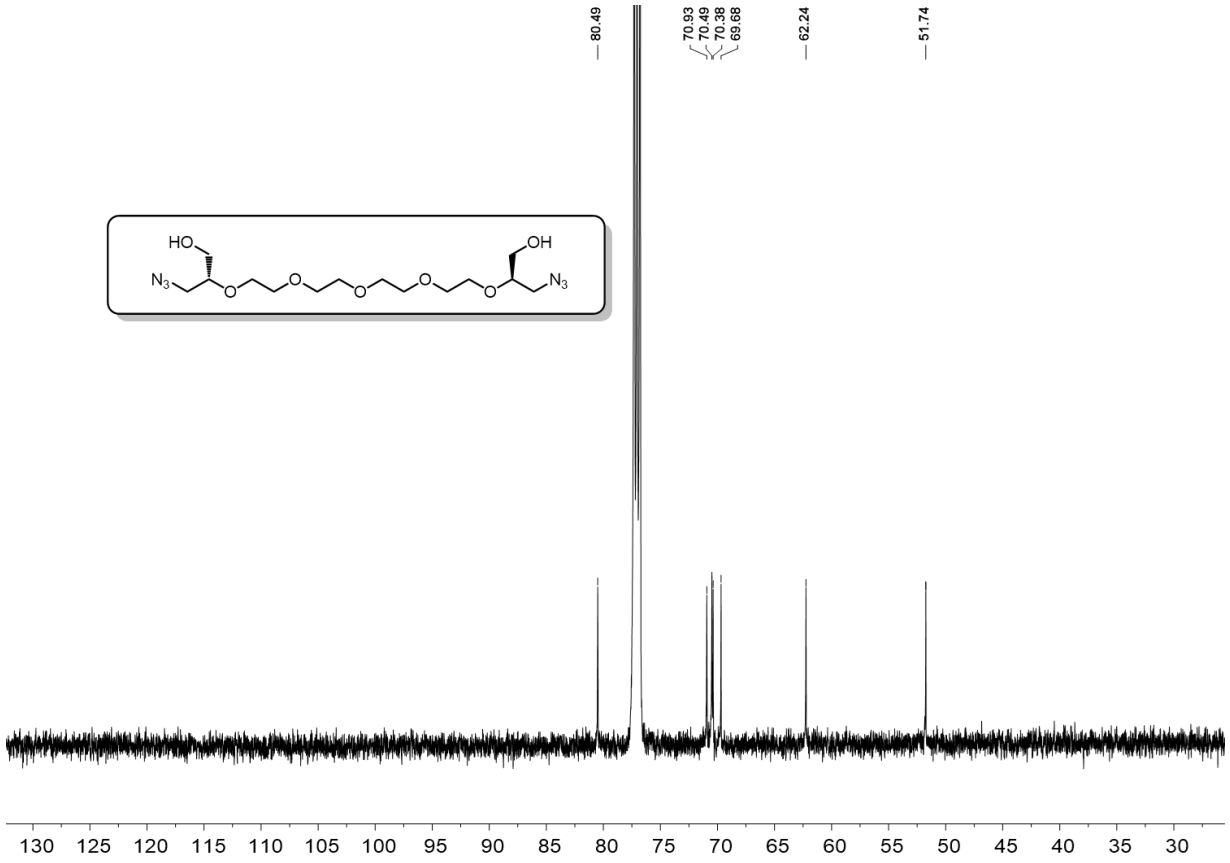

Figure 2.6.24. Hexaethyleneglycol diazide ^{13}C NMR.

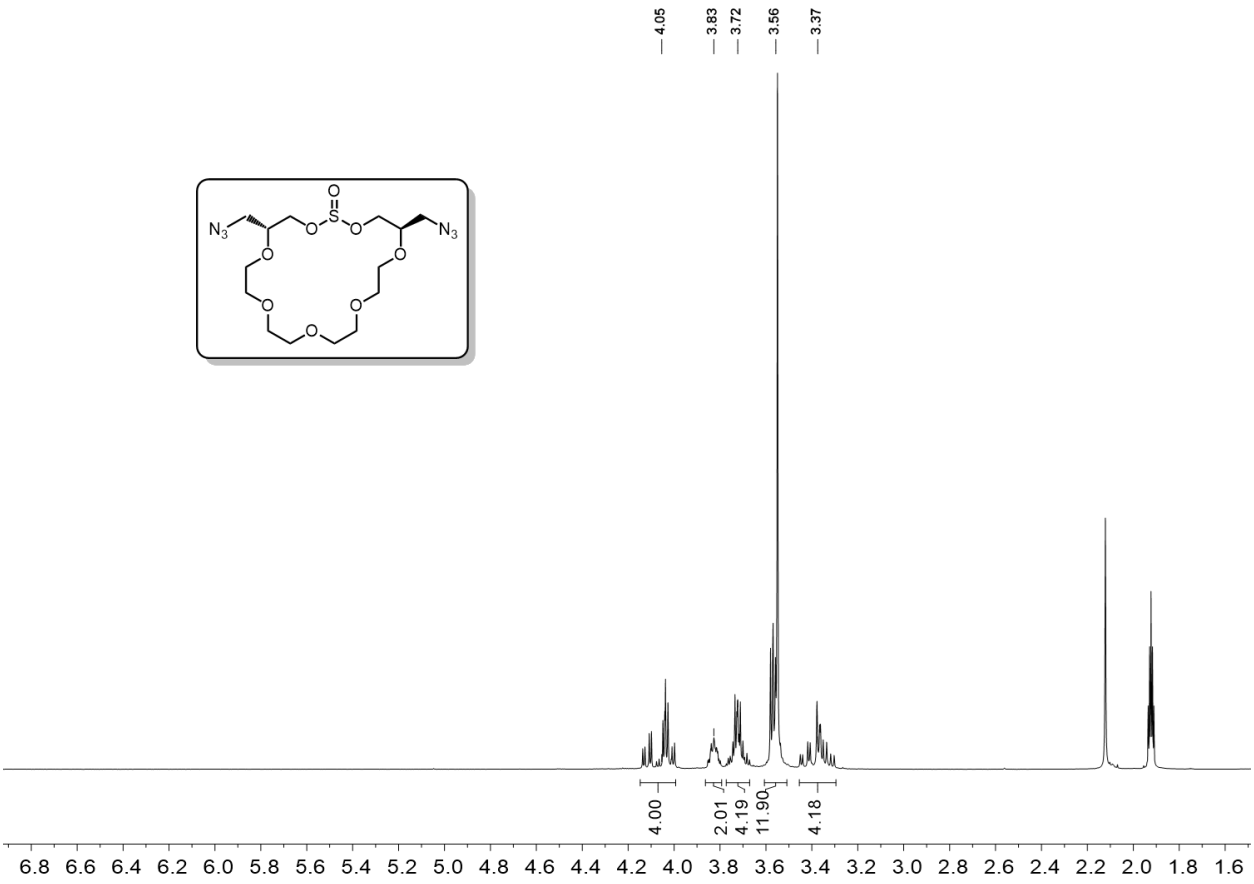

Figure 2.6.25. Hexaethyleneglycol diazide macrocyclic sulfite ^{1}H NMR.

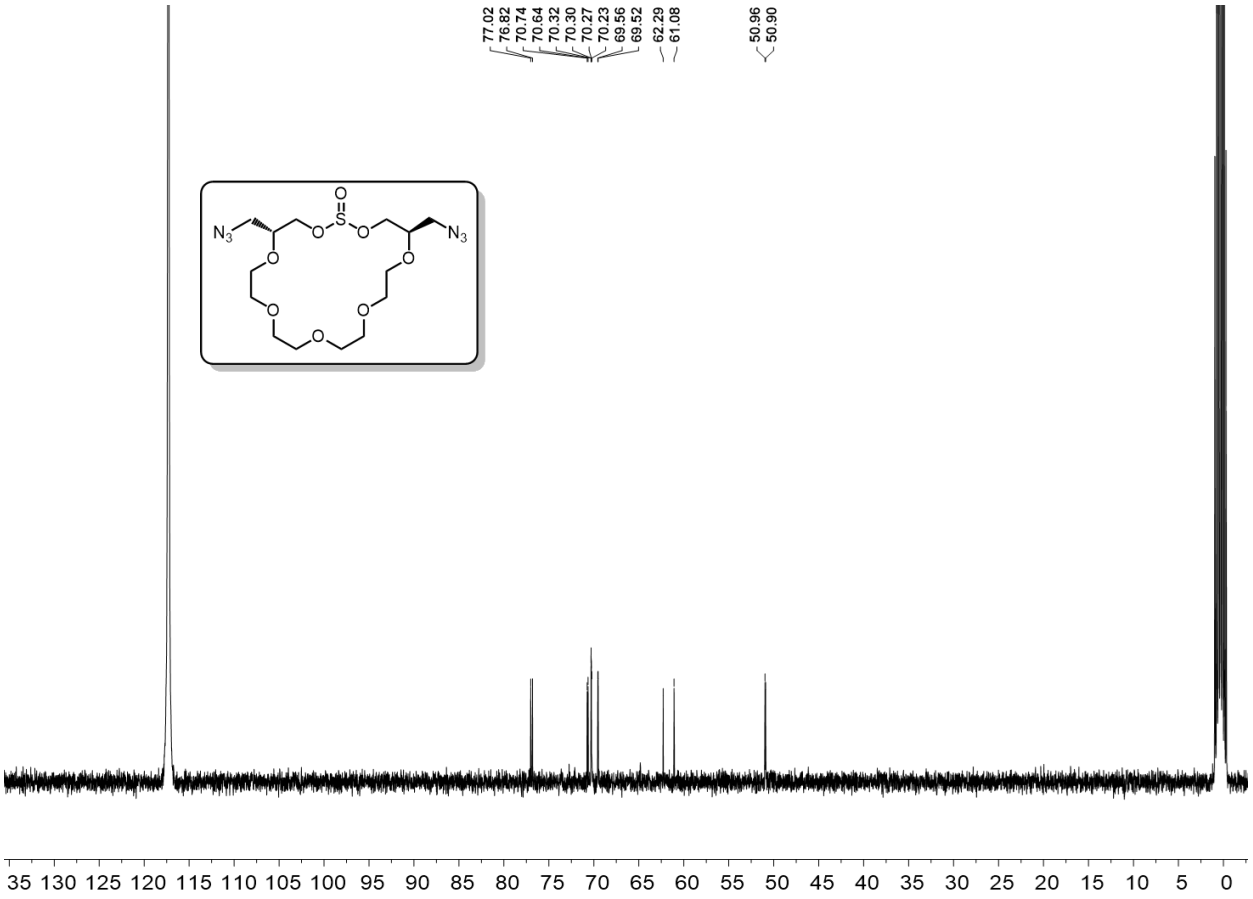

Figure 2.6.26. Hexaethyleneglycol diazide macrocyclic sulfite ^{13}C NMR.

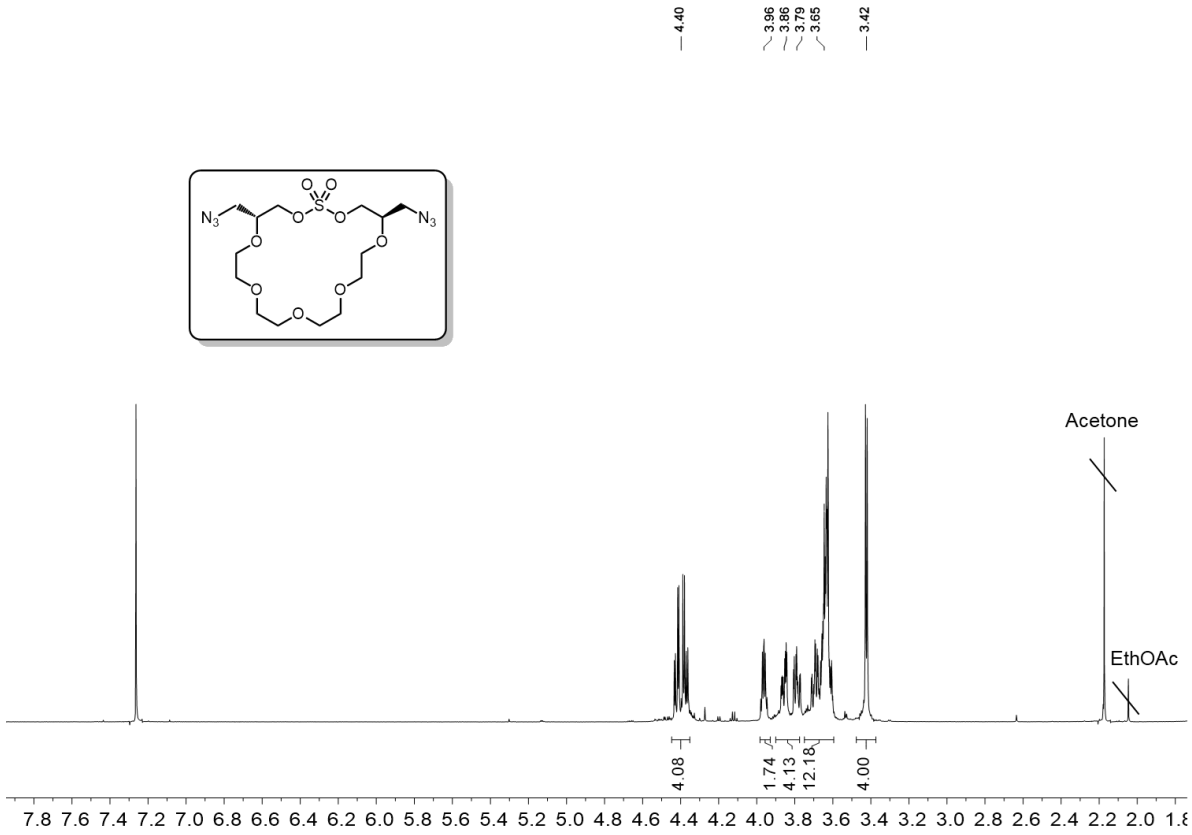

Figure 2.6.27. Hexaethyleneglycol diazide macrocyclic sulfate ^{1}H NMR.

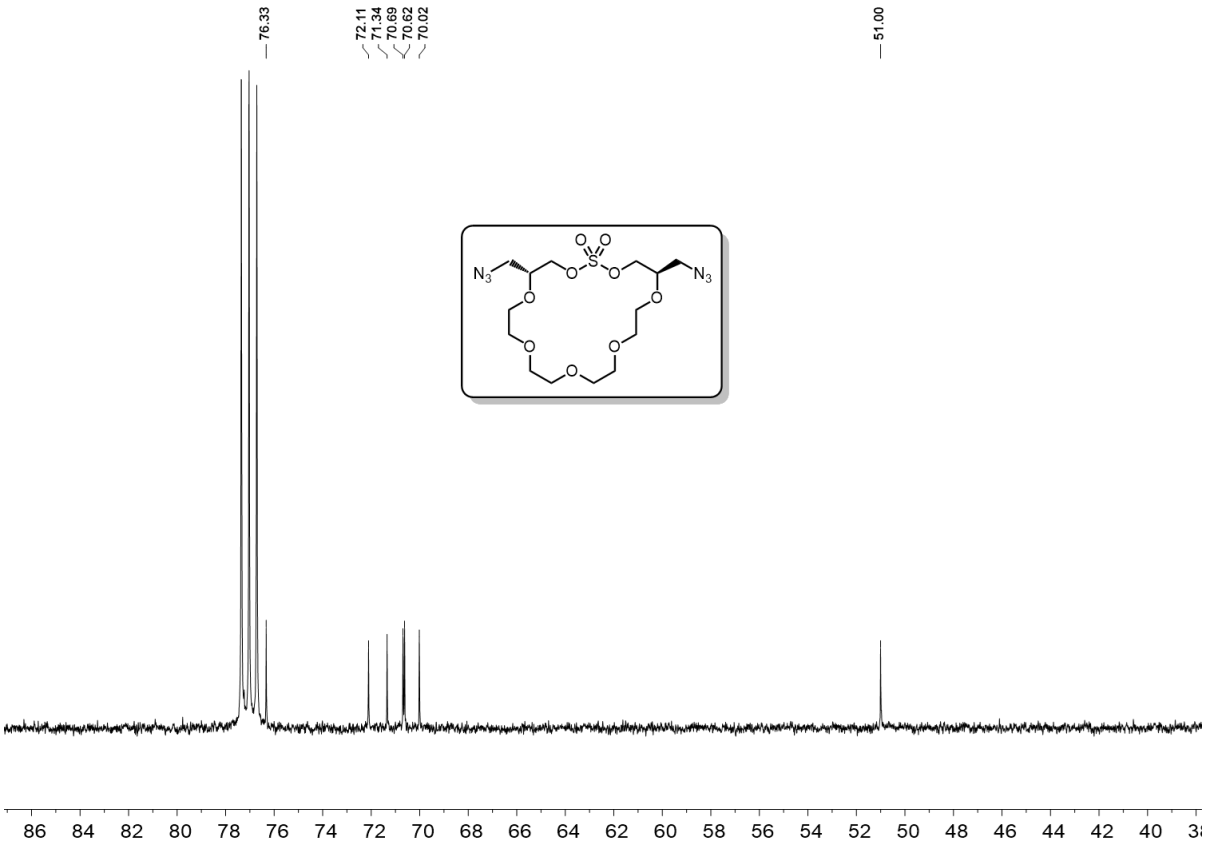

Figure 2.6.28. Hexaethyleneglycol diazide macrocyclic sulfate ^{13}C NMR.

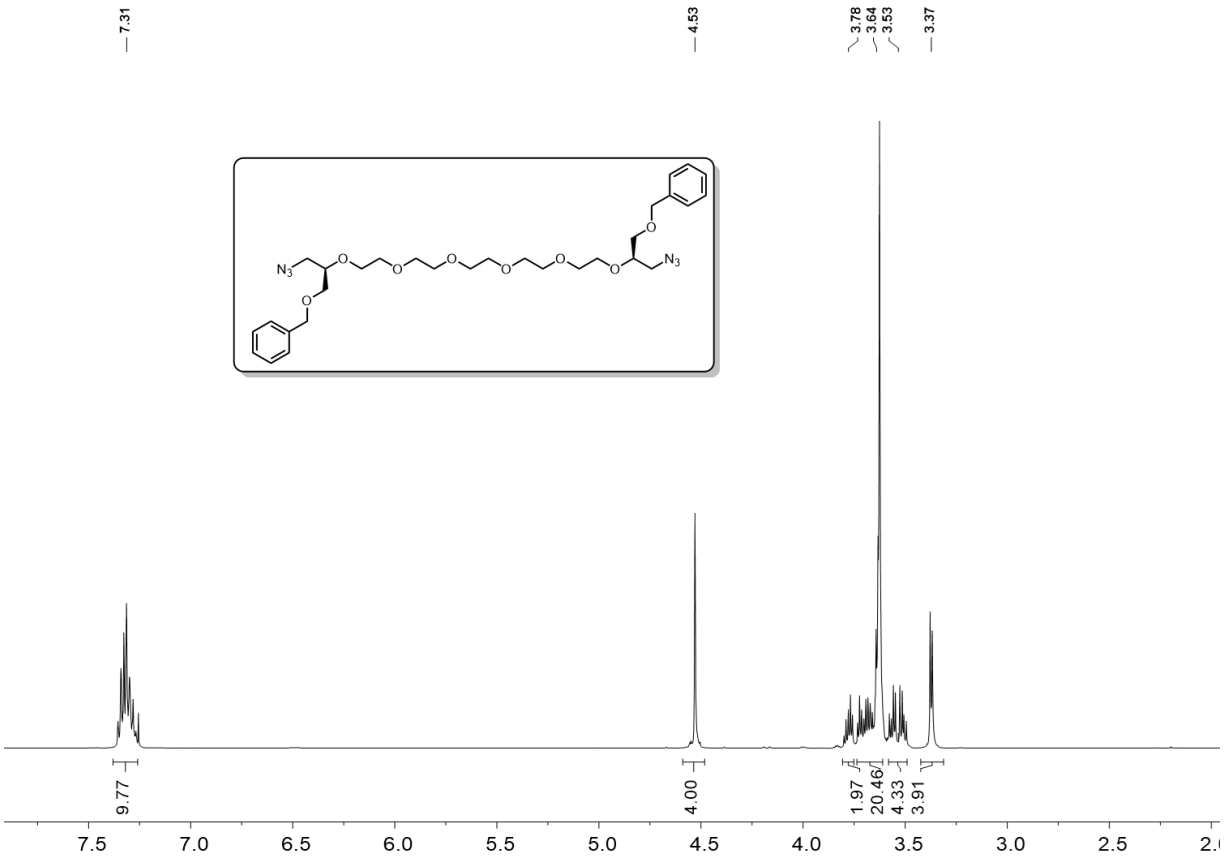

Figure 2.6.29. Dibenzylazide heptaethyleneglycol ^{1}H NMR.

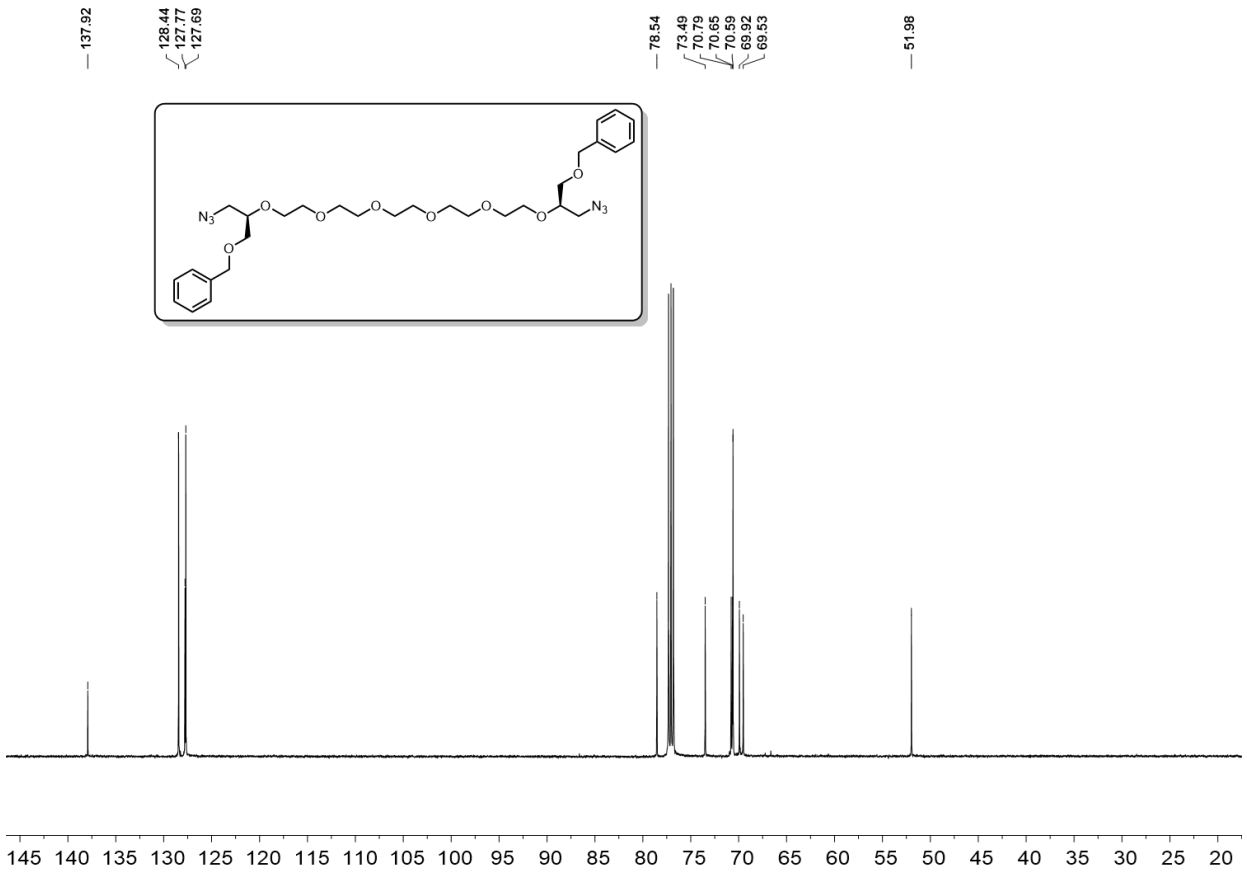

Figure 2.6.30. Dibenzylazide heptaethyleneglycol ^{13}C NMR.

Figure 2.6.31. Heptaethyleneglycol diazide ^{1}H NMR.

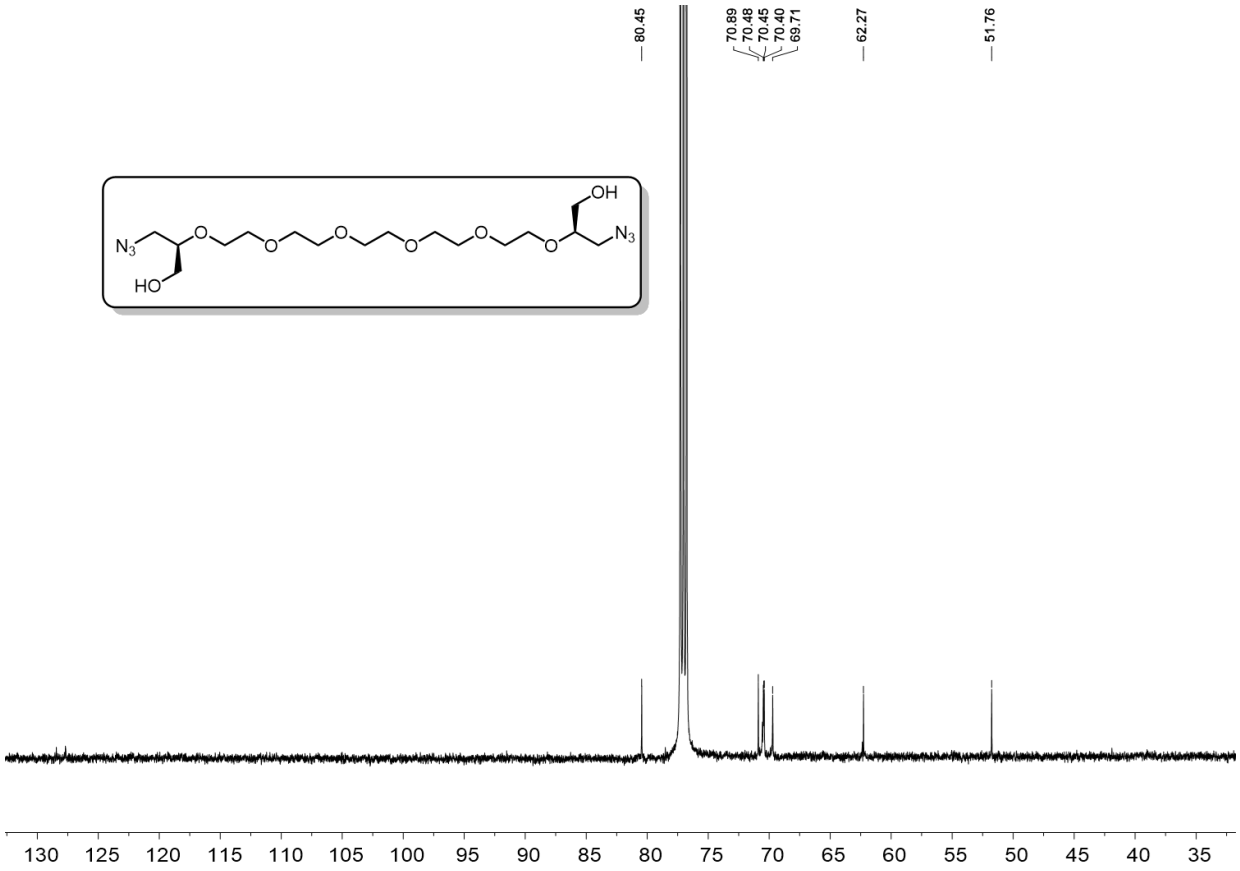

Figure 2.6.31. Heptaethyleneglycol diazide ^{13}C NMR.

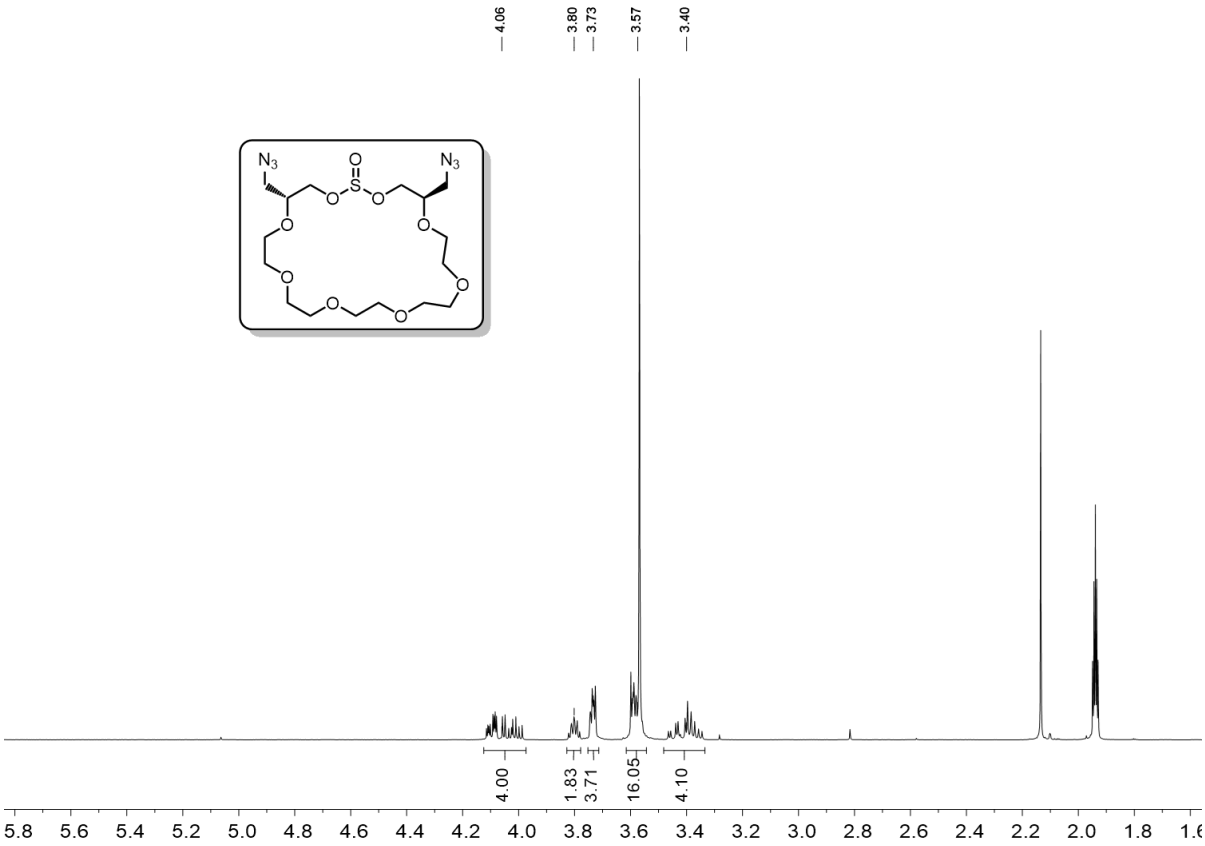

Figure 2.6.32. Heptaethyleneglycol diazide macrocyclic sulfite ^{1}H NMR.

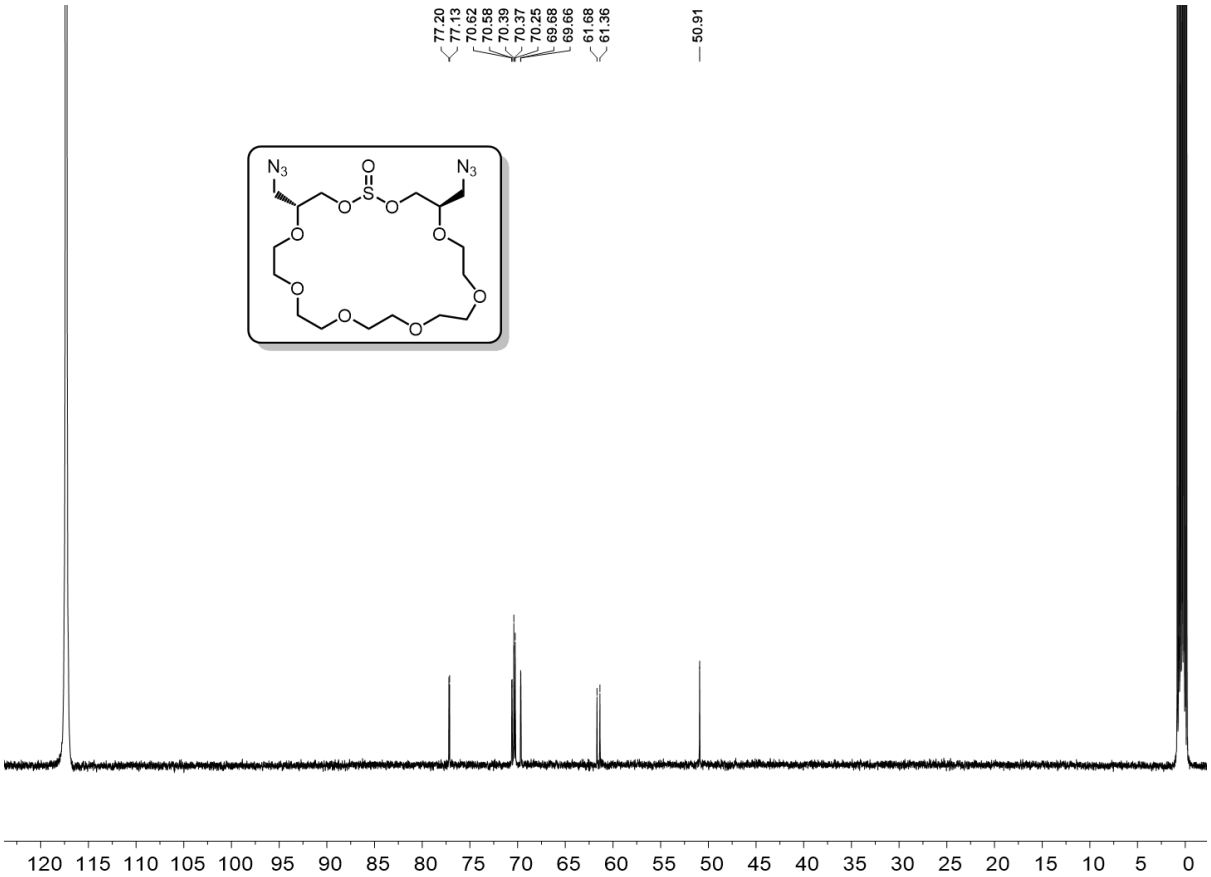

Figure 2.6.33. Heptaethyleneglycol diazide macrocyclic sulfite ^{13}C NMR.

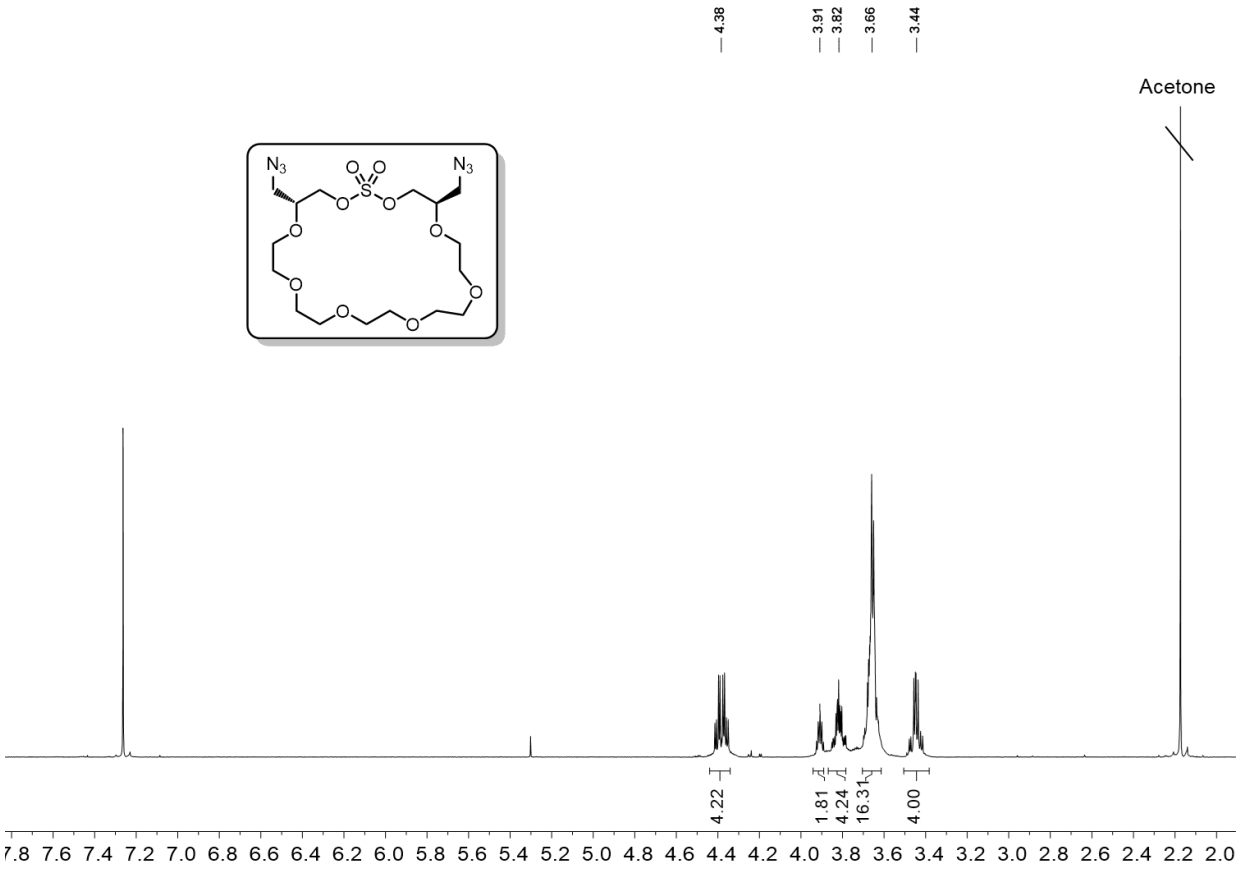

Figure 2.6.34. Heptaethyleneglycol diazide macrocyclic sulfate ^{1}H NMR.

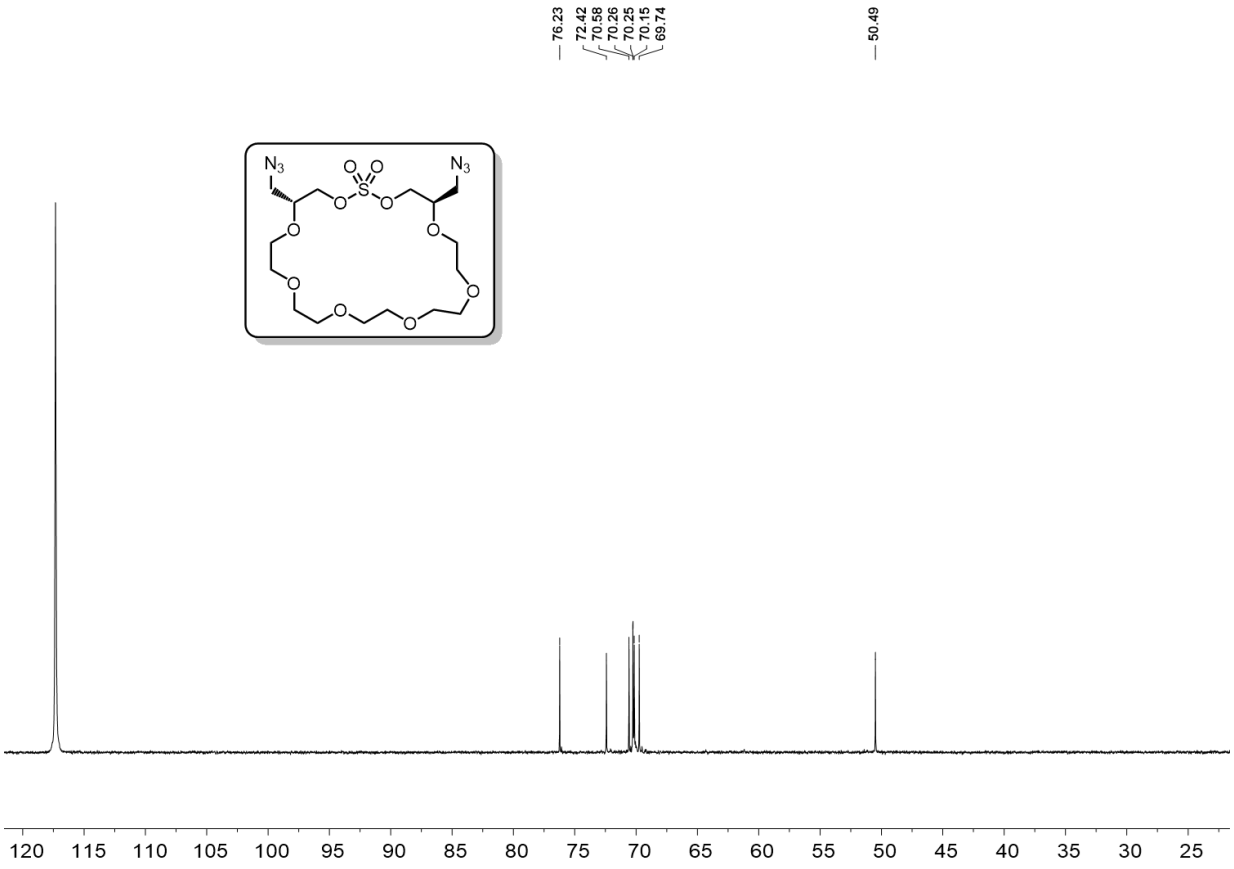

Figure 2.6.35. Heptaethyleneglycol diazide macrocyclic sulfate ^{13}C NMR.

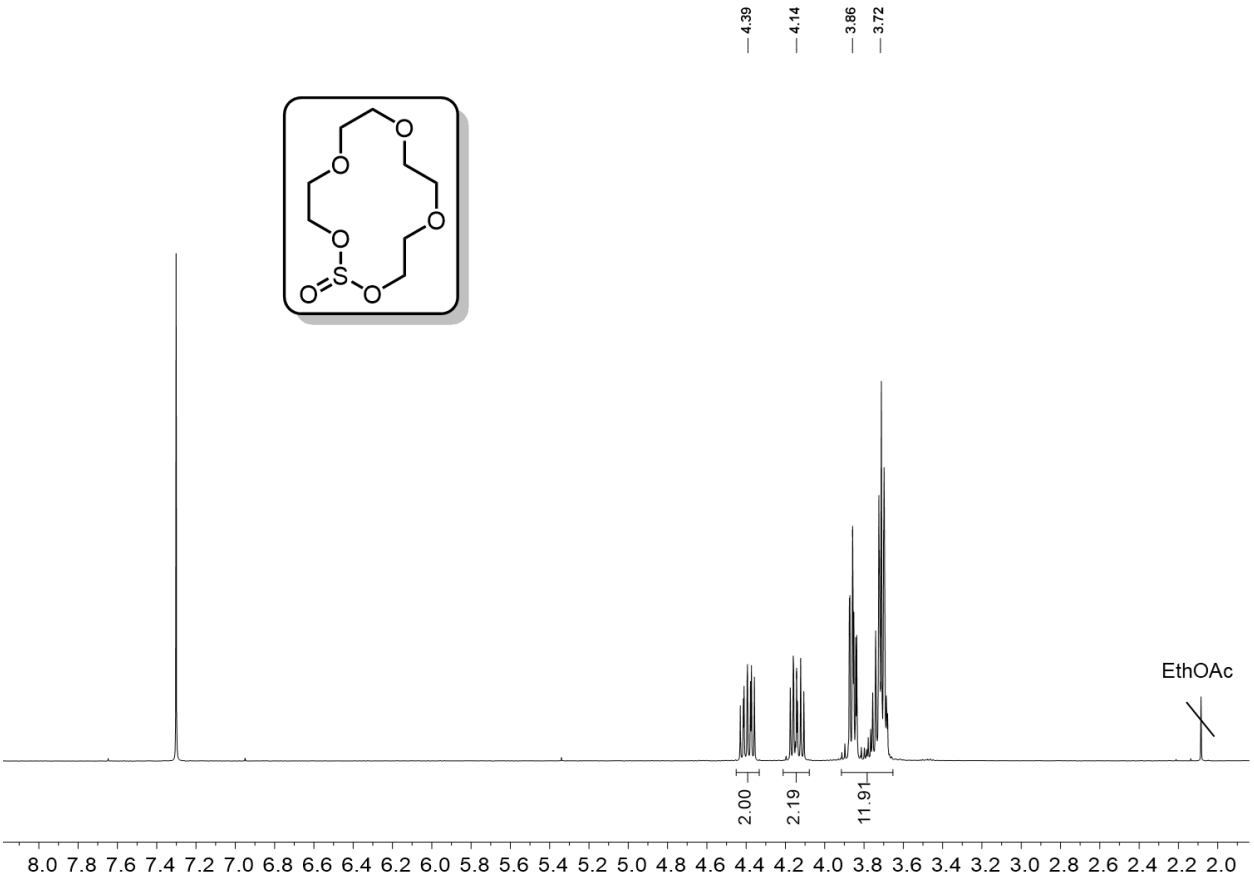

Figure 2.6.36. Tetraethyleneglycol macrocyclic sulfite ^{1}H NMR.

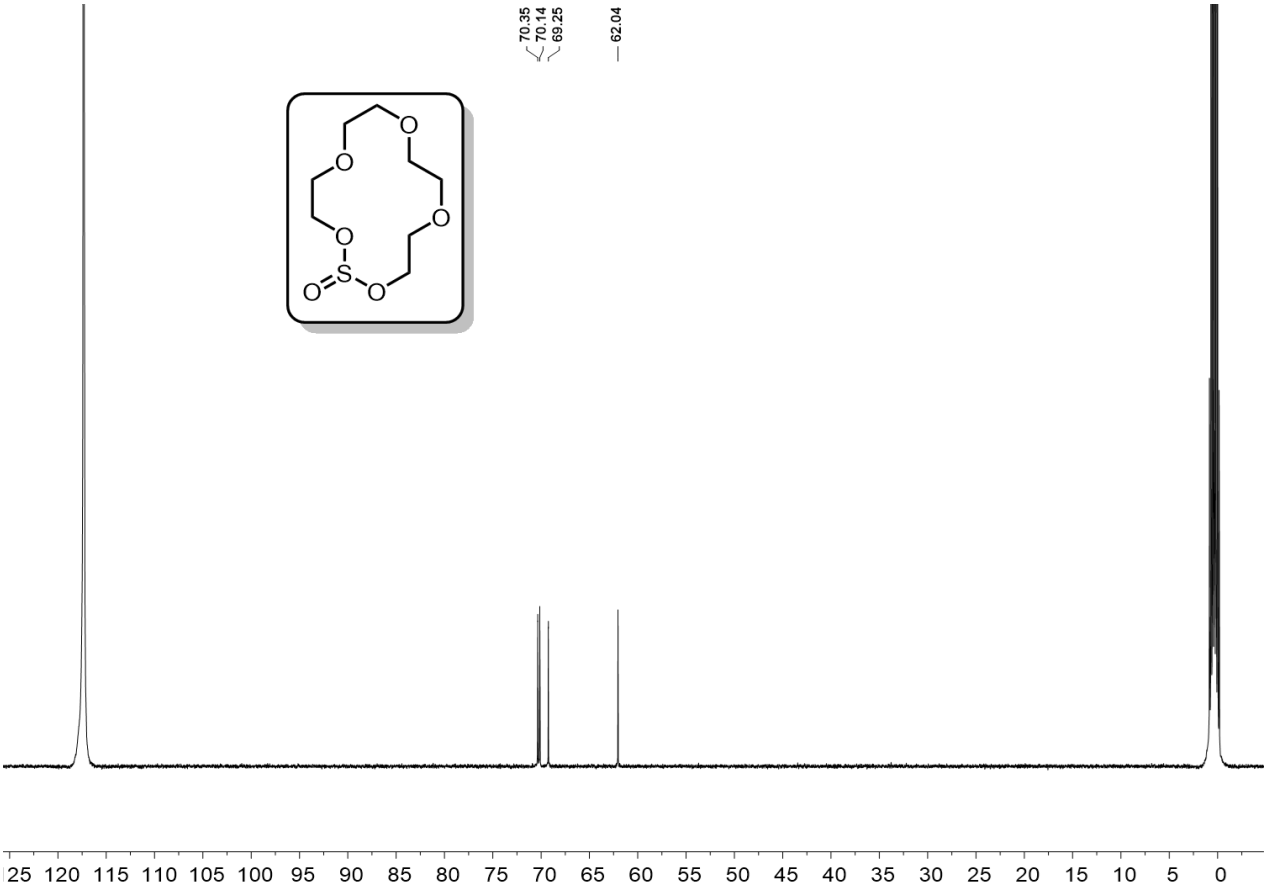

Figure 2.6.37. Tetraethyleneglycol macrocyclic sulfite ^{13}C NMR.

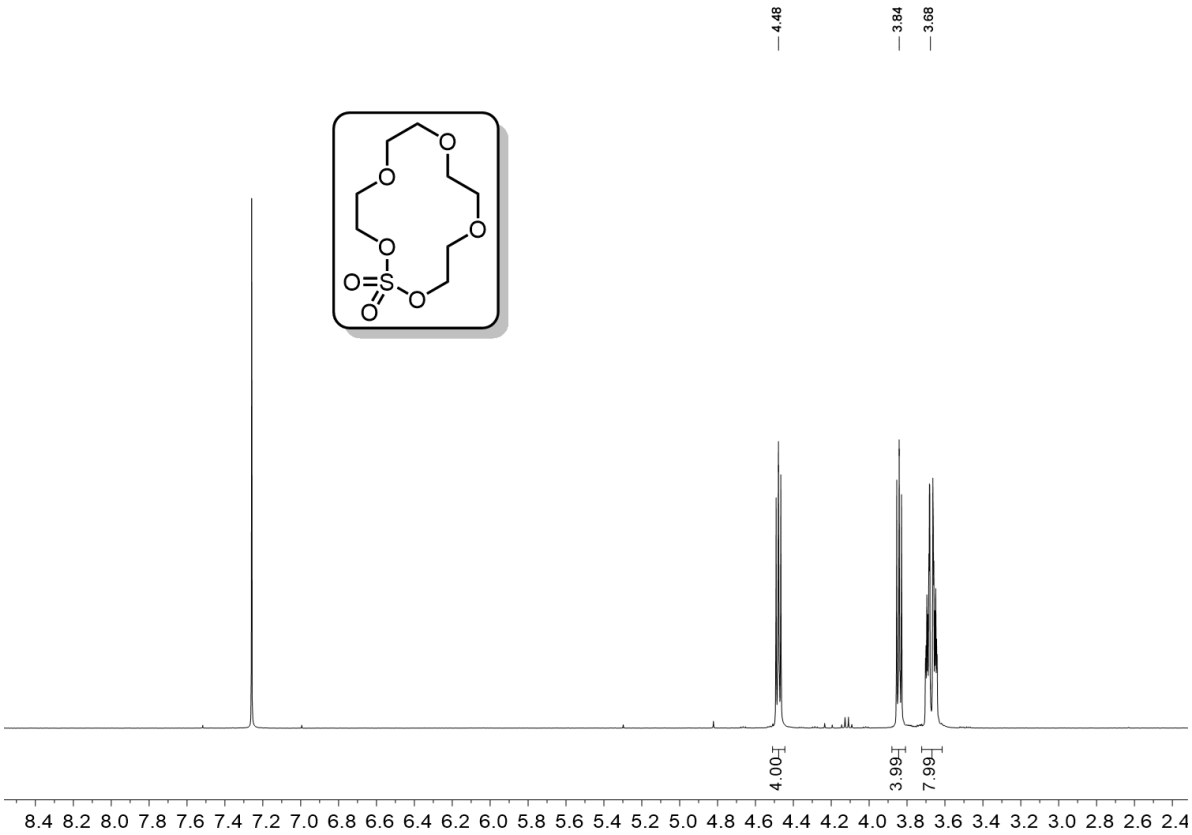

Figure 2.6.38. Tetraethyleneglycol macrocyclic sulfite ^{1}H NMR.

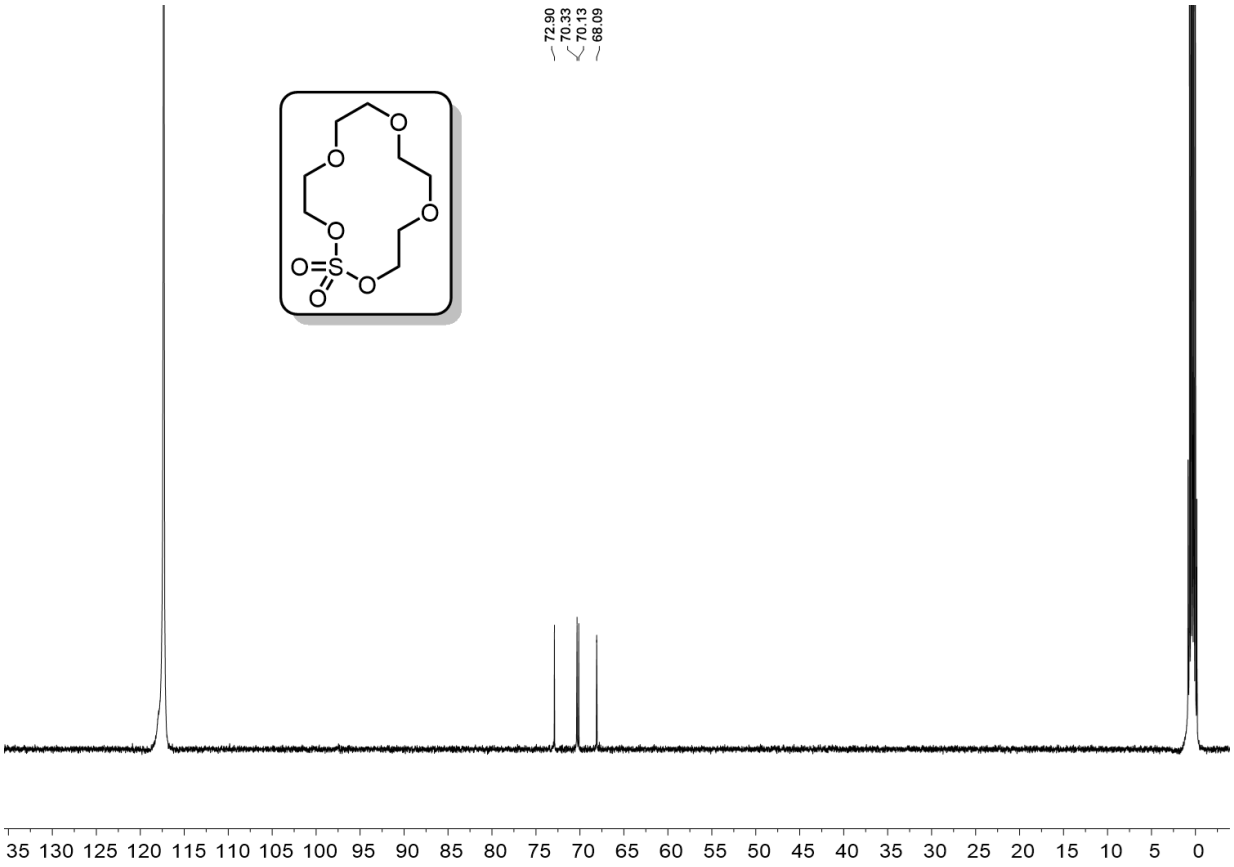

Figure 2.6.39. Tetraethyleneglycol macrocyclic sulfate ^{1}H NMR.

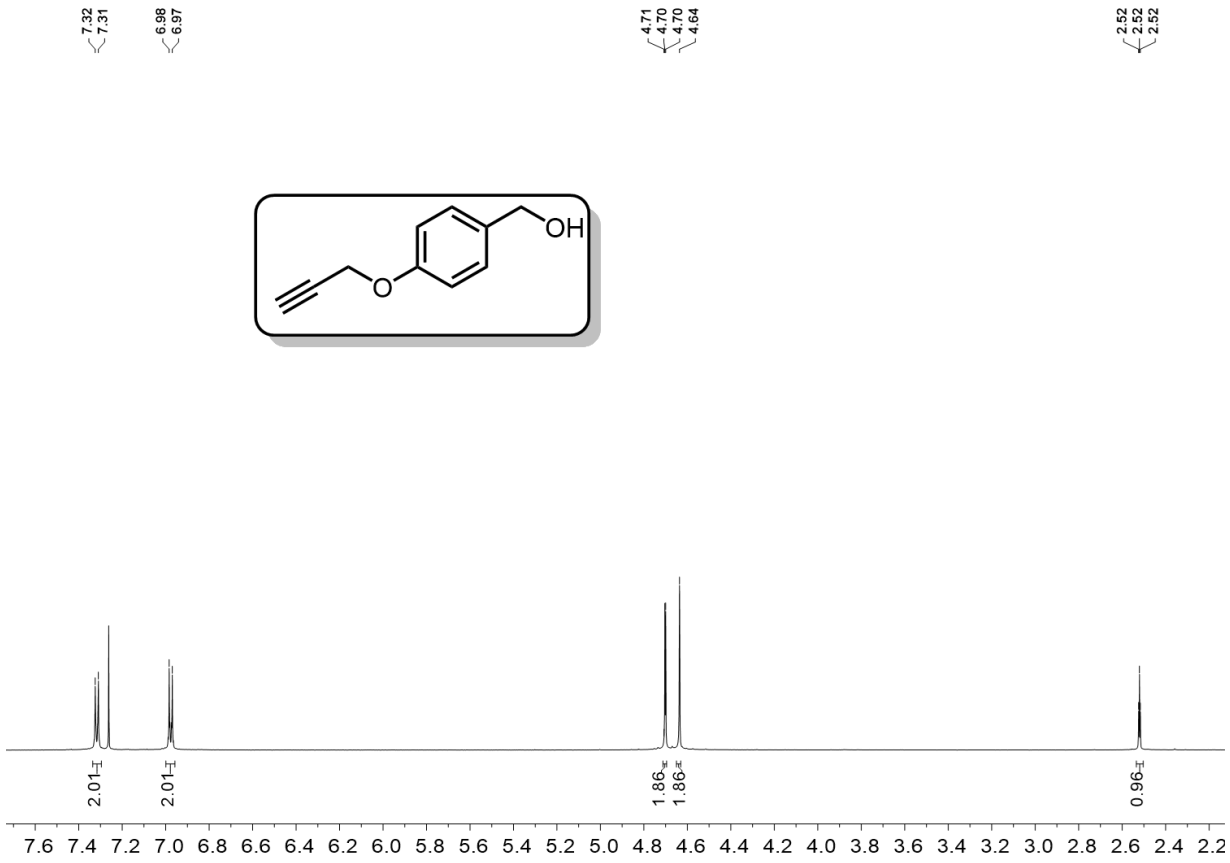

Figure 2.6.40. (4-(prop-2-yn-1-yloxy)phenyl)methanol ^{1}H NMR.

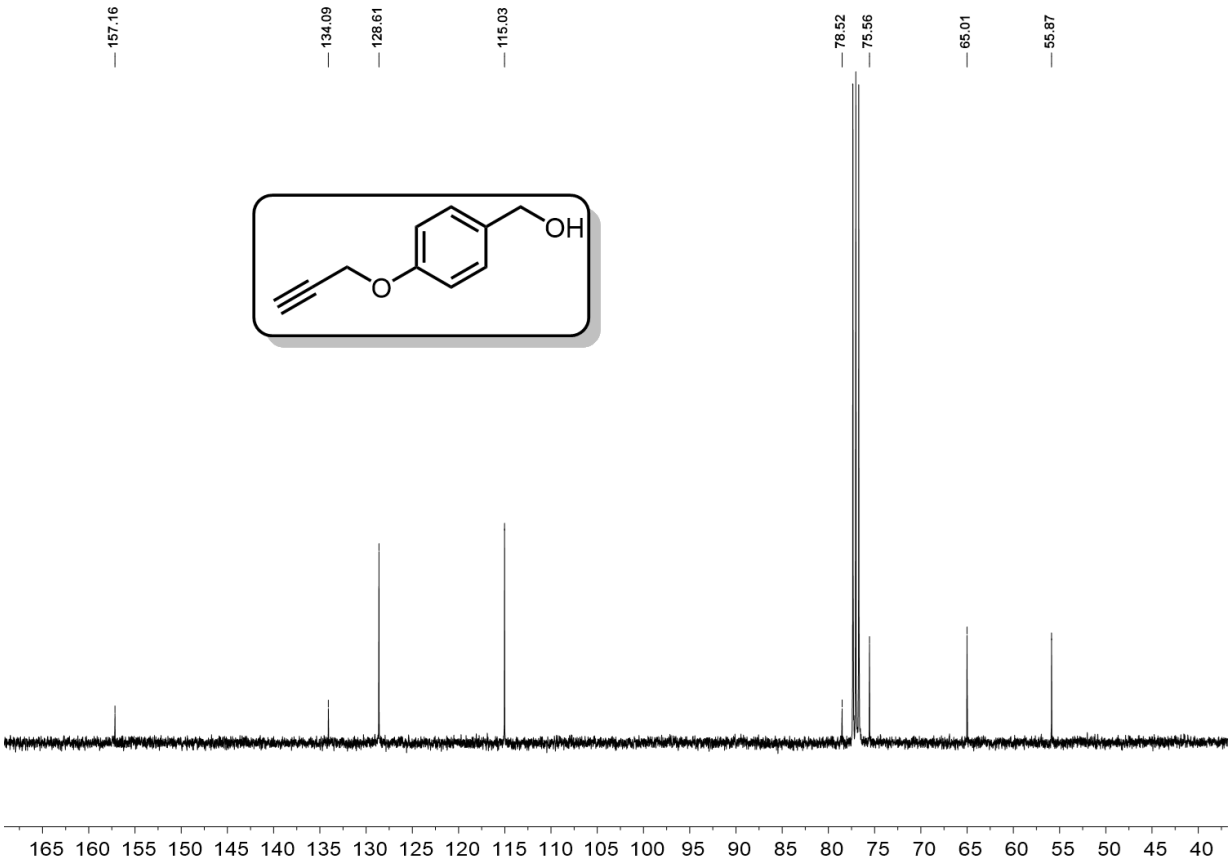

Figure 2.6.41. (4-(prop-2-yn-1-yloxy)phenyl)methanol ^{13}C NMR.

Figure 2.6.42. Diethyleneglycol ditosylate ^{1}H NMR.

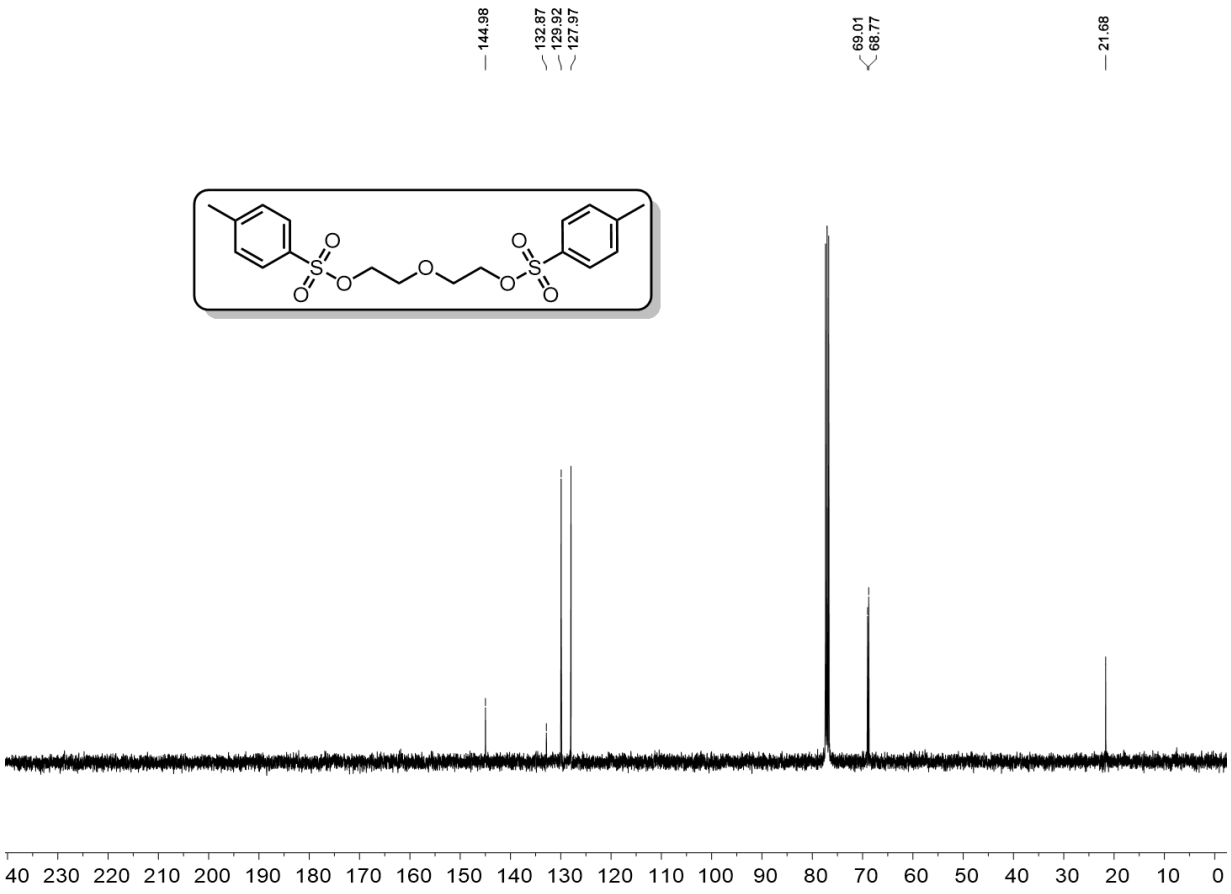

Figure 2.6.43. Diethyleneglycol ditosylate ^{13}C NMR.

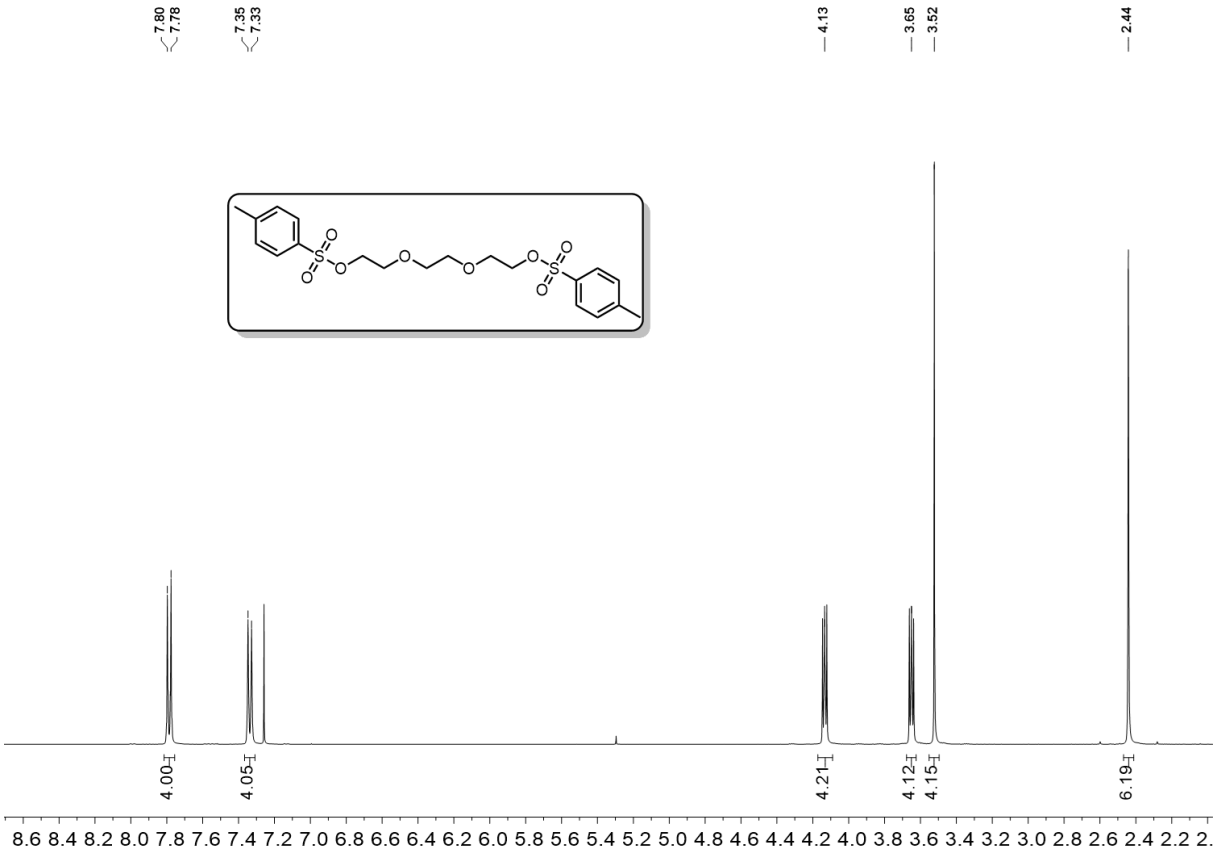

Figure 2.6.44. Triethyleneglycol ditosylate ^{1}H NMR.

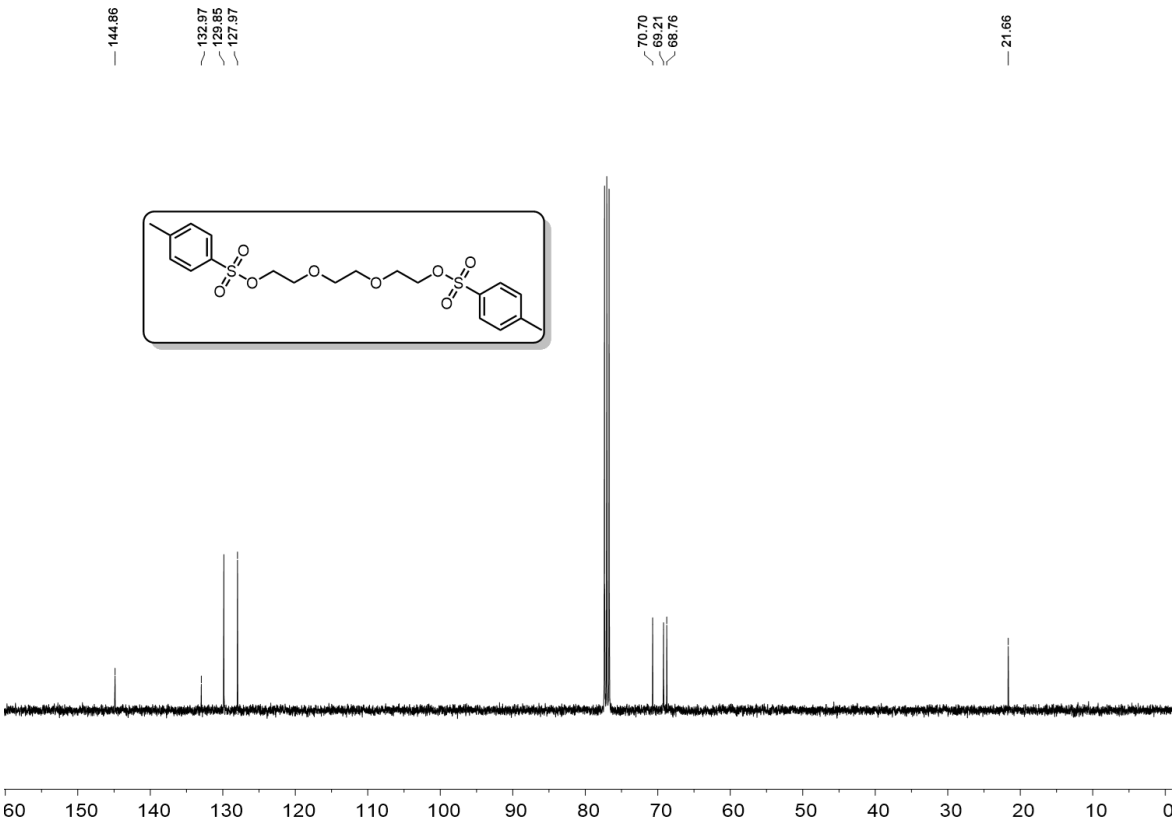

Figure 2.6.45. Triethyleneglycol ditosylate ^{13}C NMR.

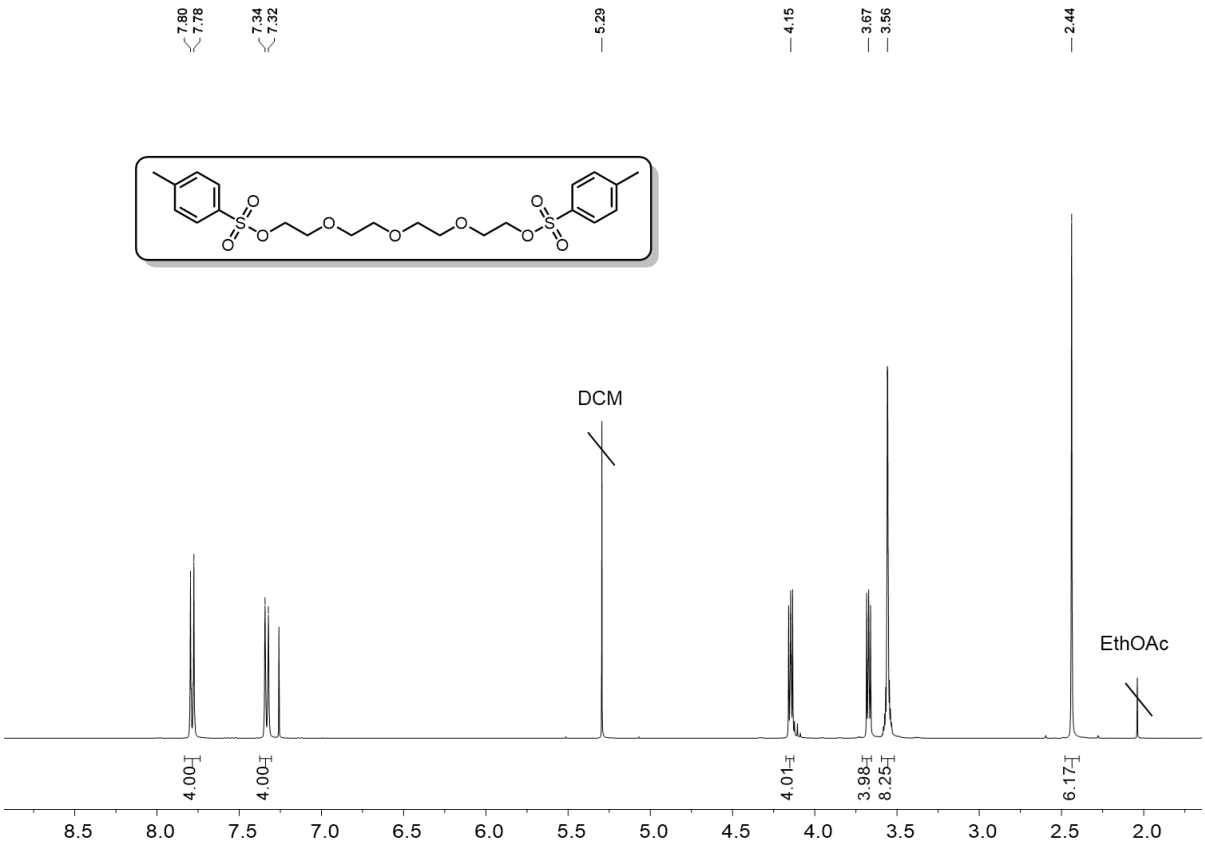

Figure 2.6.46. Tetraethyleneglycol ditosylate ^{1}H NMR.

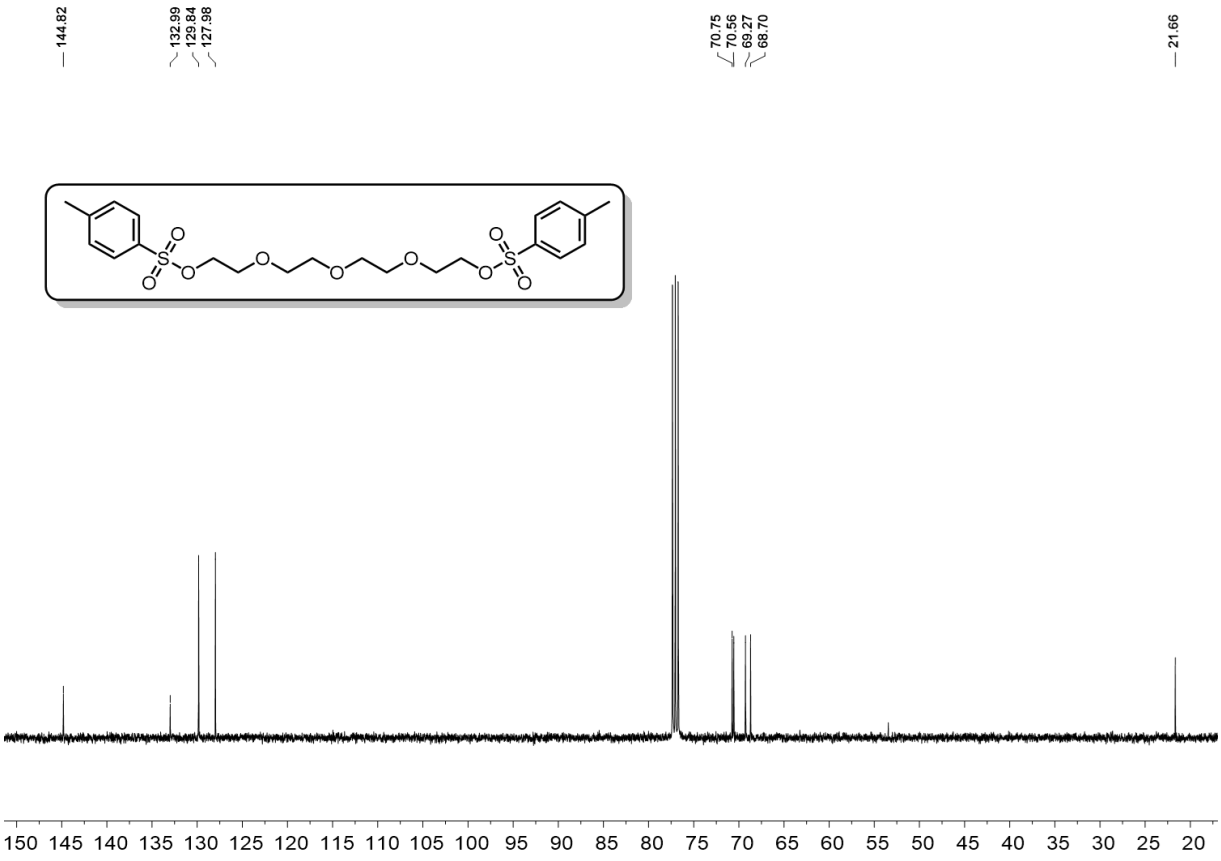

Figure 2.6.47. Tetraethyleneglycol ditosylate ^{1}H NMR.

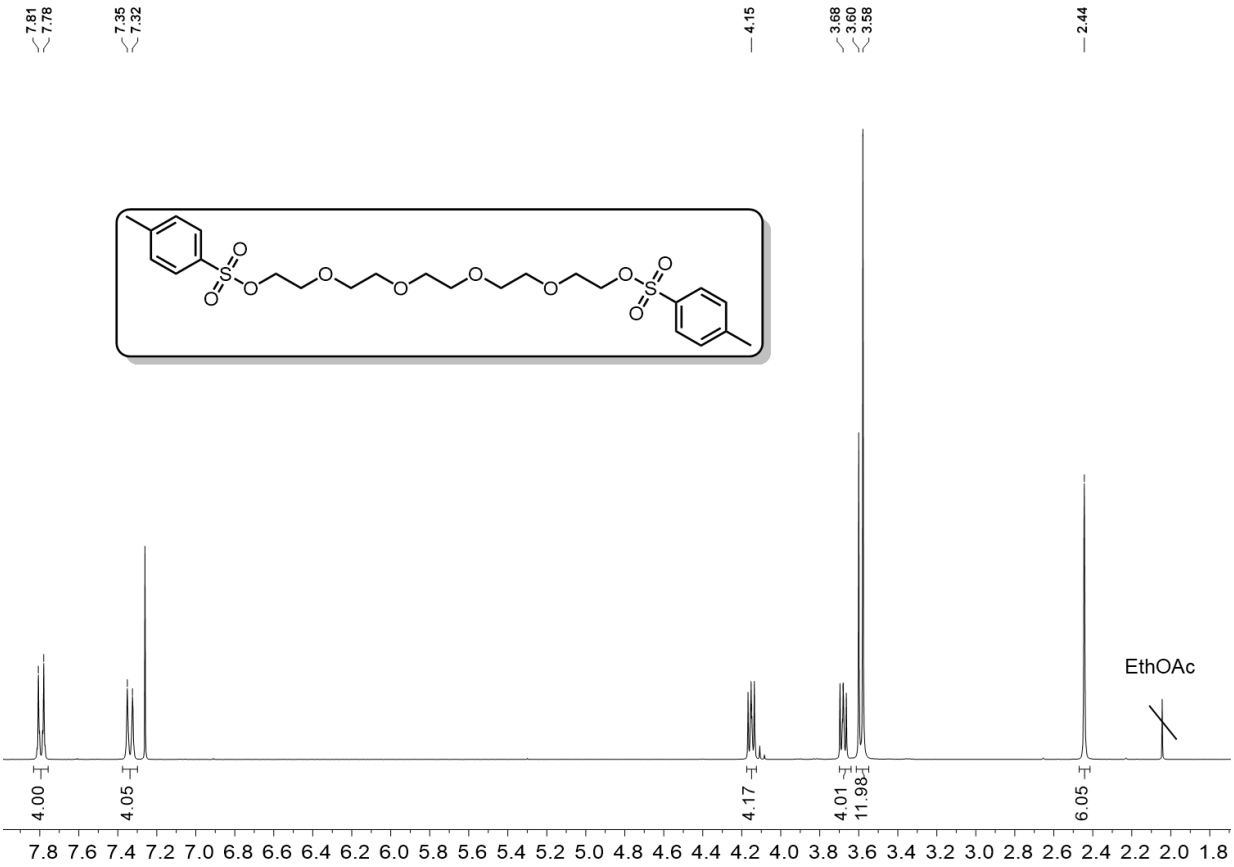

Figure 2.6.48. Pentaethyleneglycol ditosylate ^{1}H NMR.

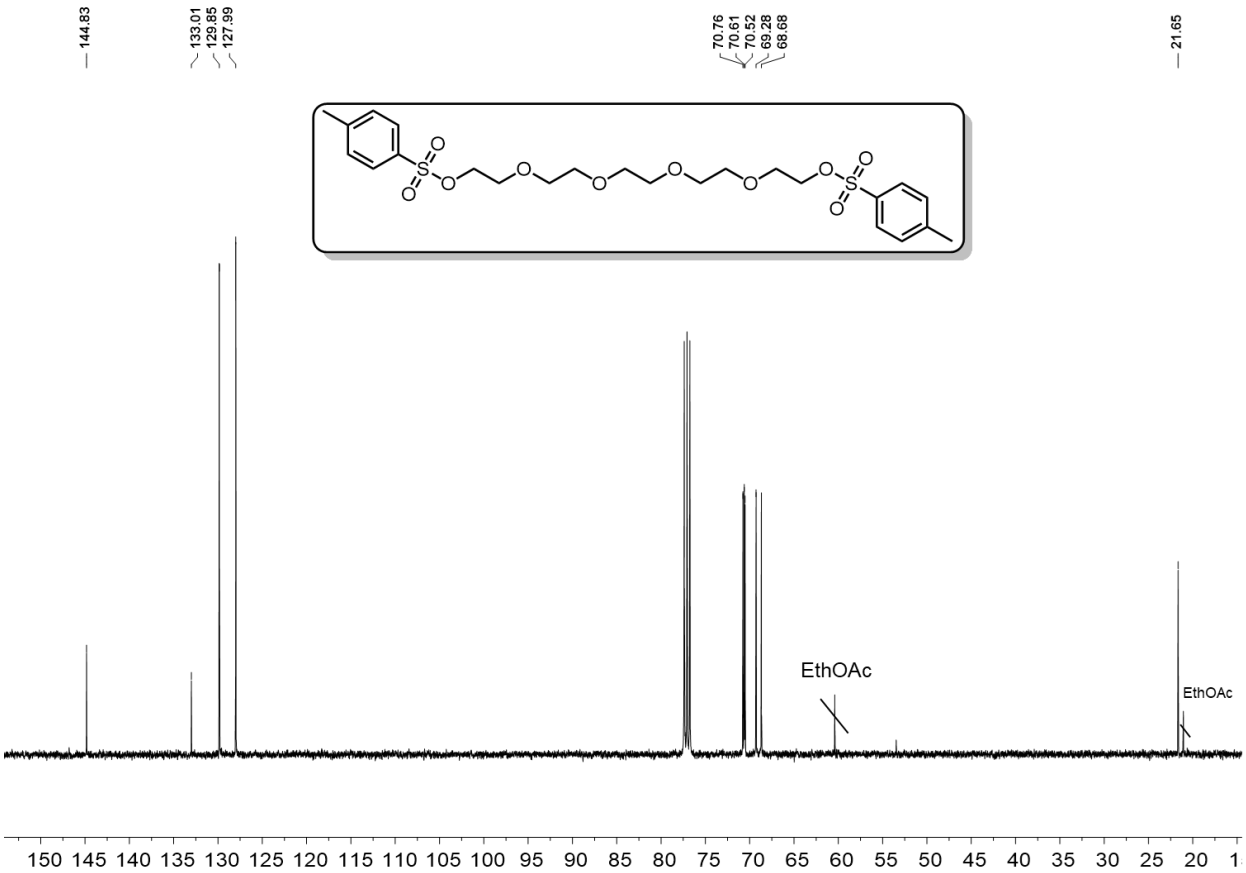

Figure 2.6.49. Pentaethyleneglycol ditosylate ^{13}C NMR.

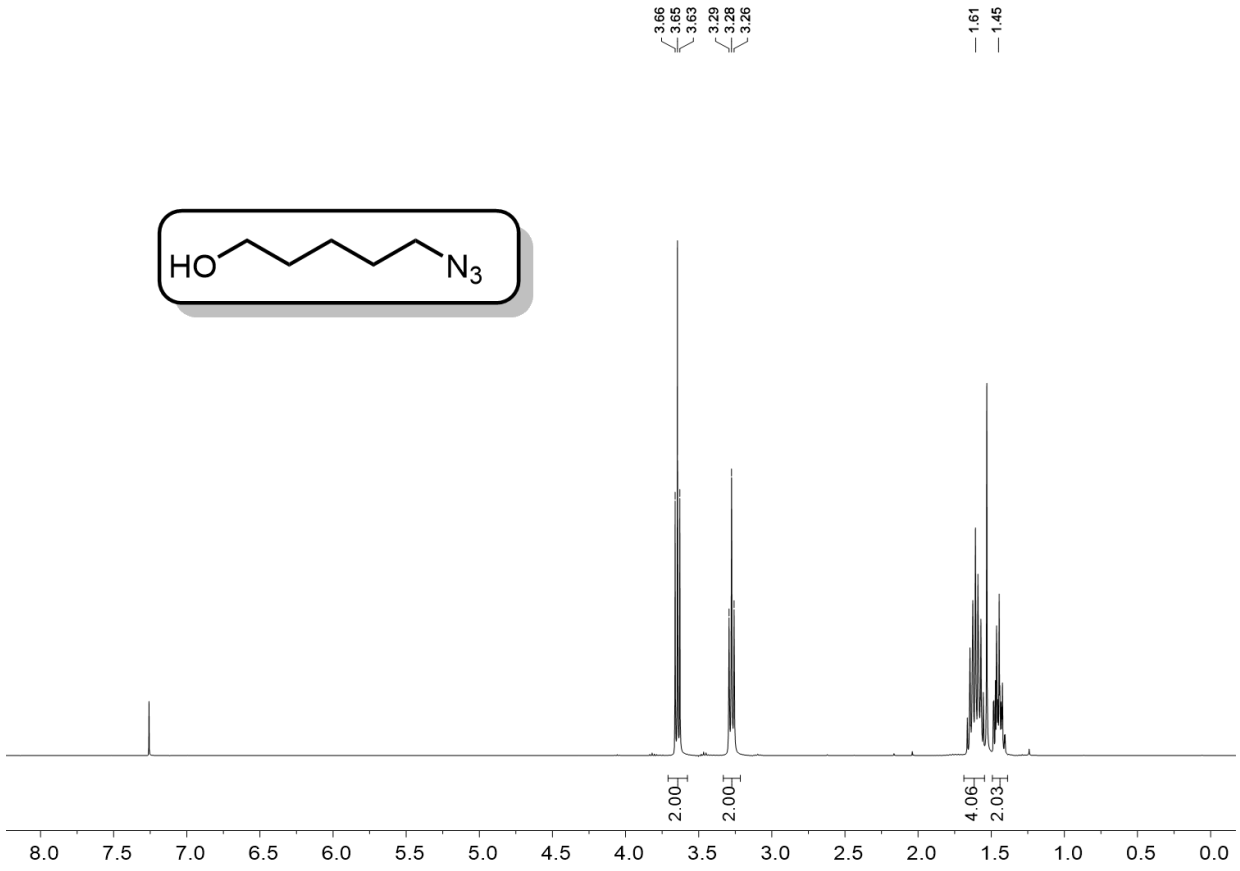

Figure 2.6.50. 5-azido-pentan-1-ol ^{1}H NMR.

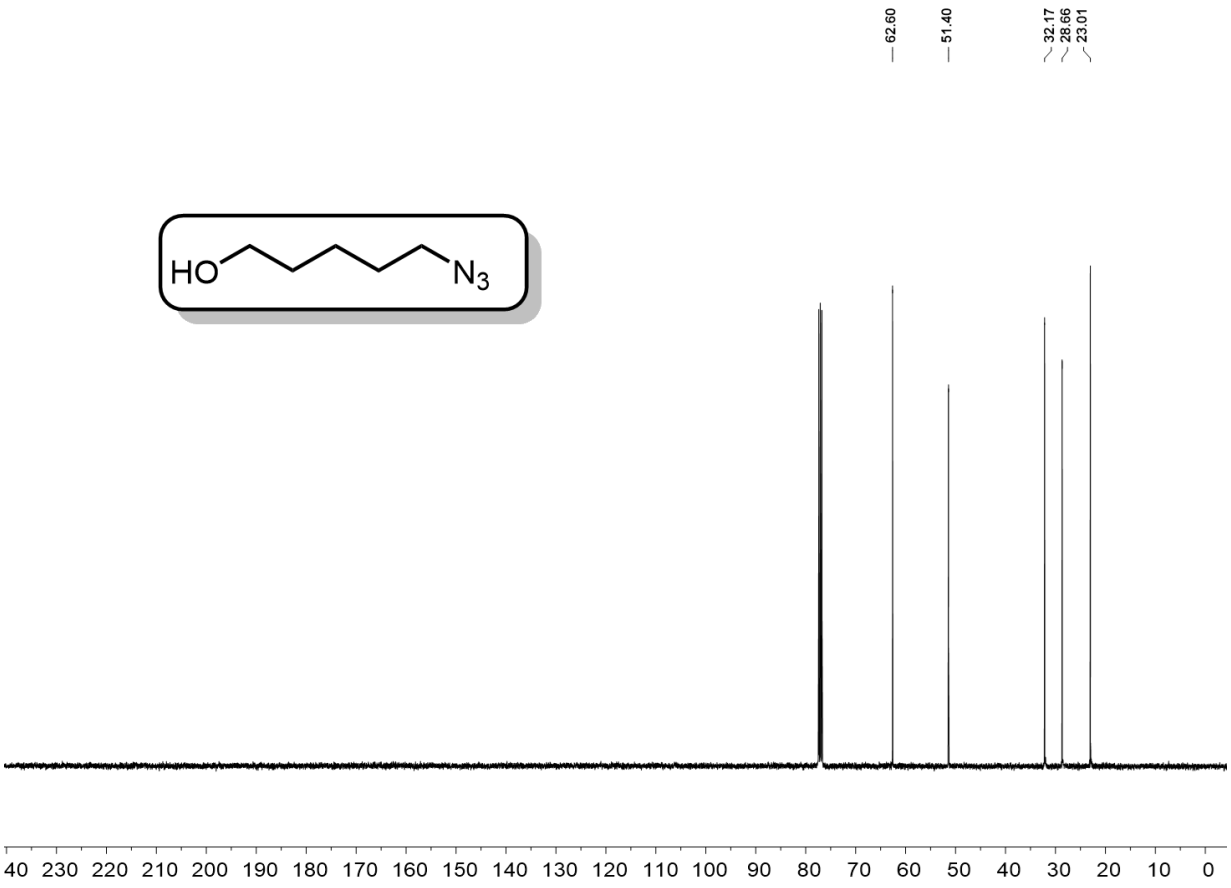

Figure 2.6.51. 5-azido-pentan-1-ol ^{13}C NMR.

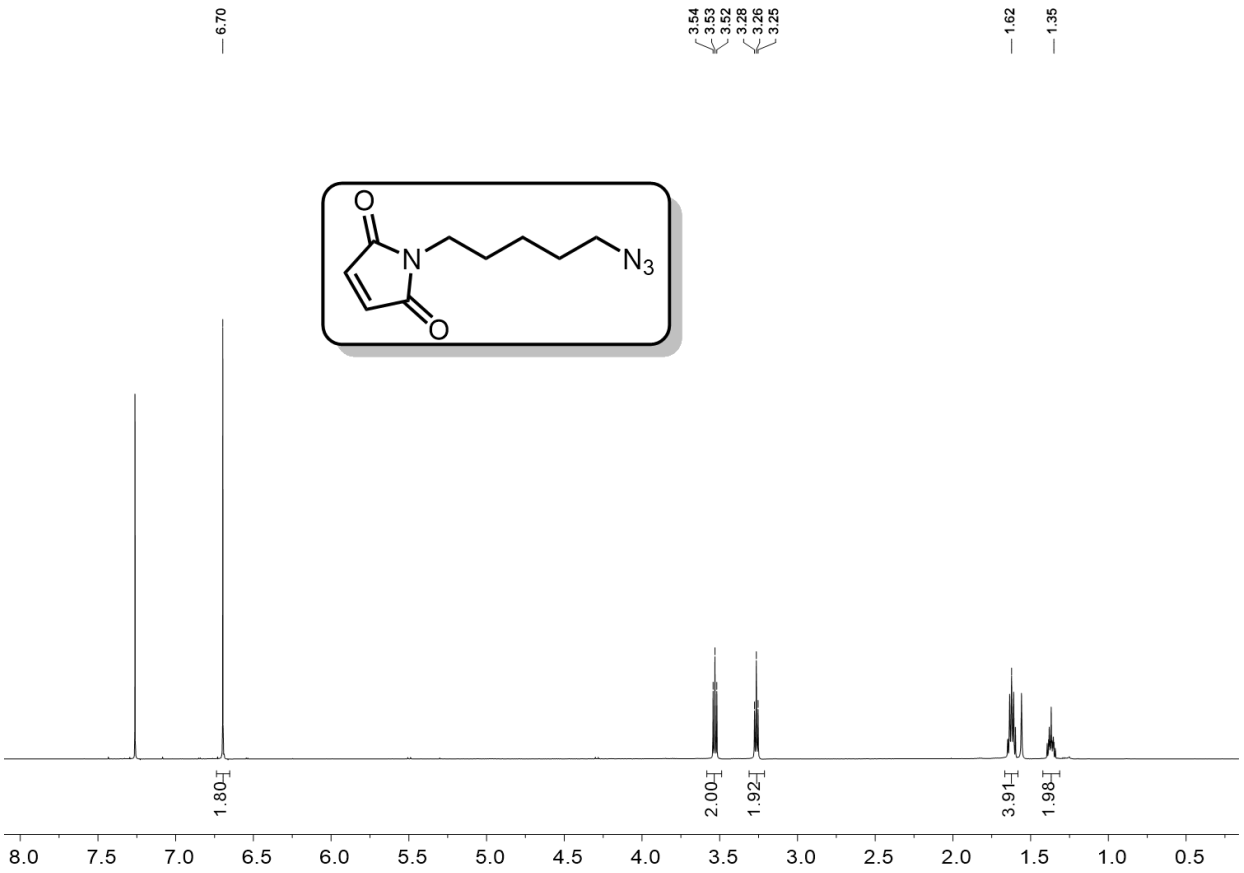

Figure 2.6.52. 5-azidopentyl-1-maleimide ^{1}H NMR.

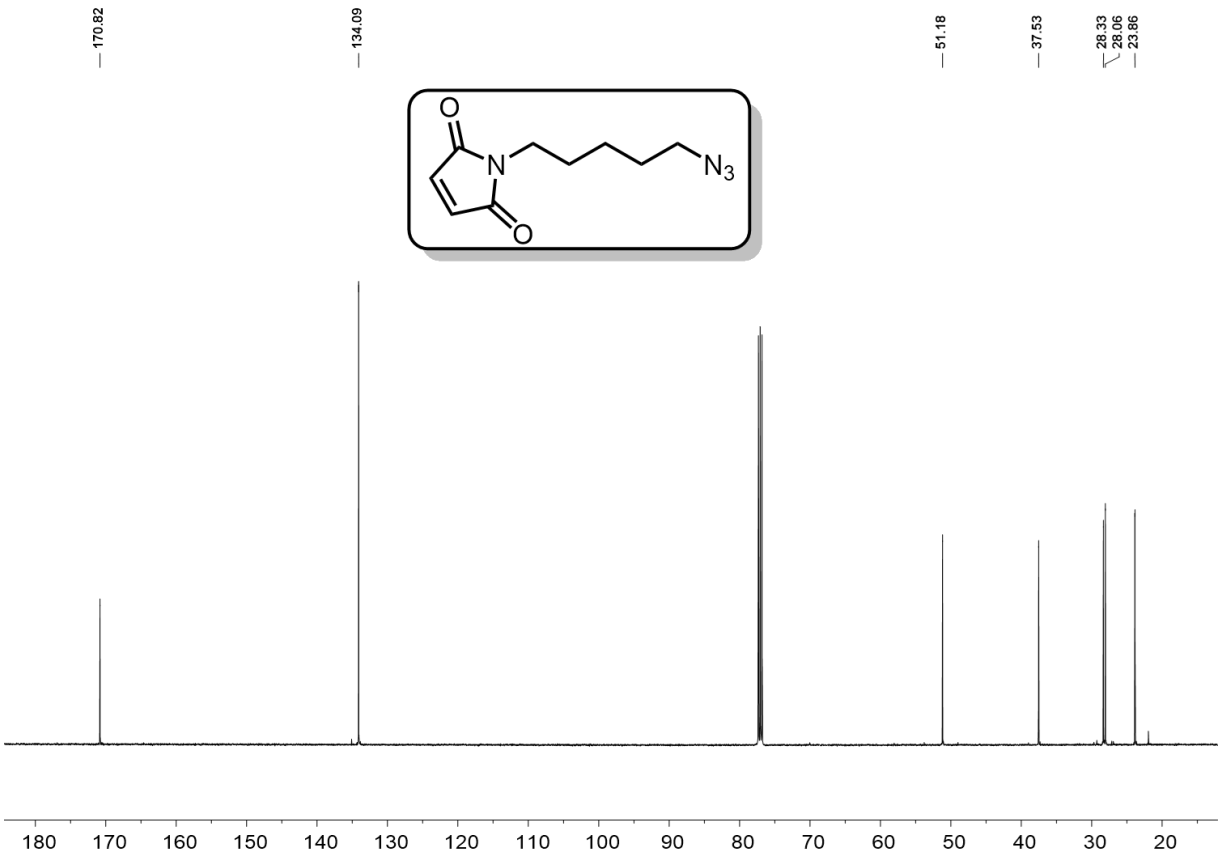

Figure 2.6.53. 5-azidopentyl-1-maleimide ^{13}C NMR.

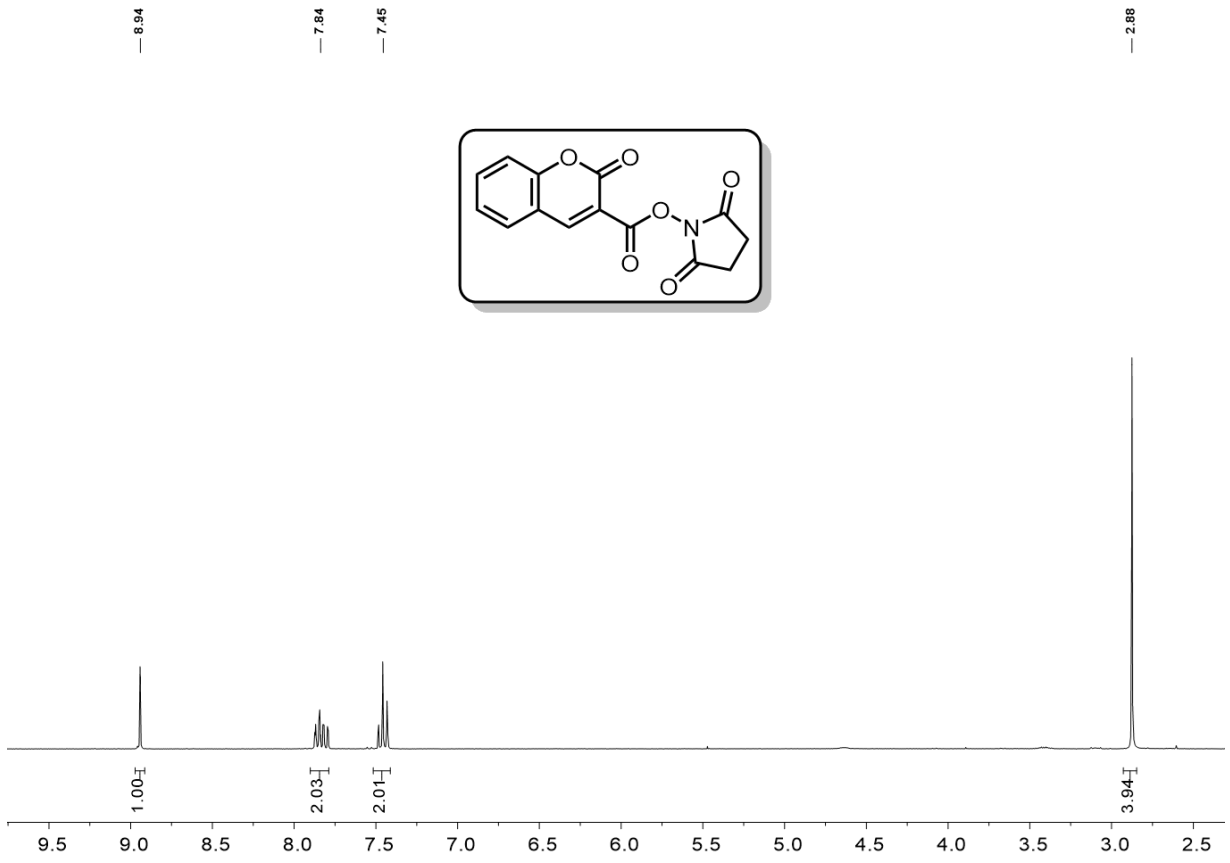

Figure 2.6.54. Coumarin-3-carboxylic acid N-succinimidyl ester ^{1}H NMR.

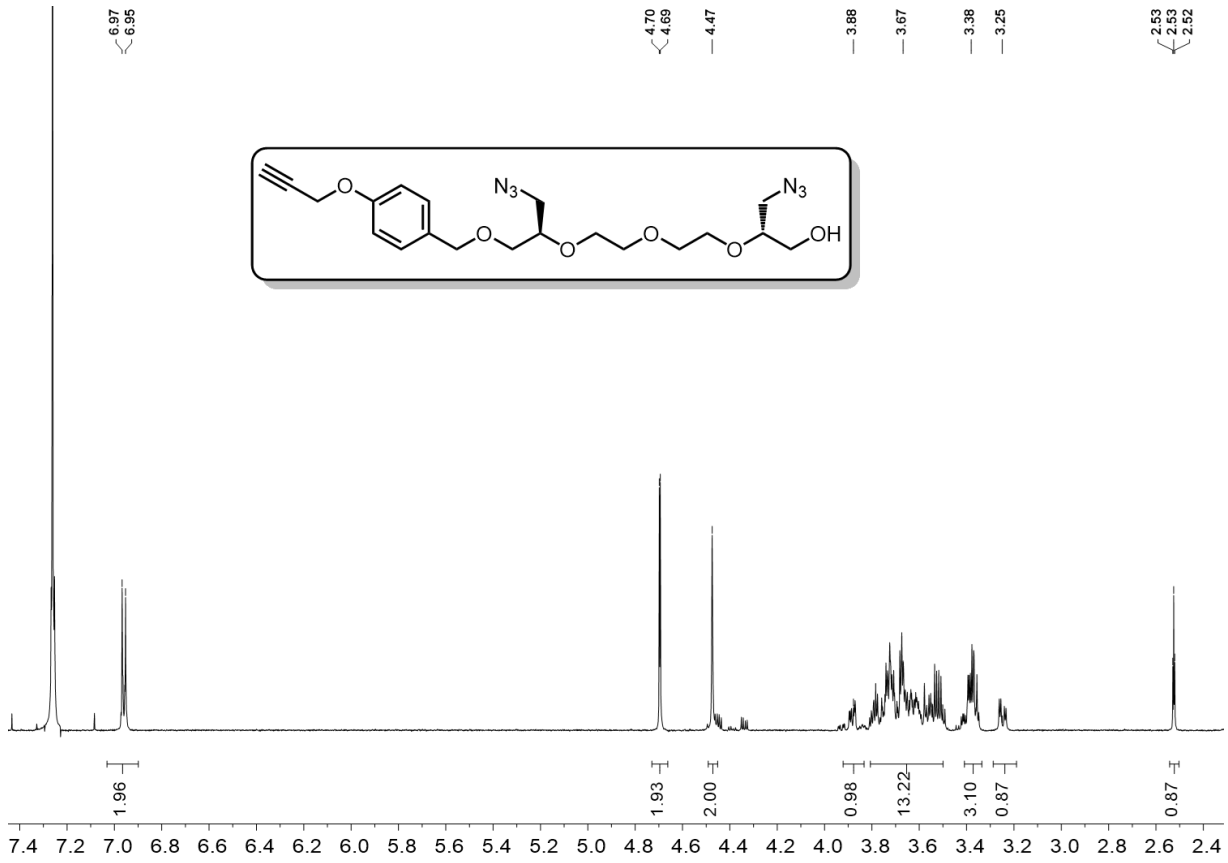

Figure 2.6.55. Propargylbenzyl diazide tetraethyleneglycol ^{1}H NMR.

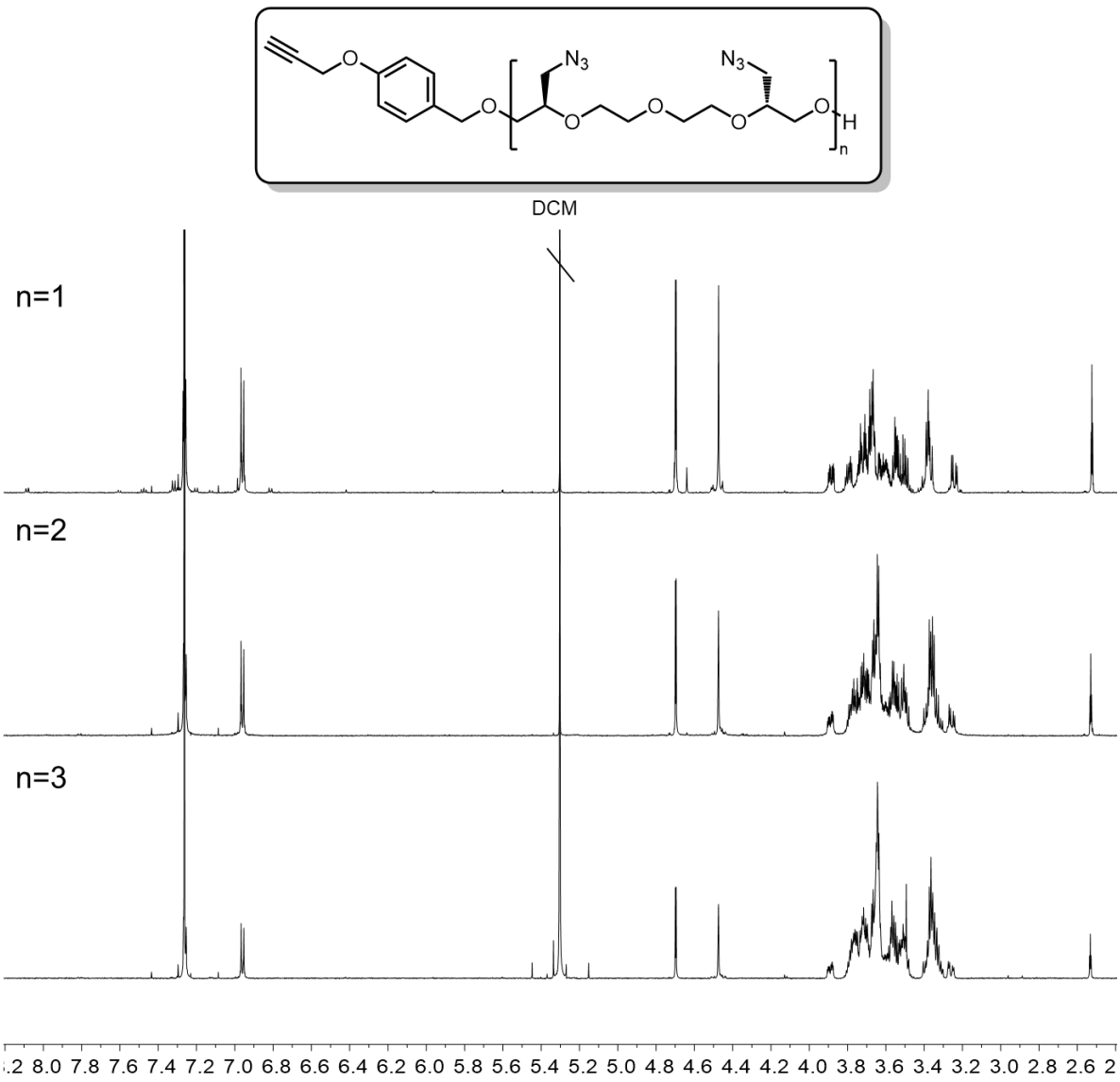

Figure 2.6.56. ^{1}H NMR of Propargylbenzy (Hexa-azide dodecaethyleneglycol) and purified intermediates.

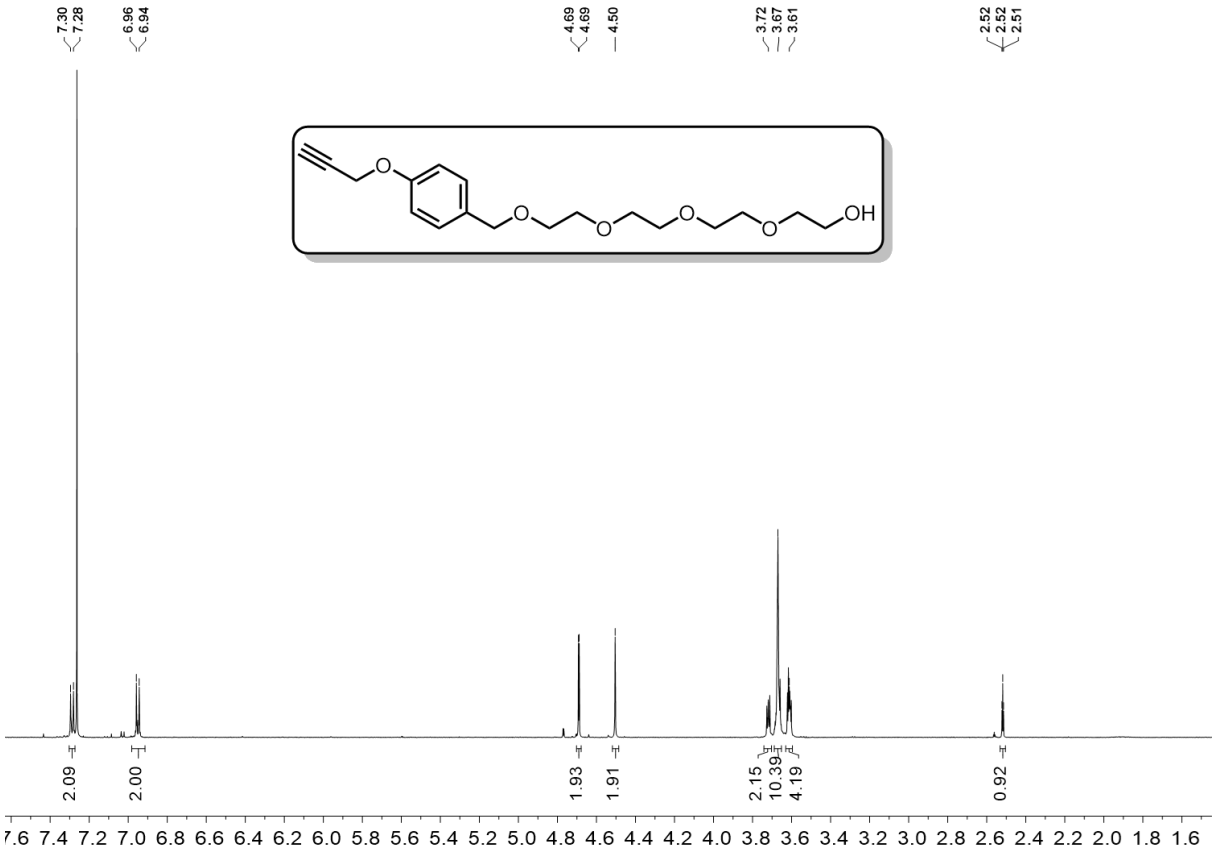

Figure 2.6.57. Propargylbenzy (tetraethyleneglycol) ^{1}H NMR.

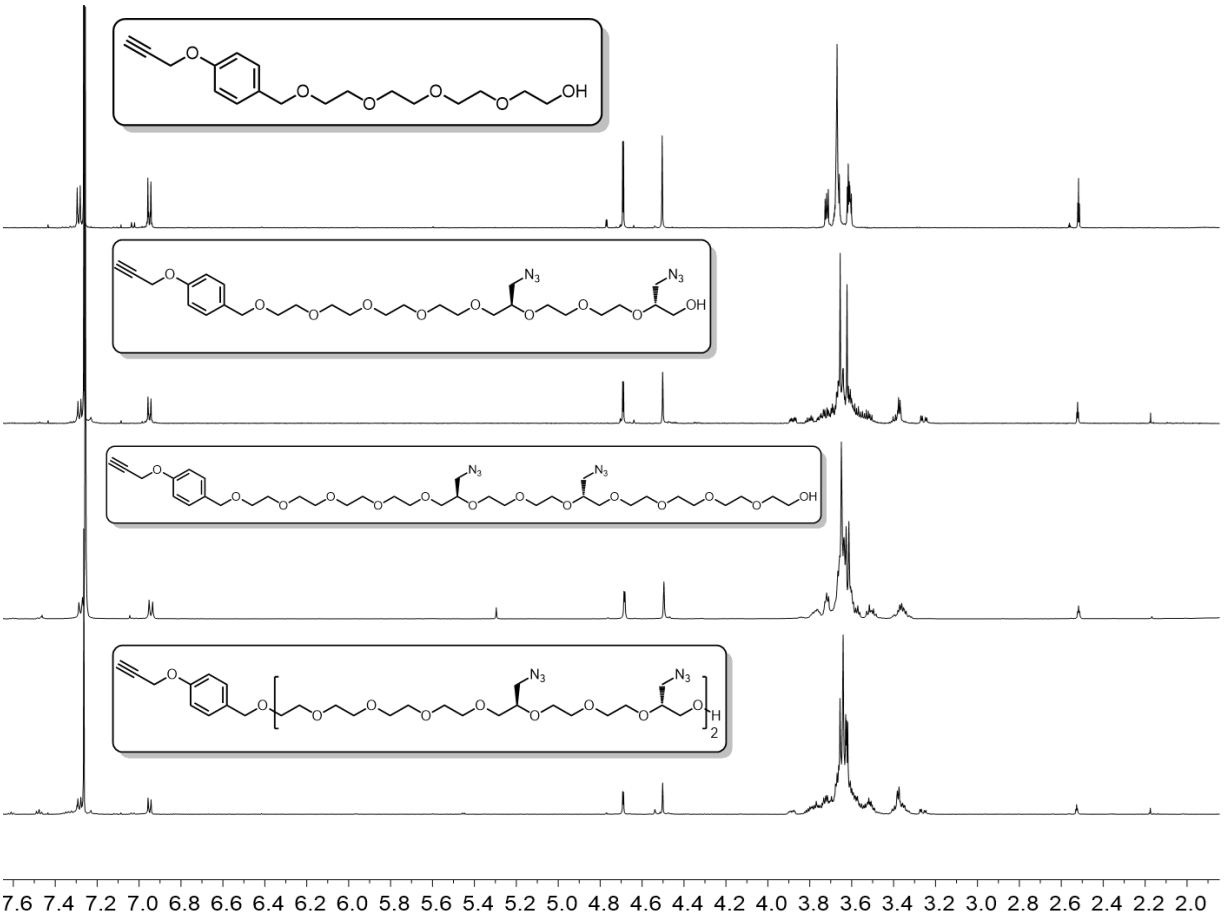

Figure 2.6.58. ^{1}H NMR of Propargylbenzy (tetra-azide hexadeca-ethyleneglycol) and purified intermediates.

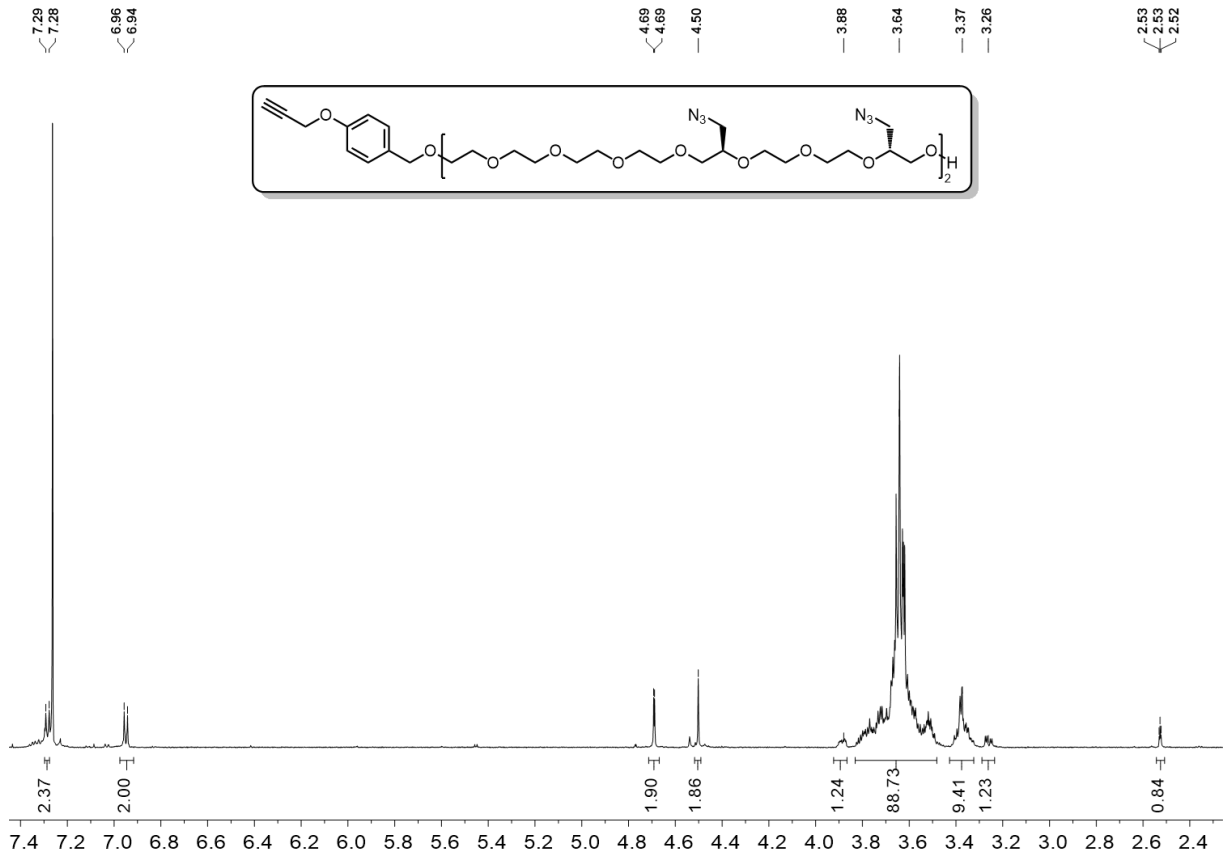

Figure 2.6.59. ^{1}H NMR of Propargylbenzy (tetra-azide hexadeca-ethyleneglycol)

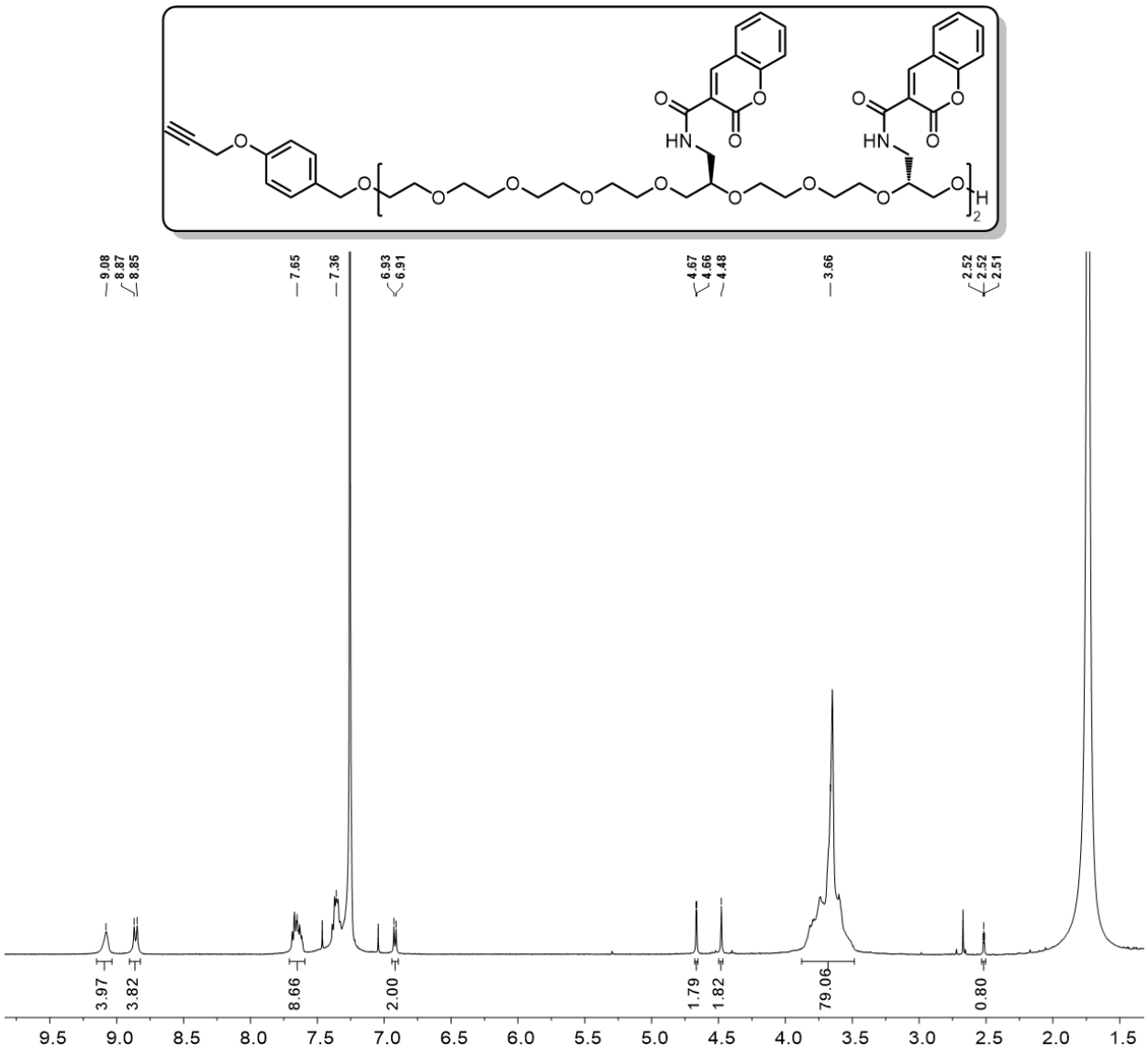

Figure 2.6.60. ^{1}H NMR of Propargylbenzy (tetra-coumarin hexadeca-ethyleneglycol).

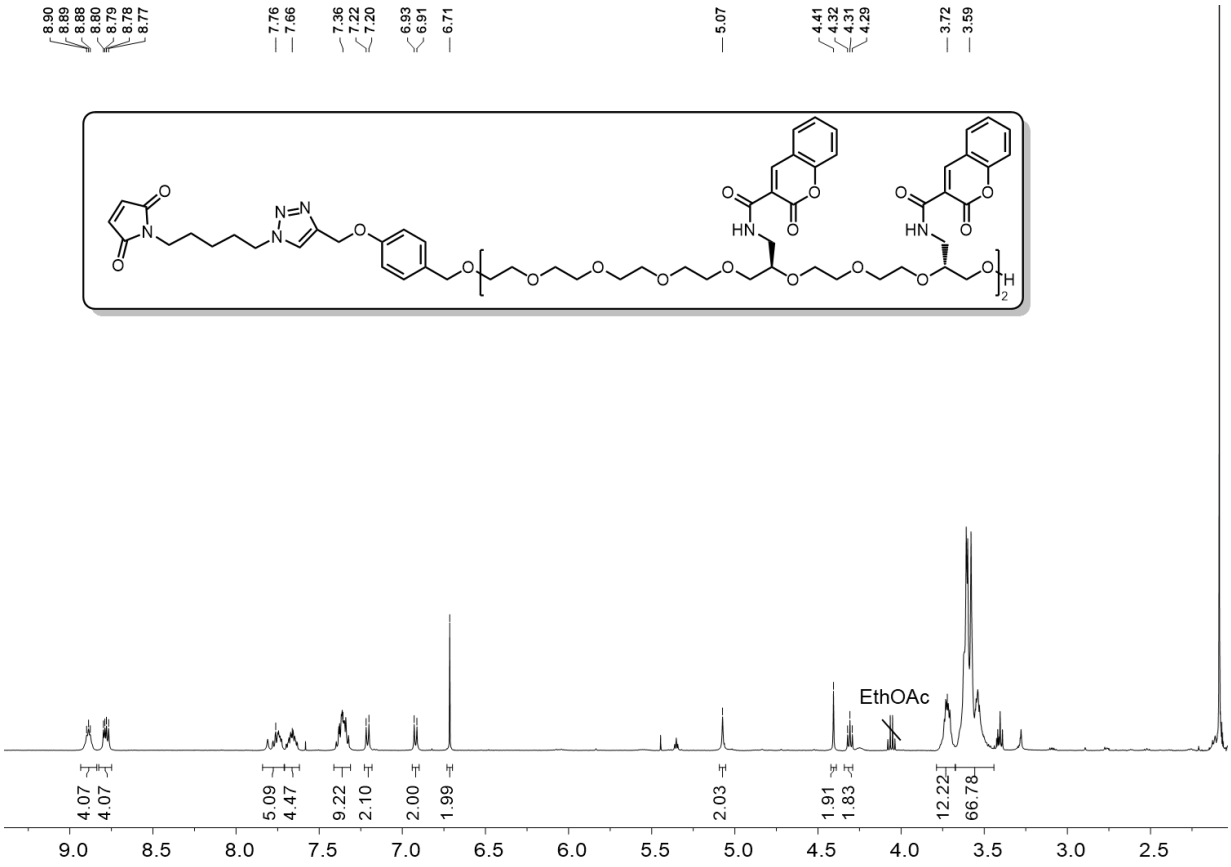

Figure 2.6.61. ^{1}H NMR of Maleimide (tetra-coumarin hexadeca-ethyleneglycol).

2.7. Experimental and Appendix References.

(1) Jamieson, M. L.; Hume, P. A.; Furkert, D. P.; Brimble, M. A. Divergent Reactivity via Cobalt Catalysis: An Epoxide Olefination. *Org. Lett.* **2016**, *18*, 468–471.

(2) Sawant, R. T.; Waghmode, S. B. Intramolecular Reductive Amination Strategy to the Synthesis of (R)-N-Boc-2-Hydroxymethylmorpholine, N-(3,4-Dichlorobenzyl)(R)-2-Hydroxymethylmorpholine, and (R)-2-Benzylmorpholine. *Tetrahedron* **2010**, *66*, 2010–2014.

(3) Zhang, H.; Li, X.; Shi, Q.; Li, Y.; Xia, G.; Chen, L.; Yang, Z.; Jiang, Z.-X. Highly Efficient Synthesis of Monodisperse Poly(Ethylene Glycols) and Derivatives through Macrocyclization of Oligo(Ethylene Glycols). *Angew. Chem.* **2015**, *127*, 3834–3838.

(4) Lewis, J. E. M.; Modicom, F.; Goldup, S. M. Efficient Multicomponent Active Template Synthesis of Catenanes. *J. Am. Chem. Soc.* **2018**, *140*, 4787–4791.

(5) Fer, M. J.; Olatunji, S.; Bouhss, A.; Calvet-Vitale, S.; Gravier-Pelletier, C. Toward Analogues of MraY Natural Inhibitors: Synthesis of 5′-Triazole-Substituted-Aminoribosyl Uridines Through a Cu-Catalyzed Azide–Alkyne Cycloaddition. *J. Org. Chem.* **2013**, *78*, 10088–10105.

(6) Zhou, L.-S.; Yang, K.-W.; Feng, L.; Xiao, J.-M.; Liu, C.-C.; Zhang, Y.-L.; Crowder, M. W. Novel Fluorescent Risedronates: Synthesis, Photodynamic Inactivation and Imaging of Bacillus Subtilis. *Bioorg. Med. Chem. Lett.* **2013**, *23*, 949–954.

(7) Forsythe, N. L.; Maynard, H. D. Synthesis of Disulfide-Bridging Trehalose Polymers for Antibody and Fab Conjugation Using a Bis-Sulfone ATRP Initiator. *Polym. Chem.* **2021**, *12*, 1217–1223.

Chapter 3

Synthesis of Disulfide-Bridging Trehalose Polymers for Antibody and Fab Conjugation Using a Bis-Sulfone ATRP Initiator

3.1 Introduction

Monoclonal antibodies are among the top selling pharmaceuticals in the US with an estimated revenue of $300 billion by 2025.[1] The marked success of this therapeutic modality is largely a result of its specificity and low toxicity, lending to their historically high success and approval rates.[2,3] Advances in antibody engineering have further leveraged this platform's modularity through the development of new formats such as Fabs and single domain antibodies that offer unique advantages for therapeutic development.[4] However, these drugs are often limited by their instability during storage and transport as well as their rapid clearance *in vivo*, thus warranting new methods to improve their performance.

The covalent attachment of function-enhancing polymers to biomolecules is a long-standing method to both overcome the shortcomings of biologic drugs or to confer new properties. This strategy has been utilized to improve the stability and enhance the applicability of antibody drugs. For instance, Fab fragments, due to the lack of an Fc domain, do not participate in neonatal gut transport receptor (FcRn) recirculation and often suffer from rapid *in vivo* clearance.[5–7] While short half-lives are often desirable for applications such as imaging, therapeutic antibody fragments often require extended residence *in vivo*. Conjugation of the polymer polyethylene glycol (PEG) is a common strategy for extending the *in vivo* half-life of proteins and has proved effective for Fab fragments, with the most notable success being the FDA-approved certolizumab pegol.[8] Aside from PEG, a large variety of polymer structures and architectures have been employed to tune the properties of antibody drugs. For one, stabilizing polymers have a long history of increasing the thermal stability of proteins to enable longer storage half-lives. Polymers such as poly(vinylpyrrolidone),[9] polysorbate,[10] and amphiphilic acrylamides[11] have shown such stabilizing properties for antibody drugs. In terms of drug delivery, polymers are used as carriers

for anticancer drugs to create more effective antibody drug conjugates. Masking the hydrophobicity of these drugs with hydrophilic polymers can enable higher drug loading by reducing the propensity towards aggregation and denaturation. Polymers such as PEG,[12] poly-1-hydroxymethylethylene hydroxymethylformal,[13,14] polysarcosine,[15] polyglutamide,[16,17] and poly(hydroxypropyl methacrylamide) (pHPMA)[18] have successfully been conjugated to antibodies. In a similar manner, contrast agents[19] and fluorophore-containing polymers[20] were used to enhance the imaging capabilities of antibodies, while polymers containing *N*-isopropylacrylamide (NIPAM) units[21] have been employed to confer stimuli responsive properties.

As the diversity of polymers used for antibody conjugates expands, it becomes increasingly important to efficiently incorporate new bioconjugation handles into polymer structures. A common strategy for protein modification is through non-specific, lysine modification with reagents containing activated esters. While this method can achieve high conjugation yields with commercially available reagents, its nonspecific nature often has a deleterious effect on antibody binding. Furthermore, the final conjugate yielded *via* this method will be highly heterogenous (between 20 to 40 different lysine residues may be modified per antibody), creating challenges in characterization and reproducibility.[22] To achieve a more selective conjugation, successive reduction and modification of inter-chain disulfide bonds with thiol-reactive reagents such as maleimides can be employed. In a similar manner, dibromo and dithiophenol maleimides are used to form conjugates through a re-bridging of interchain disulfide bonds after reduction.[23,24] These functionalized maleimides have further been incorporated into both RAFT (reversible addition–fragmentation chain transfer) agents and ATRP initiators to synthesize polymers for disulfide conjugation (Figure 3.1.1).[25,26] While maleimides and their derivatives are robust in selectivity and

efficiency, they are known to undergo deconjugation *in vivo* through a retro-Michael reaction, which can limit their applicability in long circulating antibody therapeutics.[27] Generally, challenges with maleimide reversibility can be overcome through a combination of tuning the N-substituent of the maleimide and increasing the pH of the solution to favor maleimide hydrolysis, thus imparting irreversibility to the thioether bond.[28,29] However, such strategies add additional steps and characterization to the conjugation reaction, and further require the use of less synthetically accessible N-substituted maleimides.

As a complement to the aforementioned strategies, bis-sulfone moieties are capable of irreversibly inserting into reduced disulfide bonds in one step *via* successive tosylate elimination and alkylation. This reactive handle has been used to form disulfide-bridged protein–polymer conjugates for a number of proteins.[30–32] However, previous applications of this reactive handle in polymer chemistry have relied on post-polymerization modification either through activated esters with amino-terminated polymers[30] or through late-stage oxidation of bis-sulfide terminated polymers.[33,34] While these are effective methods for polymer functionalization, the most robust method for integrating conjugation handles into polymer endgroups is through direct incorporation into a polymerization initiator or chain transfer agent. This avoids the use of excess reagent and additional purification steps that are required in post-polymerization modification strategies.

Herein we report the synthesis of a bis-sulfone ATRP initiator that is capable of creating well-defined polymers that can be used directly for disulfide conjugation without further synthetic manipulation. We demonstrate optimization of the AGET ATRP polymerization conditions to prevent cross-reactivity of the bis-sulfone in the polymerization process first using commercially available PEG methacrylate and demonstrate predictable molecular weights and low dispersity of the final polymer. Due to the instability challenges that are inherent with antibody therapies, we

applied this chemistry towards the production of more stable antibody conjugates. Given our previous work with stabilizing polymers, we chose to utilize a poly(trehalose methacrylate) that has stabilizing properties as both an excipient and a conjugate.[35,36] We were able to directly translate the optimized polymerization conditions to make well-controlled trehalose polymers with bis-sulfone end groups. Conjugation of these polymers to both an antibody and its Fab fragment proceeded to quantitative conversion and characterization of the resulting conjugates demonstrated the utility of these polymers as protein stabilizers. This study shows the applicability of the reported bis-sulfone initiator for the synthesis well-controlled, function-enhancing polymers for disulfide conjugation, as well as the applicability of trehalose polymers for antibody stabilization.

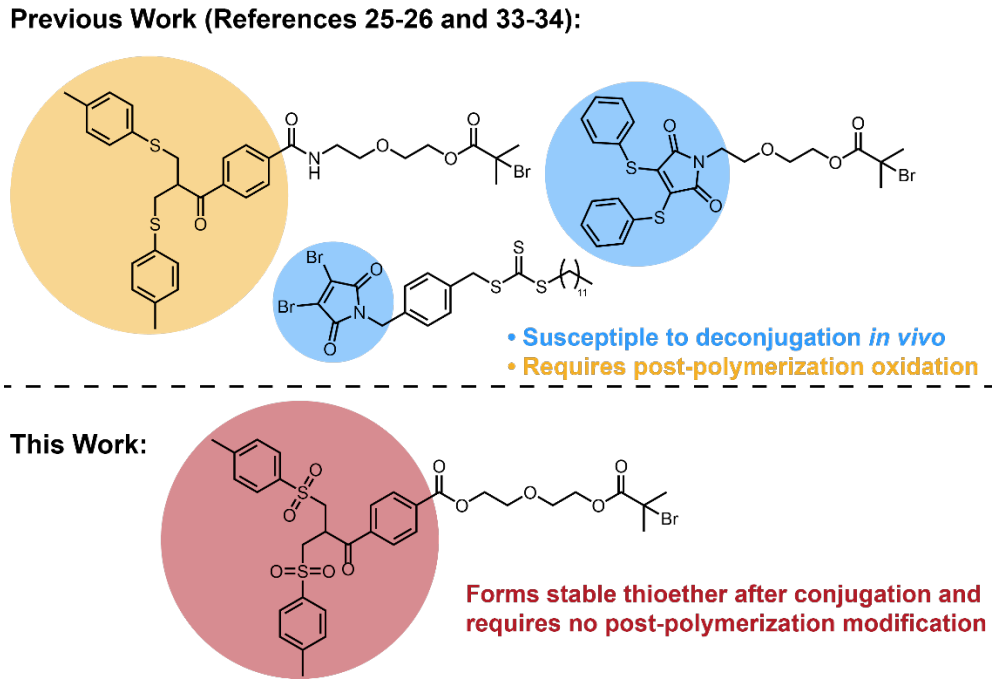

Figure 3.1.1. Comparison of disulfide-reactive ATRP initiators and CTAs.

3.2 Results and Discussion

3.2.1 Optimization of polymerization conditions.

The principal concern with the direct use of the bis-sulfone moiety in the ATRP process is its potential reactivity. The bis-sulfone initiator contains an acidic proton alpha to its ketone that

imparts its reactivity during conjugation, but under basic conditions may undergo ligand-assisted elimination to form a secondary alkene. During polymerization, this elimination could result in the coupling of polymer chains, leading to loss of polymerization control and end-group fidelity. To study this and determine optimal conditions for the polymerization, we first used a commercially available monomer, poly(ethylene glycol) methacrylate (ethylene glycol Mn = 300), as a model monomer.

Initially, using two molar equivalents of TPMA ligand and a 1 M concentration of monomer ([PEGMA] : [initiator] : [CuBr2] : [TPMA] = [200] : [1] : [1] : [2]), we observed fast polymerization kinetics with a correspondingly large increase in dispersity (**Figure 3.2.1. A and B**). We hypothesized that the excess TPMA ligand was indeed acting as a base to eliminate the tosylate in the bis-sulfone to result in polymer chain coupling. Repeating the polymerization with equimolar ligand and CuBr2 ([200] : [1] : [1] : [1]) produced a clear decrease in the dispersity (**Figure 3.2.1. A**), supporting our hypothesis. To further validate this conclusion, we conducted the same polymerization using the non-oxidized bis-sulfide initiator, as it is structurally similar to the bis-sulfone, yet unable to form the elimination product. Using identical polymerization conditions to the initial bis-sulfone polymerization ([200] : [1] : [1] : [2]), we observed considerably lower dispersity throughout the polymerization ($Đ \leq 1.2$) (**Figure 3.2.1. A**). Taken together, this data supports our hypothesis of the ligand-assisted elimination of the bis-sulfone causing a loss of control during the polymerization process.

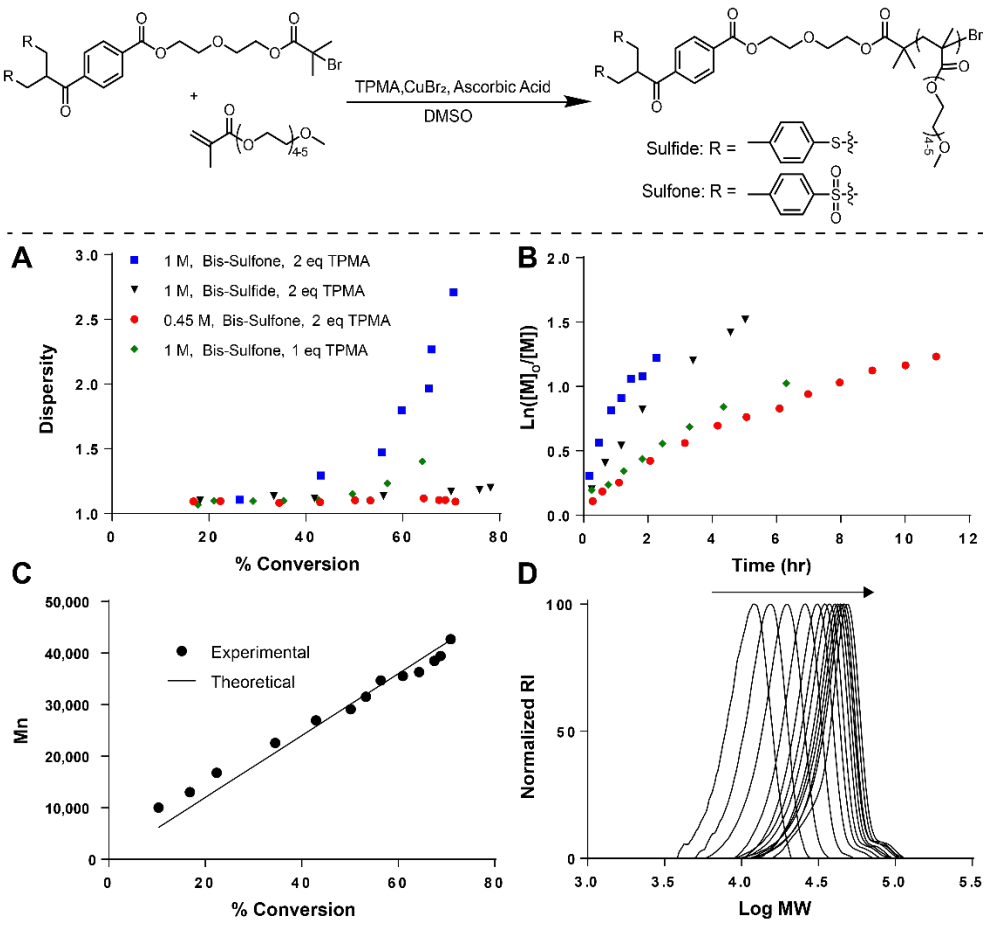

Figure 3.2.1. Optimization of PEGMA polymerization conditions: (A) molecular weight dispersity and (B) kinetics of polymers made with bis-sulfone and bis-sulfide initiators with varying conditions. (C) Theoretical and experimental molecular weights with respect to conversion and (D) overlaid GPC traces of timepoints collected for 0.45 M polymerization with the bis-sulfone initiator.

To disfavor the observed cross-reactivity, we investigated the effect of more dilute polymerization conditions as this should reduce the intermolecular side reaction. Repeating the polymerization at 0.45 M ([200]:[1]:[1]:[2]) rather than 1 M resulted in low dispersity throughout the polymerization and mono-modal GPC traces until later in the polymerization when small high molecular weight shoulders were observed (**Figure 3.2.1. A and D**). Furthermore, we found good agreement with theoretical molecular weight over a large range of monomer conversions, demonstrating a high initiator efficiency (**Figure 3.2.1. C**). It is important to note that

the rate of polymerization under these more dilute conditions is predictably slower (requiring 11 h to reach 70% conversion) (**Figure 3.2.1. B**) and that there is a slight curvature in the kinetics plot, suggesting a small amount of termination as observed in the GPC traces. However, we found this acceptable to achieve low dispersity polymers of predictable molecular weight.

3.2.2 Preparation and characterization of conjugates.

Given the success in optimizing the bis-sulfone initiator and AGET ATRP conditions, we sought to apply this system towards the generation of stabilizing polymers for antibody therapeutics. Trehalose, a non-reducing sugar composed of two glucose units linked through the anomeric position, is commonly employed in the stabilization of biologics. While not fully understood, it is hypothesized that trehalose stabilizes proteins through one or a combination of the following mechanisms: direct hydrogen bonding with the protein (water replacement), hydrogen bonding with the water molecules at the surface of the protein (water entrapment), or mechanical inhibition of protein conformational changes (vitrification).[37,38] Our lab has produced trehalose polymers and trehalose-functionalized materials and has demonstrated the ability of these polymers to stabilize a wide variety of proteins as both conjugates and excipients.[35,36,39–41] Wanting to expand the scope of these findings, we sought to make bis-sulfone functionalized trehalose polymers for conjugation to both a full antibody as well as its Fab fragment.

Trehalose methacrylate monomer functionalized at the C6 position was obtained in one step followed by preparatory HPLC purification. Polymerization using the optimized AGET ATRP conditions proceeded to high conversion while maintaining low dispersity ($Đ < 1.1$, *via* GPC) to result in a polymer of molecular weight 23 kDa (theoretical 20 kDa) (**Figure 3.2.2**). Proton NMR of the polymer showed the presence of the three expected signals from 7.0–8.0 ppm, representative of the bis-sulfone end group (Fig. 3B). Additionally, proton NMR showed smaller peaks in this

region which we believe to be the mono-sulfone that exists in equilibrium with the bis-sulfone at pH 7.0.[30]

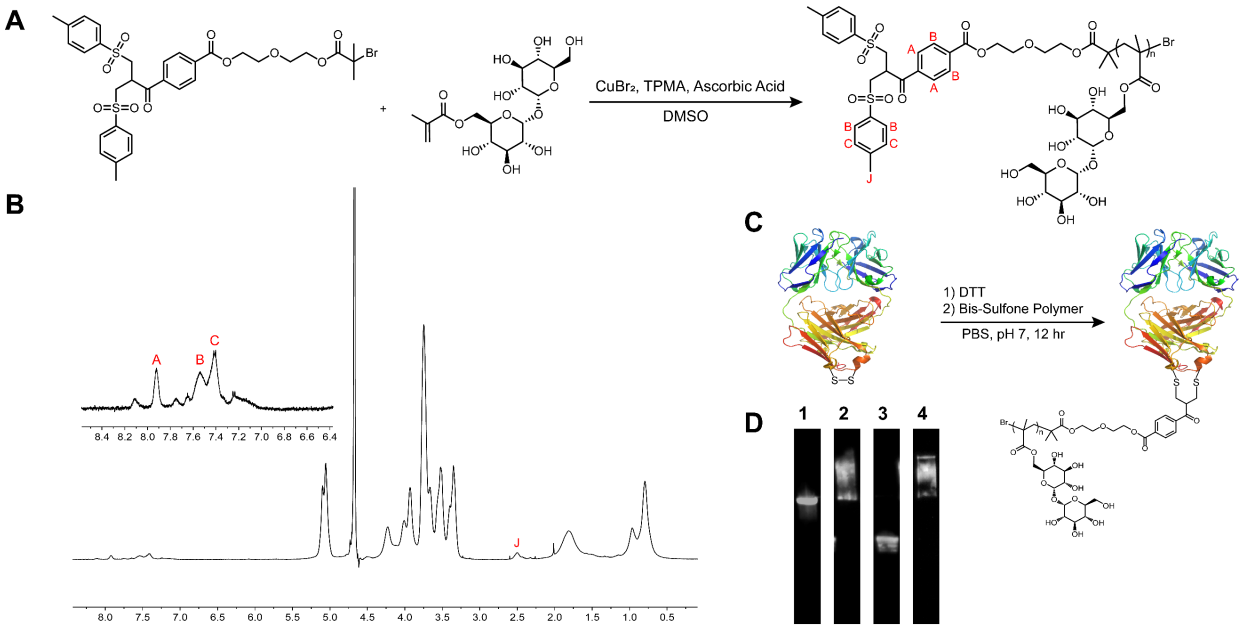

Figure 3.2.2. (A) Scheme for the synthesis of bis-sulfone trehalose polymers and (B) NMR of purified polymers in D_2O showing the presence of the bis-sulfone endgroup. (C) Scheme for the preparation of Fab conjugates and (D) Western blot of conjugates (lane 1: unmodified Fab, lane 2: Fab conjugate, lane 3: unmodified Fab reducing, and lane 4: Fab conjugate reducing).

To initially explore the reactivity of the bis-sulfone trehalose polymers, we first prepared a conjugate with a full IgG (Immunoglobulin G). Using Herceptin as a model, we first reduced the disulfide bonds followed by addition of 16 kDa bis-sulfone trehalose polymer. After removal of excess polymer *via* cation exchange chromatography, Western blot analysis showed quantitative formation of conjugate as a higher molecular weight smear. Since the full IgG molecules contains 4 interchain disulfide bonds capable of being alkylated, the isolated conjugate is likely a heterogenous distribution of both protein conjugation site as well as the number of polymers conjugated.

We next expanded this system to a more therapeutically relevant and defined system by pursuing a similar conjugation strategy for the Fab fragment of Herceptin. The antibody fragment was prepared by digesting the full antibody with papain followed by protein A chromatography to obtain pure Fab. To prepare the conjugate, a procedure of successive reduction and disulfide insertion was adapted.[31] Excess DTT was first used to reduce the native disulfide bonds. After incubating for 1-hour, excess DTT was removed with a desalting column and 10 equivalents of the bis-sulfone trehalose polymer was then added. After incubation at room temperature for 12 h, excess polymer was removed *via* cation exchange chromatography to yield pure conjugate (Fig. 3C and D). The smear was large as is typical of polymers, and thus the protein was reduced to confirm that the yield was quantitative. Western blot under reducing conditions did not reveal lower molecular weight protein, which is consistent with the thioether bond that irreversibly links the heavy and light chains of the Fab. This further suggests that conjugation occurred through the interchain disulfide bonds and was quantitative as no unmodified protein was present.

To further characterize the Fab conjugate, we wanted to investigate if only one trehalose polymer was added to the Fab fragment. While intact mass spectrometry of the conjugate would be the ideal method for this determination, we have found that the trehalose polymer suppresses ionization.[36] Furthermore, the inherent dispersity of the polymer as well as multiple charge states of the protein adds an additional layer of complexity to the analysis of the conjugate. To circumvent this issue, we pursued an indirect method wherein we cleaved the polymer from the conjugate under basic conditions at pH 10 followed by LCMS to characterize the remaining benzoic acid fragment on the protein. This method yielded a mass that corresponded well with the expected mass (**Figure 3.2.3**), confirming single modification of the Fab. This result is also

consistent with the literature, which holds that only the interchain disulfides of the Fab are accessible to conjugation.[42]

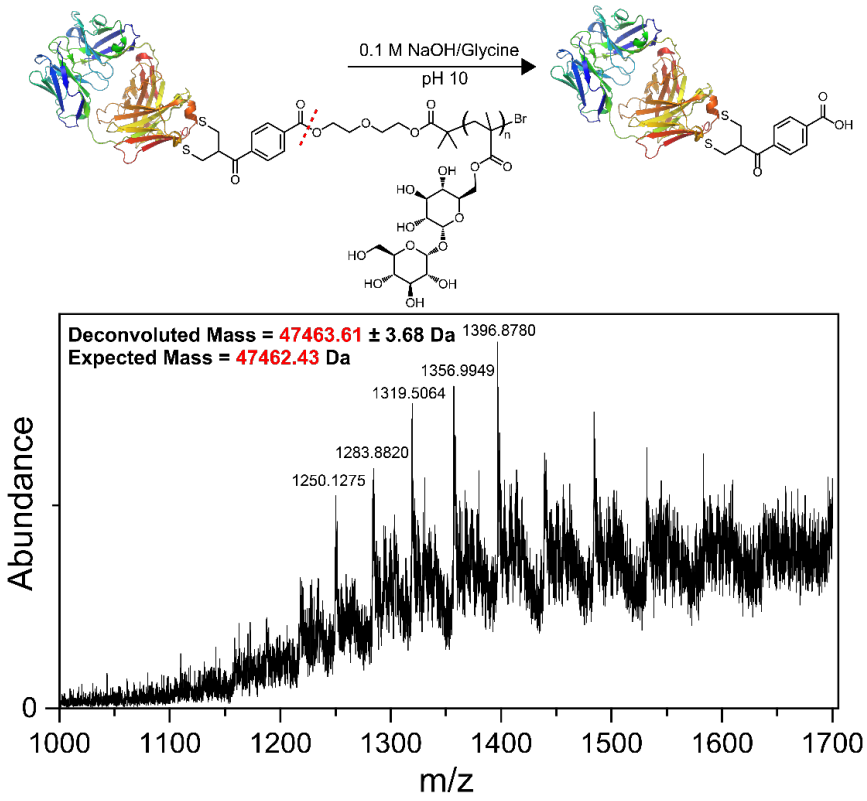

Figure 3.2.3. Mass spectrometry of conjugate after cleavage of polymer. Deconvolution was performed using ESIprot online software using the labeled m/z peaks.

3.2.4 Binding Studies of Conjugates

It is well understood and expected that conjugation of macromolecules to antibodies effects their affinity towards their antigen. This trade-off between the activity/binding of a protein and the added benefit of the polymer is a fundamental dichotomy of any protein–polymer conjugate. To determine the effect of polymer conjugation in our system, we used indirect ELISA to determine comparative binding of the conjugates. In this experiment, Her2 antigen was immobilized onto a 96 well plate followed by addition of the appropriate proteins and conjugates at a range of

concentrations. Extrapolation of EC_{50} from the corresponding dose response allows us to quantify the effect the polymer has for both the full Herceptin antibody as well as its Fab fragment. From this experiment, we found that the heterogenous Herceptin conjugate (16 kDa polymer) had approximately 3.5-fold lower affinity and the Fab conjugate (23 kDa polymer) had a reduced affinity of 4.2-fold (**Figure 3.2.4**).

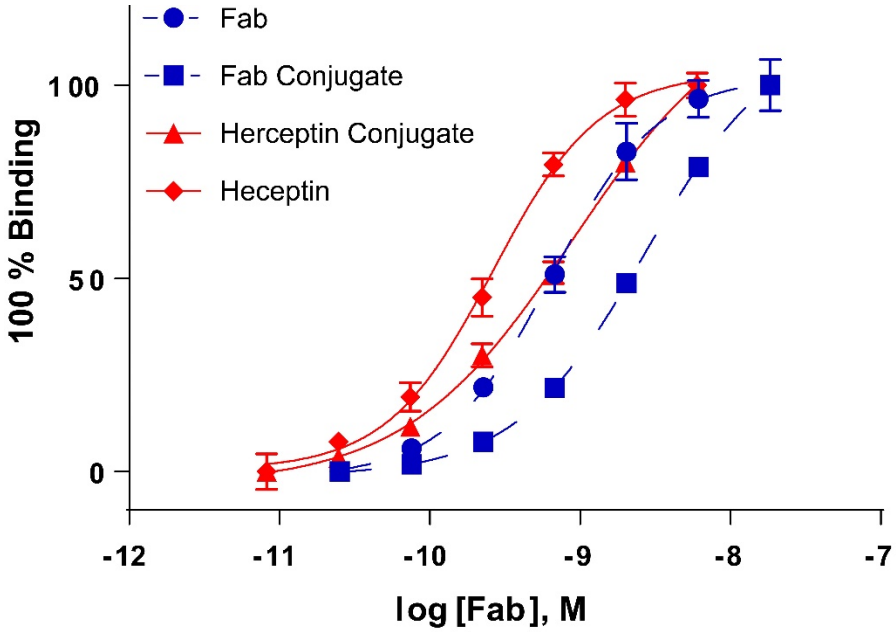

Sample	EC50 (nM)	95% CI (nM)
Herceptin	0.26	0.23 - 0.31
Hercpetin Conjutage	0.90	0.65 - 1.24
Fab	0.65	0.54 - 0.78
Fab Conjugate	2.74	2.52 - 2.97

Figure 3.2.4. ELISA Dose–response for Herceptin, Fab, and their respective conjugates (16 kDa polymer for the Herceptin and 23 kDa polymer for the Fab). IC50 values for both Fab and Herceptin conjugates were found to be statistically different via t-test. 95% confidence intervals are provided as a measure of variance.

While we do observe an expected decrease in activity, we believe that this conjugation method helps minimize interference of the polymer with binding. By conjugating through the disulfide

bonds, the polymer is at the maximal distance from the antigen binding domain for the Fab conjugate. It has previously been reported that the location of PEGylation can have a significant effect on the affinity of the resulting conjugate.[43] Given that most macromolecular conjugations will have an effect on binding to an antigen, we postulate that this distal, disulfide-insertion conjugation method is ideal for mitigating activity loss.

3.2.5 Heat Stability of Conjugates

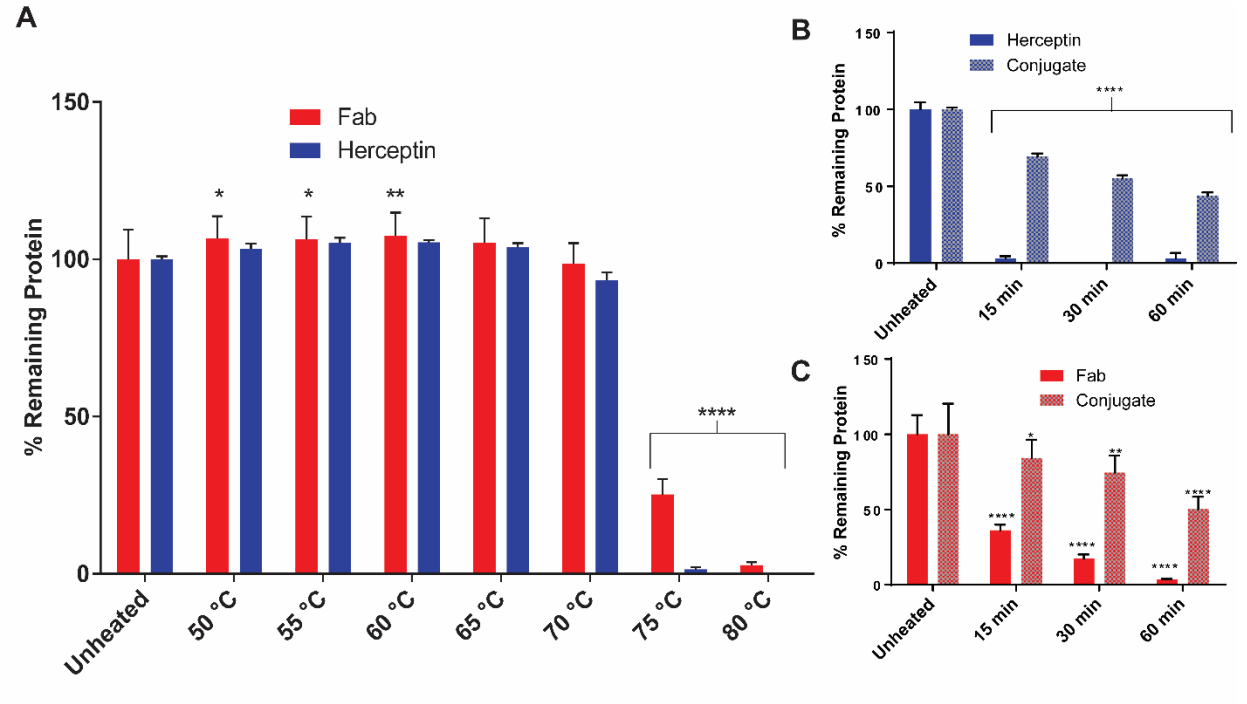

Figure 3.2.5. (A) Heat ramp of Fab and Herceptin. (B) Herceptin and Herceptin conjugate stability at 75 °C for 1 h, and (C) Fab and Fab conjugate stability at 75 °C for 1 h. Percent remaining protein was calculated *via* analytical HPLC after filtration through a 0.22 µM filter ($n = 3$). Statistical significance determined *via* two-way anova with: * = $p \leq 0.05$, ** = $p \leq 0.01$, **** = $p \leq 0.0001$ compared against the unheated sample in each data set.

Minimizing aggregation in antibody therapies is essential to maintain consistent and safe dosing for the patient. Aggregated antibodies are linked to a variety of poor health outcomes including renal failure and anaphylactoid reactions.[10,44] While excipients can often help to mitigate this instability, a large excess of stabilizing molecule is required. For instance, in the therapeutic

Herceptin formulation, almost 400 molar equivalents of trehalose per antibody are used. We have shown that significantly lower equivalents of trehalose polymers are required to stabilize proteins, especially when conjugated, and that the polymers have a distinct advantage compared to trehalose with regard to preventing heat-induced protein aggregation.[32] Thus, we hypothesize that localizing the trehalose polymer stabilizer through direct conjugation can help enhance antibody stability, particularly in more dilute solutions.

Before testing the stability of the conjugates, we first studied the heat stress conditions through a temperature ramp of the unmodified Herceptin and Fab (**Figure 3.2.5**). Both the Fab and the full Herceptin showed a large drop off in soluble protein concentration at 75 °C. Based on this, we chose 75 °C as our accelerated heat stress condition and monitored soluble protein over one hour at this temperature (**Figure 3.2.5**). For both the Herceptin and Fab conjugates, we observed only a 50% loss of soluble protein wherein the unmodified proteins showed little to no signal after one hour, demonstrating that the trehalose conjugates are able to inhibit Herceptin aggregation under these accelerated stress conditions. We further explored the mechanism of this stabilization *via* dynamic light scattering (DLS). While the unmodified Fab showed large aggregates greater than 1000 nm after heating at 75 °C for 1 h, the conjugate only showed a slight increase in size from 10 nm to 30 nm, suggesting the formation of soluble trimers/oligomers rather than insoluble particulates (**Figure 3.2.6**). From this, we hypothesize that the trehalose conjugate is largely stabilizing through inhibition of irreversible protein precipitation. Furthermore, despite the formation of higher-order oligomers for the conjugate under these stress conditions, there is evidence that soluble aggregates such as these can be reversible given the appropriate conditions.[45] We plan to continue investigation and optimization of the trehalose polymers to

further stabilize antibodies and their fragments by preventing such oligomerization and additionally studying the reversibility of this process in the future.

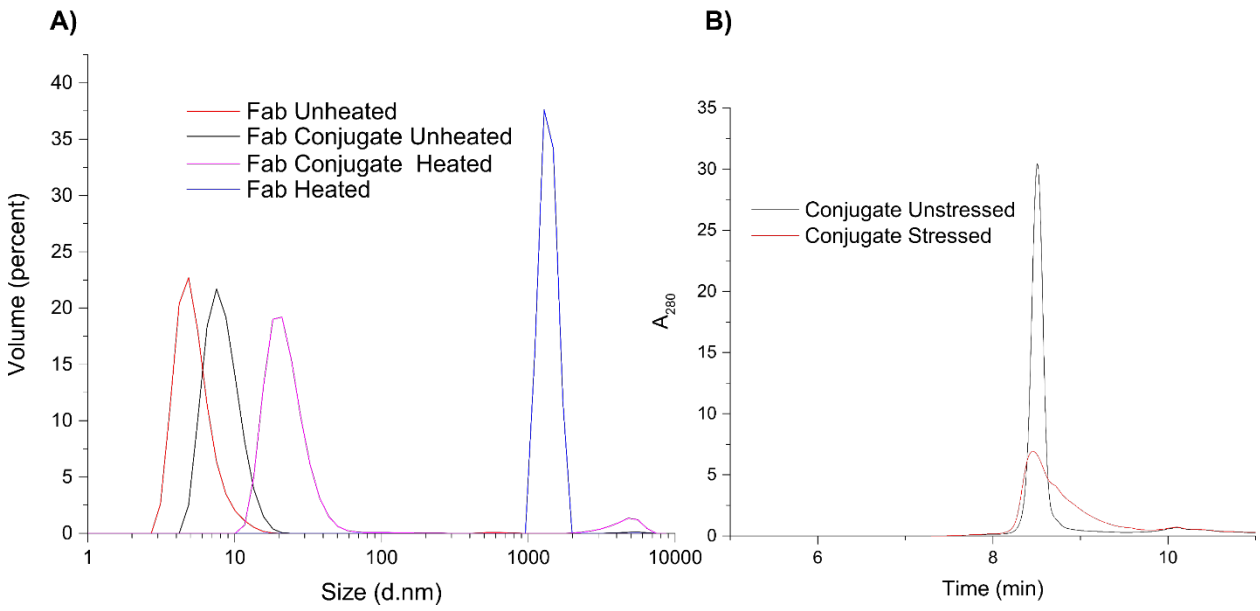

Figure 3.2.6. DLS and HPLC analysis of stressed antibodies and their conjugates.

We postulate that direct conjugation of a stabilizing, trehalose polymer can offer significant advantages to the therapeutic that justifies the decreased binding affinity. Primarily, from the accelerated stabilization data, we infer that the trehalose polymer is able to stabilize the antibodies from bulk aggregation when conjugated. This stabilizing property could be leveraged to increase the shelf life of the therapies and decrease the need for refrigerated storage. Furthermore, since the polymers increase the overall molecular weight of the protein, we envision, much like PEGylation, that the trehalose polymers could increase the *in vivo* half-life of the Fab conjugate. This would allow for a dual-stabilization of the protein wherein it would be able to withstand stressors both during storage and after administration.

3.3. Conclusions

A bis-sulfone initiator was prepared and polymerization conditions were optimized to produce well-controlled polymers of predictable molecular weight. This system was then applied to prepare disulfide-reactive trehalose polymers with low dispersity. Subsequent conjugation of these polymers to both a full IgG and its Fab fragment proceeded to quantitative conversion. The resulting conjugates retained activity towards their antigen and further demonstrated stability against bulk aggregation in an accelerated heat stress study. We believe this initiator and polymerization strategy to be useful platform for both the polymer and bioconjugation communities given that it provides good monomer compatibility without the need for post-polymerization modification. Additionally, we believe that the trehalose polymer platform convincingly stabilizes antibodies and their Fab fragments, and we anticipate its continued exploration in the field of antibody and protein conjugation.

3.4 References

(1) Lu, R.-M.; Hwang, Y.-C.; Liu, I.-J.; Lee, C.-C.; Tsai, H.-Z.; Li, H.-J.; Wu, H.-C. Development of Therapeutic Antibodies for the Treatment of Diseases. *Journal of Biomedical Science* **2020**, *27*, 1.

(2) Ecker, D. M.; Jones, S. D.; Levine, H. L. The Therapeutic Monoclonal Antibody Market. *MAbs* **2014**, *7*, 9–14.

(3) Reichert, J. M. Monoclonal Antibodies as Innovative Therapeutics. *Current pharmaceutical biotechnology* **2008**, *9*, 423–430.

(4) Nelson, A. L. Antibody Fragments. *MAbs* **2010**, *2*, 77–83.

(5) Junghans, R. P.; Anderson, C. L. The Protection Receptor for IgG Catabolism Is the Beta2-Microglobulin-Containing Neonatal Intestinal Transport Receptor. *Proc Natl Acad Sci U S A* **1996**, *93*, 5512–5516.

(6) Dennis, M. S.; Jin, H.; Dugger, D.; Yang, R.; McFarland, L.; Ogasawara, A.; Williams, S.; Cole, M. J.; Ross, S.; Schwall, R. Imaging Tumors with an Albumin-Binding Fab, a Novel Tumor-Targeting Agent. *Cancer Res* **2007**, *67*, 254–261.

(7) Batra, S. K.; Jain, M.; Wittel, U. A.; Chauhan, S. C.; Colcher, D. Pharmacokinetics and Biodistribution of Genetically Engineered Antibodies. *Current Opinion in Biotechnology* **2002**, *13*, 603–608.

(8) Goel, N.; Stephens, S. Certolizumab Pegol. *MAbs* **2010**, *2*, 137–147.

(9) Gombotz, W. R.; Pankey, S. C.; Phan, D.; Drager, R.; Donaldson, K.; Antonsen, K. P.; Hoffman, A. S.; Raff, H. V. The Stabilization of a Human IgM Monoclonal Antibody with Poly(Vinylpyrrolidone). *Pharm Res* **1994**, *11*, 624–632.

(10) Wang, W.; Singh, S.; Zeng, D. L.; King, K.; Nema, S. Antibody Structure, Instability, and Formulation. *Journal of Pharmaceutical Sciences* **2007**, *96*, 1–26.

(11) Ma, D.; Martin, N.; Herbet, A.; Boquet, D.; Tribet, C.; Winnik, F. M. The Thermally Induced Aggregation of Immunoglobulin G in Solution Is Prevented by Amphipols. *Chem. Lett.* **2012**, *41*, 1380–1382.

(12) Lyon, R. P.; Bovee, T. D.; Doronina, S. O.; Burke, P. J.; Hunter, J. H.; Neff-LaFord, H. D.; Jonas, M.; Anderson, M. E.; Setter, J. R.; Senter, P. D. Reducing Hydrophobicity of

Homogeneous Antibody-Drug Conjugates Improves Pharmacokinetics and Therapeutic Index. *Nature Biotechnology* **2015**, *33*, 733–735.

(13) Yurkovetskiy, A. V.; Yin, M.; Bodyak, N.; Stevenson, C. A.; Thomas, J. D.; Hammond, C. E.; Qin, L.; Zhu, B.; Gumerov, D. R.; Ter-Ovanesyan, E.; Uttard, A.; Lowinger, T. B. A Polymer-Based Antibody–Vinca Drug Conjugate Platform: Characterization and Preclinical Efficacy. *Cancer Res* **2015**, *75*, 3365–3372.

(14) Schneider, H.; Deweid, L.; Pirzer, T.; Yanakieva, D.; Englert, S.; Becker, B.; Avrutina, O.; Kolmar, H. Dextramabs: A Novel Format of Antibody-Drug Conjugates Featuring a Multivalent Polysaccharide Scaffold. *ChemistryOpen* **2019**, *8*, 354–357.

(15) Viricel, W.; Fournet, G.; Beaumel, S.; Perrial, E.; Papot, S.; Dumontet, C.; Joseph, B. Monodisperse Polysarcosine-Based Highly-Loaded Antibody-Drug Conjugates. *Chem. Sci.* **2019**, *10*, 4048–4053.

(16) Lu, Y.; Ngo Ndjock Mbong, G.; Liu, P.; Chan, C.; Cai, Z.; Weinrich, D.; Boyle, A. J.; Reilly, R. M.; Winnik, M. A. Synthesis of Polyglutamide-Based Metal-Chelating Polymers and Their Site-Specific Conjugation to Trastuzumab for Auger Electron Radioimmunotherapy. *Biomacromolecules* **2014**, *15*, 2027–2037.

(17) Ngo Ndjock Mbong, G.; Lu, Y.; Chan, C.; Cai, Z.; Liu, P.; Boyle, A. J.; Winnik, M. A.; Reilly, R. M. Trastuzumab Labeled to High Specific Activity with 111In by Site-Specific Conjugation to a Metal-Chelating Polymer Exhibits Amplified Auger Electron-Mediated Cytotoxicity on HER2-Positive Breast Cancer Cells. *Mol. Pharmaceutics* **2015**, *12*, 1951–1960.

(18) Satchi-Fainaro, R.; Wrasidlo, W.; Lode, H. N.; Shabat, D. Synthesis and Characterization of a Catalytic Antibody–HPMA Copolymer-Conjugate as a Tool for Tumor Selective Prodrug Activation. *Bioorganic & Medicinal Chemistry* **2002**, *10*, 3023–3029.

(19) L. Villaraza, A. J.; Bumb, A.; Brechbiel, M. W. Macromolecules, Dendrimers, and Nanomaterials in Magnetic Resonance Imaging: The Interplay between Size, Function, and Pharmacokinetics. *Chem. Rev.* **2010**, *110*, 2921–2959.

(20) Zhang, L.; Zhao, W.; Liu, X.; Wang, G.; Wang, Y.; Li, D.; Xie, L.; Gao, Y.; Deng, H.; Gao, W. Site-Selective in Situ Growth of Fluorescent Polymer–Antibody Conjugates with Enhanced Antigen Detection by Signal Amplification. *Biomaterials* **2015**, *64*, 2–9.

(21) Roy, D.; Nehilla, B. J.; Lai, J. J.; Stayton, P. S. Stimuli-Responsive Polymer-Antibody Conjugates via RAFT and Tetrafluorophenyl Active Ester Chemistry. *ACS Macro Lett.* **2013**, *2*, 132–136.

(22) Behrens, C. R.; Liu, B. Methods for Site-Specific Drug Conjugation to Antibodies. *mAbs* **2014**, *6*, 46–53.

(23) Schumacher, F. F.; Nobles, M.; Ryan, C. P.; Smith, M. E. B.; Tinker, A.; Caddick, S.; Baker, J. R. In Situ Maleimide Bridging of Disulfides and a New Approach to Protein PEGylation. *Bioconjugate Chem.* **2011**, *22*, 132–136.

(24) Morais, M.; Nunes, J. P. M.; Karu, K.; Forte, N.; Benni, I.; Smith, M. E. B.; Caddick, S.; Chudasama, V.; Baker, J. R. Optimisation of the Dibromomaleimide (DBM) Platform for Native Antibody Conjugation by Accelerated Post-Conjugation Hydrolysis. *Org. Biomol. Chem.* **2017**, *15*, 2947–2952.

(25) Jones, M. W.; Strickland, R. A.; Schumacher, F. F.; Caddick, S.; Baker, J. R.; Gibson, M. I.; Haddleton, D. M. Highly Efficient Disulfide Bridging Polymers for Bioconjugates from Radical-Compatible Dithiophenol Maleimides. *Chem. Commun.* **2012**, *48*, 4064–4066.

(26) Robin, M. P.; Jones, M. W.; Haddleton, D. M.; O'Reilly, R. K. Dibromomaleimide End Functional Polymers by RAFT Polymerization Without the Need of Protecting Groups. *ACS Macro Lett.* **2012**, *1*, 222–226.

(27) Alley, S. C.; Benjamin, D. R.; Jeffrey, S. C.; Okeley, N. M.; Meyer, D. L.; Sanderson, R. J.; Senter, P. D. Contribution of Linker Stability to the Activities of Anticancer Immunoconjugates. *Bioconjugate Chem.* **2008**, *19*, 759–765.

(28) Ryan, C. P.; Smith, M. E. B.; Schumacher, F. F.; Grohmann, D.; Papaioannou, D.; Waksman, G.; Werner, F.; Baker, J. R.; Caddick, S. Tunable Reagents for Multi-Functional Bioconjugation: Reversible or Permanent Chemical Modification of Proteins and Peptides by Control of Maleimide Hydrolysis. *Chem. Commun.* **2011**, *47*, 5452–5454.

(29) Lyon, R. P.; Setter, J. R.; Bovee, T. D.; Doronina, S. O.; Hunter, J. H.; Anderson, M. E.; Balasubramanian, C. L.; Duniho, S. M.; Leiske, C. I.; Li, F.; Senter, P. D. Self-Hydrolyzing Maleimides Improve the Stability and Pharmacological Properties of Antibody-Drug Conjugates. *Nature Biotechnology* **2014**, *32*, 1059–1062.

(30) Khalili, H.; Godwin, A.; Choi, J.; Lever, R.; Brocchini, S. Comparative Binding of Disulfide-Bridged PEG-Fabs. *Bioconjugate Chem.* **2012**, *23*, 2262–2277.

(31) Brocchini, S.; Balan, S.; Godwin, A.; Choi, J.-W.; Zloh, M.; Shaunak, S. PEGylation of Native Disulfide Bonds in Proteins. *Nat. Protocols* **2006**, *1*, 2241–2252.

(32) Balan, S.; Choi, J.; Godwin, A.; Teo, I.; Laborde, C. M.; Heidelberger, S.; Zloh, M.; Shaunak, S.; Brocchini, S. Site-Specific PEGylation of Protein Disulfide Bonds Using a Three-Carbon Bridge. *Bioconjugate Chem.* **2007**, *18*, 61–76.

(33) Brocchini, S. J.; Godwin, A. R.; Tang, Y.; Lewis, A. L. Derivatisation of Biological Molecules. US8575397B2, November 5, 2013.

(34) Lewis, A.; Tang, Y.; Brocchini, S.; Choi, J.; Godwin, A. Poly(2-Methacryloyloxyethyl Phosphorylcholine) for Protein Conjugation. *Bioconjugate Chem.* **2008**, *19*, 2144–2155.

(35) Lee, J.; Lin, E.-W.; Lau, U. Y.; Hedrick, J. L.; Bat, E.; Maynard, H. D. Trehalose Glycopolymers as Excipients for Protein Stabilization. *Biomacromolecules* **2013**, *14*, 2561–2569.

(36) Liu, Y.; Lee, J.; Mansfield, K. M.; Ko, J. H.; Sallam, S.; Wesdemiotis, C.; Maynard, H. D. Trehalose Glycopolymer Enhances Both Solution Stability and Pharmacokinetics of a Therapeutic Protein. *Bioconjugate Chem.* **2017**, *28*, 836–845.

(37) Lins, R. D.; Pereira, C. S.; Hünenberger, P. H. Trehalose–Protein Interaction in Aqueous Solution. *Proteins: Structure, Function, and Bioinformatics* **2004**, *55*, 177–186.

(38) Sakurai, M. Biological Functions of Trehalose as a Substitute for Water. In *Water and Biomolecules: Physical Chemistry of Life Phenomena*; Kuwajima, K., Goto, Y., Hirata, F., Kataoka, M., Terazima, M., Eds.; Biological and Medical Physics, Biomedical; Springer: Berlin, Heidelberg, 2009; pp 219–240.

(39) Mancini, R. J.; Lee, J.; Maynard, H. D. Trehalose Glycopolymers for Stabilization of Protein Conjugates to Environmental Stressors. *Journal of the American Chemical Society* **2012**, *134*, 8474–8479.

(40) Messina, M. S.; Ko, J. H.; Yang, Z.; Strouse, M. J.; Houk, K. N.; Maynard, H. D. Effect of Trehalose Polymer Regioisomers on Protein Stabilization. *Polym. Chem.* **2017**, *8*, 4781–4788.

(41) Mansfield, K. M.; Maynard, H. D. Site-Specific Insulin-Trehalose Glycopolymer Conjugate by Grafting from Strategy Improves Bioactivity. *ACS Macro Lett.* **2018**, *7*, 324–329.

(42) Liu, H.; Chumsae, C.; Gaza-Bulseco, G.; Hurkmans, K.; Radziejewski, C. H. Ranking the Susceptibility of Disulfide Bonds in Human IgG1 Antibodies by Reduction, Differential Alkylation, and LC−MS Analysis. *Anal. Chem.* **2010**, *82*, 5219–5226.

(43) Selis, F.; Focà, G.; Sandomenico, A.; Marra, C.; Di Mauro, C.; Saccani Jotti, G.; Scaramuzza, S.; Politano, A.; Sanna, R.; Ruvo, M.; Tonon, G. Pegylated Trastuzumab Fragments Acquire an Increased in Vivo Stability but Show a Largely Reduced Affinity for the Target Antigen. *Int J Mol Sci* **2016**, *17*.

(44) Demeule, B.; Gurny, R.; Arvinte, T. Where Disease Pathogenesis Meets Protein Formulation: Renal Deposition of Immunoglobulin Aggregates. *Eur J Pharm Biopharm* **2006**, *62*, 121–130.

(45) Arosio, P.; Barolo, G.; Müller-Späth, T.; Wu, H.; Morbidelli, M. Aggregation Stability of a Monoclonal Antibody During Downstream Processing. *Pharm Res* **2011**, *28*, 1884–1894.

3.5 Materials and Methods

All chemicals were purchased from Sigma-Aldrich and Fisher Scientific and were used without purification unless otherwise noted. For PEGMA, inhibitor was removed by passing through a plug of basic alumina. Herceptin® was purchased from the UCLA pharmacy. Fab specific (anti-Human IgG, Fab Specific−Peroxidase antibody produced in goat) and whole molecule (Anti-Human IgG (whole molecule) −Peroxidase antibody produced in rabbit) imaging antibodies were purchased from Sigma-Aldrich. MilliporeSigma™ Millex™ hydrophilic PTFE filters were used for stability studies. Trehalose was purchased from The Healthy Essential Management Corporation (Houston, TX) and was azeotropically dried with ethanol and kept under vacuum until use. Recombinant Her_2 antigen (Erb2 Fc Chimera) was purchased from R&D Solutions.

Analytical Techniques. Nuclear Magnetic Resonance (NMR) spectra were recorded on a Bruker DRX 500 MHz, Bruker AV 500 MHz, and Bruker AV 600 MHz spectrometer. Proton NMR spectra were acquired with a relaxation delay of 2 s for small molecules and 10 seconds for polymers. Mass spectrometry for both proteins and small molecules was obtained on an Agilent Q-TOF 6530 LC/MS. For trehalose polymers, size exclusion chromatography (SEC) was conducted on a Malvern Viscotek GPCmax equipped with a TDA 305-040 Quadruple Detector Array (RI + Viscosity + LALS/RALS + UV) and 0.05 M sodium sulfate in water + 10 % methanol as eluent at a flow rate of 1.0 mL/min. For PEGMA polymerizations, SEC was conducted on a Shimadzu high performance liquid chromatography (HPLC) system with a refractive index detector (RID-10A), one Phenomenex Phenogel 10 μm guard column, and two Polymer Laboratories PLgel 5 μm mixed D columns in DMF eluent with LiBr (0.1 M) at 50 °C (flow rate: 0.80 mL/min). Trehalose monomer was purified by preparatory reverse phase high performance liquid chromatography (HPLC) on a Shimadzu system equipped with a UV detector using a Luna

5 μm C18 100A column (5 μm, 250 x 21.2 mm) with monitoring at λ = 215 nm and 254 nm. Gradient solvent system (water:methanol = 90:10 to 40:60 over 20 min) was used as the mobile phase at a flow rate of 20 mL/min. For SDS PAGE, BioRad Any kD Mini-PROTEAN-TGX™ gels were used for the Fab and Fab conjugate while 4–15% Mini-PROTEAN® TGX™ gels were used for Herceptin and the Herceptin conjugate. SDS-PAGE protein standards were obtained from Bio-Rad (Precision Plus Protein Prestained Standards). Protein and conjugate purifications were conducted via FPLC on a Bio-Rad BioLogic DuoFlow chromatography system with UV monitoring at 280 nm (cation exchange column: 1mL GE Healthcare SPHP column, protein A: 1 mL MabSelect protein A GE Healthcare). Western blot was imaged with SuperSignal West Pico Chemiluminescent substrate paired with a CCD camera. Small molecule purification was done via flash chromatography was conducted on a Biotage Isolera One auto-column system.

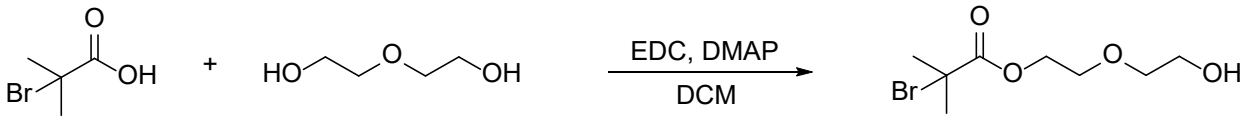

Ethylene glycol initiator synthesis. To an oven-dried scintillation vial with a stir bar, α-bromoisobutyric acetic acid (0.5 g, 2.99 mmol, 1 equivalent) and diethylene glycol (1.42 mL, 15 mmol, 5 equivalents) were added. The reagents were dissolved in 10 mL of dry DCM and cooled to 0 ºC. To the reaction mixture, *N*-(3-dimethylaminopropyl)-N′-ethylcarbodiimide hydrochloride (EDC, 0.69 g, 3.6 mmol, 1.2 equivalents) and 4-dimethylaminopyridine (DMAP, 0.037g, 0.299 mmol, 0.1 equivalents) was added. The reaction was allowed to warm to 22 ºC and proceed for 3 hrs. The product was purified via flash column chromatography with a 1:1 hexanes:ethyl acetate mobile phase (R_f product ~ 0.3) to afford 492 mg (64.5 % yield) of product as a clear oil. ^{1}H NMR (500 MHz, Chloroform-d) δ 4.37 – 4.32 (m, 2H), 3.78 – 3.70 (m, 4H), 3.64 – 3.59 (m, 2H), 1.94

(s, 6H). ^{13}C NMR (126 MHz, Chloroform-*d*) δ 171.70, 72.36, 68.73, 64.96, 61.76, 55.68, 30.73. IR: ν = 3442, 2873, 1732, 1462 cm^{-1}. HRMS calculated for $C_8H_{15}BrO_4Na$ ([M + Na]$^+$) = 277.0051, observed = 276.9304.

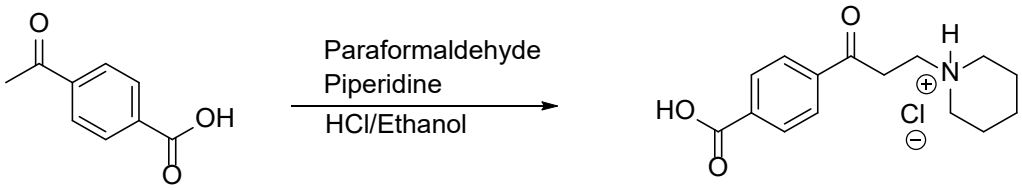

Mannich Salt Synthesis. Product was synthesized from modified procedure by Brocchini *et al.*[1] To a 250 mL round bottom flask with a stirbar absolute ethanol (25 mL), 4-acetyl benzoic acid (2 g, 12.2 mmol, 1 equivalent), piperidine (1.2 mL, 12.2 mmol, 1 equivalent), and paraformaldehyde (1.1 g, 36.5 mmol, 3 equivalents) were added. To this solution, concentrated HCl (1.13 mL of 37%, 13.7 mmol, 1.1 equivalents) was added. The reaction mixture was refluxed at 105 ºC for 12 h and then allowed to cool to 22 ºC. After cooling, 20 mL of acetone was added and the product was isolated via vacuum filtration to yield 4.47 g (61.6% yield) of a white powder. ^{1}H NMR (500 MHz, Deuterium Oxide) δ 8.03 – 7.95 (m, 4H), 3.57 (t, *J* = 6.8 Hz, 2H), 3.52 – 3.39 (m, 4H), 2.91 (td, *J* = 12.5, 3.1 Hz, 2H), 1.85 (dt, *J* = 15.3, 3.6 Hz, 2H), 1.76 – 1.55 (m, 3H), 1.39 (qt, *J* = 11.9, 3.7 Hz, 1H). ^{13}C NMR (126 MHz, Deuterium Oxide) δ 199.12, 170.43, 138.60, 135.75, 129.77, 128.20, 53.55, 51.60, 33.10, 22.67, 20.96. HRMS calculated for $C_{15}H_{19}NO_3$ ([M+H]$^+$) = 262.1443, observed =262.1348.

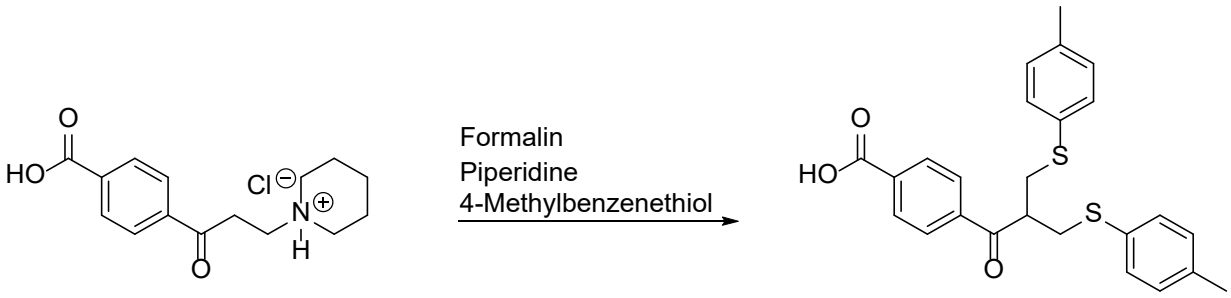

Bis-sulfide acid synthesis. Product was synthesized from modified procedure by Brocchini *et al.*[1] To a 15 mL round bottom flask, Mannich salt (0.7 g, 2.35 mmol, 1 equivalent), 4-methylbenzene thiol (0.58g, 4.7 mmol, 2 equivalents), piperidine (0.1 mL, 1.01 mmol, 0.43 equivalents), formaldehyde (37% solution, 1 mL), ethanol (2 mL), and methanol (1 mL) were added. The solution was refluxed at 105 °C for 1 hr. After 1 h, the reaction was allowed to cool to 22 °C before adding formaldehyde (37% solution, 1 mL) again. The reaction was then refluxed for 3 more hours at 105 °C. The solution was then cooled to 22 °C and the solvent was removed *in vacuo*. To the crude, ~2 mL of methanol was added and heated to dissolve the suspension. The product was allowed to crystalize for 12 h at -20 °C and the product was isolated 400 mg (52.1% yield) via vacuum filtration as white crystals. ^{1}H NMR (500 MHz, Chloroform-*d*) δ 8.05 – 7.99 (m, 2H), 7.63 – 7.57 (m, 2H), 7.16 – 7.10 (m, 4H), 7.09 – 6.98 (m, 4H), 3.80 (p, *J* = 8.4 Hz, 1H), 3.24 (dd, *J* = 13.6, 7.4 Hz, 2H), 3.15 (dd, *J* = 13.6, 6.1 Hz, 2H), 2.35 (s, 6H). ^{13}C NMR (126 MHz, Chloroform-*d*) δ 200.45, 168.80, 140.44, 137.29, 132.75, 131.58, 131.06, 130.27, 129.87, 128.34, 45.85, 36.39, 21.12. IR: ν =3015, 2919, 2650,1678 cm^{-1}. HRMS calculated for $C_{25}H_{24}O_3S_2$ ([M+K]$^+$) = 475.0804, observed = 474.9805.

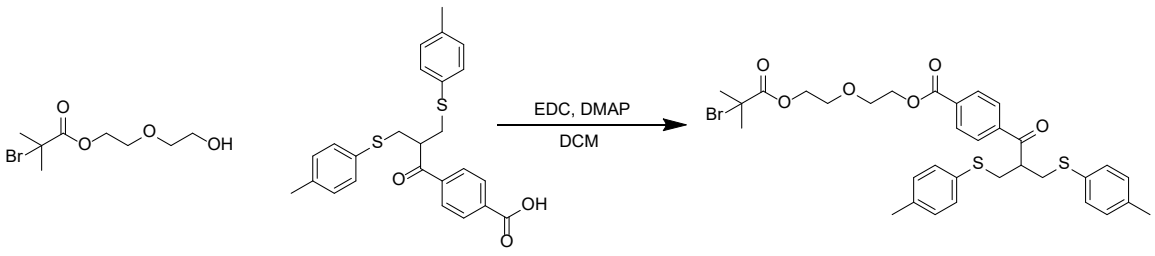

Bis-sulfide synthesis initiator. To a 20 mL scintillation with a stir bar, diethylene glycol initiator (140 mg, 0.55 mmol, 1.2 equivalent), bis-sulfide acid (200 mg, 0.46 mmol, 1 equivalent), EDC (176 mg, 0.916 mmol, 2 equivalents), and DMAP (11.2 mg, 0.0916, 0.2 equivalents) were added and dissolved in 5 mL of dry DCM. Coupling was allowed to proceed overnight for 12 h followed

by concentration via rotovap. Product was purified with via flash chromatography with a gradient of Hex:EtOAc from 0% to 45% over 18 column volumes to yield 155 mg (56%) of a clear oil. ^{1}H NMR (400 MHz, Chloroform-*d*) δ 8.03 – 7.95 (dt, *J* = 8.7, 1.7 Hz, 2H), 7.59 (dt, *J* = 8.5, 1.7 Hz, 2H), 7.17 – 7.09 (dt, *J* = 8.2, 2.3 Hz, 4H), 7.09 – 7.01 (d, *J* = 7.9 Hz, 4H), 4.53 – 4.47 (m, 2H), 4.39 – 4.30 (m, 2H), 3.92 – 3.72 (m, 5H), 3.24 (dd, *J* = 13.6, 7.3 Hz, 2H), 3.15 (dd, *J* = 13.6, 6.2 Hz, 2H), 2.35 (s, 6H), 1.91 (s, 6H). ^{13}C NMR (126 MHz, Chloroform-*d*) δ 200.49, 137.23, 133.84, 131.52, 131.12, 129.88, 129.83, 128.26, 69.15, 68.81, 64.99, 64.45, 45.79, 36.40, 30.72, 21.13. IR: ν = 2921, 1723, 1684, 1269, 1103, 805 cm^{-1}. ESI-MS calculated for $C_{33}H_{37}BrO_6S_2$ ([M + Na]$^{+}$) = 695.1112, observed = 695.1142

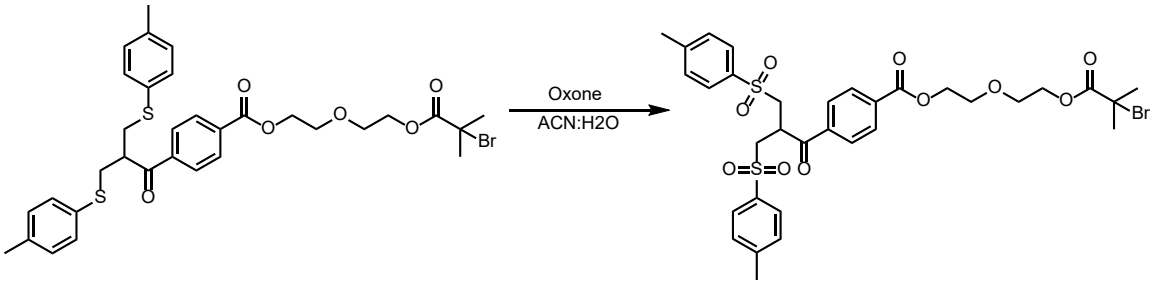

Bis-sulfone initiator synthesis. Bis sulfide (149 mg, 0.221 mmol, 1 equivalent) and oxone monopersulfate (1.63 g, 5.3 mmol, 24 equivalents) were dissolved in 10 mL of 1:1 acetonitrile:H_2O in a scintillation vial with stir bar. Reaction was stirred vigorously for 4 h, after which complete conversion was observed via LCMS. Acetonitrile was removed via rotovap and DCM and water were added to the vial. The reaction was transferred to a separatory funnel and the organic layer was collected. The aqueous layer was extracted three times with DCM and organic layers were pooled before drying with $MgSO_4$. Solvent was removed via rotary evaporation and the resulting oil was re-dissolved in acetonitrile. The product was then precipitated into 15 mL of water, centrifuged, and the supernatant was discarded. The resulting residue was lyophilized to yield 137

mg (84%) of a white foam. It was found that without the final precipitation step, the product failed to initiate polymerization. We attribute this to excess oxone that likely interferes with the reduction of $CuBr_2$ during the AGET ATRP process. ^{1}H NMR (500 MHz, Chloroform-*d*) δ 8.04 (dt, *J* = 8.5, 1.7, 2H), 7.69 (m, 6H), 7.36 (d, *J* = 7.9 Hz, 4H), 4.51 (m, 2H), 4. (m, 3H), 3.87 (m, 2H), 3.80 (m, 2H), 3.61 (dd, *J* = 14.3, 6.6 Hz, 2H), 3.48 (dd, *J* = 14.3, 5.9 Hz, 2H), 2.48 (s, 6H), 1.92 (s, 6H). ^{13}C NMR (126 MHz, Chloroform-*d*) δ 195.31, 171.62, 165.36, 145.57, 137.53, 135.33, 134.60, 130.22, 130.14, 128.48, 128.34, 69.11, 68.83, 64.98, 64.58, 55.65, 55.59, 35.70, 30.72, 21.75. IR: ν = 2926, 1723, 1694, 1271, 1141, 1106, 1085, 742 cm^{-1}. ESI-MS calculated for $C_{33}H_{37}BrO_{10}S_2$ ($[M+NH_4]^+$) = 754.1355, observed = 754.0900.

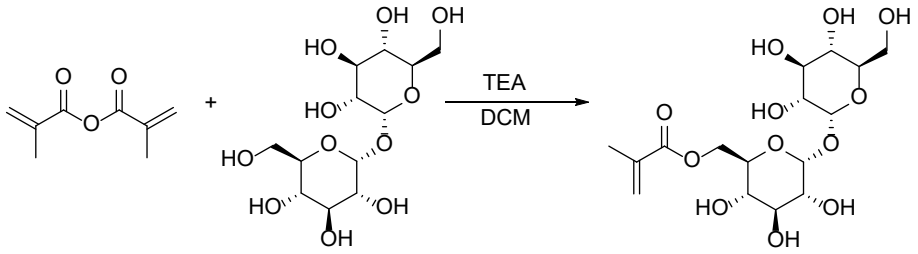

Trehalose methacrylate synthesis. Trehalose monomer was synthesized as previously reported.[2] To an oven-dried 250 mL flask, azeotropically dried trehalose (6.92 g, 20.2 mmol, 5 equivalents) was added and dissolved in dry DMSO. Dry TEA (8.41 mL, 60.7 mmol, 15 equivalents) and methacrylic anhydride (0.6 mL, 4.05 mmol, 1 equivalent) were added sequentially and the reaction was allowed to proceed for 16 h under argon. The crude was then precipitated into a chilled flask of 1800 mL of 8:2 Hex/DCM. The antisolvent was poured off and the remaining oil was dissolved in 70 mL of water. The sample was the purified via preparatory high-performance liquid chromatograph (10-60% gradient over 20 minutes). Fractions containing product were combined and 150 ppm of 4-methoxy phenol was added to prevent auto-polymerization. Methanol was removed via rotary evaporation in a 2-neck round bottom and a septum with a needle bubbling

into the solution to provide oxygen and prevent autopolymerization. The remaining water was then lyophilized and 698 mg (41.4 %) of product was recovered via lyophilization as a fluffy solid. ^{1}H NMR (600 MHz, Deuterium Oxide) δ 6.01 (s, 1H), 5.60 (s, 1H), 5.04-5.01 (dd, J = 3.9 Hz, 2H), 4.35 (d, J = 12.3, 2.2 Hz, 1H), 4.22 (dd, J = 12.3, 5.2 Hz, 1H), 3.94 (m, J = 10.1, 5.3, 2.1 Hz, 1H), 3.75 – 3.64 (m, 4H), 3.61 (dd, J = 12.1, 5.2 Hz, 1H), 3.53 (dd, J = 9.9, 3.9 Hz, 1H), 3.48 (dd, J = 10.0, 3.9 Hz, 1H), 3.40 (t, J = 9.6 Hz, 1H), 3.29 (t, J = 9.5 Hz, 1H), 1.79 (s, 3H). ESI-MS calculated for $C_{16}H_{26}O_{12}$ ([M+Na]$^{+}$) = 433.1322, observed = 433.1458.

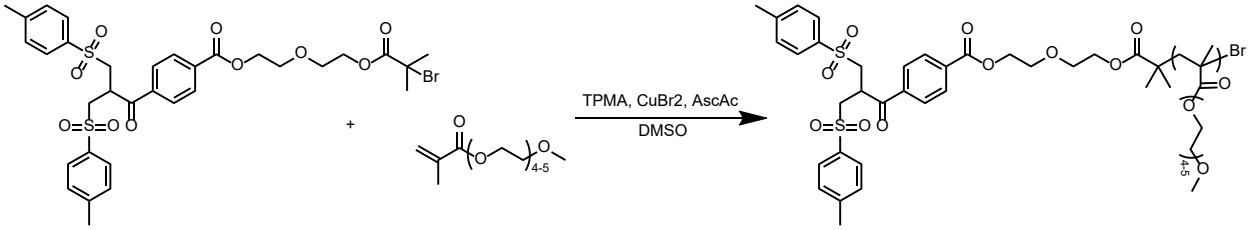

Representative PEGMA Polymerization. Stock solutions of $CuBr_2$ (16 mg/mL), tris (2-pyridylmethyl) amine (TPMA, 43 mg/mL), and bis-sulfone initiator (54 mg/mL) were prepared in DMSO in individual dram vials. To a scintillation vial containing PEGMA monomer (0.4 mL, 1.5 mmol, 200 equivalents), 100 µL of the $CuBr_2$ (1.6 mg, 7.4 µmol, 1 equivalent), 100 µL of the TPMA stock (4.3 mg, 15 µmol, 2 equivalents), and 100 µL of initiator (5.4 mg, 7.4 µmol, 1 equivalent) were added along with 2.8 mL of DMSO (0.45 M with respect to monomer). For percent conversion analysis, 40 µL of tetralin was added as an internal standard. The mixture was then transferred to a Schlenk tube and three freeze-pump-thaw cycles were conducted. Meanwhile, a stock solution (7.8 mg/mL) of ascorbic acid was sparged with argon. After the final freeze-pump-thaw cycle, the polymerization was initiated by adding 100 µL of the sparged ascorbic acid solution (0.78 mg, 4.43 µmol, 0.6 equivalents) to the Schlenk flask.

For kinetics, timepoints were collected through an argon-purged syringe and frozen immediately in liquid nitrogen to quench. After thawing, the timepoint was diluted in ~0.1 mL of DMF. A portion of the sample was used for GPC analysis while a separate aliquot was diluted 5-fold in acetonitrile for HPLC analysis. Percent conversion was determined via analytical HPLC by comparing the PEGMA monomer integration against the tetralin internal standard.

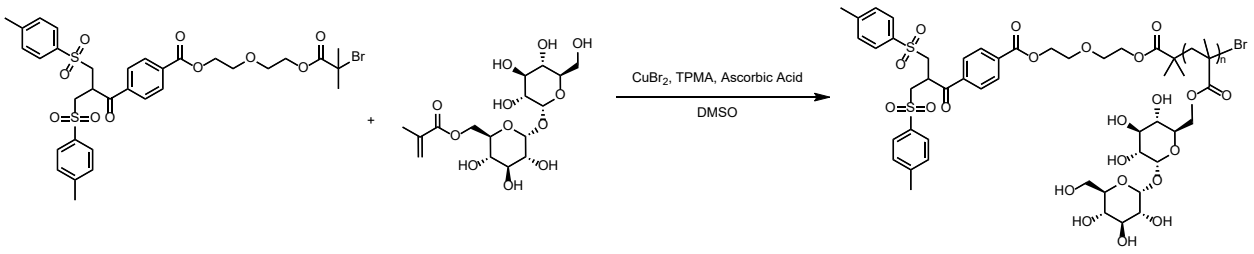

Polymerization of trehalose monomer. Stock solutions of $CuBr_2$ (21.8 mg/mL), TPMA (56.6 mg/mL), and sulfone initiator (72.0 mg/mL) were prepared in dry DMSO in individual dram vials. To a scintillation vial containing trehalose monomer (100 mg, 0.24 mmol, 25 equivalents), 100 µL of the $CuBr_2$ stock (2.18 mg, 9.7 µmol, 1 equivalent), 100 µL of the TPMA stock (5.7 mg, 19.4 µmol, 2 equivalents), and 100 µL of the sulfone initiator (7.2 mg, 9.7 µmol, 1 equivalent) were added and the resulting solution transferred to a Schlenk tube. An additional 50 µL of DMSO was used to dissolve remaining reagents and also transferred to the Schlenk flask. Meanwhile, an 18.4 mg/mL solution of ascorbic acid was sparged with argon in dram vial with a septum for ~15 min. The solution in the Schlenk flask was degassed via 3 freeze-pump-thaw cycles and 56 µL of the sparged ascorbic acid solution (1.03 mg, 5.8 µmol, 0.6 equivalents) was added to initiate polymerization (final reaction volume = 406 µL, 0.6 M with respect to monomer). The polymerization was allowed to proceed for 16 h before quenching with liquid N_2. The polymer was purified via dialysis (MWCO = 3.5 kDa) against water for 2 days and recovered via

lyophilization. ^{1}H NMR (500 MHz, Deuterium Oxide) δ 5.10, 5.05, 4.23, 4.01, 3.93, 3.75, 3.66, 3.53, 3.35, 1.81, 0.97, 0.79.

NMR used calculate molecular weight in addition to GPC. Proton A was set to an integration of 2 and used to determine the integration of peak D. The values were then plugged into the following formula: $\frac{\text{Integration of D}}{2} * 410.37$

Fab preparation. The FAB preparation was adapted from a reported literature reports.[3,4] First, 224 mg of cysteine was added to 12 mL of digestion buffer (20 mM NaH_2PO_4, pH 7.4, 10 mM EDTA) immediately before use. Then, 1.6 mL of immobilized papain resin was added to 2.4 mL of digestion buffer and the resulting suspension was centrifuged (1000xg, 2 min). The supernatant was discarded and the resin was resuspended in 2.4 mL of digestion buffer. This procedure was repeated a total of 3 times. After resuspending the final time, the slurry was added to a 15 mL conical tube. To the suspension, 4 milligrams of Herceptin (previously dissolved in 200 µL of digestion buffer) was added. The sample was purged with argon and incubated in thermoshaker (300 rpm, 37 °C) for 20 hrs. The crude reaction mixture was then centrifuged (1000xg, 2 min) and the supernatant was collected. Resin was resuspended in 2 mL of digestion buffer and the previous process of centrifugation followed by supernatant collection was repeated twice. The pooled supernatants were then purified via fast-protein liquid chromatography as outlined below.

A 1 mL Mabselect SuRe® was equilibrated with phosphate buffered saline (pH 7.4) at a flowrate of 0.7 mL/min. Sample was loaded and Fab was eluted from column with 12 column volumes (CV) of isocratic PBS. The F_c was eluted with a linear gradient of 0-100% 50 mM glycine buffer (pH 2.7) over 20 column volumes. Fractions containing Fab were pooled, dialyzed into PBS buffer, concentrated via ultracentrifugation, and stored at 4 °C. Deconvoluted ESI-mass spectrometry of

the reduced Fab displayed 3 masses corresponding to light chain of Herceptin (calculated = 24204.14, observed = 24203.64) and two different heavy chain papain cleavage sites differing by the tripeptide KTH (calculated without KTH peptide = 23443.10, observed = 23441.26 and calculated with KTH= 23837.72, observed = 23836.71).

Representative conjugation to Fab. 1 mL of Fab stock was concentrated via Amicon 30 kDa ultra centrifugal filtration to a concentration of 9.1 mg/mL (91 μL volume, 832 ug protein, 1.7 x 10^{-8} mol). To this sample, 1 weight equivalent of DTT was added and reduction was allowed to proceed at 22 °C for 1 hr. The sample was then buffer exchanged via 0.5 mL ZEBA desalting column into PBS+10 mM EDTA. A 100 mg/mL stock of 23 kDa trehalose polymer dissolved in MilliQ water was then added (4.16 mg, 1.72 x 10^{-7} mol, 10 equivalents). Conjugation was allowed to proceed at 22 °C for 12 h. Conjugate was purified from excess polymer via cation exchange chromatography using 1 mL GE Healthcare SPHP columns. Free polymer was eluted with isocratic 20 mM MES, pH 5.7 over 12 CV's. Conjugate was eluted with a linear gradient of 20 mM MES, pH 5.7, 300 mM NaCl over 15 CVs.

Representative Herceptin Conjugation. Herceptin (10 mg/mL, 100 μL) was dissolved in 20 mM sodium phosphate buffer with 20 mM EDTA. Next, 3.5 μL of a 1 mg/mL solution of TCEP was added and incubated for 2 h at 37 °C. TCEP was then removed via Amicon ultrafiltration (100 kDa cutoff) and 50 equivalents of 16 kDa bis-sulfone trehalose polymer (dissolved in water) was added. The conjugation was allowed to proceed overnight for 16 h at 40 °C. The conjugate was purified via cation exchange chromatography with a HiTrap SPHP column. Free polymer was eluted with 8 column volumes of isocratic MES buffer (pH 5.6) followed by elution of the conjugate with a gradient of MES buffer (pH 5.6) + 300 mM NaCl over 12 column volumes.

General ELISA Protocol. To the wells of a high-binding 96 well plate, 100 µL of a 1 µg/mL solution (diluted in 0.1 M carbonate buffer, pH 9.6) of recombinant Her_2 was added. The plate was covered with foil and incubated at 4 °C overnight for 12 h. The following day, the solution was aspirated and the plate was washed four times with ELISA wash buffer (PBS + 0.3% Tween 20). To the wells, 200 µL of blocking buffer (1% BSA in PBS, filtered with 0.22 µM filter) was added and incubated at 22 °C for 2 h. Again, 4 washes were performed with wash buffer before adding 100 µL of antibody and conjugate samples at appropriate dilution (dilution buffer = 1% BSA in PBS). The plate was incubated at 22 °C for 1 h before repeating aspiration and wash procedure. FAB-specific peroxidase labeled anti-human IgG (diluted 1:40,000 in dilution buffer) was then added (100 µL per well) and the plate was incubated at 37 °C for 45 min. After aspirating and washing the plate a final time, 100 µL of TMB (3,3',5,5'-Tetramethylbenzidine) substrate solution was added to the wells via a multichannel pipette and the plate was incubated in the dark for ~5 min. After sufficient development of blue color, 50 µL of 1 M sulfuric acid was added via multichannel pipette and absorbance of each well was measured at 450 nm.

Stability Heat Ramp. Fab protein was diluted to 0.1 mg/mL in PBS and 50 µL aliquots were divided among 24 separate 0.5 mL Lo-Bind Eppendorf tubes. Three of the aliquots were stored at 4 °C to serve as a control. The remaining tubes were placed in a pre-heated water bath at 50 °C. At 30-minute intervals, 3 samples (triplicate samples) were removed and stored at 4 °C, and the temperature of the bath was increased by 5 °C. This procedure was repeated to a final temperature of 80 °C. Samples were then filtered through a 0.22 µM and remaining protein was analyzed via analytical HPLC (C3 stationary phase, 10-95% acetonitrile+0.1% TFA, 5% isocratic isopropanol + 0.1% TFA, 70 °C column temperature).

Stability at 75 °C. Fab and Fab conjugate were diluted to 0.1 mg/mL in PBS. For both sets of samples, 12 aliquots of 50 µL divided into separate lo-bind Eppendorf tubes. Three samples were stored at 4 °C for both the conjugate and Fab to serve as controls. The remaining samples were placed in a preheated 75 °C water bath. Three samples were removed from each group at 15 minutes, 30 minutes, and 60 minutes and stored at 4 °C until analysis. Samples were then filtered through a 0.22 µM and remaining protein was analyzed via analytical HPLC (C3 stationary phase,10-95% acetonitrile+0.1% TFA, 5% isocratic isopropanol + 0.1% TFA, 70 °C column temperature).

3.6 Appendix with Supplementary Figures.

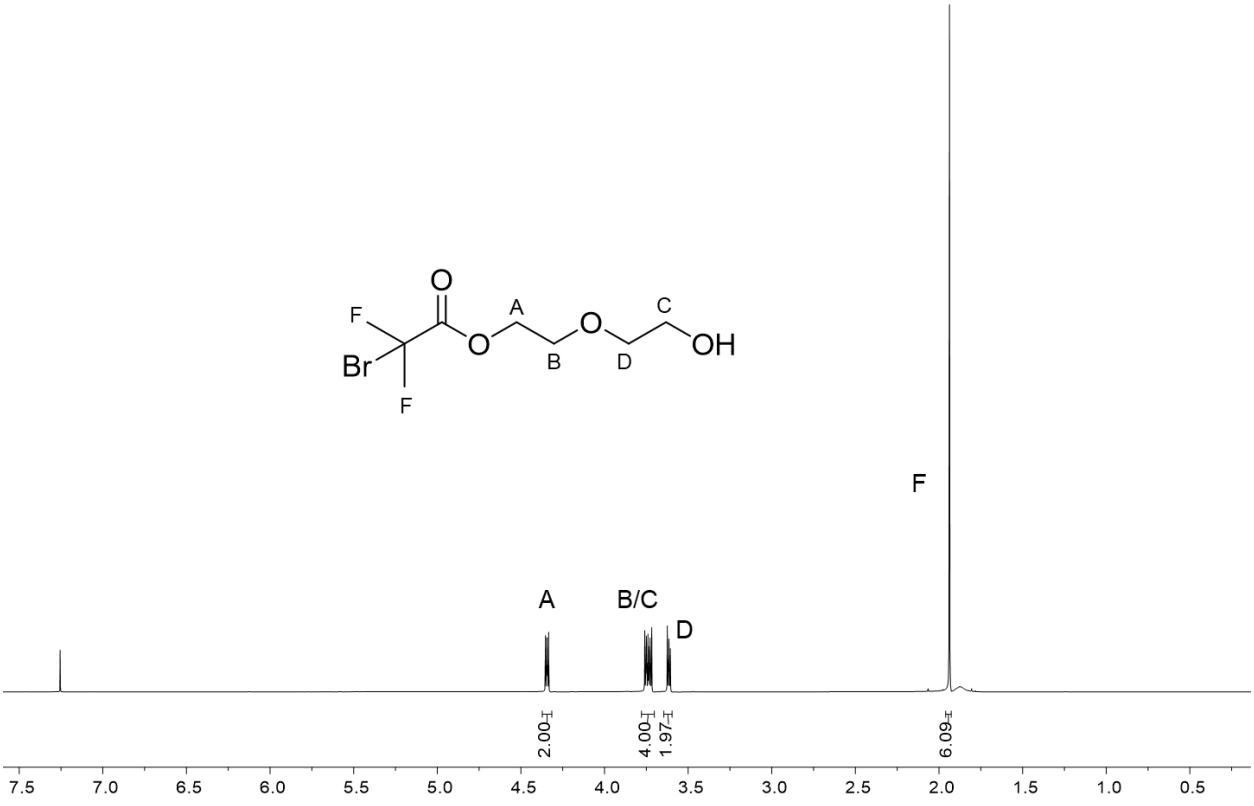

Figure 3.6.1. ^{1}H NMR of ethylene glycol initiator ($CDCl_3$).

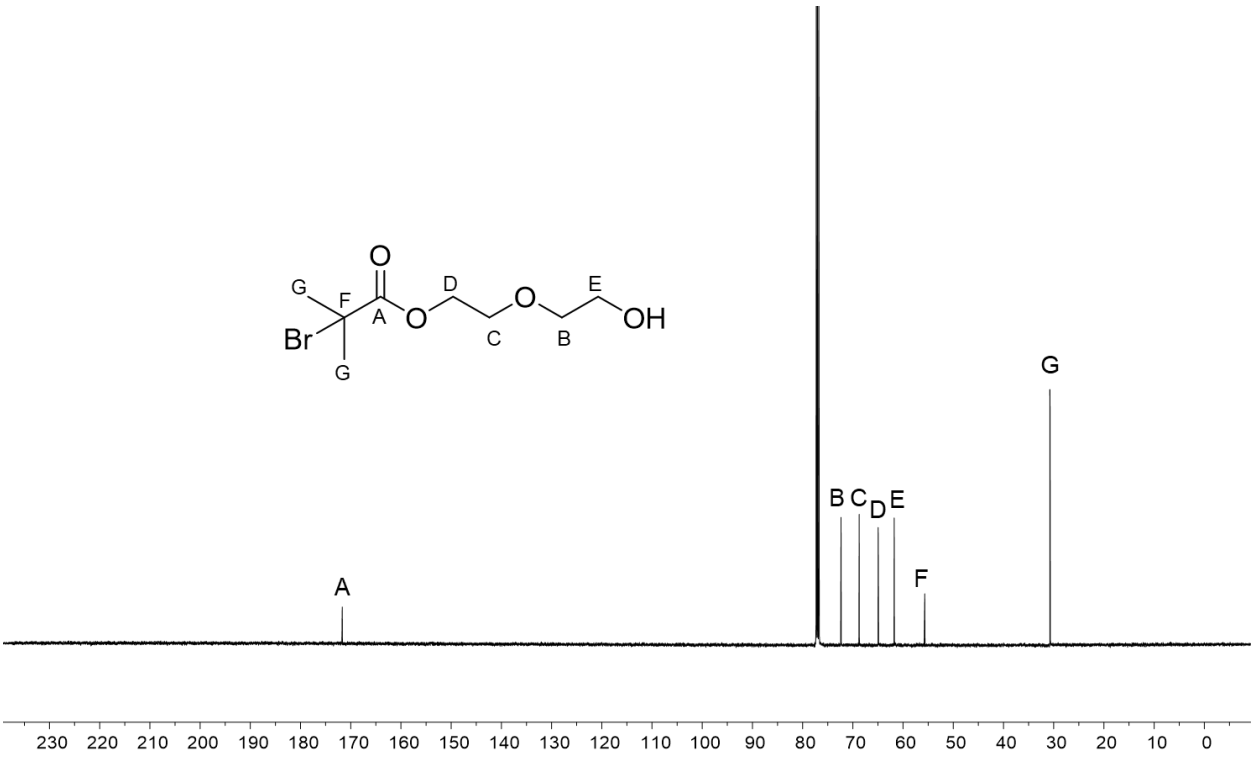

Figure 3.6.2. ^{13}C NMR of ethylene glycol initiator ($CDCl_3$).

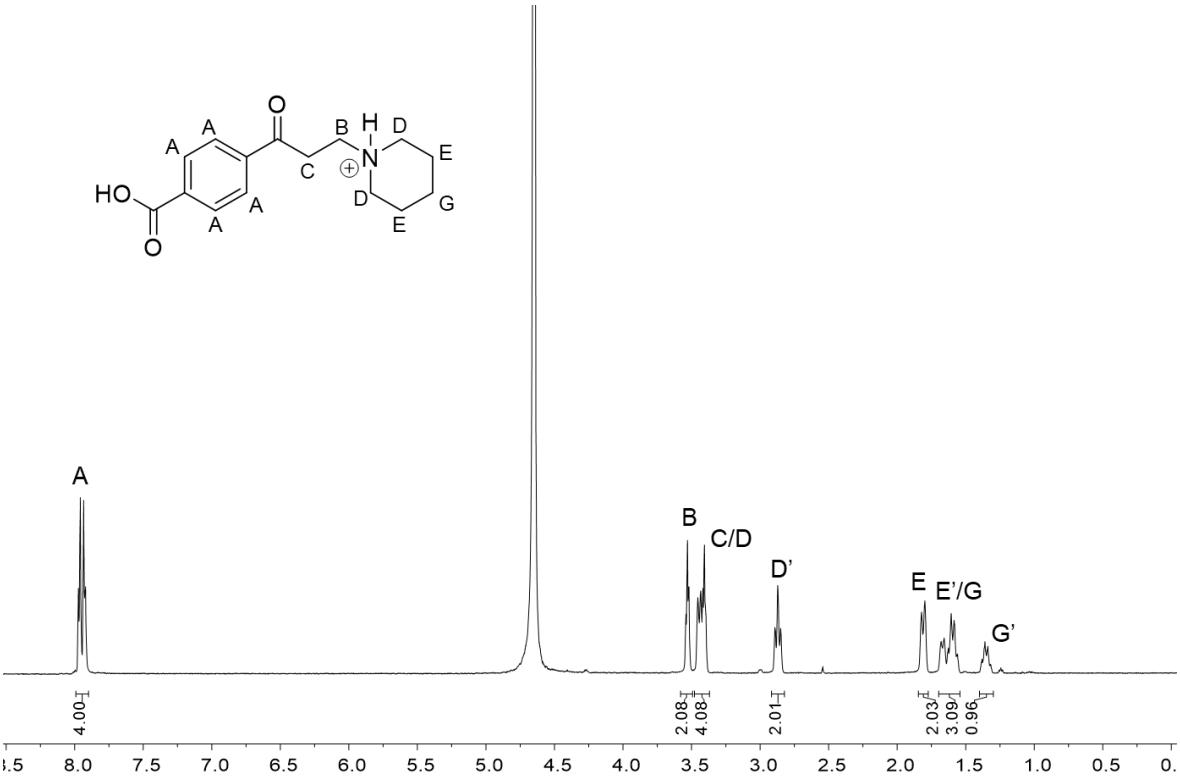

Figure 3.6.3. [1]H NMR of mannich salt (D2O).

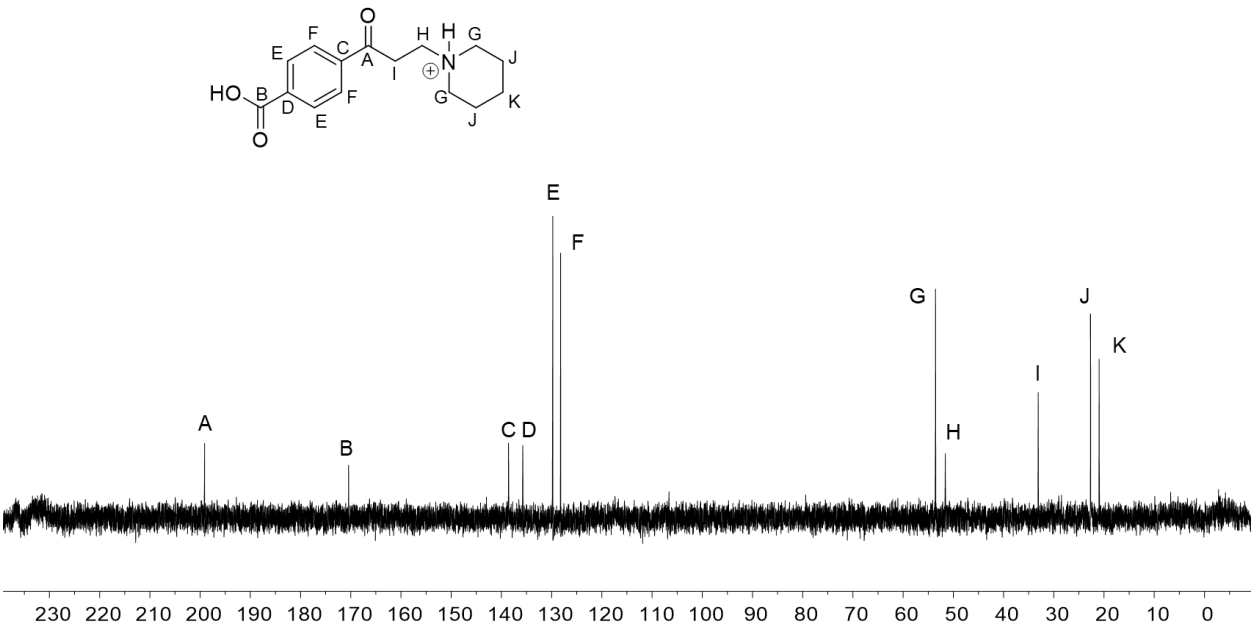

Figure 3.6.4. [13]C NMR of mannich salt (D_2O).

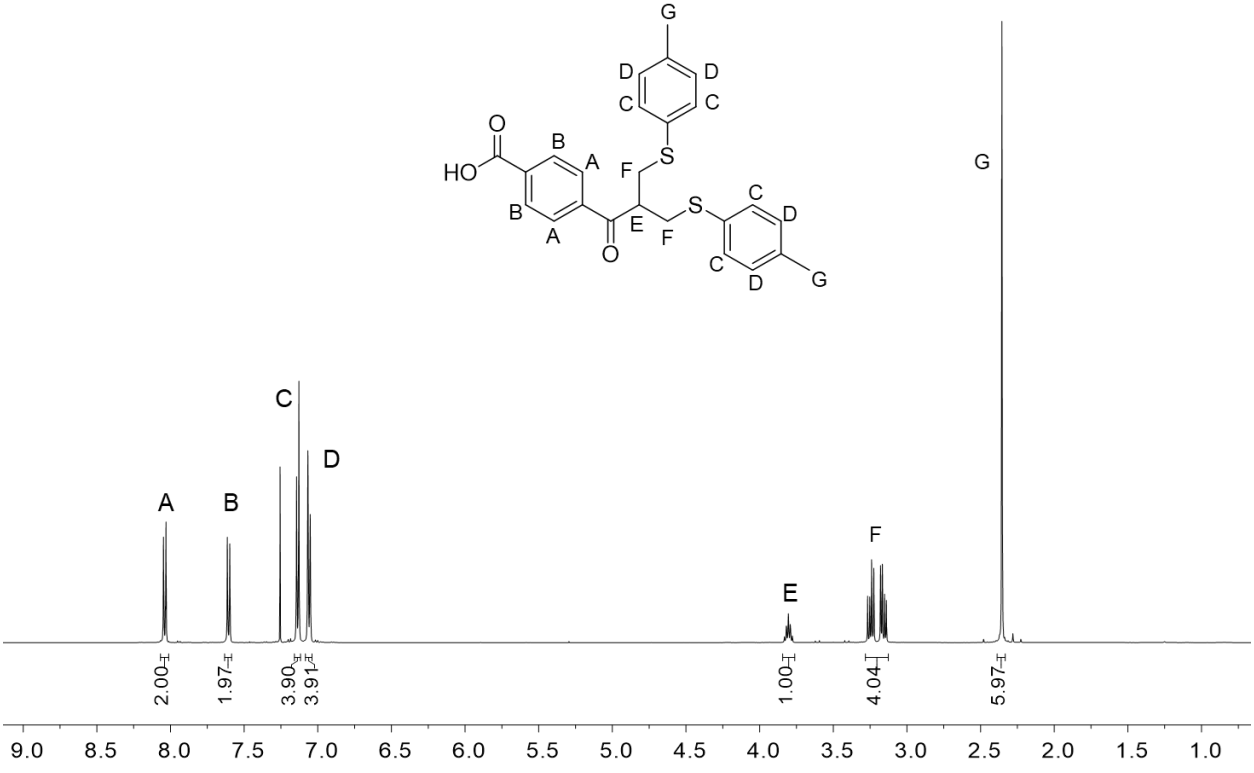

Figure 3.6.5. ^{1}H NMR of bis-sulfide acid (CDCl3).

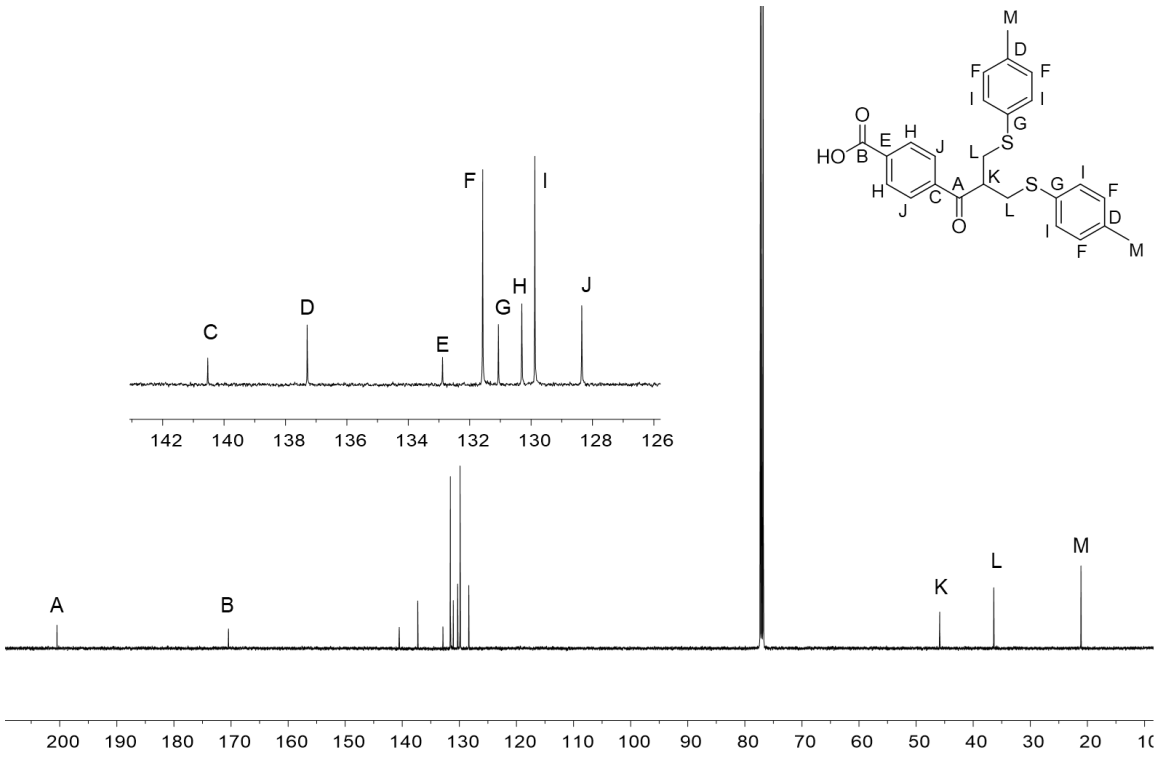

Figure 3.6.6. ^{13}C NMR of bis-sulfide acid ($CDCl_3$).

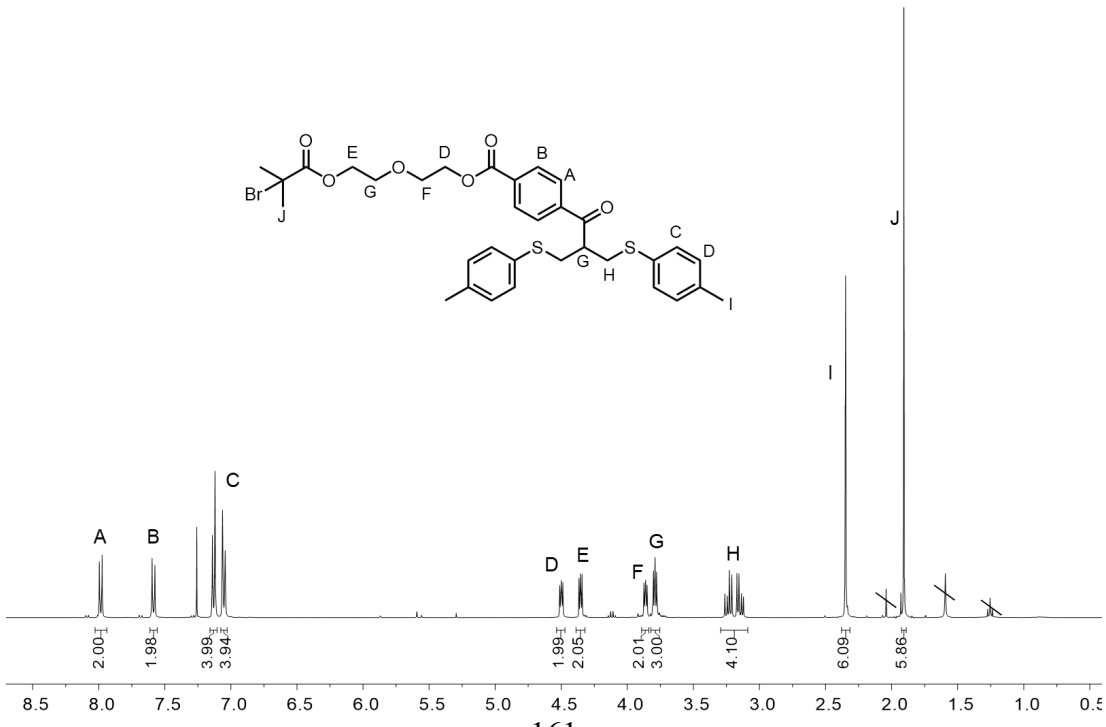

Figure 3.6.7. 1H proton bis-sulfide initiator (CDCl3).

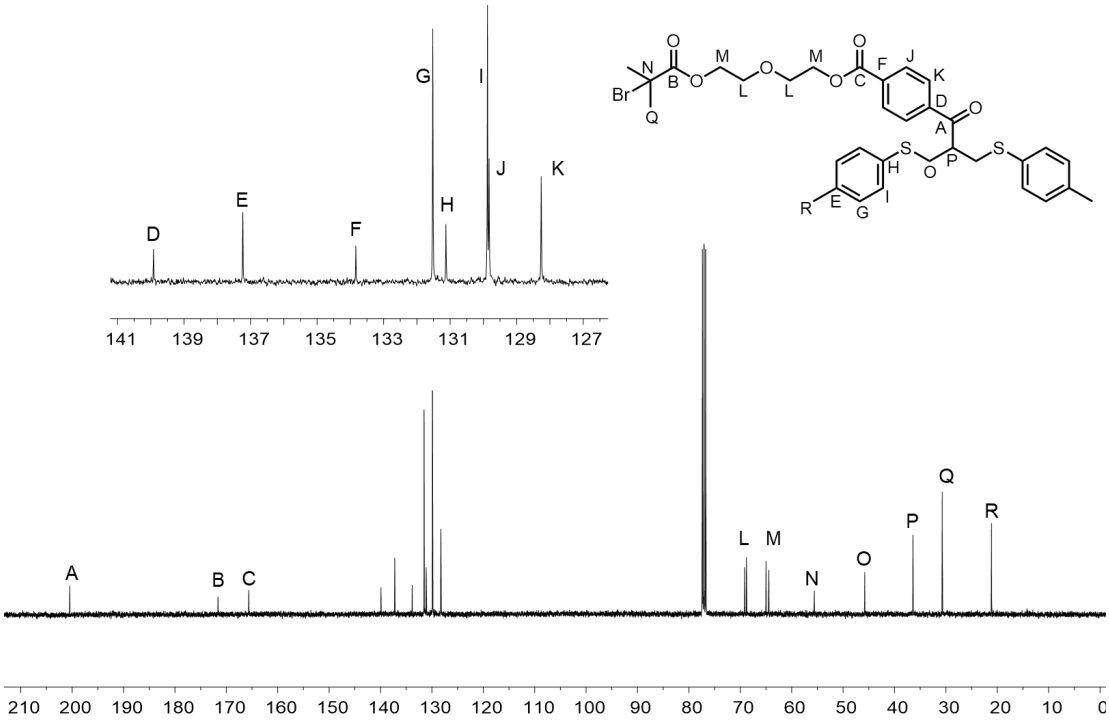

Figure 3.6.8. ^{13}C NMR of bis-sulfide initiator (CDCl3).

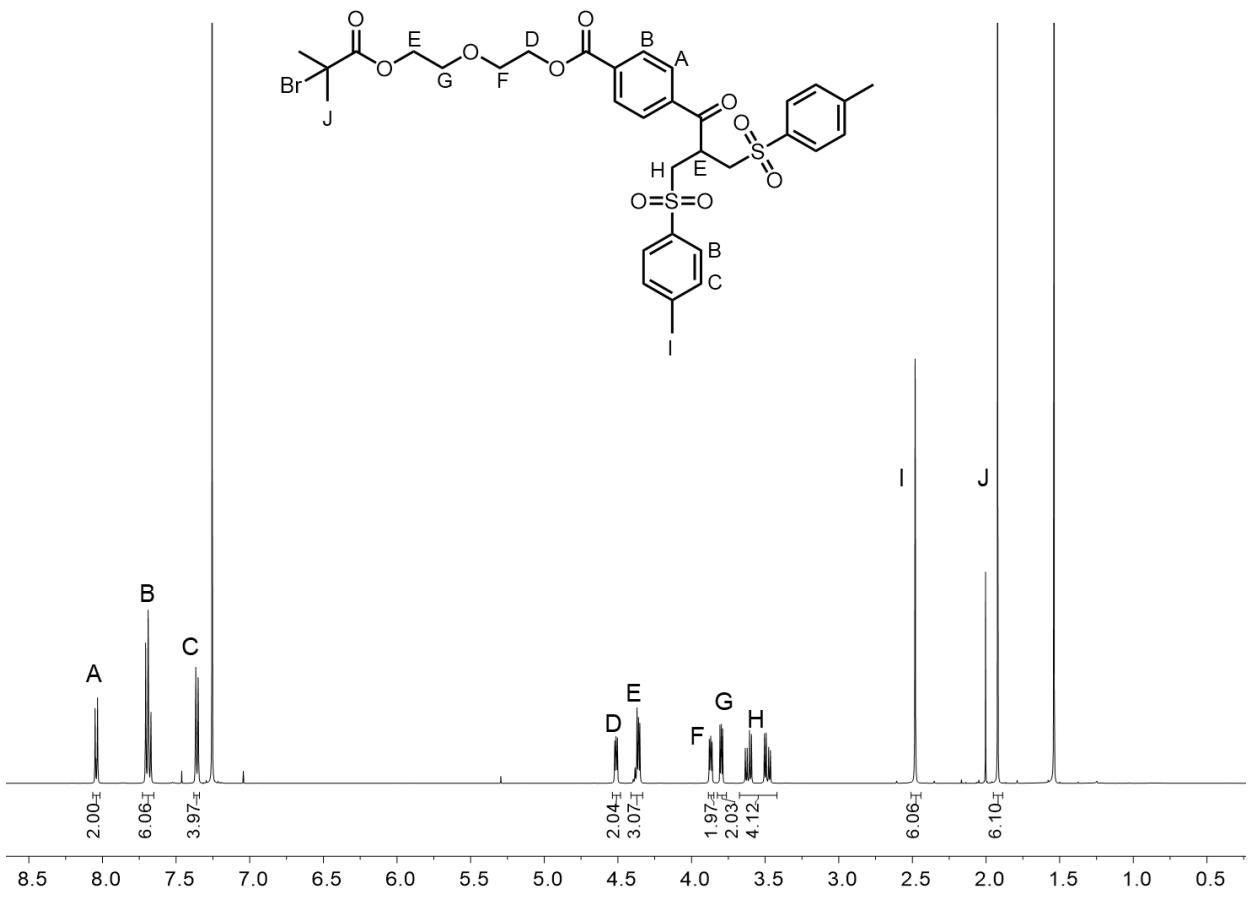

Figure 3.6.9. ^{1}H NMR of bis-sulfone initiator ($CDCl_3$).

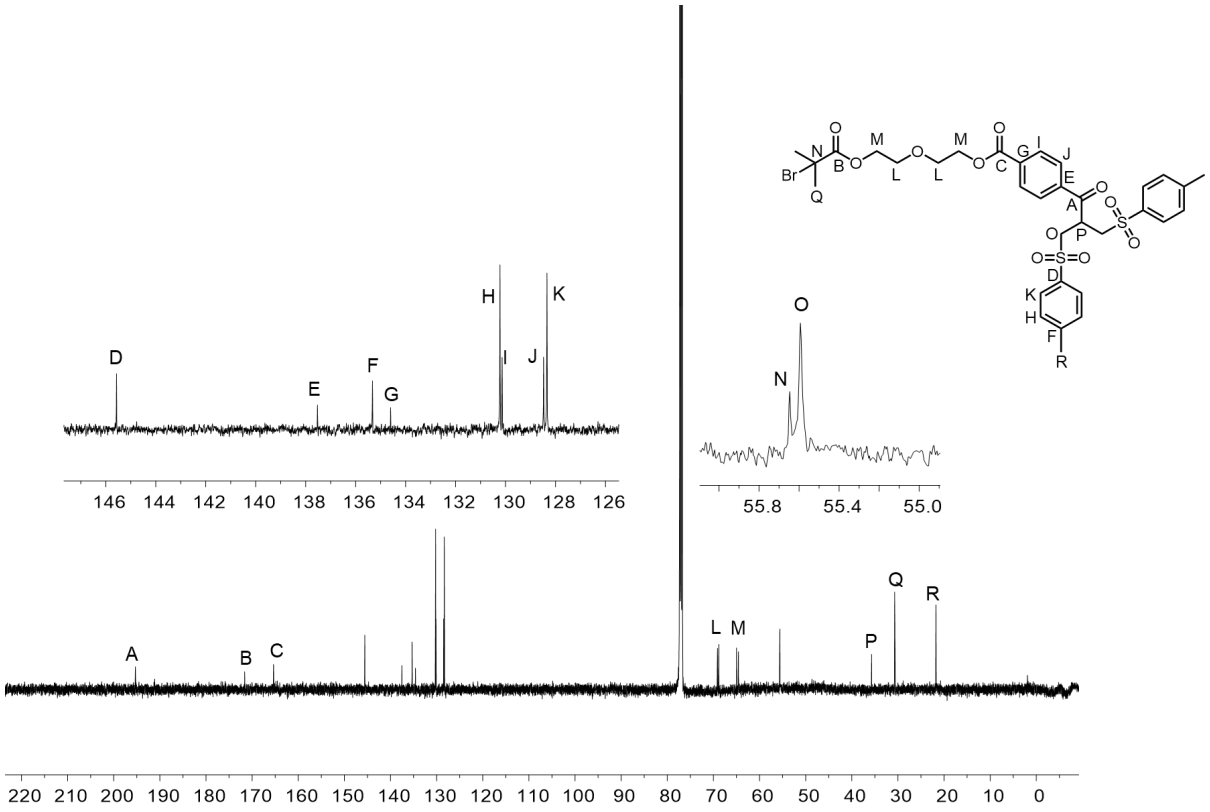

Figure 3.6.10. ^{13}C NMR of bis-sulfone initiator ($CDCl_3$).

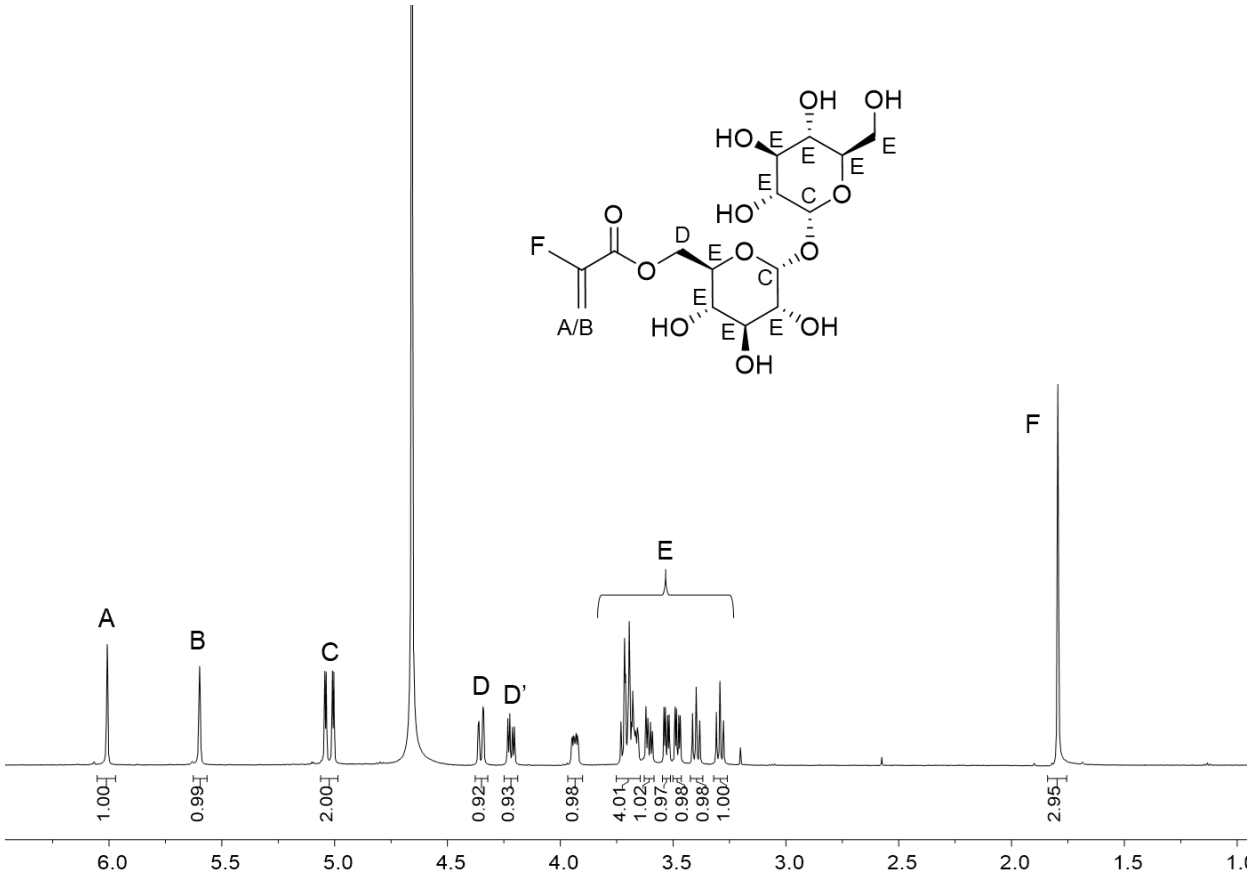

Figure 3.6.11. ^{1}H NMR of trehalose methacrylate (D_2O).

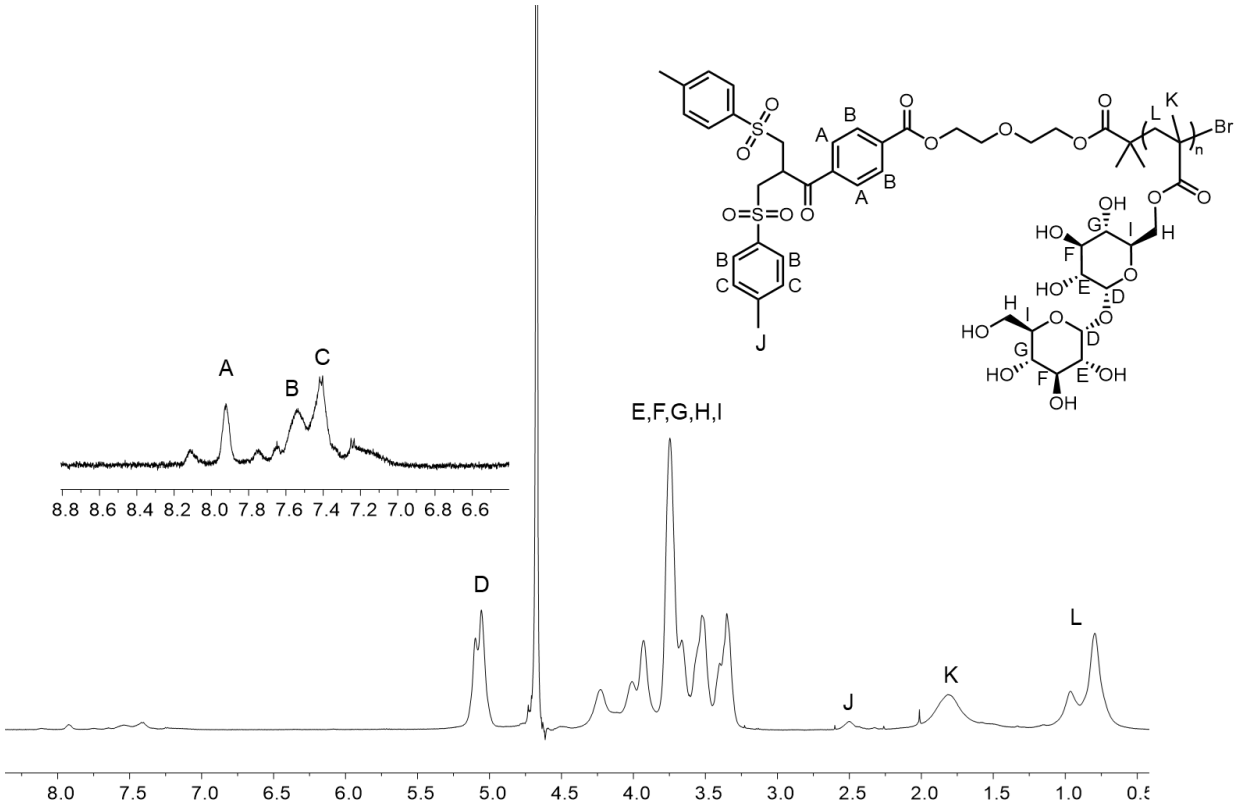

Figure 3.6.12. ^{1}H NMR of bis-sulfone trehalose polymer (D_2O).

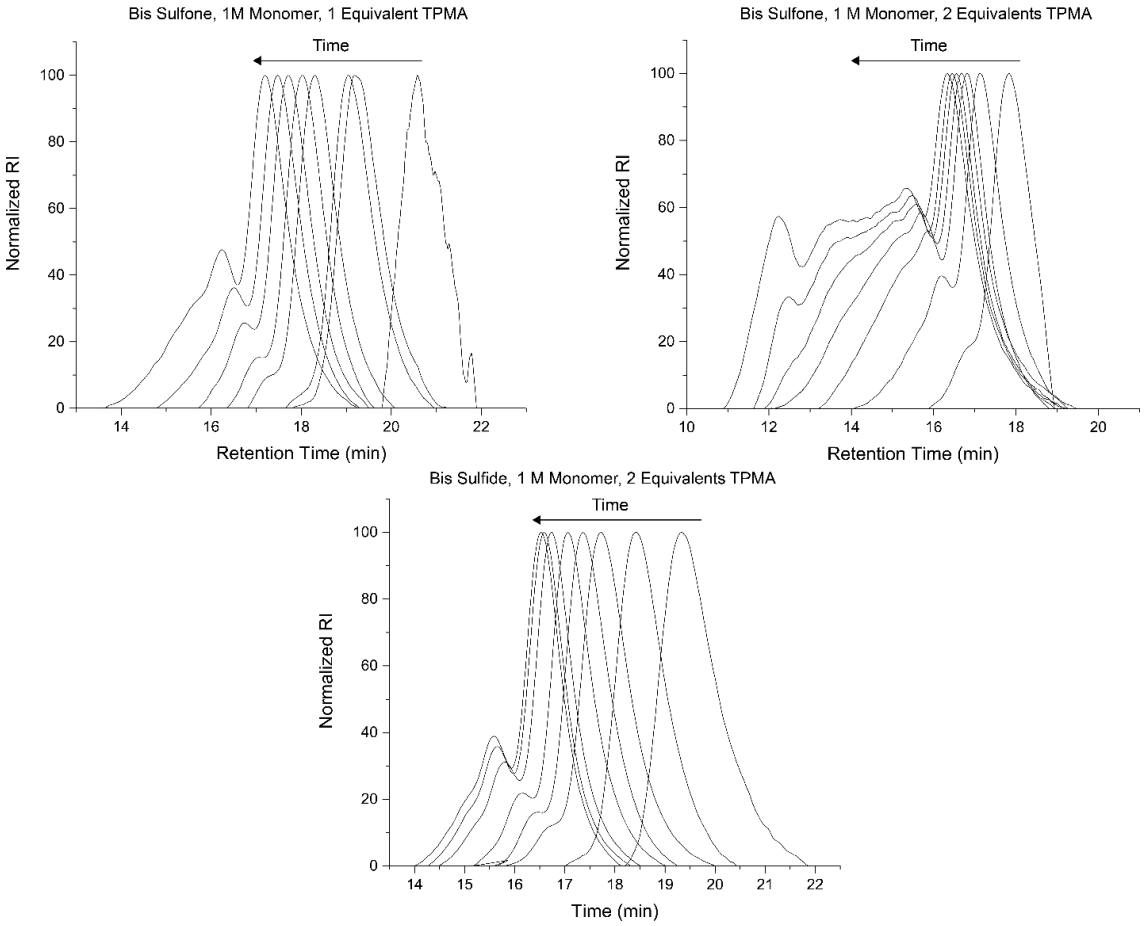

Figure 3.6.13. Overlaid GPC traces of tested conditions for polymerization optimization.

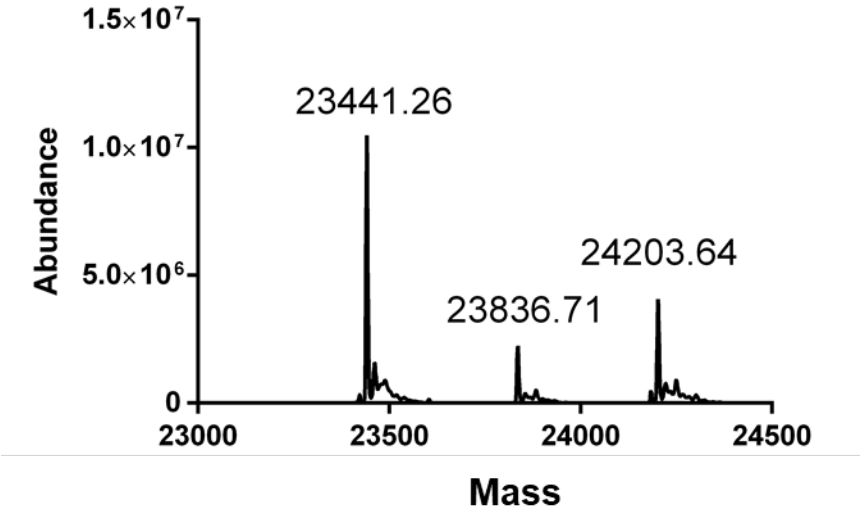

Figure 3.6.14. ESI-MS of purified, reduced Fab.

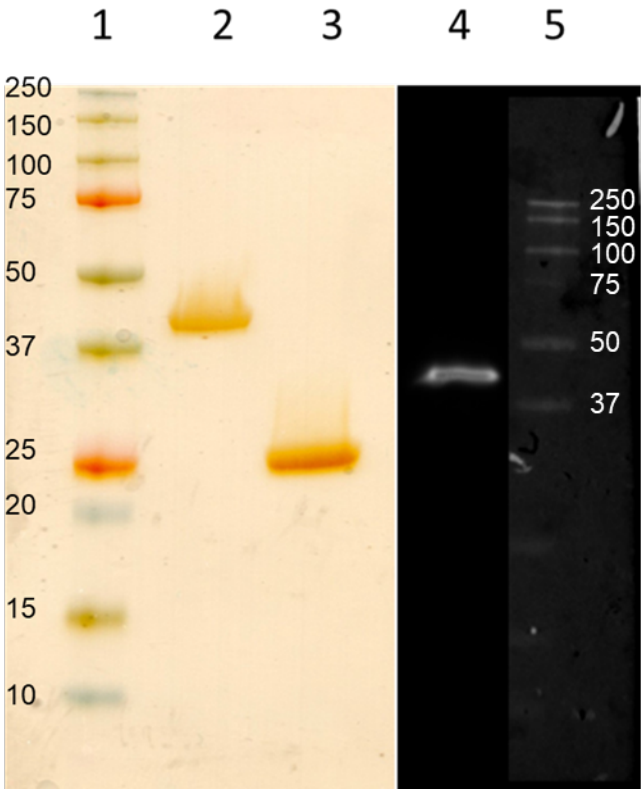

Figure 3.6.15. SDS PAGE visualized via silver staining (lane 1: ladder, lane 2: Fab, lane 3: Fab reducing) and western blot (lane 4: Fab, lane 5: protein ladder) of purified Fab

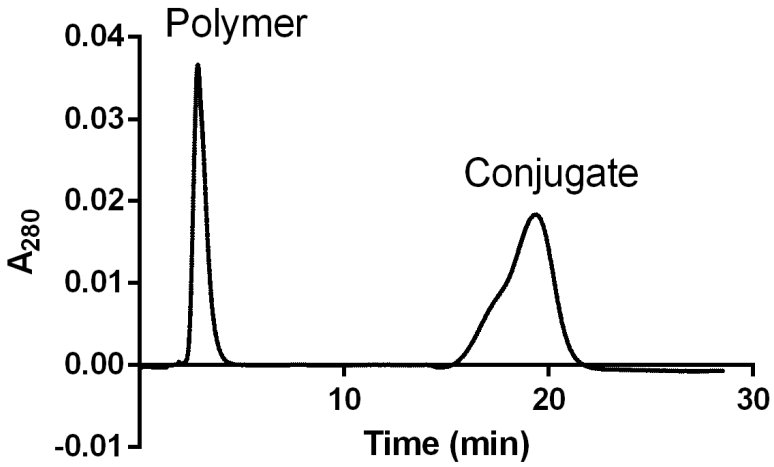

Figure 3.6.16. Representative FPLC trace of conjugates.

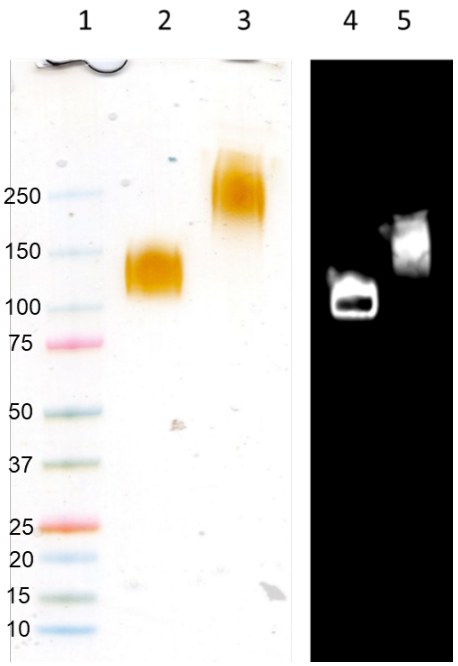

Figure 3.6.17. SDS PAGE visualized via silver staining (lane 1: ladder, lane 2: Herceptin, lane 3: Herceptin conjugate) and western blot (lane 4: Herceptin, lane 5: Herceptin conjugate) of Herceptin conjugate.

3.7. Experimental and Appendix References.

(1) Brocchini, S.; Balan, S.; Godwin, A.; Choi, J.-W.; Zloh, M.; Shaunak, S. PEGylation of Native Disulfide Bonds in Proteins. *Nat. Protoc.* **2006**, *1*, 2241–2252.

(2) Boehnke, N.; Kammeyer, J. K.; Damoiseaux, R.; Maynard, H. D. Stabilization of Glucagon by Trehalose Glycopolymer Nanogels. *Adv. Funct. Mater.* **2018**, *28*, 1705475.

(3) Selis, F.; Focà, G.; Sandomenico, A.; Marra, C.; Di Mauro, C.; Saccani Jotti, G.; Scaramuzza, S.; Politano, A.; Sanna, R.; Ruvo, M.; Tonon, G. Pegylated Trastuzumab Fragments Acquire an Increased in Vivo Stability but Show a Largely Reduced Affinity for the Target Antigen. *Int. J. Mol. Sci.* **2016**, *17*.

(4) Khalili, H.; Godwin, A.; Choi, J.; Lever, R.; Brocchini, S. Comparative Binding of Disulfide-Bridged PEG-Fabs. *Bioconjug. Chem.* **2012**, *23*, 2262–2277.

Chapter 4

Templated Enzyme Nanogels via a Photo-Removable Linkage: Applications in the Treatment of Phenylketonuria.

4.1 Introduction

Enzymes are critical to life and are utilized extensively in a scope of industries including the production of detergents, sensors, sweeteners, textiles, cosmetics, and pharmaceuticals.[1] The inherent specificity of enzymes along with high turnover rates make them attractive catalysts for the synthesis and production of structurally complex molecules. For example, recent developments in DNA synthesis and sequencing, directed evolution, and bioanalytical techniques now enable the biosynthesis of stereochemically complex natural products and medicines.[2,3] Biocatalysis has the additional advantage over traditional synthetic approaches in that it can often provide a greener and more sustainable process in a cost-effective manner.[4] Outside of the production of chemicals and materials, enzymes have also become increasingly important as therapies themselves. For instance, enzyme replacement therapies (ERTs) are successful in treating a number of lysosomal storage diseases and immunodeficiencies.[5] While these enzymatic approaches to solving problems in both organic chemistry and biology have their merits, the use of enzymes as such are not without their challenges.

Due to their amino acid composition and general reliance on tertiary structure for substrate turnover, enzymes, like all proteins, are often unstable. External factors such as temperature, organic solvent, pH, mechanical agitation, proteases, and light can all lead to irreversible denaturation or inactivation of enzymes.[6] In both biocatalysis and ERT applications, these limitations can often be prohibitive. Biocatalysis processes often require cosolvents, agitation, or temperature variation to support sufficient product formation while *in vivo* application of therapeutic enzymes can suffer from immune-mediated clearance, protease degradation, and/or renal clearance. To combat this, a number of strategies have been developed to help increase enzyme stability.[7] For instance, covalent attachment of polymers such as poly ethylene glycol

(PEG), poly hydroxypropyl methacrylamide (pHPMA), polysaccharide/sugar derivatives, and poly N-isopropylacrylamide (pNIPAM) have proved effective at increasing the stability of enzymes to stressors including heat, pH change, and protease degradation.[8] Outside of the direct conjugation of linear polymers, a variety of methods can be pursued to increase enzyme stability. These include site-directed mutagenesis to remove degradation prone regions from the protein structure;[9] covalent or non-covalent immobilization onto a matrix;[10,11] or direct encapsulation within a nanoparticle, liposome, or micelle.[7] Each methodology has its inherent advantages depending on the application with trade-offs in either stability, activity, or preparation. For instance, while immobilization into a polymer matrix may offer protection from proteases, pH changes, or agitation, a densely crosslinked network can limit substrate diffusion leading to decreased activity. While every technology is a dichotomy between activity and stability, tunability is the most desirable characteristic so that the final material can be tailored to the specific application. One rapidly developing methodology that offers such flexibility in design with broad applicability across chemistry and biology are enzyme nanogels.

Fundamentally, the synthesis of enzyme nanogels involves the localization of monomers and crosslinkers around the surface of the protein followed by polymerization to yield a protective, polymer shell around the enzyme.[12] First generation nanogels involved covalent attachment of acroyl groups to the lysine residues of the protein followed by polymerization of acrylamide monomers.[13,14] This strategy has been effectively expanded to a number of enzymes including chymotrypsin,[15,16] carbonyic anhydrase,[14,17] glucose oxidase,[18] green fluorescent protein,[19] and lipase.[20,21] While this can be an effective strategy with certain enzymes, this method requires the direct conjugation of monomers to surface residues of the protein, which can lead to a reduction in enzyme activity and even denaturation of the protein. Due to these challenges, a number of

approaches have been developed to support non-covalent formation of enzyme nanogels. Gu *et al.*[22] developed a strategy wherein positively charged monomers are used to localize around a negatively charged protein. Subsequent polymerization yields nanogels without the need for covalent modification. This strategy has been expanded to a number or proteins and applications.[23–25] Additionally, Beloqui *et al*[26] demonstrated an effective, one-pot synthesis of non-covalent protein nanogel through the addition of excipients such as sucrose. The authors show this technique to be applicable to a number of proteins with the capability of tuning the shell thickness through adjustment of the protein concentration. While such methods of non-covalent nanogel formation are effective, they rely on intramolecular/electrostatic interactions which inherently limits the pH range, proteins, or monomers that can be used in nanogel formation.

In the work described herein, we present a method for the formation of protein nanogels through the use of a photo-removable monomer. Conjugation of a bifunctional acrylamide-nitrobenzyl-carbonate (ANC) to lysines yields a polymerization handle on the protein surface linked through a photocleavable carbamate (**Figure 4.1.1**). Subsequent polymerization and photo-irradiation with 365 nm light yields an active, noncovalent protein nanogel that provides a protective shell around the enzyme. This traceless and templated method for nanogel formation eliminates the need electrostatic/intramolecular localizations of monomer at the protein surface, expanding the scope of monomers and proteins that can be utilized in nanogel formation.

In order to demonstrate the relevance and applicability of this method, we chose encapsulate the enzyme phenylalanine ammonia lyase (PAL), which is used in the treatment of phenylketonuria. This disease is characterized by an individual's inability to process dietary phenylalanine, leading to an accumulation of the amino acid and resulting in cognitive impairment.[27] PAL enzymatically transforms phenylalanine into the natural metabolite trans-

cinnamic acid and has been extensively examined as potential treatment for PKU.[28] Study of this disease and enzyme have recently led to the development and FDA approval of a PEGylated variant of PAL, which is administered subcutaneously. While this drug is an excellent alternative to current treatments, its reliance on injection is not only an inconvenience to patients, but additionally presents added risk. Due to the bacterial derived nature of the enzyme, immune reactions such as hypersensitivity and rapid clearance of the drug have been reported.[29,30] Because of this risk, it is necessary to titrate the drug carefully over the first 5 weeks of administration, requiring a tailored dosing schedule for each patient. An alternative to systemic delivery of the drug is oral administration. If dietary phenylalanine can be removed from food as it passes through the digestive tract and before it is absorbed, the disease could be effectively treated without the need for regular injections. The main challenge with this strategy, however, is the uniquely harsh environment of the digestive tract, requiring that the protein not be degraded by the large variation in pH and high concentrations of promiscuous proteases. A number of attempts at addressing these challenges have been attempted and range from genetically engineering PAL via directed evolution or encapsulation/adsorption of the enzyme onto membranes or other materials.[31–34] We believe enzyme nanogels to be a uniquely suitable approach for the delivery of PAL through the digestive system as it allows for greater tunability as everything from monomer type to crosslinker density can be adjusted. Using our aforementioned methodology of noncovalent protein nanocapusles formation, we demonstrate this strategy and convincingly show the formation of well-defined PAL nanogels with stability against the protease tryspin. We further believe that this technology can be expanded and applied to a host of different enzymes with applications in both oral and systemic protein delivery.

In this chapter, the aspects regarding the design and synthesis of the photocleavable monomer as well as the expression of PAL are discussed and presented. Work regarding the preparation of the nanogels, characterization of their activity, and stability assays against trypsin will be discussed in follow-up publications since they are the work of another graduate student.

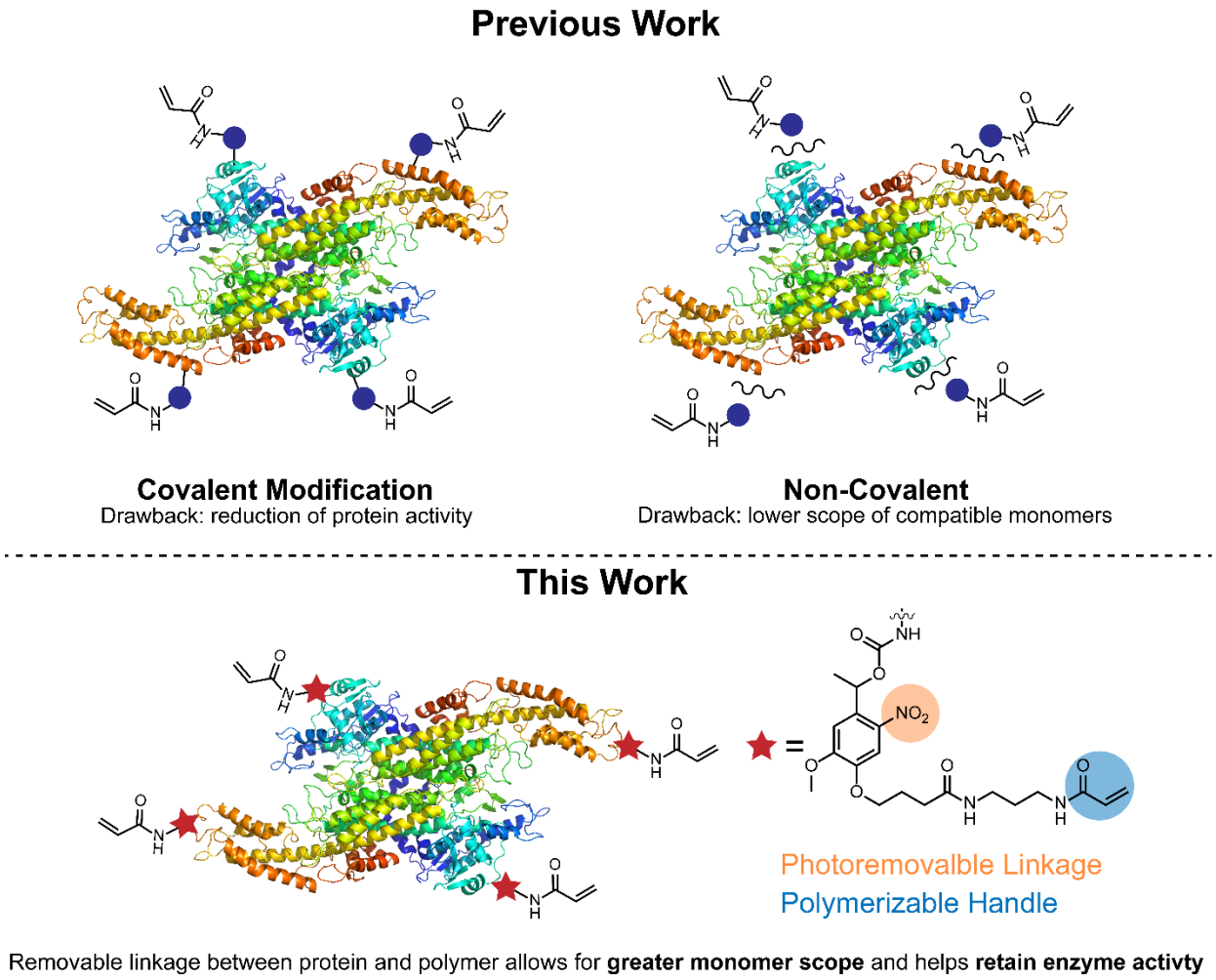

Figure 4.1.1. comparison of strategies for the synthesis of enzyme nanogels.

4.2 Results and Discussion

4.2.1 Design and synthesis of photocleavable acrylamide.

While covalent and non-covalent methodologies for nanogel preparation have their advantages, we imagined a hybrid strategy wherein the covalent linkage between the protein and monomer could be removed after nanogel formation. In an indirect manner, this allows for the synthesis of noncovalent protein nanogels that can maintain higher activity (due to the lack of covalent attachment to the matrix) while making available a wider scope of proteins and monomers. To facilitate this post-polymerization removal of a covalent linkage, we settled on the use of an ortho-nitro carbamate as it could provide a stable linkage throughout the polymerization process while offering a rapid and traceless mechanism for cleavage using UV-light, which has been widely used in chemical biology applications and is biocompatible.

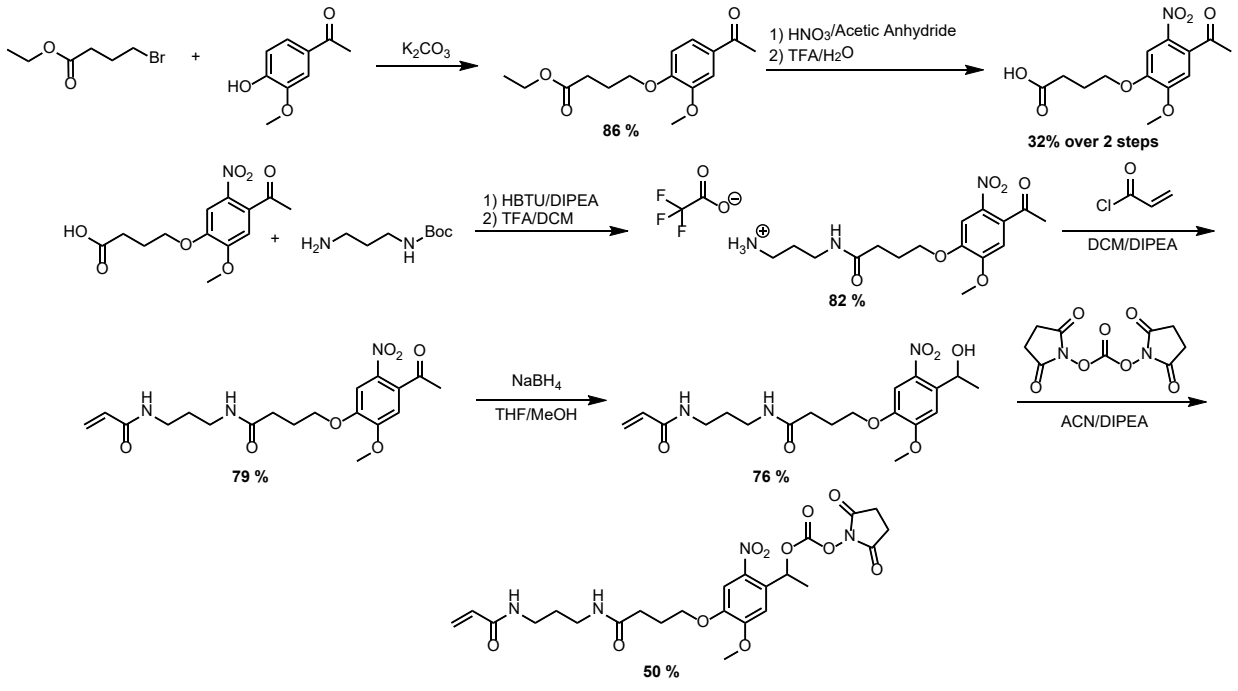

Figure 4.2.1. Synthesis of photocleavable acrylamide for templated nanogel synthesis

For the synthesis of the heterobifunctional ANC linker, we chose to start with acetovanillone, which could be purchased cheaply at less than $1 per gram (**Figure 4.2.1**). Alkylation of the phenol and the ortho-nitration were performed as reported in the literature.[35] Coupling and deprotection of N-Boc-1,3 propanediamine to the nitrated acid then yielded a free amine, which was used to install the acrylamide polymerization handle. Subsequent reduction of the ketone using sodium borohydride followed by alkylation with N,N'-disuccinimidyl carbonate resulted in the final, lysine reactive ANC monomer in good yield.

4.2.2 Expression of Phenylalanine Ammonia Lyase.

Phenylalanine ammonia lyase (PAL) is a large, tetrameric protein that converts phenylalanine into trans-cinnamic acid. The enzyme is produced by a large range of plants and fungi and has gained popularity recently due to its implications in the treatment of Phenylketonuria. For our applications, we sought to recombinantly express the PAL variant in E. coli from *Rhodosporidium toruloides* (Rt), which has been used in PEGylation studies for the development of longer-lasting therapies.[36]

Using Rt-PAL gene (GeneBank accession no. X51513), we first performed a codon optimization, which is particularly important in this application as we are using E. coli to express a native yeast protein (optimized cDNA sequence: **Figure 4.4.2**.). Additionally, in order to provide for more facile purification, we installed a His_6-TEV affinity-tag sequence at the N-terminus of the protein that would allow for Ni-NTA purification that could be later be removed with TEV protease. The optimized sequence was order through Twist Biosciences as a pre-cloned expression vector (Ndel_Xhol restriction sites in a pET-29b(+) vector). The plasmid was transformed into chemically competent BL21 (DE3) E. coli. While initial, small scale expression of the protein showed a strong induction band after the addition of Isopropyl β-d-1-thiogalactopyranoside

(IPTG), we exclusively found the protein in the insoluble fraction after lysis and centrifugation. In an attempt to improve protein solubility, we lowered the expression temperature from 37 °C to 18 °C, and were pleased to observe the majority of the protein remained soluble. Further Ni-NTA purification followed by His_6 cleavage yielded the active protein in good yield of approximately 70 mg/Liter (**Figure 4.2.2**).

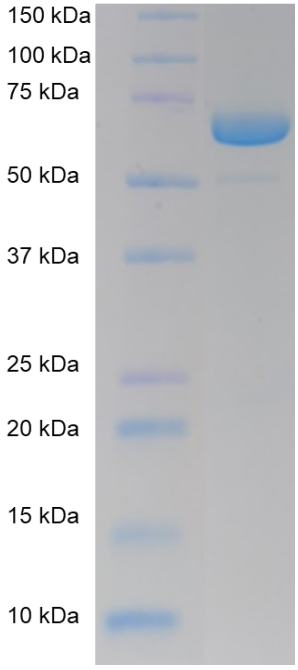

Figure 4.2.2. SDS PAGE of His-cleaved PAL product.

4.2.3 Conjugation of photocleavable acrylamide to PAL.

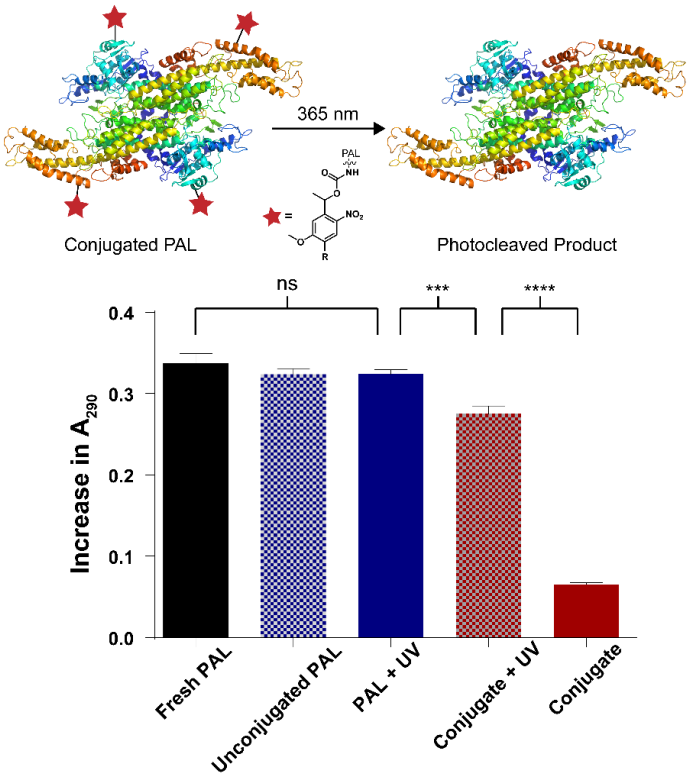

Figure 4.2.3. Photocleavage activity model study showing the recovery of enzyme activity after cleavage. Activity measured as an increase in absorbance at 290 nm over the course of 90 min.

Before proceeding with the formation of the nanogels, we first wanted to do a proof-of-concept model system with the ANC monomer in order quantify the added benefit of our strategy. Conjugating an ANC monomer to the lysines of PAL to form the resulting carbamate produced a large decrease in activity when compared to fresh protein that was not exposed to conjugation conditions (**Figure 4.2.3**). However, after exposing the conjugate to UV light, we saw a large recovery in protein activity (81 ± 4%) when compared to fresh protein). This result helps both exemplify the deleterious effect conjugation can have on enzyme activity while simultaneously demonstrating the added benefit of going through a removable linkage in the future nanogel. Furthermore, this experiment also elucidated that the conjugation conditions of DMSO as a cosolvent (Unconjugated PAL in **Figure 4.2.3**) and additionally the UV light (PAL + UV in **Figure**

4.2.3) did not have a statistically significant effect on PAL activity. Based on these proof-of-concept studies, we are encouraged in the use of this photo-removable strategy for the future production of enzyme nanogels for protein delivery.

4.3 Conclusion

Current methodologies for the synthesis of protein nanogels either relies on the covalent attachment of monomers to protein amino acids or non-covalent assembly of monomers to the protein surface. While each of these strategies can be effective in the preparation of protein nanogels, their application is limited by tradeoffs in either activity or monomer compatibility. In this work, we demonstrate a new methodology for the preparation of protein nanogels that relies on a photo-releasable linkage between the nanogel and the protein surface. By using this strategy in the synthesis of PAL nanogels, we show the applicability of this chemistry in the synthesis of active enzyme nanogels for therapeutic purposes.

4.4 References

(1) Gurung, N.; Ray, S.; Bose, S.; Rai, V. A Broader View: Microbial Enzymes and Their Relevance in Industries, Medicine, and Beyond https://www.hindawi.com/journals/bmri/2013/329121/ (accessed Oct 23, 2020).

(2) Cravens, A.; Payne, J.; Smolke, C. D. Synthetic Biology Strategies for Microbial Biosynthesis of Plant Natural Products. *Nature Communications* **2019**, *10*, 2142.

(3) Arnold, F. H. Directed Evolution: Bringing New Chemistry to Life. *Angewandte Chemie International Edition* **2018**, *57*, 4143–4148.

(4) Role of Biocatalysis in Sustainable Chemistry | Chemical Reviews https://pubs.acs.org/doi/10.1021/acs.chemrev.7b00203 (accessed Oct 23, 2020).

(5) Desnick, R. J.; Schuchman, E. H. Enzyme Replacement and Enhancement Therapies: Lessons from Lysosomal Disorders. *Nature Reviews Genetics* **2002**, *3*, 954–966.

(6) Silva, C.; Martins, M.; Jing, S.; Fu, J.; Cavaco-Paulo, A. Practical Insights on Enzyme Stabilization. *Critical Reviews in Biotechnology* **2018**, *38*, 335–350.

(7) Chapman, R.; Stenzel, M. H. All Wrapped up: Stabilization of Enzymes within Single Enzyme Nanoparticles. *J. Am. Chem. Soc.* **2019**.

(8) Gauthier, M. A.; Klok, H.-A. Polymer–Protein Conjugates: An Enzymatic Activity Perspective. *Polymer Chemistry* **2010**, *1*, 1352.

(9) Nisthal, A.; Wang, C. Y.; Ary, M. L.; Mayo, S. L. Protein Stability Engineering Insights Revealed by Domain-Wide Comprehensive Mutagenesis. *PNAS* **2019**, *116*, 16367–16377.

(10) Liu, Y.; Yu, J. Oriented Immobilization of Proteins on Solid Supports for Use in Biosensors and Biochips: A Review. *Microchim Acta* **2016**, *183*, 1–19.

(11) Mohamad, N. R.; Marzuki, N. H. C.; Buang, N. A.; Huyop, F.; Wahab, R. A. An Overview of Technologies for Immobilization of Enzymes and Surface Analysis Techniques for Immobilized Enzymes. *Biotechnology & Biotechnological Equipment* **2015**, *29*, 205–220.

(12) Jia, X.; Wang, L.; Du, J. In Situ Polymerization on Biomacromolecules for Nanomedicines. *Nano Res.* **2018**, *11*, 5028–5048.

(13) Yan, M.; Ge, J.; Liu, Z.; Ouyang, P. Encapsulation of Single Enzyme in Nanogel with Enhanced Biocatalytic Activity and Stability. *J. Am. Chem. Soc.* **2006**, *128*, 11008–11009.

(14) Yan, M.; Liu, Z.; Lu, D.; Liu, Z. Fabrication of Single Carbonic Anhydrase Nanogel against Denaturation and Aggregation at High Temperature. *Biomacromolecules* **2007**, *8*, 560–565.

(15) Hegedűs, I.; Nagy, E. Improvement of Chymotrypsin Enzyme Stability as Single Enzyme Nanoparticles. *Chemical Engineering Science* **2009**, *64*, 1053–1060.

(16) Kim, J.; Jia, H.; Lee, C.; Chung, S.; Kwak, J. H.; Shin, Y.; Dohnalkova, A.; Kim, B.-G.; Wang, P.; Grate, J. W. Single Enzyme Nanoparticles in Nanoporous Silica: A Hierarchical Approach to Enzyme Stabilization and Immobilization. *Enzyme and Microbial Technology* **2006**, *39*, 474–480.

(17) Yadav, R.; Labhsetwar, N.; Kotwal, S.; Rayalu, S. Single Enzyme Nanoparticle for Biomimetic CO2 Sequestration. *J Nanopart Res* **2011**, *13*, 263–271.

(18) Liu, Y.; Du, J.; Yan, M.; Lau, M. Y.; Hu, J.; Han, H.; Yang, O. O.; Liang, S.; Wei, W.; Wang, H.; Li, J.; Zhu, X.; Shi, L.; Chen, W.; Ji, C.; Lu, Y. Biomimetic Enzyme Nanocomplexes and Their Use as Antidotes and Preventive Measures for Alcohol Intoxication. *Nature Nanotechnology* **2013**, *8*, 187–192.

(19) Yan, M.; Du, J.; Gu, Z.; Liang, M.; Hu, Y.; Zhang, W.; Priceman, S.; Wu, L.; Zhou, Z. H.; Liu, Z.; Segura, T.; Tang, Y.; Lu, Y. A Novel Intracellular Protein Delivery Platform Based on Single-Protein Nanogels. *Nature Nanotechnology* **2010**, *5*, 48–53.

(20) Ge, J.; Lu, D.; Wang, J.; Yan, M.; Lu, Y.; Liu, Z. Molecular Fundamentals of Enzyme Nanogels. *J. Phys. Chem. B* **2008**, *112*, 14319–14324.

(21) Ge, J.; Lu, D.; Wang, J.; Liu, Z. Lipase Nanogel Catalyzed Transesterification in Anhydrous Dimethyl Sulfoxide. *Biomacromolecules* **2009**, *10*, 1612–1618.

(22) Gu, Z.; Yan, M.; Hu, B.; Joo, K.-I.; Biswas, A.; Huang, Y.; Lu, Y.; Wang, P.; Tang, Y. Protein Nanogel Weaved with Enzymatically Degradable Polymeric Network. *Nano Lett.* **2009**, *9*, 4533–4538.

(23) Zhao, M.; Biswas, A.; Hu, B.; Joo, K.-I.; Wang, P.; Gu, Z.; Tang, Y. Redox-Responsive Nanogels for Intracellular Protein Delivery. *Biomaterials* **2011**, *32*, 5223–5230.

(24) Biswas, A.; Joo, K.-I.; Liu, J.; Zhao, M.; Fan, G.; Wang, P.; Gu, Z.; Tang, Y. Endoprotease-Mediated Intracellular Protein Delivery Using Nanogels. *ACS Nano* **2011**, *5*, 1385–1394.

(25) Wen, J.; Anderson, S. M.; Du, J.; Yan, M.; Wang, J.; Shen, M.; Lu, Y.; Segura, T. Controlled Protein Delivery Based on Enzyme-Responsive Nanogels. *Advanced Materials* **2011**, *23*, 4549–4553.

(26) Beloqui, A.; Yu Kobitski, A.; Ulrich Nienhaus, G.; Delaittre, G. A Simple Route to Highly Active Single-Enzyme Nanogels. *Chemical Science* **2018**, *9*, 1006–1013.

(27) Al Hafid, N.; Christodoulou, J. Phenylketonuria: A Review of Current and Future Treatments. *Transl Pediatr* **2015**, *4*, 304–317.

(28) Sarkissian, C. N.; Gámez, A. Phenylalanine Ammonia Lyase, Enzyme Substitution Therapy for Phenylketonuria, Where Are We Now? *Molecular Genetics and Metabolism* **2005**, *86, Supplement*, 22–26.

(29) Rutsch, F. Antibodies against PEGylated Enzymes: Treat Them with Respect! *EBioMedicine* **2018**, *38*, 15–16.

(30) Gupta, S.; Lau, K.; Harding, C. O.; Shepherd, G.; Boyer, R.; Atkinson, J. P.; Knight, V.; Olbertz, J.; Larimore, K.; Gu, Z.; Li, M.; Rosen, O.; Zoog, S. J.; Weng, H. H.; Schweighardt, B. Association of Immune Response with Efficacy and Safety Outcomes in Adults with Phenylketonuria Administered Pegvaliase in Phase 3 Clinical Trials. *EBioMedicine* **2018**, *37*, 366–373.

(31) Huisman, G. W.; Agard, N. J.; Mijts, B.; Vroom, J.; Zhang, X. Engineered Phenylalanine Ammonia Lyase Polypeptides. US20170191050A1, July 6, 2017.

(32) Pereira de Sousa, I.; Gourmel, C.; Berkovska, O.; Burger, M.; Leroux, J.-C. A Microparticulate Based Formulation to Protect Therapeutic Enzymes from Proteolytic Digestion: Phenylalanine Ammonia Lyase as Case Study. *Scientific Reports* **2020**, *10*, 3651.

(33) Cui, J. D.; Li, L. L.; Bian, H. J. Immobilization of Cross-Linked Phenylalanine Ammonia Lyase Aggregates in Microporous Silica Gel. *PLOS ONE* **2013**, *8*, e80581.

(34) Ambrus, C. M.; Ambrus, J. L.; Horvath, C.; Pedersen, H.; Sharma, S.; Kant, C.; Mirand, E.; Guthrie, R.; Paul, T. Phenylalanine Depletion for the Management of Phenylketonuria: Use of Enzyme Reactors with Immobilized Enzymes. *Science* **1978**, *201*, 837–839.

(35) Kloxin, A. M.; Kasko, A. M.; Salinas, C. N.; Anseth, K. S. Photodegradable Hydrogels for Dynamic Tuning of Physical and Chemical Properties. *Science* **2009**, *324*, 59–63.

(36) Sarkissian, C. N.; Shao, Z.; Blain, F.; Peevers, R.; Su, H.; Heft, R.; Chang, T. M. S.; Scriver, C. R. A Different Approach to Treatment of Phenylketonuria: Phenylalanine Degradation with Recombinant Phenylalanine Ammonia Lyase. *PNAS* **1999**, *96*, 2339–2344.

(37) Tropea, J. E.; Cherry, S.; Waugh, D. S. Expression and Purification of Soluble His(6)-Tagged TEV Protease. *Methods Mol Biol* **2009**, *498*, 297–307.

4.5 Materials and Methods

Acetovanillone was purchased form Oakwood Chemicals. All other chemicals were purchased from Sigma-Aldrich and Fisher Scientific and were used without purification unless otherwise

noted. For PEGMA, inhibitor was removed by passing through a plug of basic alumina. Plasmid for PAL expression was ordered from Twist Biosciences with the sequence cloned between Ndel_Xhol restriction sites in a pET-29b(+) vector. TEV protease was expressed following reported procedures and stored at -80 °C in 50% glycerol and thawed immediately before use.[37]

Analytical Techniques. Nuclear Magnetic Resonance (NMR) spectra were recorded on a Bruker AV 400 MHz, Bruker DRX 500 MHz, Bruker AV 500 MHz, and Bruker AV 600 MHz spectrometer. Proton NMR spectra were acquired with a relaxation delay of 2 s for small molecules and 10 seconds for polymers. Mass spectrometry for both proteins and small molecules was obtained on an Agilent Q-TOF 6530 LC/MS. For SDS PAGE, BioRad Any kD Mini-PROTEAN-TGX™ gels were used for Fab and Fab conjugate while 4–15% Mini-PROTEAN® TGX™ gels were used for Herceptin and Herceptin conjugate. SDS-PAGE protein standards were obtained from Bio-Rad (Precision Plus Protein Prestained Standards). Small molecule purification was done via flash chromatography was conducted on a Biotage Isolera One auto-column system.

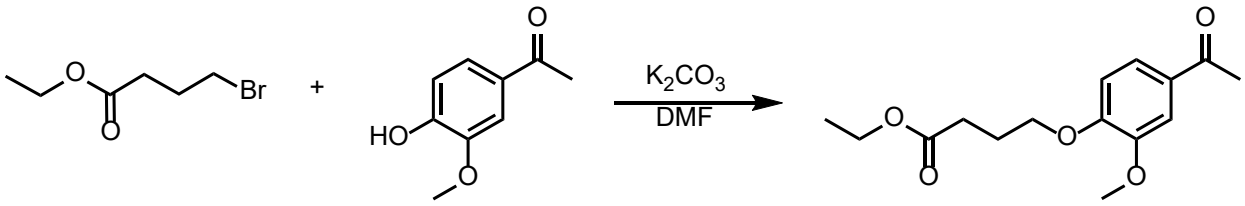

Acetovanillone Alkylation.[35] Acetovanillone (5.0 g, 30 mmol,1 equivalent) and K_2CO_3 (6.2 g, 45 mmol, 1.5 equivalents) were dissolved in 40 mL of DMF. Ethyl 4-bromobutyrate (5.2 mL, 36 mmol, 1.2 equivalents) was added dropwise and reaction was allowed to proceed overnight for 12 hrs. The crude was then poured into 400 mL of cold water and the resulting solid was collected via filtration, washed with excess water, and dried to yield 7.28 g (86%) of a brown powder. ^{1}H NMR (600 MHz, Chloroform-*d*) δ 7.55 (dd, *J* = 8.3, 2.0 Hz, 1H), 7.52 (d, *J* = 2.0 Hz, 1H), 6.89 (d, *J* = 8.4 Hz, 1H), 4.14 (q, *J* = 6.6, 6.0 Hz, 4H), 3.91 (s, 3H), 2.56 (s, 3H), 2.54 (t, *J* = 7.2 Hz,

2H), 2.19 (p, J = 6.8 Hz, 2H), 1.25 (t, J = 7.1 Hz, 3H). ^{13}C NMR (101 MHz, Chloroform-*d*) δ 196.90, 173.08, 152.67, 149.30, 130.53, 123.24, 111.29, 110.50, 67.83, 60.54, 56.02, 30.61, 26.23, 24.32, 14.23. IR: ν = 2613, 2940, 1730, 1672, 1587, 1509, 1466, 1416, 1356, 1266, 1218, 1176, 1149, 1134, 1027, 876, 807 cm^{-1}. ESI-MS calculated for $C_{15}H_{20}O_5$ $[M+H]^+$ = 281.1389, observed = 281.1391.32%

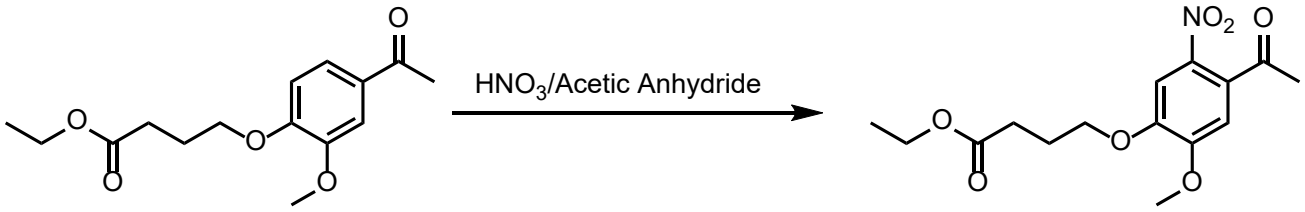

Nitration. Alkylated acetovanillone (7.28 g, 26 mmol, 1 equivalent) was dissolved in acetic anhydride (30 mL, 320 mmol, 12 equivalents) and added dropwise to 70 mL of 70% Nitric acid at 0 °C. After 30 minutes, the reaction was warmed to room temperature and allowed to proceed for 1.5 hrs. The mixture was them precipitated into 400 mL of cold water and the resulting solid was collected via filtration. The product was further purified via recrystallization from ethanol followed by vacuum filtration to yield 3.50 g (41%) of a yellow powder. ^{1}H NMR (400 MHz, Chloroform-*d*) δ 7.61 (s, 1H), 6.74 (s, 1H), 4.22 – 4.11 (m, 4H), 3.95 (s, 3H), 2.54 (t, J = 7.2 Hz, 2H), 2.49 (s, 3H), 2.20 (p, J = 6.7, 2H), 1.26 (t, J = 7.1 Hz, 3H). ^{13}C NMR (101 MHz, Chloroform-*d*) δ 200.11, 172.82, 154.32, 148.90, 138.41, 132.88, 108.79, 108.04, 68.51, 60.63, 56.61, 30.53, 30.41, 24.20, 14.24. IR: ν = 2298, 1731, 1708, 1521, 1337, 1284, 1214, 1182, 1039 cm^{-1}. ESI-MS calculated for $C_{15}H_{19}NO_7$ $[M+H]^+$ = 326.1240, observed = 326.1289.

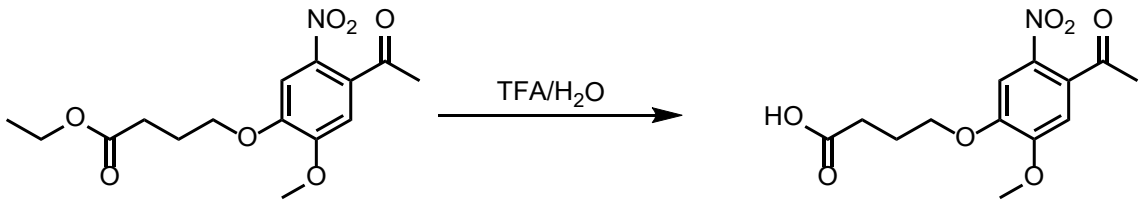

Ethyl Deprotection. Ethyl protected starting material was added to a round bottom flask and suspended in 50 mL of water along with 20 mL of trifluoro acetic acid. The reaction was heated to 105 °C and stirred for 2 hrs. The reaction was then cooled and TFA was removed via Hi Vac. The resulting precipitate was collected via vacuum filtration, washed with water, and dried to yield 2.57 g (80%) of a yellow solid. ^{1}H NMR (500 MHz, DMSO-d_6) δ 12.16 (s, 1H), 7.62 (s, 1H), 7.20 (s, 1H), 4.10 (t, J = 6.5 Hz, 2H), 3.91 (s, 3H), 2.49 (s, 3H), 2.37 (t, J = 7.3 Hz, 2H), 1.94 (p, J = 6.9 Hz, 2H). ^{13}C NMR (126 MHz, DMSO-d_6) δ 199.77, 174.43, 153.76, 148.97, 138.82, 131.61, 110.31, 108.49, 68.63, 57.14, 30.48, 30.33, 24.36. IR: ν = 2309, 1697, 1518, 1503, 1330, 1281, 1213 cm^{-1}. ESI-MS calculated for $C_{13}H_{15}NO_7$ $[M+H]^+$ = 298.0926, observed = 298.0982.

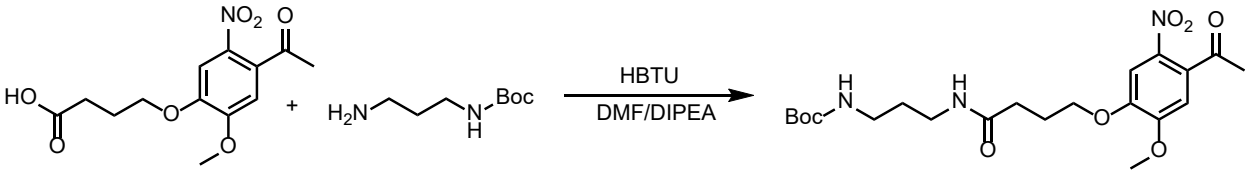

Boc Propyl Amine Coupling. Nitrated acid (1.05 g, 3.53 mmol, 1 equivalent), HBTU (2.01 g, 5.30 mmol, 1.5 equivalents), and N,N-diisopropylethylamine (1.54 mL, 8.83 mmol, 2.5 equivalents) were dissolved in 30 mL DMF. The reaction was stirred for 30 min to form the activated complex (it forms an insoluble precipitate). N-Boc-1,3-propanediamine (678 µL, 3.89 mmol, 1.1 equivalents) was then added and reaction was allowed to proceed for 12 hrs overnight. The mixture was then poured into 300 mL of cold water and the precipitate was collected via filtration. The product was then dissolved in DCM, dried with $MgSO_4$, and concentrated to yield 1.32 g (82 %) of a yellow powder. ^{1}H NMR (400 MHz, Chloroform-d) δ 7.61 (s, 1H), 6.74 (s, 1H), 6.39 (s, 1H), 4.84 (s, 1H), 4.16 (t, J = 6.2 Hz, 2H), 3.96 (s, 3H), 3.30 (q, J = 6.2 Hz, 2H), 3.14 (m, 2H), 2.49 (s, 3H), 2.44 (t, J = 7.2 Hz, 2H), 2.22 (p, J = 6.7 Hz, 2H), 1.61 (p, J = 6.5 Hz, 2H), 1.43 (s, 9H). ^{13}C NMR (126 MHz, Chloroform-d) δ 200.14, 172.24, 156.75, 154.25, 148.91, 138.43,

132.81, 108.76, 108.08, 79.53, 68.79, 56.61, 35.91, 32.60, 30.42, 30.27, 28.38, 24.76. IR: ν = 3352, 2309, 1736, 1525, 1364, 1287, 1216 cm^{-1}. ESI-MS calculated for $C_{21}H_{31}N_3O_8$ $[M + Na]^+$ = 476.2008 observed = 476.2077.

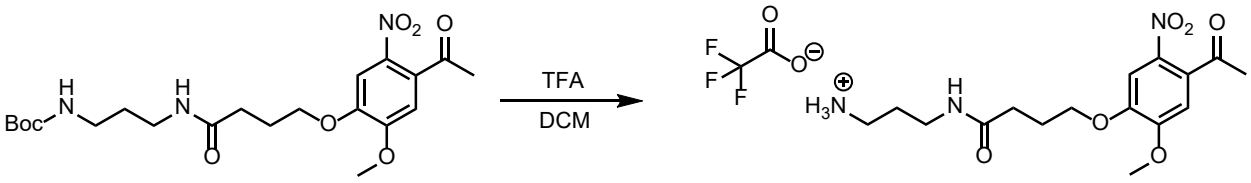

Boc Deprotection. Boc protected starting material was dissolved in 10 mL of 50/50 TFA:DCM in a scintillation vial and stirred for 30 min. TFA was then removed via vacuum and the crude was then dissolved in DCM and precipitated/triturated in 50 mL of diethyl ether to yield the product quantitatively as a yellow wax. ^{1}H NMR (500 MHz, DMSO-d_6) δ 8.03 (t, J = 5.8 Hz, 1H), 7.70 (s, 3H), 7.61 (s, 1H), 7.21 (s, 1H), 4.09 (t, J = 6.4 Hz, 2H), 3.91 (s, 3H), 3.10 (q, J = 6.5 Hz, 2H), 2.81 – 2.71 (m, 2H), 2.53 (s, 1H), 2.50 (s, 3H), 2.24 (t, J = 7.5 Hz, 2H), 1.95 (p, J = 6.7 Hz, 2H), 1.65 (p, J = 7.0 Hz, 2H). ^{13}C NMR (126 MHz, DMSO-d_6) δ 199.78, 172.38, 153.73, 149.00, 138.81, 131.60, 110.30, 108.41, 68.99, 57.13, 37.27, 36.01, 31.90, 30.49, 27.95, 24.98. IR: ν = 2942, 1677, 1645, 1518, 1335, 1282, 1199, 1175, 1132, 1036. ESI-MS calculated for $C_{16}H_{24}N_3O_6$ $[M]^+$ = 354.1665, observed = 354.1828.

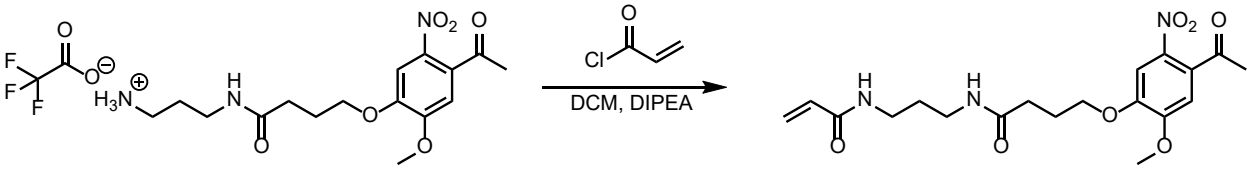

Acrylamide Addition. Trifluoroacetate salt (200 mg, 428 μmol) was dissolved in 5 mL of DCM with DIPEA (298 μL, 1.71 mmol, 4 equivalents) and added to a scintillation vial. The reaction was then cooled to 0 °C and acroyl chloride (52 μL, 642 μmol) was added dropwise. The reaction was

stirred for 30 min at 0 °C and then at 22 °C for 1 hr. The crude was then concentrated and purified via column chromatography with a 95:5 DCM:MeOH mobile phase (via gradient on autocolumn). 137 mg (79 %) of product was isolated as a yellow powder. ^{1}H NMR (600 MHz, Chloroform-*d*) δ 7.64 (s, 1H), 6.75 (s, 1H), 6.38 (s, 1H), 6.29 (dd, *J* = 17.0, 1.4 Hz, 2H), 6.13 (dd, *J* = 17.0, 10.3 Hz, 1H), 5.67 (dd, *J* = 10.3, 1.4 Hz, 1H), 5.30 (s, 1H), 4.17 (t, *J* = 6.2 Hz, 2H), 3.97 (s, 3H), 3.36 (q, *J* = 6.3 Hz, 2H), 3.31 (q, *J* = 6.2 Hz, 2H), 2.50 (s, 3H), 2.46 (t, *J* = 7.1 Hz, 2H), 2.23 (p, *J* = 6.7 Hz, 2H), 1.67 (m, 2H). ^{13}C NMR (126 MHz, Chloroform-*d*) δ 200.14, 172.64, 166.28, 154.26, 148.88, 138.42, 132.85, 130.82, 126.60, 108.75, 108.10, 68.78, 56.63, 35.80, 32.64, 30.42, 29.78, 24.74. IR: ν = 3002, 1737, 1365, 1217. ESI-MS calculated for $C_{19}H_{25}N_3O_7$ $[M+H]^+$ = 408.1771, observed = 408.1875.

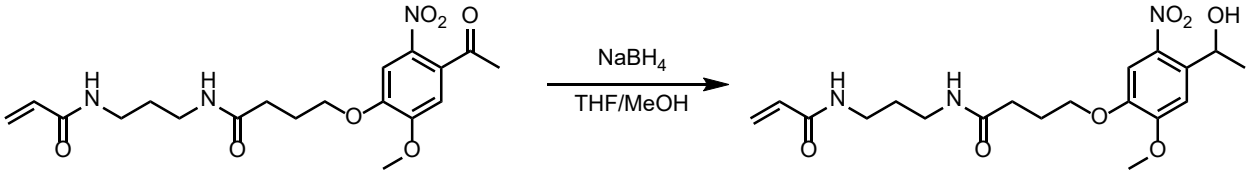

Ketone Reduction. Ketone acrylamide (158 mg, 388 µmol, 1 equivalent) was dissolved in 5 mL of 3:2 THF/MeOH with a stir bar in a scintillation vial. Sodium borohydride (88 mg, 2.33 mmol, 6 equivalents) was then added in portions, resulting in the evolution of H_2. The reaction was allowed to proceed at room temperature for 3 hrs. Saturated NH_4Cl was then added to quench and the organic layer was collected. The aqueous layer was then extracted 3x with ethyl acetate. The organic layers were combined, dried with $MgSO_4$, and concentrated to yield 120 mg of (76%) of a yellow solid. ^{1}H NMR (500 MHz, DMSO-d_6) δ 8.03 (t, *J* = 5.7 Hz, 1H), 7.84 (t, *J* = 5.7 Hz, 1H), 7.50 (s, 1H), 7.33 (s, 1H), 6.17 (dd, *J* = 17.1, 10.1 Hz, 1H), 6.03 (dd, *J* = 17.1, 2.3 Hz, 1H), 5.54 (dd, *J* = 10.1, 2.3 Hz, 1H), 5.38 (s, 1H), 5.23 (q, *J* = 6.2 Hz, 1H), 4.01 (t, *J* = 6.5 Hz, 2H), 3.88 (s, 3H), 3.10 (q, *J* = 6.6 Hz, 2H), 3.03 (q, *J* = 6.6 Hz, 2H), 2.49 (s, 1H), 2.21 (t, *J* = 7.4 Hz, 2H), 1.92

(p, J = 6.96 Hz, 2H), 1.53 (p, J = 7.0 Hz, 2H), 1.34 (d, J = 6.3 Hz, 3H). ^{13}C NMR (126 MHz, DMSO-d_6) δ 171.83, 164.99, 153.85, 146.72, 139.35, 138.41, 132.26, 125.36, 109.52, 108.79, 68.74, 64.36, 56.51, 36.89, 36.87, 32.08, 29.66, 25.64, 25.17. IR: ν = 3214, 1737, 1653, 1515, 1267, 1212, 1102, 1018, 804. ESI-MS calculated for $C_{19}H_{27}N_3O_7$ $[M+H]^+$ = 410.1927, observed = 410.1984.

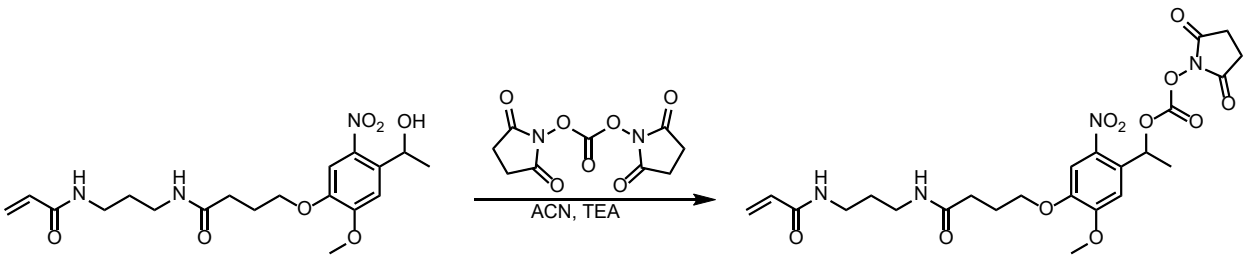

NHS Carbonate Addition. Alcohol (308 mg, 752 μmol, 1 equivalent) and triethyl amine (524 μL, 3.76 mmol, 5 equivalents) were dissolved in dry acetonitrile in an oven-dried round bottom flask. N,N′-Disuccinimidyl carbonate (964 mg, 3.76 mmol, 5 equivalents) was then added and reaction was allowed to proceed overnight for 16 hrs. The product was then concentrated and partially purified via column chromatography with a DCM+4% MeOH mobile phase. Fractions containing the product were combined and concentrated. Residual electrophile was then removed by redissolving in DCM and washing twice with sodium bicarbonate. The product was then dried with $MgSO_4$ and concentrated to yield 205 mg (50%) of the product as a yellow foam. ^{1}H NMR (600 MHz, Chloroform-d) δ 7.63 (s, 1H), 7.06 (s, 1H), 6.53 (t, J = 6.4 Hz, 1H), 6.48 (q, J = 6.4 Hz, 1H), 6.26 (dd, J = 17.0, 1.4 Hz, 1H), 6.12 (dd, J = 17.0, 10.3 Hz, 1H), 5.64 (dd, J = 10.3, 1.4 Hz, 1H), 4.18 – 4.05 (m, 2H), 4.03 (s, 3H), 3.34 – 3.23 (m, 2H), 2.80 (s, 4H), 2.44 (t, J = 7.2 Hz,

2H), 2.20 (p, *J*=6.55, 2H), 1.76 (d, *J* = 6.4 Hz, 3H), 1.63 (p, *J* = 6.15, 2H). ^{13}C NMR (126 MHz, Chloroform-*d*) δ 172.69, 168.40, 166.05, 154.42, 147.59, 139.19, 131.03, 130.82, 126.25, 109.07, 107.23, 76.45, 68.44, 56.41, 35.76, 35.64, 32.67, 29.64, 25.31, 24.70, 21.81. IR: ν = 1737, 1365, 1217.

Expression of Phenylalanine Ammonia Lyase from Rhodosporidium toruloides. The plasmid containing the His_6-TEV-PAL expression vector was transformed into chemically competent BL21 (DE3) E. coli and starter cultures were grown in terrific broth (TB) with 50 µg/mL kanamycin. The following day, these starter cultures were used to inoculate 2x750 mL shaker flasks of TB broth (containing 50 µg/mL kanamycin). The cells were grown at 37 °C until a OD_{600} of 1.3 was reached. The cells were then induced with 1 mM IPTG and expression was allowed to occur overnight for 16 hrs at 18 °C. After expression, the cells were pelleted via centrifugation and resuspended in lysis buffer (50 mM Tris, pH 7.8, 300 mM NaCl, 10 mM imidazole, cOmplete protease inhibitor tablet). The cells were then lysed with an emulsifier and the supernatant was clarified via centrifugation. The supernatant was then incubated with NiNTA resin and rocked at 4 °C for 15 min. The resin slurry was then poured into a gravity column and the flowthrough was collected. The bound protein was then washed with 200 mL of wash buffer (50 mM Tris, pH 7.8, 300 mM NaCl, 10 mM imidazole). The bound his-tagged protein was then eluted with 50 mL of elution buffer (50 mM Tris, pH 7.8, 300 mM NaCl, 300 mM imidazole) and then dialyzed into 50 mM Tris, pH 7.8, 300 mM NaCl overnight.

For removal of the His tag, the His_6-TEV-PAL was incubated with 1:10 weight equivalents of TEV protease and allowed to incubate for 9 hrs at 4 °C. To the mixture, NiNTA resin was added and the slurry was rocked at 4 °C for 15 mins. The slurry was added to a gravity column and the flow through was collected. The unbound protein was then eluted with 50 mL of wash buffer (50

mM Tris, pH 7.8, 300 mM NaCl, 10 mM imidazole). The TEV-cleaved protein was then dialyzed into 50 mM Tris, pH 7.8, 90 mM NaCl overnight and the protein was stored at -80 °C until use.

4.6 Appendix with Supplementary Figures

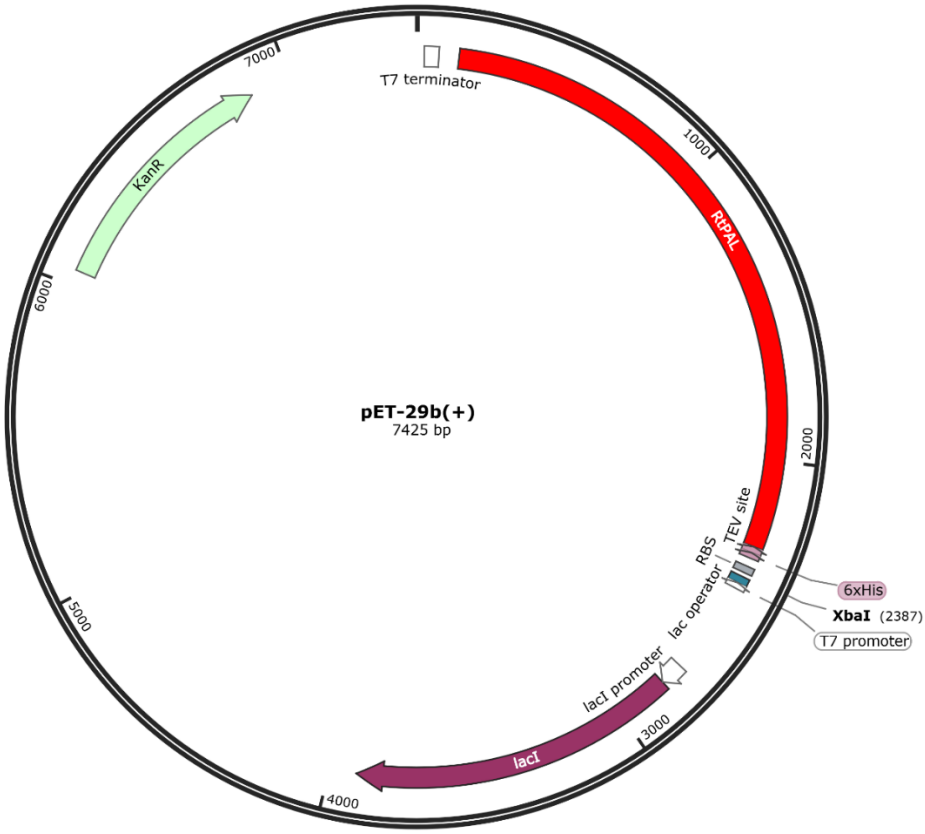

Figure 4.6.1. pET-29b Plasmid map for the expression of Phenylalanine Ammonia Lyase

GGATCTGATAAAATTCATCATCATCATCACGAAAACCTGTACTTCCAGGGCATG
GCGCCTAGCTTAGACAGCATCTCCCATAGCTTCGCTAATGGCGTTGCATCTGCTAAG
CAAGCAGTTAATGGGGCATCTACTAACTTAGCCGTTGCCGGCTCCCATTTACCTACG
ACGCAAGTAACGCAGGTTGACATCGTGGAAAAGATGCTTGCTGCGCCGACTGACAG
TACCCTTGAGTTAGACGGTTACTCTCTGAATCTTGGGGACGTTGTTAGTGCTGCACG
CAAAGGTCGCCCCGTCCGCGTCAAGGACAGTGATGAAATTCGCTCCAAAATTGATA
AATCAGTGGAATTCTTACGTTCGCAGTTGAGCATGTCGGTTTACGGAGTCACCACAG
GGTTTGGCGGGTCAGCCGATACCCGTACTGAAGATGCGATTTCGTTACAGAAAGCTC
TTCTTGAGCATCAACTTTGTGGCGTTTTGCCTAGTTCTTTCGATTCATTTCGCTTAGG
ACGTGGTCTGGAAAATAGCTTGCCGTTAGAAGTGGTTCGTGGAGCGATGACAATCC
GCGTGAATTCACTTACGCGCGGCCACTCGGCTGTCCGTCTTGTCGTCTTAGAAGCTTT

GACTAATTTTCTTAATCATGGAATTACCCCGATCGTCCCTTTGCGCGGTACAATTAGT
GCTAGCGGAGATTTATCGCCCCTGAGCTACATCGCCGCAGCGATTAGCGGACATCCC
GACTCAAAGGTGCATGTTGTCCATGAAGGTAAGGAAAAGATCCTTTACGCACGCGA
AGCAATGGCTCTGTTTAACCTGGAGCCCGTCGTGTTAGGTCCGAAGGAGGGCCTTGG
CTTAGTAAATGGCACAGCTGTGTCAGCGTCAATGGCGACTCTGGCGTTGCATGATGC
GCACATGCTTTCTCTTTTGTCTCAAAGTCTGACAGCCATGACCGTTGAGGCCATGGTT
GGGCATGCCGGCTCCTTTCACCCATTCTTACATGACGTCACGCGTCCTCATCCAACC
CAGATTGAGGTGGCAGGCAACATCCGCAAGCTGTTAGAGGGGTCCCGCTTCGCGGT
CCATCATGAGGAAGAAGTTAAAGTTAAAGACGACGAGGGCATTCTGCGTCAGGACC
GCTACCCCTTGCGCACAAGTCCTCAGTGGCTTGGACCTCTTGTTTCCGATCTTATTCA
TGCACACGCCGTCCTGACAATTGAAGCGGGTCAAAGCACAACCGACAATCCATTAA
TCGATGTCGAGAACAAGACTTCTCACCACGGTGGCAATTTTCAGGCTGCGGCAGTGG
CGAATACGATGGAAAAAACTCGTCTTGGATTAGCGCAAATTGGGAAGCTGAATTTC
ACCCAGCTGACGGAAATGCTGAACGCAGGTATGAACCGTGGCTTACCATCCTGTTTG
GCCGCAGAGGATCCAAGCCTGTCTTACCACTGTAAAGGTCTGGATATTGCAGCGGCC
GCGTATACCTCGGAATTAGGTCACTTGGCTAACCCAGTGACGACTCATGTGCAGCCT
GCCGAAATGGCAAACCAGGCTGTAAACTCTTTAGCTTTGATCAGTGCCCGTCGCACG
ACTGAGTCAAACGACGTCTTATCGTTGCTGTTGGCGACCCACTTATACTGCGTATTA
CAAGCGATTGATCTGCGTGCGATTGAGTTTGAATTCAAAAAGCAATTCGGACCGGCT
ATCGTAAGCCTTATTGACCAACACTTTGGGTCGGCTATGACTGGCTCTAACTTGCGC
GATGAATTAGTCGAGAAAGTTAACAAGACGTTAGCGAAGCGTCTGGAACAGACGAA
CTCTTACGATCTGGTACCTCGTTGGCACGATGCTTTCTCATTTGCCGCAGGAACCGTT
GTCGAGGTGTTAAGCTCGACATCTTTGTCATTGGCAGCTGTTAACGCATGGAAGGTG
GCAGCGGCGGAGTCAGCTATCAGTCTTACACGCCAAGTTCGTGAGACATTTTGGTCT
GCCGCTTCCACAAGCTCCCCGGCACTGAGTTATTTGAGTCCACGTACTCAGATCCTT
TACGCTTTTGTACGTGAGGAATTGGGCGTAAAAGCACGTCGCGGGGATGTGTTCTTA
GGCAAGCAGGAAGTCACCATCGGCTCTAACGTATCGAAGATTTACGAAGCGATTAA
ATCCGGGCGTATTAACAATGTACTTTTGAAGATGCTGGCCTAATGA

Figure 4.6.2. cDNA used for Rt-PAL expression. Yellow highlighted region indicates His_6 tag while the green region indicates the TEV cleavage site.

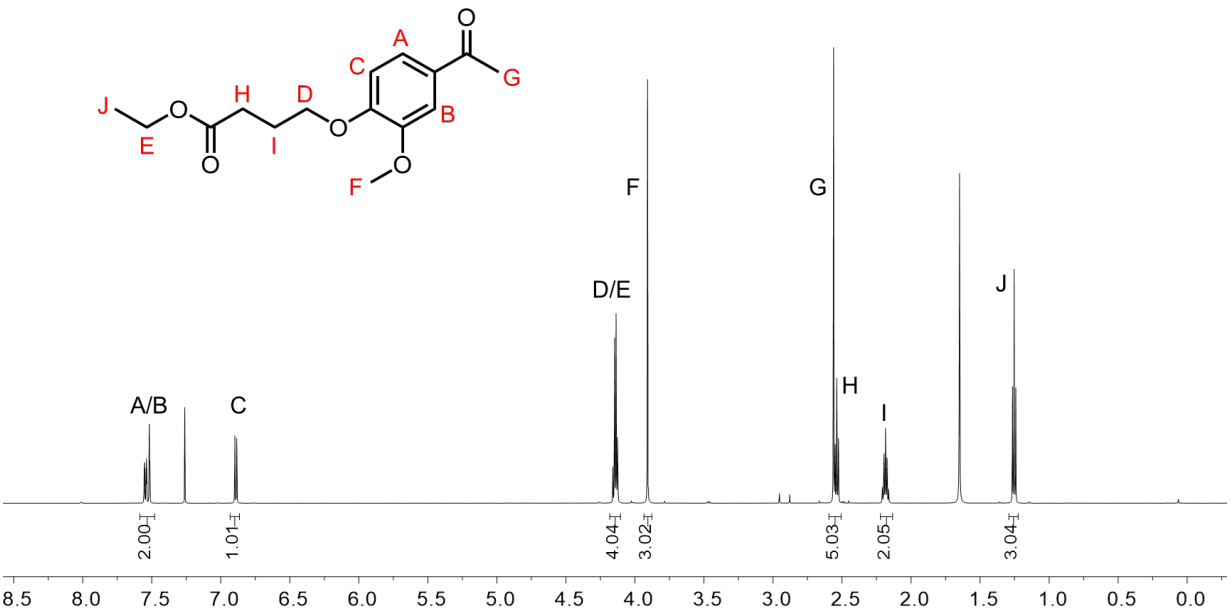

Figure 4.6.3. [1]H NMR of alkylated acetovanillone.

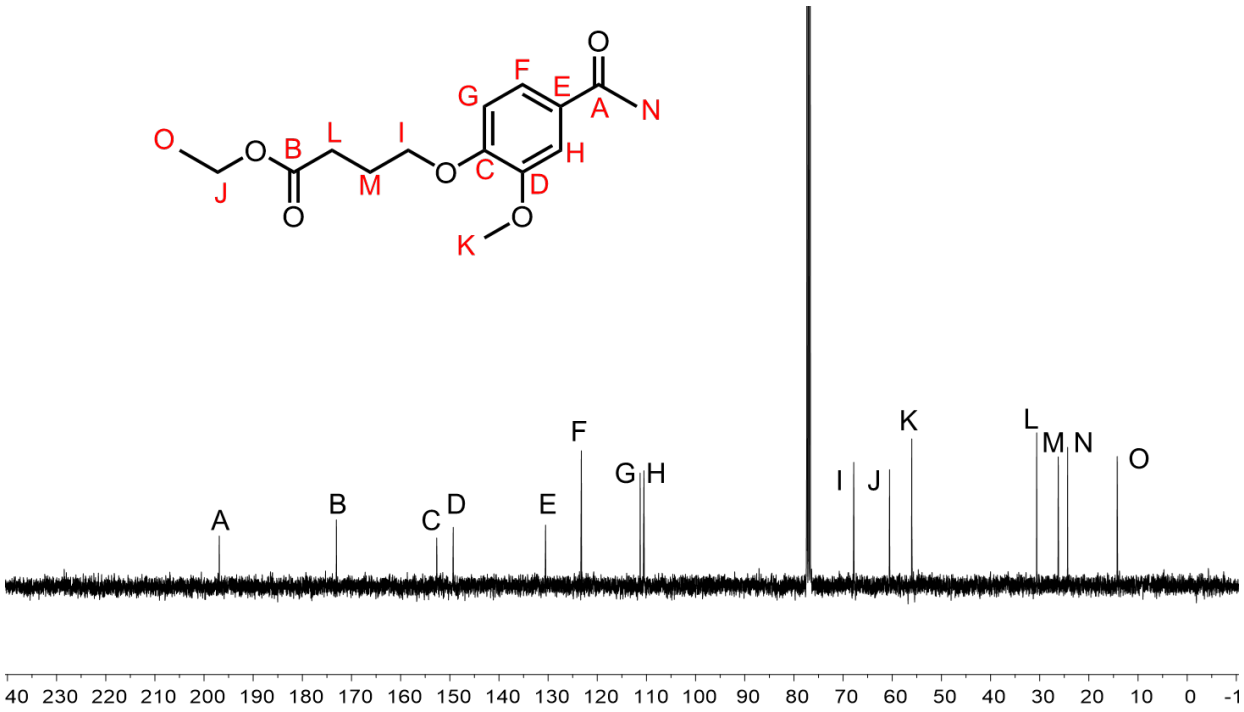

Figure 4.6.4. [13]C NMR of alkylated acetovanillone.

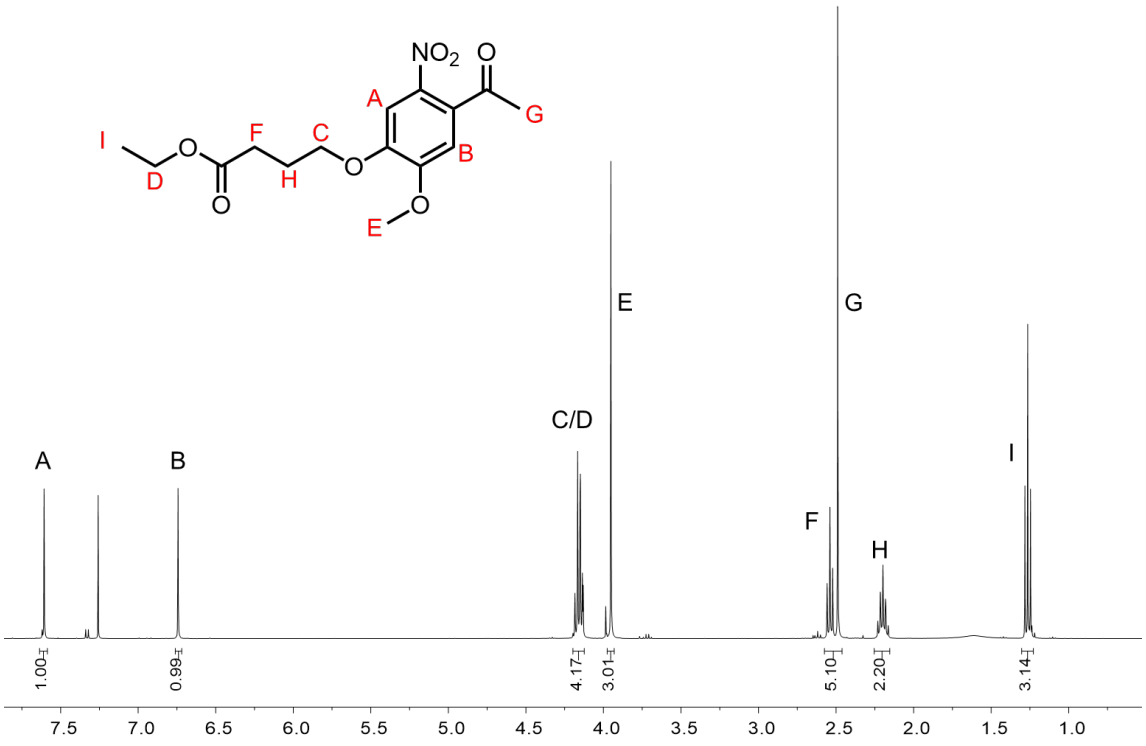

Figure 4.6.5. ^{1}H NMR of nitrated acetovanillone.

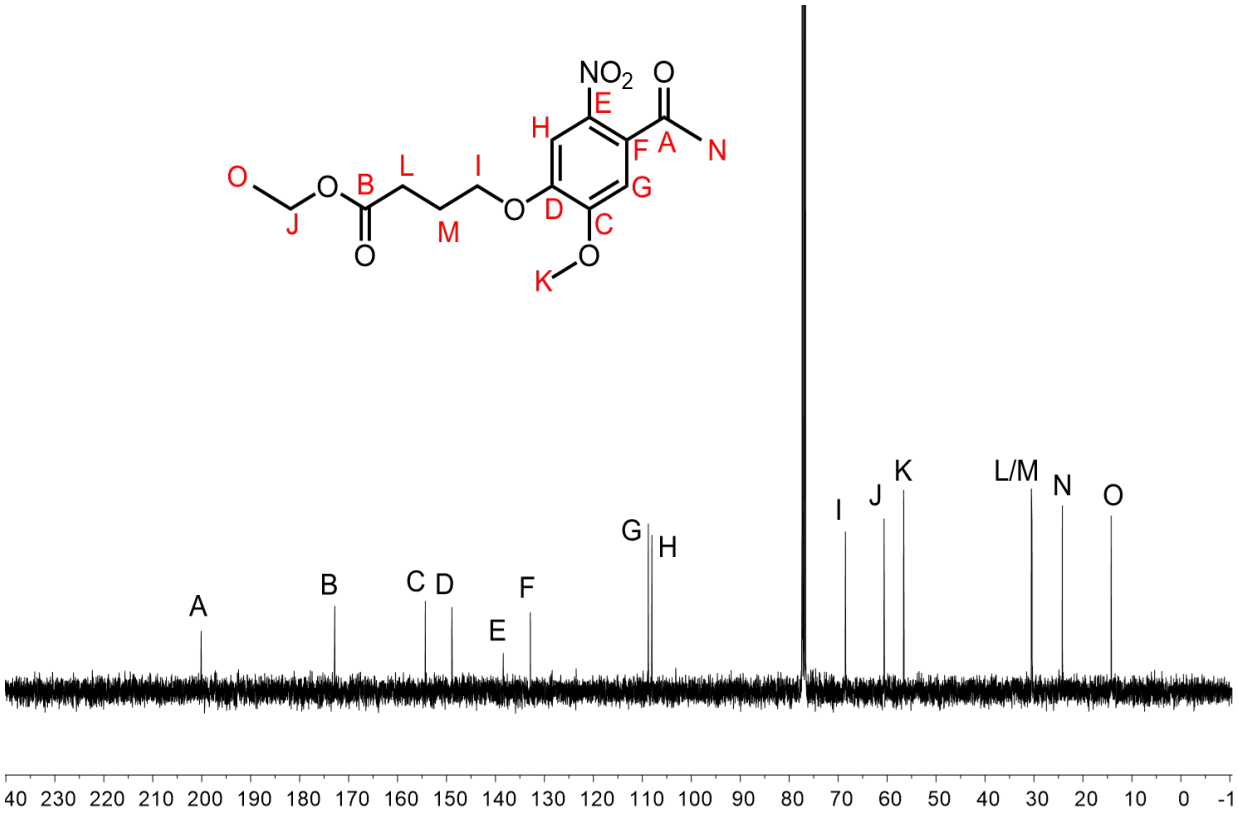

Figure 4.6.6. ^{13}C NMR of nitrated acetovanillone.

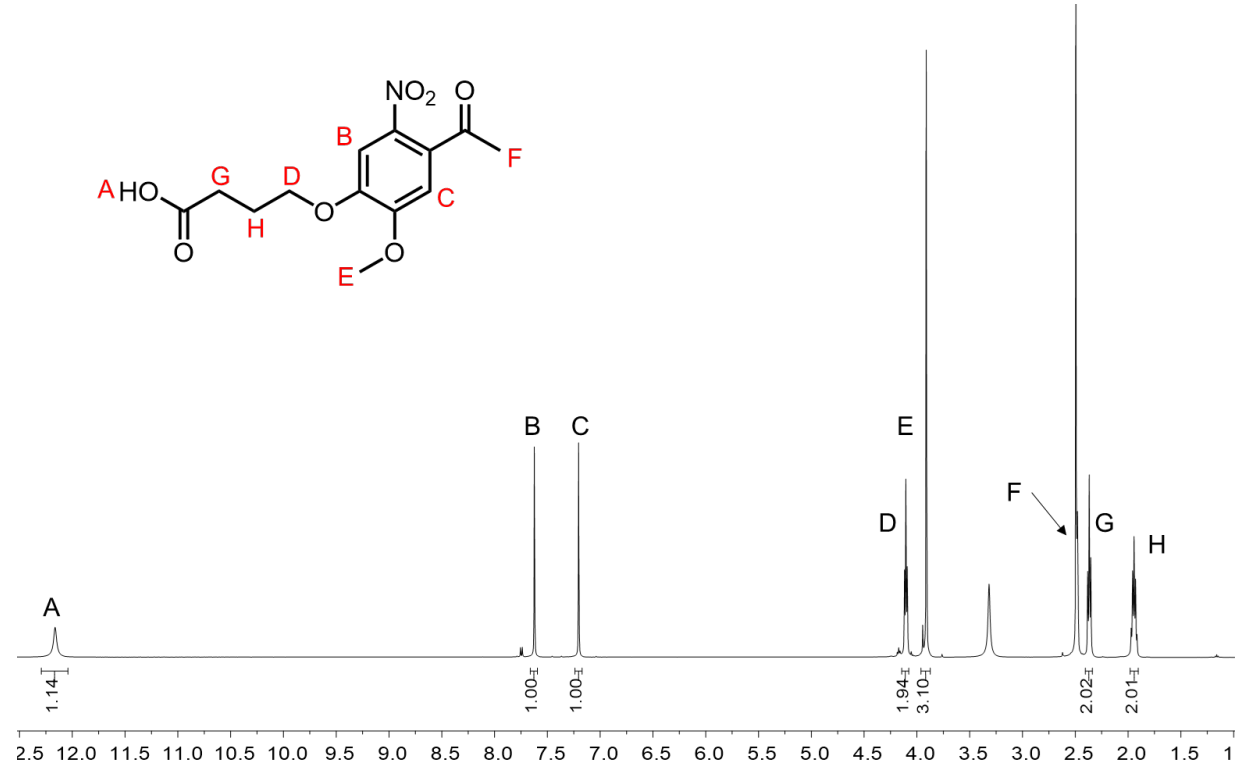

Figure 4.6.7. ^{1}H NMR of nitrated acid.

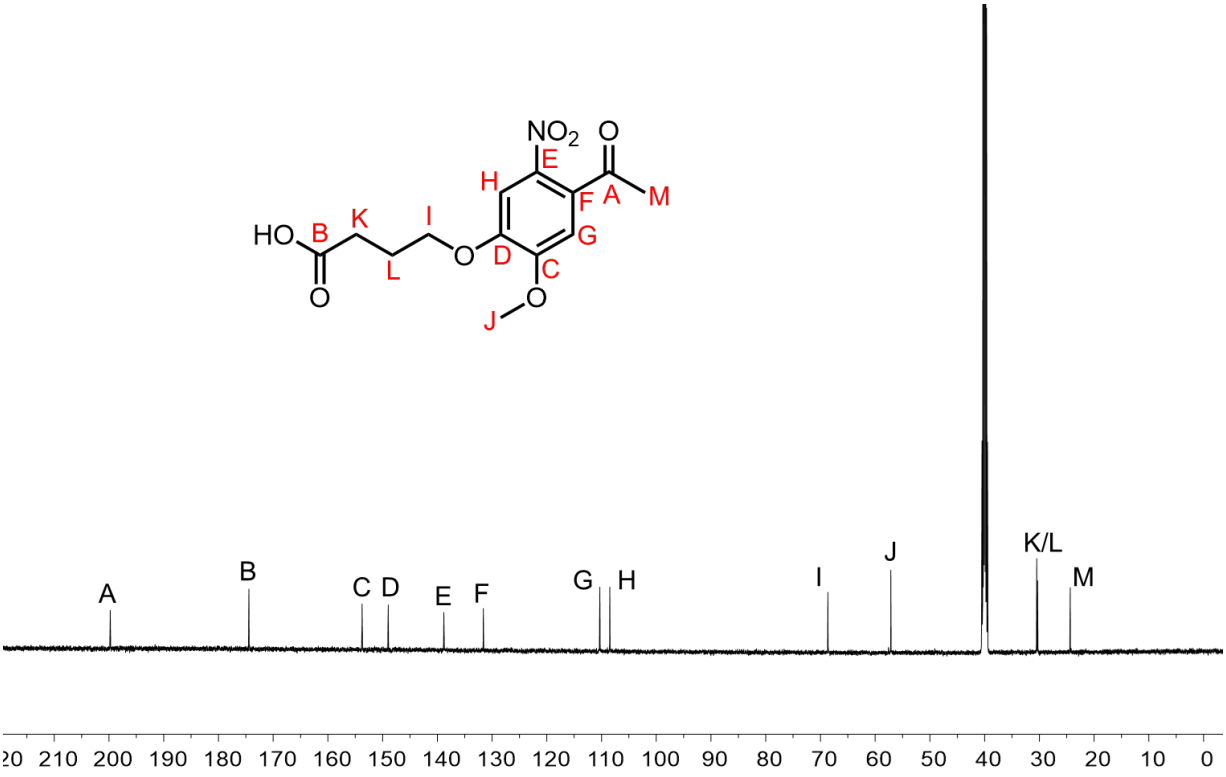

Figure 4.6.8. ^{13}C of nitrated acid.

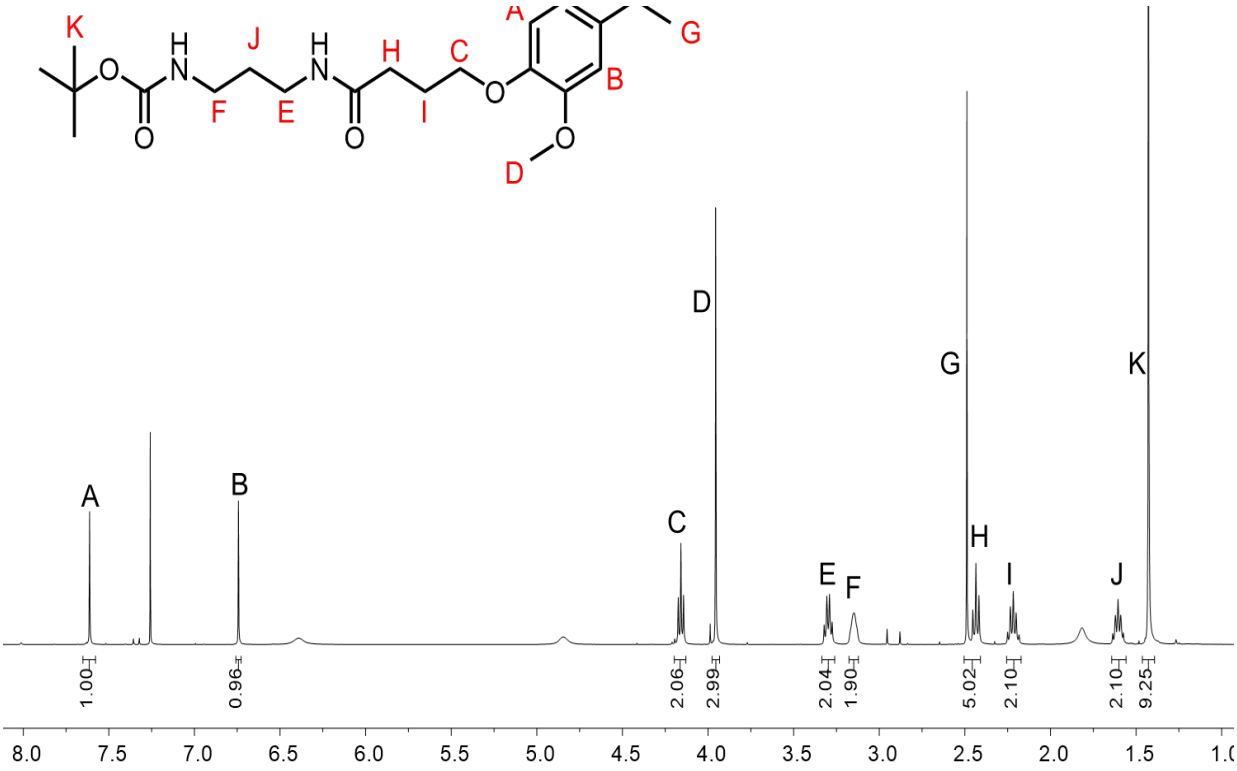

Figure 4.6.9. ^{1}H NMR of nitrated mono-boc acetovanillone.

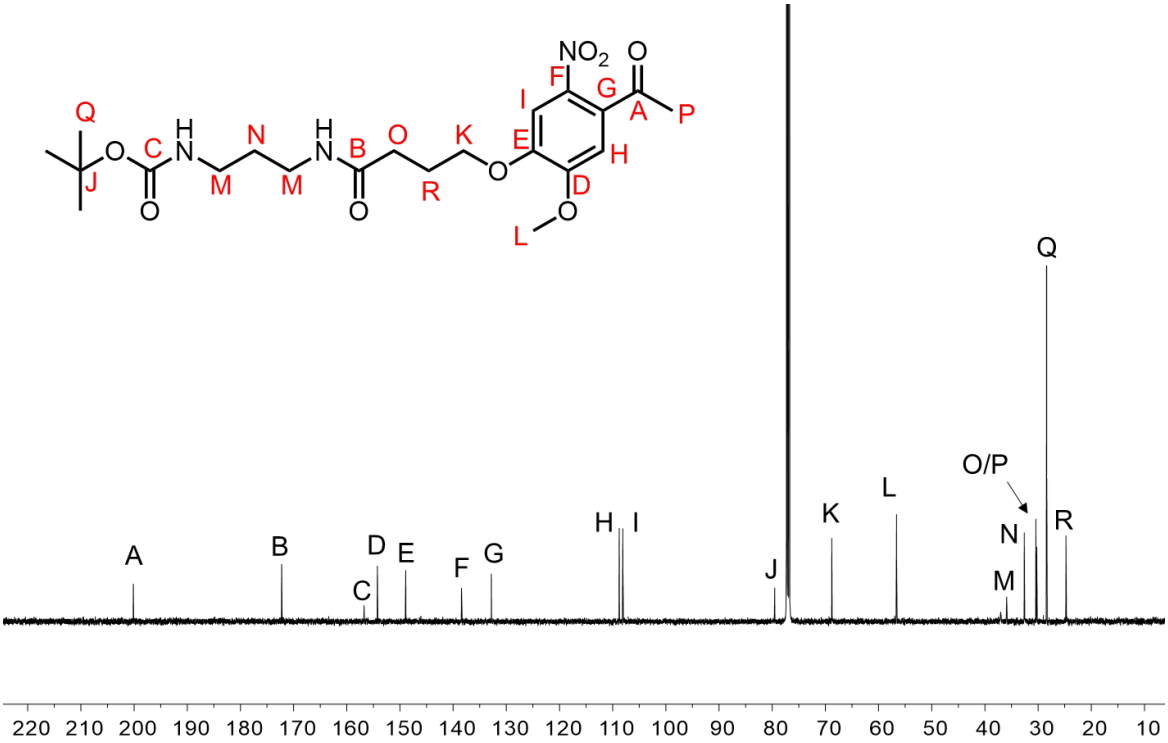

Figure 4.6.10. ^{13}C NMR of nitrated mono-boc acetovanillone.

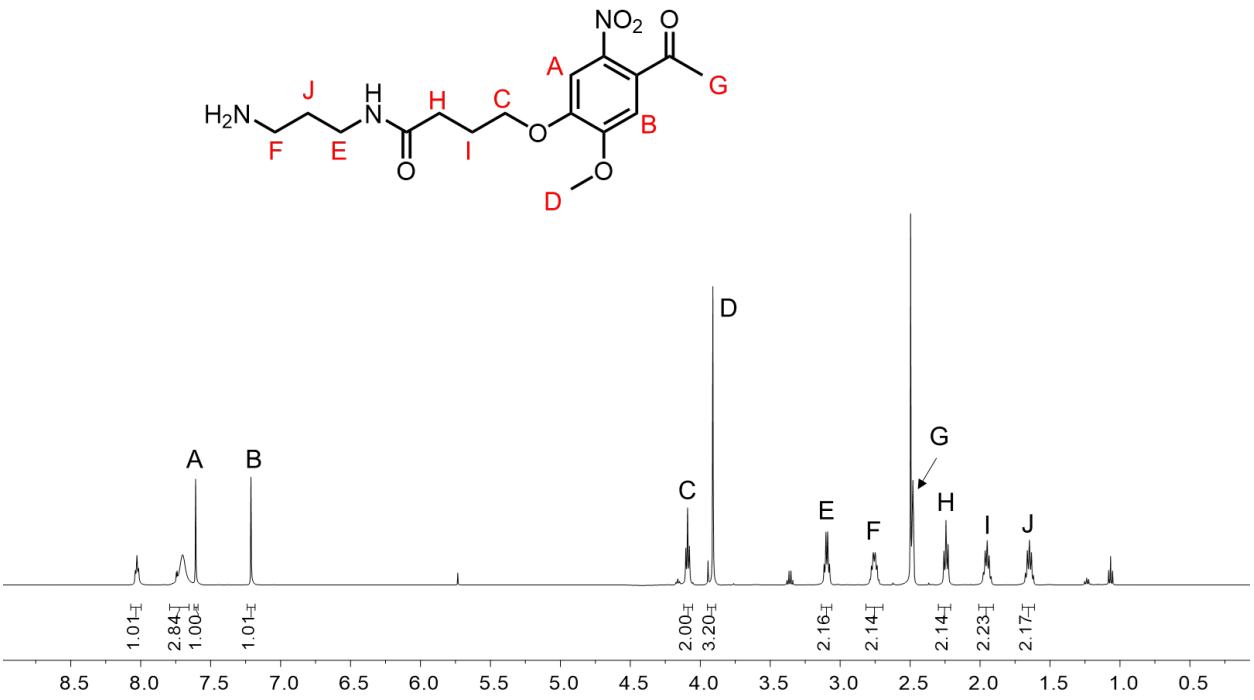

Figure 4.6.11. [1]H NMR of amino acetovanillone.

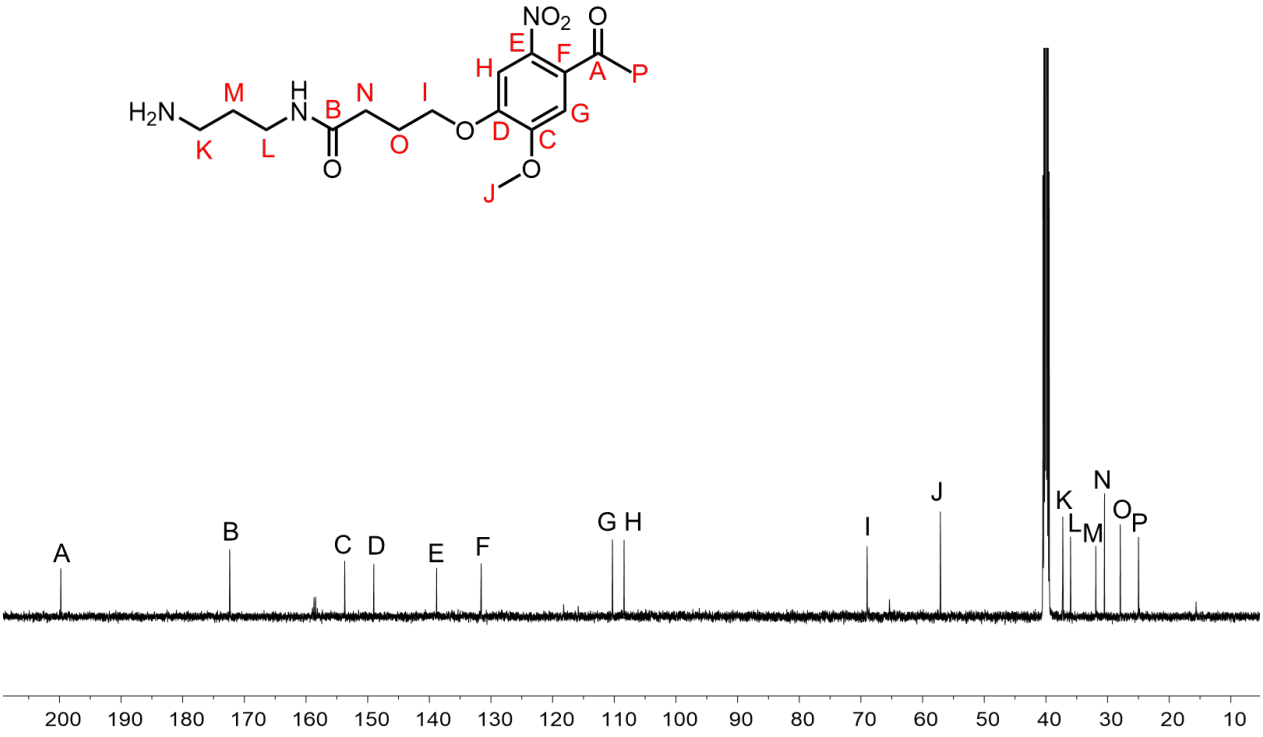

Figure 4.6.12. [13]C NMR of amino acetovanillone.

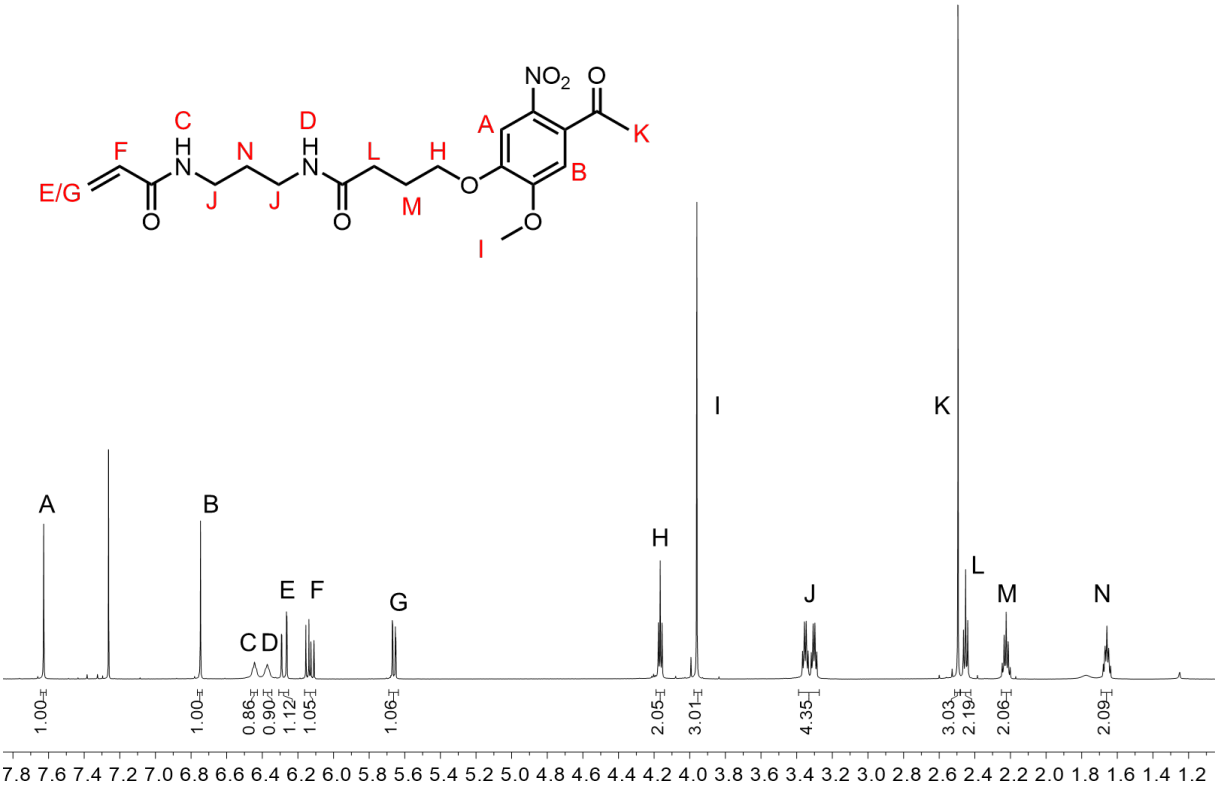

Figure 4.6.13. ^{1}H NMR of acetovanillone acrylamide.

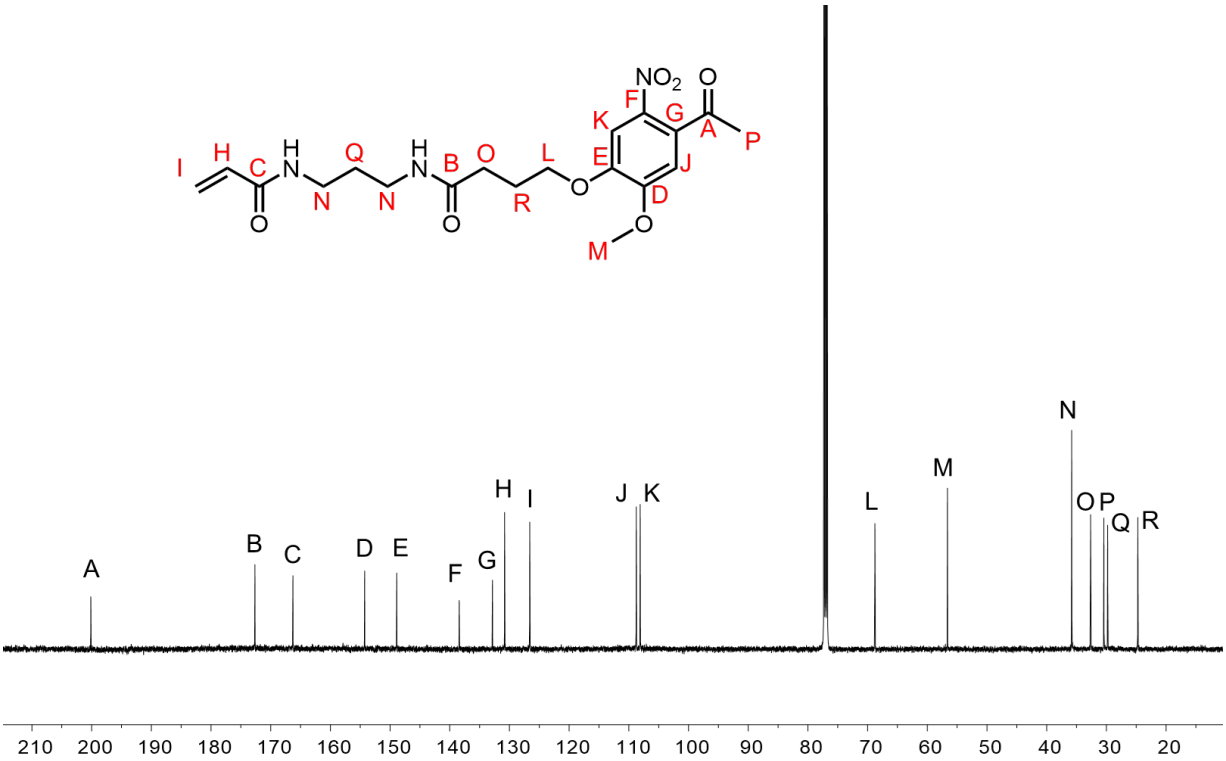

Figure 4.6.14. ^{13}C NMR of acetovanillone acrylamide.

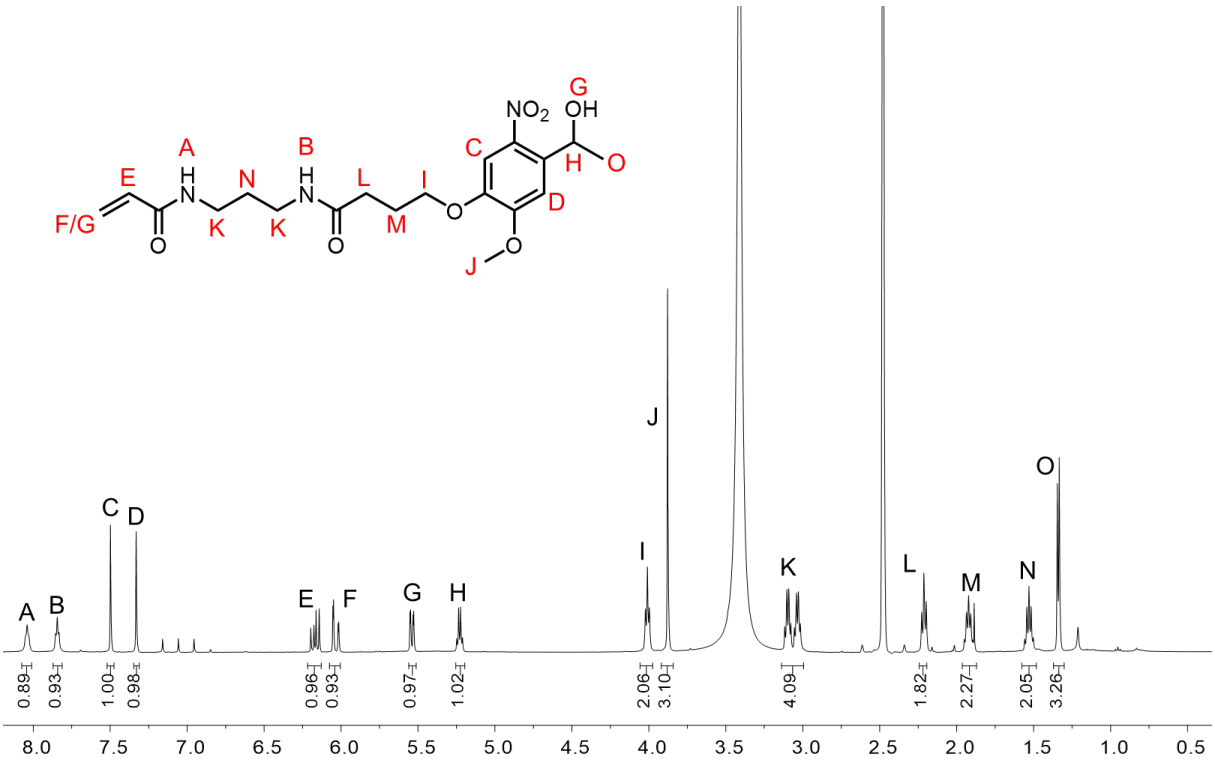

Figure 4.6.15. ^{1}H NMR of acetovanillone acrylamide alcohol.

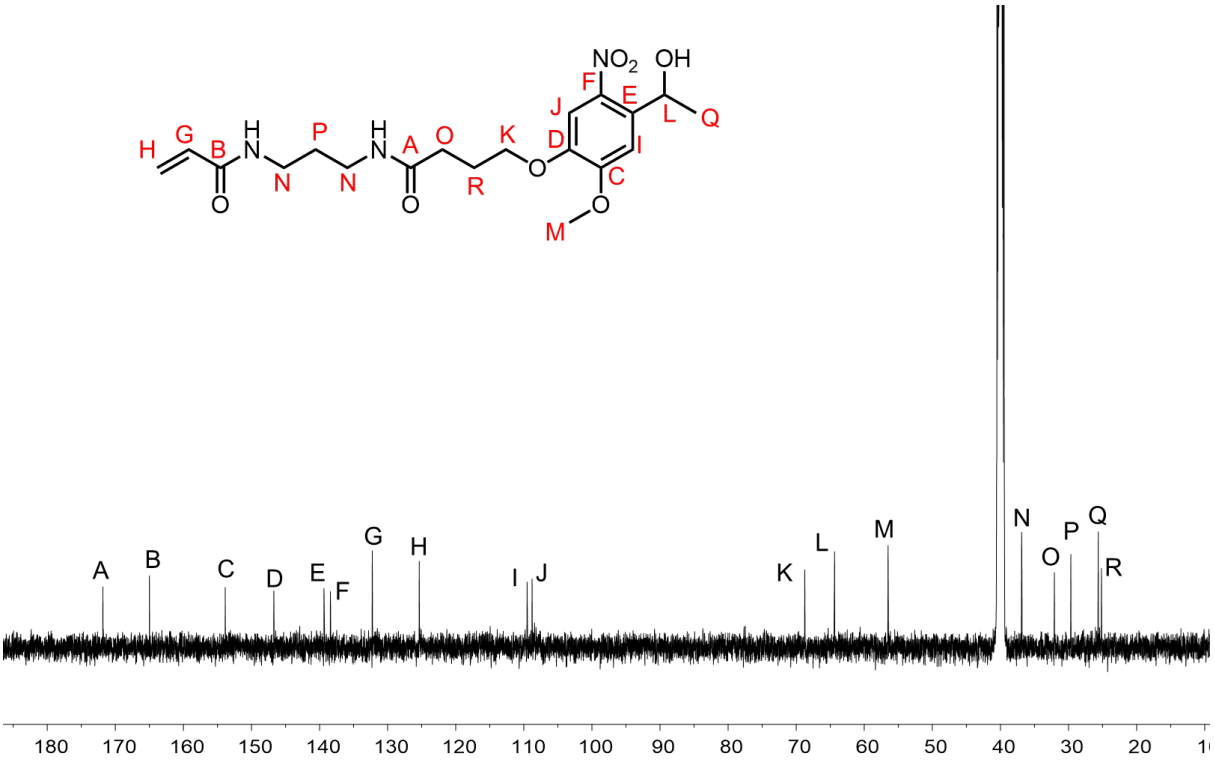

Figure 4.6.16. ^{12}C NMR of acetovanillone acrylamide alcohol.

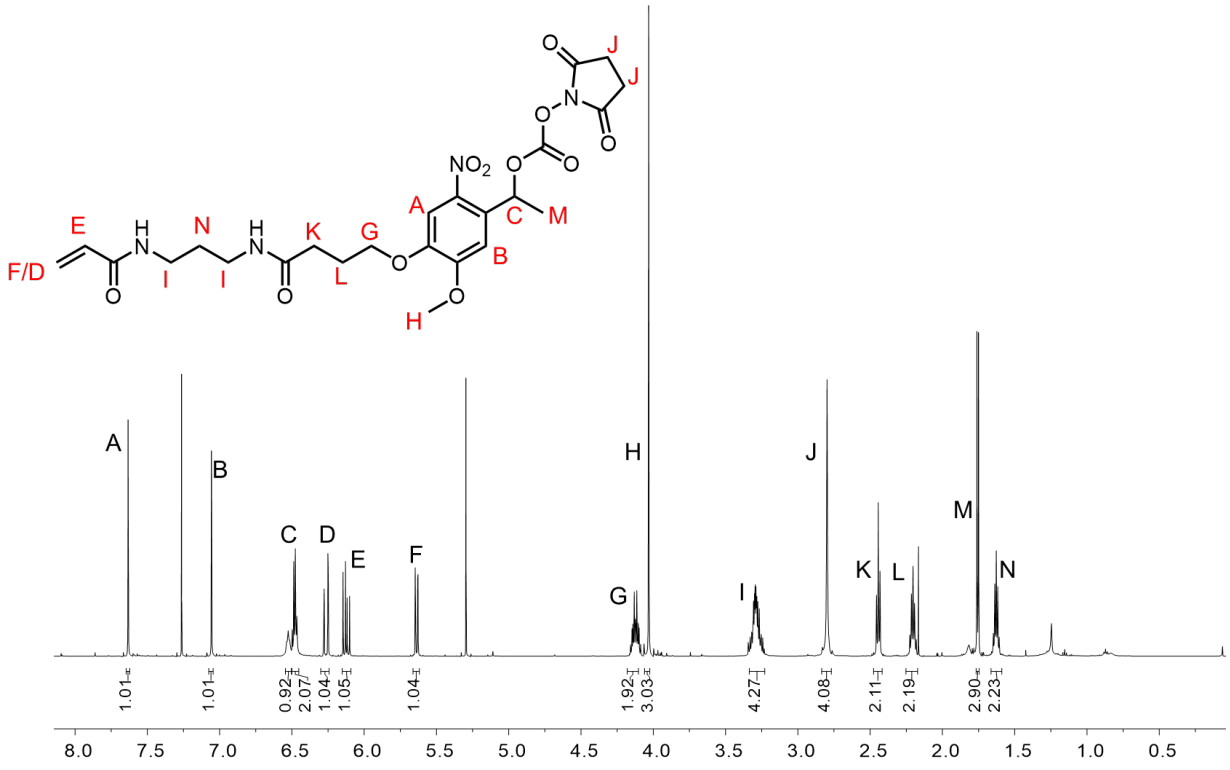

Figure 4.6.17. ^{1}H NMR of acetovanillone acrylamide NHS carbonate.

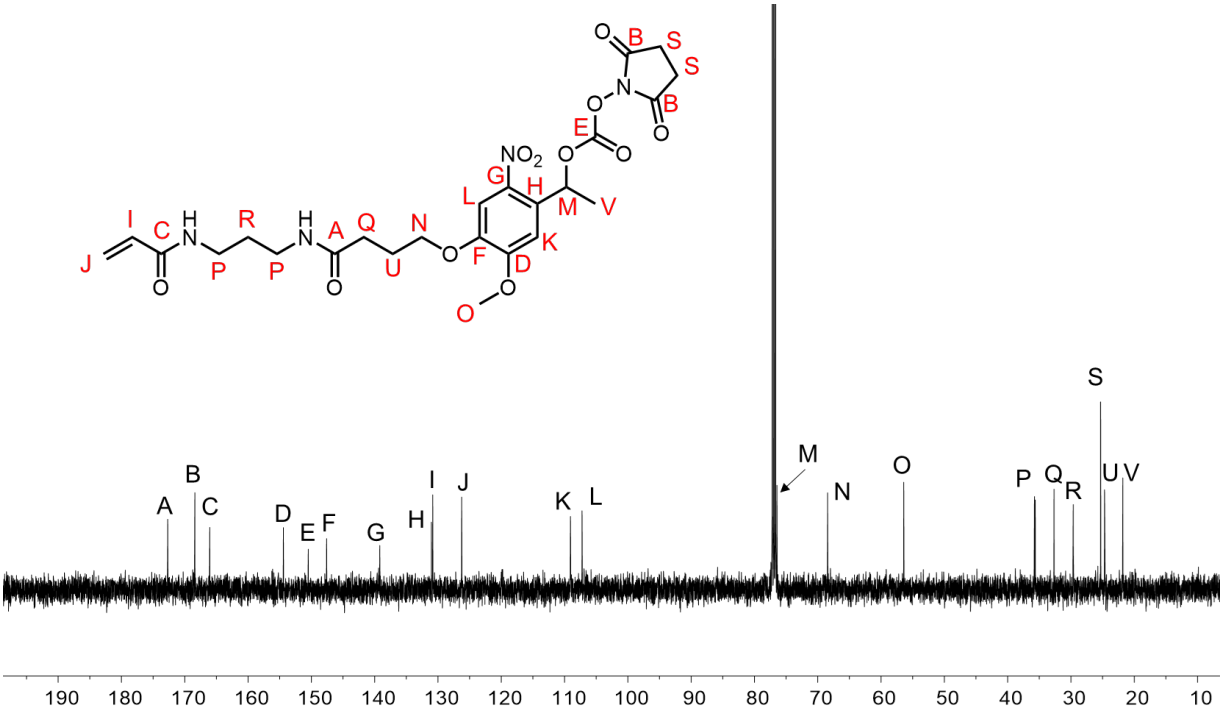

Figure 4.6.18. ^{13}C NMR of acetovanillone acrylamide NHS carbonate.

4.7. Experimental and Appendix References

(1) Tropea, J. E.; Cherry, S.; Waugh, D. S. Expression and Purification of Soluble His(6)-Tagged TEV Protease. *Methods Mol. Biol. Clifton NJ* **2009**, *498*, 297–307.

(2) Kloxin, A. M.; Kasko, A. M.; Salinas, C. N.; Anseth, K. S. Photodegradable Hydrogels for Dynamic Tuning of Physical and Chemical Properties. *Science* **2009**, *324*, 59–63.

Chapter 5

Efficient and Scalable Production of Granulocyte Colony-Stimulating Factor Conjugates via a Heterobifunctional Benzaldehyde Maleimide Linker

5.1 Introduction

Patients undergoing chemotherapy can develop a condition known as febrile neutropenia, that, if left untreated, can lead to a compromised immune system. Patients suffering from this condition often have poor health outcomes due to greater susceptibility to sepsis and bacterial infections.[1] Granulocyte colony-stimulating factor (G-CSF), or Neupogen®, is an approved therapy for use in the treatment of neutropenia as it elicits a powerful stimulus for the production of progenitor cells.[2] Since its initial approval for neutropenia, G-CSF has further been expanded to six additional indications for treatment of other diseases involving immunodeficiencies.[3] Despite its marked success, however, G-CSF suffers from a relatively short half-life of 3.5-3.8 hrs, requiring a daily dosing regimen.[4] These poor pharmacokinetic outcomes are largely due to its small size as the cytokine is only 175 amino acids in length (18.8 kDa), leading to rapid renal clearance.[5]

One commonly employed method to improve the half-life of protein drugs is PEGylation. Through attachment of polymers with a large hydrodynamic radius such as polyethylene glycol (PEG), protein conjugates are able to avoid *in vivo* clearance mechanisms through the kidneys and immune system.[7] As a means to improve the half-life of G-CSF, Neulasta® was developed as a PEGylated form of Neuopogen®. Chemically, a 20,000 kDa PEG was conjugated selectively to the N-terminus using reductive amination of a monomethoxy-PEG aldehyde.[4] This method for site-specific conjugation is especially important in the case of G-CSF as conjugation relies on receptor-mediated binding, meaning that heterogenous conjugation through lysine residues could significantly inhibit activity. By this modification, the half-life is improved to 42 hours, allowing for a single dose per 21-day chemotherapy cycle rather than the daily injections required for the non-pegylated variant. [5,8] While these developments significantly expand the therapeutic

availability of G-CSF *in vivo*, G-CSF has one additional limitation that significantly limits its application: poor stability to storage and stressors.

The solution stability of G-CSF is impeded largely by its propensity towards aggregation. Variations in pH, concentration, and ionic strength can all lead to irreversible aggregation, which, in turn, can lead to poor health outcomes and wasted products.[9–11] While PEGylation is a robust method to increase the *in vivo* stability and clearance of G-CSF, PEG does not necessarily confer stabilization of the protein to storage and stress conditions. Previous work in the Maynard lab has extensively demonstrated ability of trehalose-functionalized polymers to stabilize proteins to environmental stressor as well as extend the *in vivo* half-life.[12–15] We therefore envisioned that trehalose polymers could offer significant advantages over PEG as we could achieve both protection from aggregation during transport and storage, while additionally providing improved pharmacokinetics through the increased hydrodynamic radius of the conjugate. In order to test this hypothesis, however, we first needed a robust and high yielding method to produce G-CSF. This chapter presents the optimization of G-CSF expression in E. coli and the development of a heterobifunctional linker for improved polymer conjugation.

5.2 Results and Discussion

5.2.1 G-CSF Expression Optimization

As G-CSF is not a native protein to E. coli, expression in this host requires optimization. For our purposes, we initially expressed G-CSF using maltose-binding protein (MBP) fusion via a soluble preparation. This construct contained a tobacco etch virus (TEV) cleavage site between the MBP-His_6 sequence and G-CSF that would afford pure G-CSF after protease cleavage. We initially were drawn to this expression system as G-CSF is not normally soluble during E. coli expression, resulting in the formation of inclusion bodies. To counter inclusion body formation,

MBP is commonly employed as the 42 kDa protein is highly soluble and stable at a range of pH values, making it an excellent candidate in our design of a fusion construct. Additionally, we were hopeful that this MBP fusion strategy would increase the stability of G-CSF during processing and conjugation given the sensitivity of G-CSF to aggregation. While this method did prove successful in obtaining pure G-CSF (**Figure 5.2.1**), the yield was poor (< 0.5 mg/L of culture). We largely attribute this to truncation during the expression as we exclusively observed free MBP and the expected MBP-GCSF fusion. In an attempt to optimize and prevent truncation, we attempted expression in other E. coli strains such as Rosetta and Rosetta-gami cells in order to rule out the potential for codon-bias. However, these attempts resulted in similar levels of truncation with reduced overall expression yields.

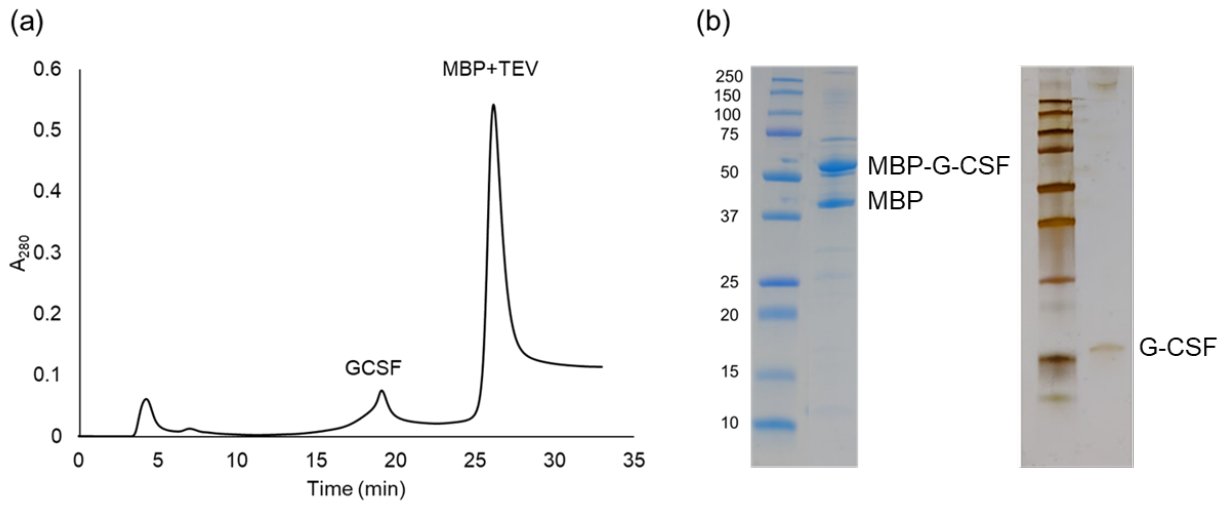

Figure 5.2.1. (a) FPLC trace of MBP-G-CSF TEV digest purification and (b) SDS PAGE of MBP-G-CSF stained with Coomassie (left) and purified G-CSF after TEV digest (right) stained with silver.

Given the challenges with truncation and low yield in the MBP fusion construct, we next pursued an insoluble, inclusion body expression of the protein.[16–18] The first construct we employed contained an N-terminal His_6-TEV cleavage sequence (abbreviated His_6-TEV hereafter) for purification. This construct showed high levels of expression as indicated by the strong

induction band. Harvesting and resolubilization of the inclusion bodies in 2 M urea at pH 12 proceeded as expected, yielding highly pure, unfolded G-CSF (**Figure 5.2.2**). Refolding of the His_6-TEV-G-CSF was done via dilution, acidification, and final dialysis into pH 7.8 Tris buffer. Native-polyacrylamide gel electrophoresis (PAGE) of the refolded G-CSF (**Figure 5.2.2**) showed a single band, indicating successful refolding. Final TEV cleavage and Ni-nitrilotriacetic acid (Ni-NTA) purification yielded pure G-CSF with a final expression yield of 137 mg/L of culture, which is approximately 300-fold higher than the initial soluble expression (< 0.5 mg/L).

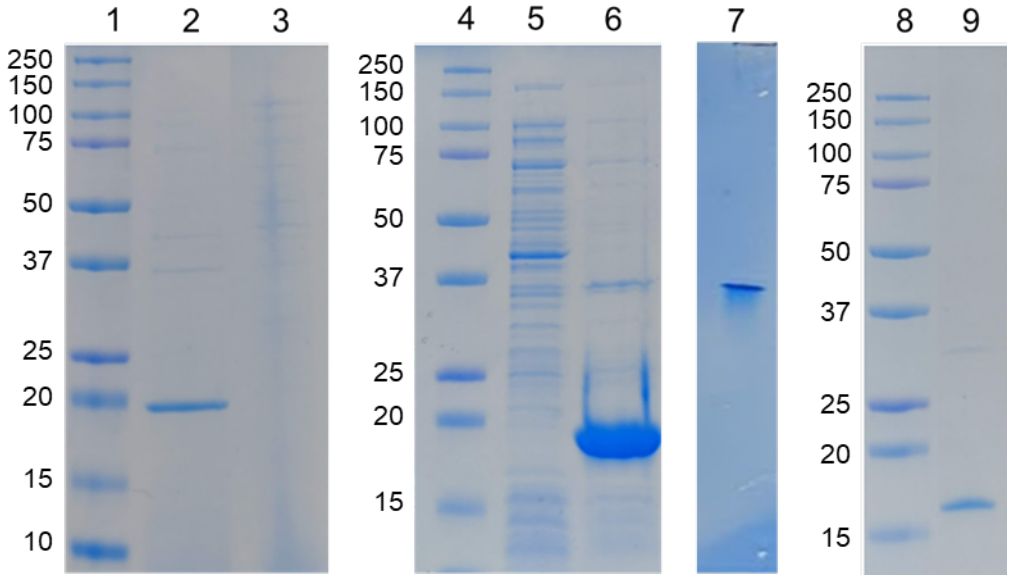

Figure 5.2.2 Expression of His-tagged G-CSF. Lane 1: ladder, lane 2: crude induced cells, lane 3: uninduced cells, lane 4: ladder, lane 5: soluble lysate, lane 6: insoluble lysate, lane 7: Native PAGE of refolded protein, lane 8: ladder, lane 9: Ni-NTA purified protein after TEV digest.

In order to expand our study in the expression of G-CSF, we also developed an alternative method that does not require Ni-NTA chromatography. We observed that the resolubilized inclusion bodies were sufficiently pure and hypothesized that the His_6-TEV purification tag is unnecessary. Therefore, we tried directly expressing untagged G-CSF. Interestingly, we did not observe the expression of G-CSF after induction with this untagged variant. We hypothesized that

this result may be due to the presence of secondary structures in the mRNA that prevents entry into the ribosome. To address this issue, we used an altered codon sequence that contains greater AT content, which is hypothesized to minimize mRNA secondary structure.[19] With this codon-optimized sequence, we were able to obtain untagged G-CSF after appropriate resolubilization and refolding (**Figure 5.2.3**). The yield was lower than the His_6-TEV fusion approach (54 mg/L vs. 137 mg/L), but this method may be desirable because Ni-NTA chromatography purification is avoided. Thus, there are fewer overall steps. These optimized approaches are important for scaled production of G-CSF in the future for conjugation and are summarized in **Table 5.2.1**.

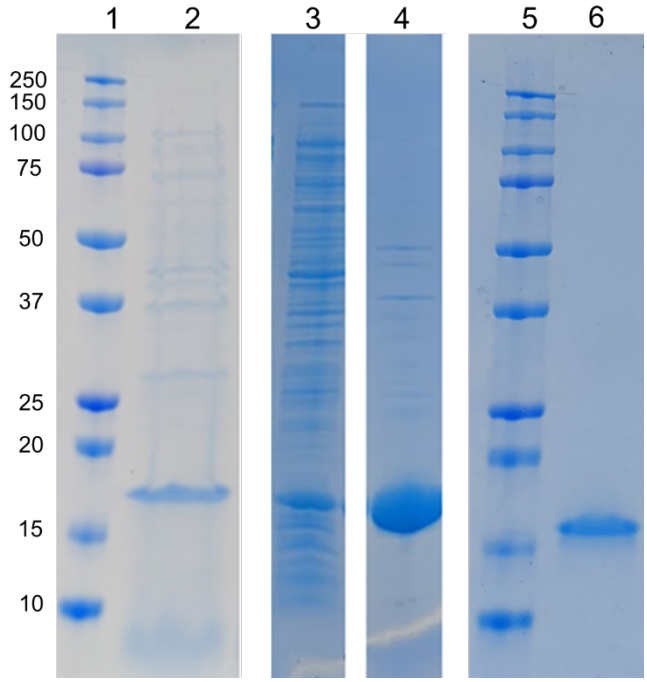

Figure 5.2.3. Untagged G-CSF Expression. Lane 1: ladder, lane 2: induction of crude cells, lane 3: soluble lysate, lane 4: insoluble lysate, lane 5: ladder, lane 6: final purified and refolded G-CSF.

Table 5.2.1. Summary of G-CSF expression constructs tested.

Construct	Pros / cons
MBP-His_6-G-CSF (soluble prep)	MBP stabilizes G-CSF to neutral pH Low yield (< 0.5 mg/L culture)
His_6-G-CSF (insoluble prep)	Highest yield (137 mg/L culture)
G-CSF (insoluble prep)	Easy purification High yield (54 mg/L culture)

5.2.2. Heterobifunctional linker for selective protein conjugation.

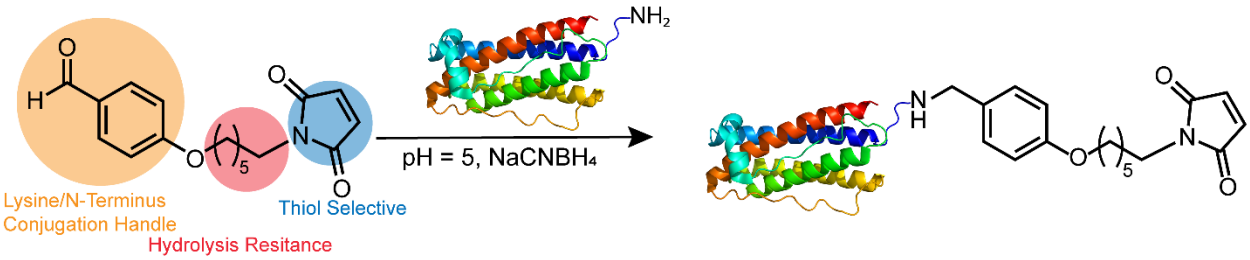

Figure 5.2.4. Scheme for the conjugation of benzaldehyde maleimide heterobifunctional linker to G-CSF.

After developing an efficient and scalable method to produce G-CSF, we wanted to additionally demonstrate a method to prepare G-CSF polymer conjugates that would be facile to characterize. As mentioned previously, G-CSF can be selectively PEGylated at the N-terminus using reductive amination of a PEG aldehyde at acidic pH. While this one-step method for conjugation is advantageous in terms of processing, it can lead to challenges in characterization, particularly if the resulting conjugate does not ionize well for mass spectrometry. While PEG conjugates can be characterized with relative ease via mass spectrometry, we have found that attachment of trehalose polymers suppresses ionization of conjugates, creating challenges in effective characterization.[12,20] Therefore, we decided to use a strategy that employed a small

molecule heterobifunctional linker that would allow for a two-step conjugation procedure. By first conjugating a polymer-reactive functionality to the protein, we could more effectively characterize the intermediate via mass spectrometry before attaching the polymer. In order to design an effective heterobifunctional linker for these purposes, we settled on two important criteria: the protein reactive functionality should be selective, yielding a uniform intermediate and that the polymer-reactive handle should rely on efficient and fast chemistry to enable high-yielding conjugation of the two macromolecules. Based on this, we settled on a benzaldehyde for lysine/N-terminal conjugation and a maleimide for attachment of a thiol containing polymer (**Figure 5.2.4**). The benzaldehyde functionality has been demonstrated as an effective handle for creating lysine protein-polymer conjugates via reductive amination. Furthermore, when conjugated to proteins in more acidic environments (which is more amenable to the stability of G-CSF), selectivity to the N-terminus can be achieved using this strategy.[21] In regards to polymer attachment using this strategy, we imagined the maleimide to be an effective reactive handle as a wide range of commercially available polymers contain thiol end groups. Furthermore, if using a polymer made via reversible addition−fragmentation chain-transfer polymerization (RAFT), the trithiocarbonate end group can be cleaved, liberating a free thiol for conjugation.[22]

While we believed that this could be an effective two-step conjugation strategy, we had two principal concerns regarding the maleimide. For one, maleimides are known to undergo hydrolysis in aqueous solutions, which would render the linker non-reactive towards thiol polymers. Therefore, in order to increase the stability of the maleimide to hydrolysis, we incorporated a hexyl chain between the benzaldehyde and the maleimide as this functionality has been reported to stabilize maleimides.[23] Additionally, there was the concern that a free cysteine residue on G-CSF could conjugate onto to the maleimide. While G-CSF does contain one free

cysteine, previous reports have indicated that it is buried and largely inaccessible to conjugation when the protein is folded, making it unlikely that we would have background addition into the maleimide.[24] In order to verify this along with the stability of the maleimide, we monitored to conjugation of the linker over the course of 96 hrs (**Figure 5.2.5**). From this, we observe the expected mass that would result from reductive amination through the aldehyde (19111 m/z) rather than addition through the cysteine and additionally we do not observe any hydrolysis-related by-product. Furthermore, we were pleased to see that by performing the conjugation at a low pH, we were able to achieve the addition of only a single linker rather than a distribution of lysine conjugations.

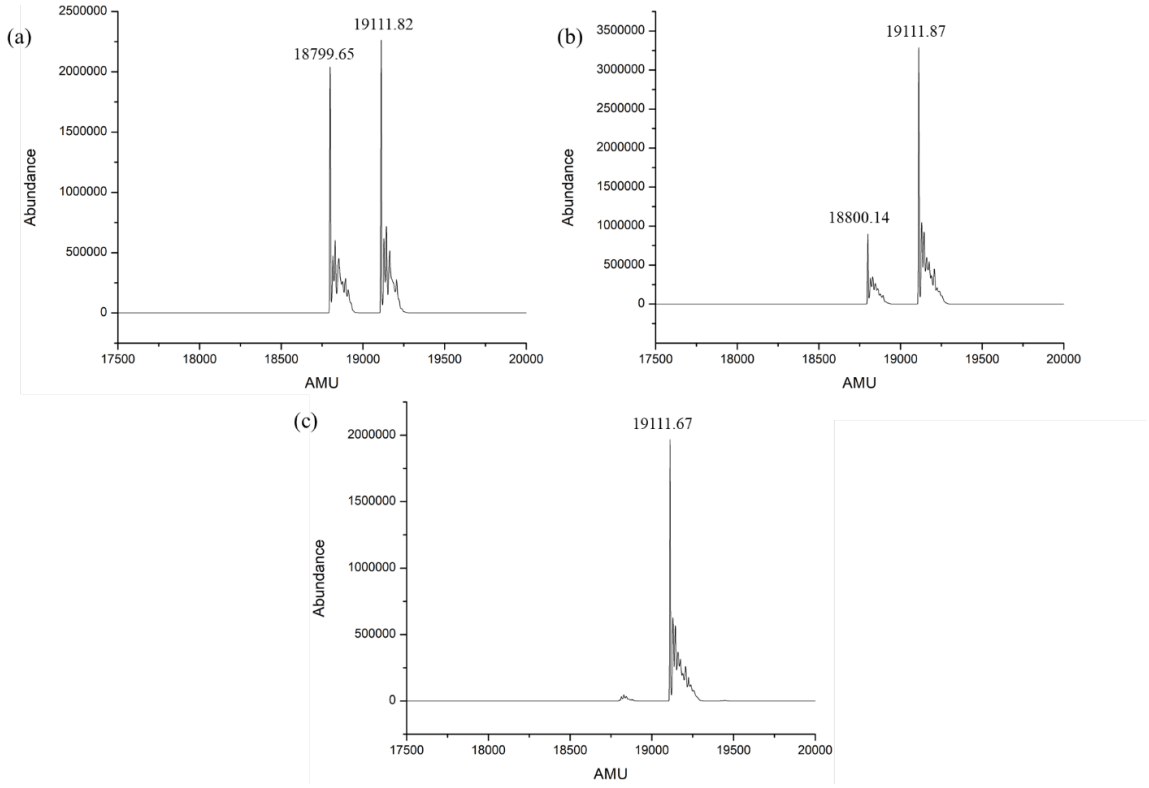

Figure 5.2.5. Conjugation kinetics of heterobifunctional linker to G-CSF at (a) 24 hrs, (b) 48 hrs, and (c) 96 hrs at 4 °C. The mass of 18799 corresponds to the unmodified G-CSF while the mass of 19111 corresponds to the conjugate. The expected mass for maleimide hydrolysis would be 1930 and is not observed due to the stabilizing hexyl linker.

After addition of the linker, we wanted to further demonstrate the applicability of this strategy for the preparation of protein-polymer conjugates. Employing a 10 kDa PEG-thiol, we conducted the conjugation to the linker-modified G-CSF. Analysis by SDS-PAGE demonstrated the expected increase in size associated with conjugation, demonstrating how this two-step conjugation strategy can lead to the facile synthesis and characterization of protein-polymer conjugates (**Figure 5.2.6**). Incomplete conversion of the conjugation is likely a result of the slower kinetics associated with the size of PEG and G-CSF, which is a known challenge in the synthesis of protein-polymer conjugates. Future work in this area involves using this strategy to create well-defined and characterized trehalose-G-CSF conjugates for applications in stabilization. However, we believe this strategy of conjugation to be a generally applicable method for protein conjugation as it allows for the addition of thiol-containing molecules to a protein in a selective manner.

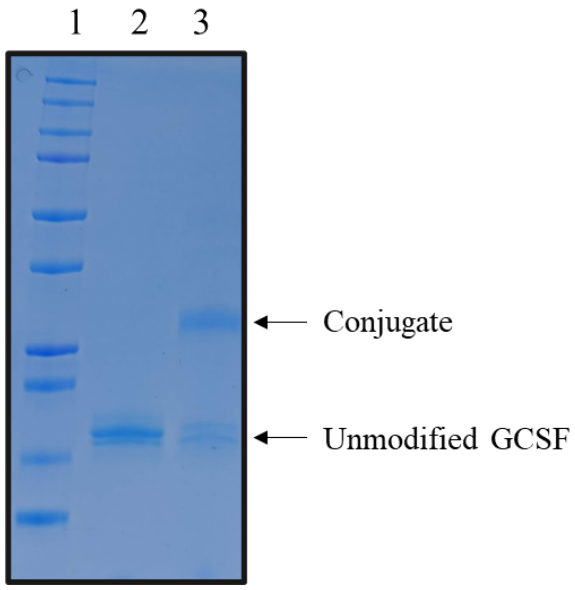

Figure 5.2.6 10 kDa PEG-thiol conjugation to G-CSF maleimide conjugate.

5.3. References

(1) Maher, D. W.; Lieschke, G. J.; Green, M.; Bishop, J.; Stuart-Harris, R.; Wolf, M.; Sheridan, W. P.; Kefford, R. F.; Cebon, J.; Olver, I.; McKendrick, J.; Toner, G.; Bradstock, K.; Lieschke, M.; Cruickshank, S.; Tomita, D. K.; Hoffman, E. W.; Fox, R. M.; Morstyn, G. Filgrastim in Patients with Chemotherapy-Induced Febrile Neutropenia: A Double-Blind, Placebo-Controlled Trial. *Ann Intern Med* **1994**, *121*, 492–501.

(2) Dührsen, U.; Villeval, J.-L.; Boyd, J.; Kannourakis, G.; Morstyn, G.; Metcalf, D. Effects of Recombinant Human Granulocyte Colony-Stimulating Factor on Hematopoietic Progenitor Cells in Cancer Patients. *Blood* **1988**, *72*, 2074–2081.

(3) Dale, D. C.; Crawford, J.; Klippel, Z.; Reiner, M.; Osslund, T.; Fan, E.; Morrow, P. K.; Allcott, K.; Lyman, G. H. A Systematic Literature Review of the Efficacy, Effectiveness, and Safety of Filgrastim. *Support Care Cancer* **2018**, *26*, 7–20.

(4) Alconcel, S. N. S.; Baas, A. S.; Maynard, H. D. FDA-Approved Poly(Ethylene Glycol)–Protein Conjugate Drugs. *Polymer Chemistry* **2011**, *2*, 1442.

(5) G., M. The Design and Development of Pegfilgrastim (PEG-RmetHuG-CSF, Neulasta®). *Current Pharmaceutical Design* **2004**, *10*, 1235–1244.

(6) Takatani, H.; Soda, H.; Fukuda, M.; Watanabe, M.; Kinoshita, A.; Nakamura, T.; Oka, M. Levels of Recombinant Human Granulocyte Colony-Stimulating Factor in Serum Are Inversely Correlated with Circulating Neutrophil Counts. *Antimicrob Agents Chemother* **1996**, *40*, 988–991.

(7) Turecek, P. L.; Bossard, M. J.; Schoetens, F.; Ivens, I. A. PEGylation of Biopharmaceuticals: A Review of Chemistry and Nonclinical Safety Information of Approved Drugs. *Journal of Pharmaceutical Sciences* **2016**, *105*, 460–475.

(8) Vogel, C. L.; Wojtukiewicz, M. Z.; Carroll, R. R.; Tjulandin, S. A.; Barajas-Figueroa, L. J.; Wiens, B. L.; Neumann, T. A.; Schwartzberg, L. S. First and Subsequent Cycle Use of Pegfilgrastim Prevents Febrile Neutropenia in Patients With Breast Cancer: A Multicenter, Double-Blind, Placebo-Controlled Phase III Study. *JCO* **2005**, *23*, 1178–1184.

(9) Lipiäinen, T.; Peltoniemi, M.; Sarkhel, S.; Yrjönen, T.; Vuorela, H.; Urtti, A.; Juppo, A. Formulation and Stability of Cytokine Therapeutics. *JPharmSci* **2015**, *104*, 307–326.

(10) Krishnan, S.; Chi, E. Y.; Webb, J. N.; Chang, B. S.; Shan, D.; Goldenberg, M.; Manning, M. C.; Randolph, T. W.; Carpenter, J. F. Aggregation of Granulocyte Colony Stimulating Factor under Physiological Conditions: Characterization and Thermodynamic Inhibition. *Biochemistry* **2002**, *41*, 6422–6431.

(11) Chi, E. Y.; Krishnan, S.; Kendrick, B. S.; Chang, B. S.; Carpenter, J. F.; Randolph, T. W. Roles of Conformational Stability and Colloidal Stability in the Aggregation of Recombinant Human Granulocyte Colony-Stimulating Factor. *Protein Sci* **2003**, *12*, 903–913.

(12) Liu, Y.; Lee, J.; Mansfield, K. M.; Ko, J. H.; Sallam, S.; Wesdemiotis, C.; Maynard, H. D. Trehalose Glycopolymer Enhances Both Solution Stability and Pharmacokinetics of a Therapeutic Protein. *Bioconjugate Chem.* **2017**, *28*, 836–845.

(13) Mancini, R. J.; Lee, J.; Maynard, H. D. Trehalose Glycopolymers for Stabilization of Protein Conjugates to Environmental Stressors. *Journal of the American Chemical Society* **2012**, *134*, 8474–8479.

(14) Lee, J.; Lin, E.-W.; Lau, U. Y.; Hedrick, J. L.; Bat, E.; Maynard, H. D. Trehalose Glycopolymers as Excipients for Protein Stabilization. *Biomacromolecules* **2013**, *14*, 2561–2569.

(15) Messina, M. S.; Ko, J. H.; Yang, Z.; Strouse, M. J.; Houk, K. N.; Maynard, H. D. Effect of Trehalose Polymer Regioisomers on Protein Stabilization. *Polym. Chem.* **2017**, *8*, 4781–4788.

(16) Kang, S.-H.; Na, K.-H.; Park, J.-H.; Park, C.-I.; Lee, S.-Y.; Lee, Y.-I. High Level Expression and Simple Purification of Recombinant Human Granulocyte Colony-Stimulating Factor in E. Coli. *Biotechnol Lett* **1995**, *17*, 687–692.

(17) Kim, C. K.; Lee, C. H.; Lee, S.-B.; Oh, J.-W. Simplified Large-Scale Refolding, Purification, and Characterization of Recombinant Human Granulocyte-Colony Stimulating Factor in Escherichia Coli. *PLOS ONE* **2013**, *8*, e80109.

(18) Vanz, A. L.; Renard, G.; Palma, M. S.; Chies, J. M.; Dalmora, S. L.; Basso, L. A.; Santos, D. S. Human Granulocyte Colony Stimulating Factor (HG-CSF): Cloning, Overexpression, Purification and Characterization. *Microb. Cell Fact.* **2008**, *7*, 13.

(19) Krishna Rao, D. V.; Rao, J. V.; Narasu, M. L.; Bhujanga Rao, A. K. S. Optimization of the AT-Content of Codons Immediately Downstream of the Initiation Codon and Evaluation of

Culture Conditions for High-Level Expression of Recombinant Human G-CSF in Escherichia Coli. *Mol Biotechnol* **2008**, *38*, 221–232.

(20) Forsythe, N. L.; Maynard, H. D. Synthesis of Disulfide-Bridging Trehalose Polymers for Antibody and Fab Conjugation Using a Bis-Sulfone ATRP Initiator. *Polym. Chem.* **2021**, *12*, 1217–1223.

(21) Chen, D.; Disotuar, M. M.; Xiong, X.; Wang, Y.; Chou, D. H.-C. Selective N-Terminal Functionalization of Native Peptides and Proteins †Electronic Supplementary Information (ESI) Available: Experimental Details. See DOI: 10.1039/C6sc04744k Click Here for Additional Data File. *Chem Sci* **2017**, *8*, 2717–2722.

(22) Willcock, H.; O'Reilly, R. K. End Group Removal and Modification of RAFT Polymers. *Polym. Chem.* **2010**, *1*, 149–157.

(23) Lyon, R. P.; Setter, J. R.; Bovee, T. D.; Doronina, S. O.; Hunter, J. H.; Anderson, M. E.; Balasubramanian, C. L.; Duniho, S. M.; Leiske, C. I.; Li, F.; Senter, P. D. Self-Hydrolyzing Maleimides Improve the Stability and Pharmacological Properties of Antibody-Drug Conjugates. *Nature Biotechnology* **2014**, *32*, 1059–1062.

(24) Veronese, F. M.; Mero, A.; Caboi, F.; Sergi, M.; Marongiu, C.; Pasut, G. Site-Specific Pegylation of G-CSF by Reversible Denaturation. *Bioconjug Chem* **2007**, *18*, 1824–1830.

5.4 Materials and Methods

Analytical techniques. Untagged G-CSF and His6-TEV-G-CSF plasmids for expression were synthesized and cloned into pET-29b (+) expression vectors with NdeI_XhoI insertion sites by

Twist Biosciences. NMR spectra were recorded on a Bruker DRX 500 MHz or a Bruker AV 500 MHz. Silica gel column chromatography was performed on a Biotage Isolera One purification system. Fast protein liquid chromatography (FPLC) was performed on a Bio-Rad BioLogic DuoFlow chromatography system. Ni-NTA cartridge (5 mL) was used for G-CSF purification, and GE Healthcare HiTrap Heparin HP column (1 mL) eluted with 20 mM sodium acetate buffer, pH 5.0 with a salt gradient from 0 M to 1 M NaCl was used for G-CSF-polymer conjugate purification. Mass spectrometry for G-CSF fusion proteins was obtained on an Agilent Q-TOF 6530 LC/MS.

MBP-G-CSF expression. Overnight cultures of transformed BL21 (DE3) cells were used to inoculate two separate shaker flasks containing 700 mL of autoclaved Terrific Broth (TB) with 0.8% glycerol and 35 μg/mL ampicillin. Cells were grown to an OD_{600} of 0.5 before inducing with 0.5 M isopropyl β-D-1-thiogalactopyranoside (IPTG) and expression was allowed to proceed at 18 °C for 16 h. Cells were then harvested via centrifugation and resuspended at 2 g/L in lysis buffer (50 mM Tris, 300 mM NaCl, 10 mM imidazole, pH 7.8, cOmplete™ protease inhibitor cocktail). Cells were then lysed via sonication and the lysate was clarified via centrifugation. The supernatant was then equilibrated with 10 mL of Ni-NTA resin with rocking for 15 minutes. The slurry was loaded onto two gravity columns. Bound protein was washed with 200 mL of lysis buffer. Protein was then eluted with lysis buffer containing 300 mM imidazole and dialyzed against 50 mM Tris containing 300 mM NaCl (pH 7.8).

For digest, 5 mg/mL of the fusion protein was added to a 15 mL conical tube and 2.2 mg thawed TEV protease was added and the digest was allowed to proceed at 22 °C for 5 hours. The product was then purified via FPLC on a 5 mL Ni-NTA cartridge with a stepwise gradient of 0,

50, and finally 350 mM imidazole in a buffer containing 50 mM Tris, 500 mM NaCl, and 5% glycerol (pH 8). Pure G-CSF was eluted in the 50 mM imidazole section of the method (Fig. S6).

His_6-TEV-G-CSF expression. Overnight starter cultures were used to inoculate two separate shaker flasks containing 700 mL of autoclaved TB, 0.4% glycerol, and 50 µg/mL kanamycin. Cells were grown at 37 °C to an OD_{600} of 1.2 before inducing with 1 mM IPTG. After 4 hours, cells were harvested via centrifugation and the pellet was resuspended in 50 mL of lysis buffer (50 mM Tris, 300 mM NaCl, cOmplete™ protease inhibitor cocktail). Cells were then lysed with an Emulsiflex homogenizer and the lysate was clarified via centrifugation. The supernatant was discarded and the pellet was sequentially washed (for 30 min with shaking followed by centrifugation after each wash) with the following buffers: 50 mM Tris, 5 mM EDTA, 2% Triton X-100 then 50 mM Tris, 5 mM EDTA, 2% sodium deoxycholate and finally 50 mM Tris, 5 mM EDTA, 1 M NaCl. The resulting pellet was resolubilized in 2 M urea at pH 12 and stirred in a beaker for 45 min. The solution was diluted to 2 mg/mL and acetic acid was used to bring the pH to 8. Refolding was allowed to proceed for 16 h with stirring at 22 °C. The protein was then dialyzed into 50 mM Tris, pH 7.8 buffer for 12 – 16 h at 4 °C.

For TEV digest, approximately 1:10 weight equivalents of TEV:protein was mixed and digestion was allowed to proceed at 22 °C for 12 h. The sample was then equilibrated with 10 mL of Ni-NTA resin and rocked for 15 min at 4 °C. The sample was loaded onto a column and the flow through was collected. G-CSF was then eluted with 2 × 20 mL of wash buffer (20 mM imidazole, pH 7.8, 50 mM Tris). Bound TEV protease and proteolysis products were then eluted with elution buffer (300 mM imidazole, pH 7.8, 50 mM Tris). Fractions containing pure protein was then dialyzed into 25 mM, pH 4.0 sodium acetate buffer.

Untagged G-CSF expression. Overnight starter cultures were used to inoculate two separate shaker flasks containing 700 mL of TB, 0.4% glycerol, and 50 µg/mL kanamycin. Cells were grown at 37 °C to an OD_{600} of 1.2 before inducing with 1 mM IPTG. After 4 hours, cells were harvested via centrifugation and the pellet was resuspended in 50 mL of lysis buffer (50 mM Tris, 300 mM NaCl, cOmplete™ protease inhibitor cocktail). Cells were then lysed with an Emulsiflex homogenizer and the lysate was clarified via centrifugation. The supernatant was discarded and the pellet was sequentially washed (for 30 min with shaking followed by centrifugation after each wash) with the following buffers: 50 mM Tris, 5 mM EDTA, 2% Triton X-100 then 50 mM Tris, 5 mM EDTA, 2% sodium deoxycholate and finally 50 mM Tris, 5 mM EDTA, 1 M NaCl. The resulting pellet was resolubilized in 2 M urea at pH 12 and stirred in a beaker for 45 min. The solution was diluted to 2 mg/mL and acetic acid was used to bring the pH to 8. Refolding was allowed to proceed for 16 h with stirring at 22 °C. The protein was then dialyzed into 50 mM Tris, pH 7.8 buffer for 12 – 16 h at 4 °C. Finally, for storage, protein was then dialyzed into 25 mM, pH 4.0 sodium acetate buffer.

Synthesis of heterobifunctional benzaldehyde-maleimide linker.

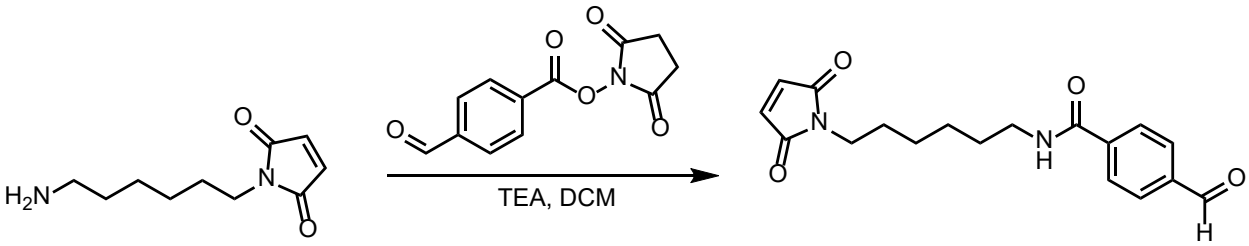

1-(6-aminohexyl)-1-maleimide (226 mg, 1.15 mmol, 1 equivalent) was added to a scintillation vial and dissolved in 5 mL of dichloromethane (DCM). N-Hydroxysuccinimide benzaldehyde (313 mg, 1.27 mmol, 1.1 equivalents) was added along with triethylamine (481 µL, 3.45 mmol, 3 equivalents) and reaction was allowed to proceed for 12 hrs. The product was then purified with a hexanes:ethyl acetate (0-100% gradient) to yield the product as an off-white solid (126 mg,

33%).[1]H NMR (400 MHz, Chloroform-d) δ 10.08 (d, J = 2.2 Hz, 1H), 7.98 – 7.91 (m, 4H), 6.69 (d, J = 2.3 Hz, 2H), 6.29 (s, 1H), 3.57 – 3.43 (m, 4H), 1.63 (q, J = 7.1 Hz, 4H), 1.44 (t, J = 7.4 Hz, 3H), 1.38 – 1.23 (m, 4H). HRMS calculated for $C_{18}H_{20}N_2O_4$ $[M+H]^+$ 329.1501, observed = 329.0267.

5.5 Appendix with Supplementary Figures.

DNA sequences

MBP-G-CSF

ATGAAAATAAAAACAGGTGCACGCATCCTCGCATTATCCGCATTAACGACGATGAT
GTTTTCCGCCTCGGCTCTCGCCAAAATCGAAGAAGGTAAACTGGTAATCTGGATTAA
CGGCGATAAAGGCTATAACGGTCTCGCTGAAGTCGGTAAGAAATTCGAGAAAGATA
CCGGAATTAAAGTCACCGTTGAGCATCCGGATAAACTGGAAGAGAAATTCCCACAG
GTTGCGGCAACTGGCGATGGCCCTGACATTATCTTCTGGGCACACGACCGCTTTGGT
GGCTACGCTCAATCTGGCCTGTTGGCTGAAATCACCCCGGACAAAGCGTTCCAGGAC
AAGCTGTATCCGTTTACCTGGGATGCCGTACGTTACAACGGCAAGCTGATTGCTTAC
CCGATCGCTGTTGAAGCGTTATCGCTGATTTATAACAAAGATCTGCTGCCGAACCCG
CCAAAAACCTGGGAAGAGATCCCGGCGCTGGATAAAGAACTGAAAGCGAAAGGTA
AGAGCGCGCTGATGTTCAACCTGCAAGAACCGTACTTCACCTGGCCGCTGATTGCTG
CTGACGGGGGTTATGCGTTCAAGTATGAAAACGGCAAGTACGACATTAAAGACGTG
GGCGTGGATAACGCTGGCGCGAAAGCGGGTCTGACCTTCCTGGTTGACCTGATTAAA
AACAAACACATGAATGCAGACACCGATTACTCCATCGCAGAAGCTGCCTTTAATAA
AGGCGAAACAGCGATGACCATCAACGGCCCGTGGGCATGGTCCAACATCGACACCA
GCAAAGTGAATTATGGTGTAACGGTACTGCCGACCTTCAAGGGTCAACCATCCAAA
CCGTTCGTTGGCGTGCTGAGCGCAGGTATTAACGCCGCCAGTCCGAACAAAGAGCT
GGCAAAAGAGTTCCTCGAAAACTATCTGCTGACTGATGAAGGTCTGGAAGCGGTTA
ATAAAGACAAACCGCTGGGTGCCGTAGCGCTGAAGTCTTACGAGGAAGAGTTGGCG
AAAGATCCACGTATTGCCGCCACTATGGAAAACGCCCAGAAAGGTGAAATCATGCC
GAACATCCCGCAGATGTCCGCTTTCTGGTATGCCGTGCGTACTGCGGTGATCAACGC
CGCCAGCGGTCGTCAGACTGTCGATGAAGCCCTGAAAGACGCGCAGACTAATTCGA
GCTCGCACCACCACCACCACCACGGAGGAGGAGAGAACCTGTATTTCCAGATGACC
CCCCTGGGCCCTGCCAGCTCCCTGCCCCAGAGCTTCCTGCTCAAGTGCTTAGAGCAA
GTGAGGAAGATCCAGGGCGATGGCGCAGCGCTCCAGGAGAAGCTGTGTGCCACCTA
CAAGCTGTGCCACCCCGAGGAGCTGGTGCTGCTCGGACACTCTCTGGGCATCCCCTG
GGCTCCCCTGAGCAGCTGCCCCAGCCAGGCCCTGCAGCTGGCAGGCTGCTTGAGCC
AACTCCATAGCGGCCTTTTCCTCTACCAGGGGCTCCTGCAGGCCCTGGAAGGGATCT

CCCCCGAGTTGGGTCCCACCTTGGACACACTGCAGCTGGACGTCGCCGACTTTGCCA
CCACCATCTGGCAGCAGATGGAAGAACTGGGAATGGCCCCTGCCCTGCAGCCCACC
CAGGGTGCCATGCCGGCCTTCGCCTCTGCTTTCCAGCGCCGGGCAGGAGGGGTCCTG
GTTGCCTCCCATCTGCAGAGCTTCCTGGAGGTGTCGTACCGCGTTCTACGCCACCTT
GCCCAGCCCTGATAAGGATCC

His$_6$-TEV-G-CSF

GGATCTGATAAAATTCATCATCATCATCATCACGAAAACCTGTACTTCCAGATGACC
CCCCTGGGCCCTGCCAGCTCCCTGCCCCAGAGCTTCCTGCTCAAGTGCTTAGAGCAA
GTGAGGAAGATCCAGGGCGATGGCGCAGCGCTCCAGGAGAAGCTGTGTGCCACCTA
CAAGCTGTGCCACCCCGAGGAGCTGGTGCTGCTCGGACACTCTCTGGGCATCCCCTG
GGCTCCCCTGAGCAGCTGCCCCAGCCAGGCCCTGCAGCTGGCAGGCTGCTTGAGCC
AACTCCATAGCGGCCTTTTCCTCTACCAGGGGCTCCTGCAGGCCCTGGAAGGGATCT
CCCCCGAGTTGGGTCCCACCTTGGACACACTGCAGCTGGACGTCGCCGACTTTGCCA
CCACCATCTGGCAGCAGATGGAAGAACTGGGAATGGCCCCTGCCCTGCAGCCCACC
CAGGGTGCCATGCCGGCCTTCGCCTCTGCTTTCCAGCGCCGGGCAGGAGGGGTCCTG
GTTGCCTCCCATCTGCAGAGCTTCCTGGAGGTGTCGTACCGCGTTCTACGCCACCTT
GCCCAGCCCTAATGA

Untagged before codon optimization

ACCCCCCTGGGCCCTGCCAGCTCCCTGCCCCAGAGCTTCCTGCTCAAGTGCTTAGAG
CAAGTGAGGAAGATCCAGGGCGATGGCGCAGCGCTCCAGGAGAAGCTGTGTGCCAC
CTACAAGCTGTGCCACCCCGAGGAGCTGGTGCTGCTCGGACACTCTCTGGGCATCCC
CTGGGCTCCCCTGAGCAGCTGCCCCAGCCAGGCCCTGCAGCTGGCAGGCTGCTTGAG
CCAACTCCATAGCGGCCTTTTCCTCTACCAGGGGCTCCTGCAGGCCCTGGAAGGGAT
CTCCCCCGAGTTGGGTCCCACCTTGGACACACTGCAGCTGGACGTCGCCGACTTTGC
CACCACCATCTGGCAGCAGATGGAAGAACTGGGAATGGCCCCTGCCCTGCAGCCCA
CCCAGGGTGCCATGCCGGCCTTCGCCTCTGCTTTCCAGCGCCGGGCAGGAGGGGTCC
TGGTTGCCTCCCATCTGCAGAGCTTCCTGGAGGTGTCGTACCGCGTTCTACGCCACC
TTGCCCAGCCCTAATGA

Untagged after codon optimization

ACACCATTAGGACCTGCTAGCTCCTTACCCCAGAGCTTCCTGCTCAAGTGCTTAGAG
CAAGTGAGGAAGATCCAGGGCGATGGCGCAGCGCTCCAGGAGAAGCTGTGTGCCAC
CTACAAGCTGTGCCACCCCGAGGAGCTGGTGCTGCTCGGACACTCTCTGGGCATCCC
CTGGGCTCCCCTGAGCAGCTGCCCCAGCCAGGCCCTGCAGCTGGCAGGCTGCTTGAG
CCAACTCCATAGCGGCCTTTTCCTCTACCAGGGGCTCCTGCAGGCCCTGGAAGGGAT
CTCCCCCGAGTTGGGTCCCACCTTGGACACACTGCAGCTGGACGTCGCCGACTTTGC
CACCACCATCTGGCAGCAGATGGAAGAACTGGGAATGGCCCCTGCCCTGCAGCCCA

CCCAGGGTGCCATGCCGGCCTTCGCCTCTGCTTTCCAGCGCCGGGCAGGAGGGGTCC
TGGTTGCCTCCCATCTGCAGAGCTTCCTGGAGGTGTCGTACCGCGTTCTACGCCACC
TTGCCCAGCCCTAATGA

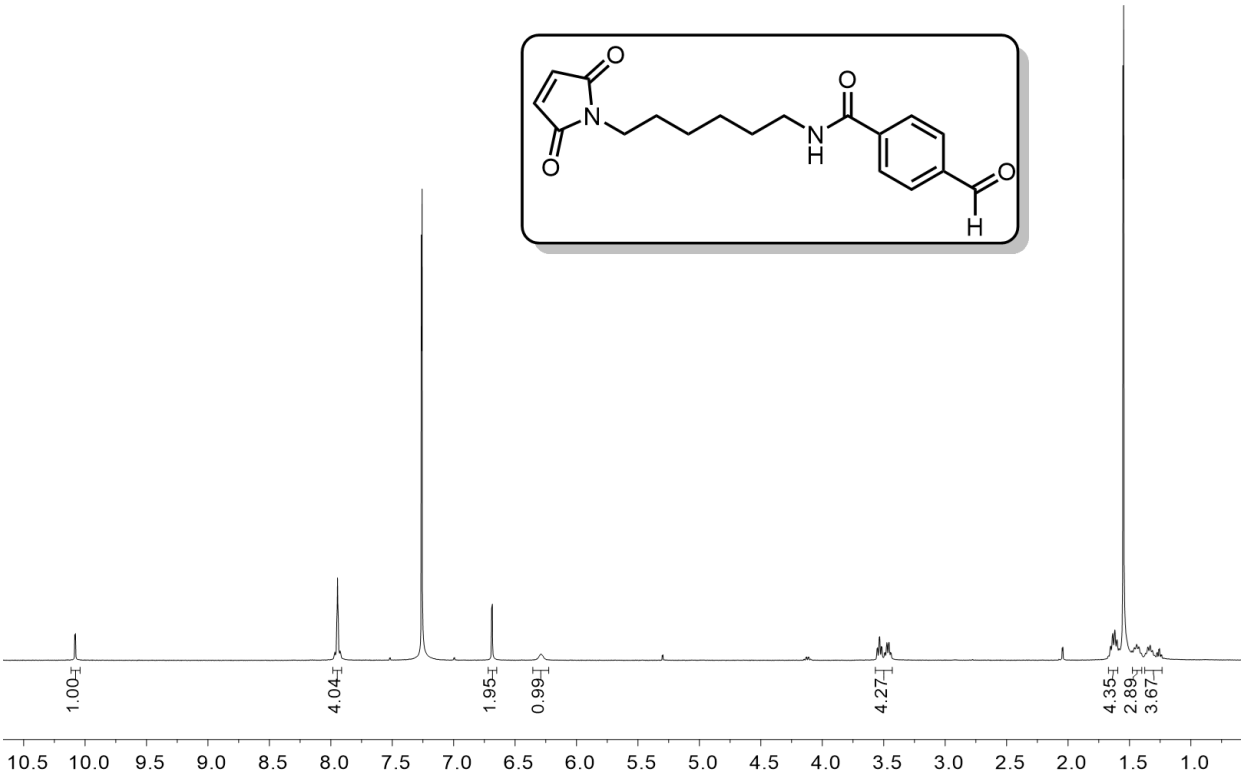

Figure 5.5.1. ^{1}H NMR of maleimide, benzaldehyde linker.

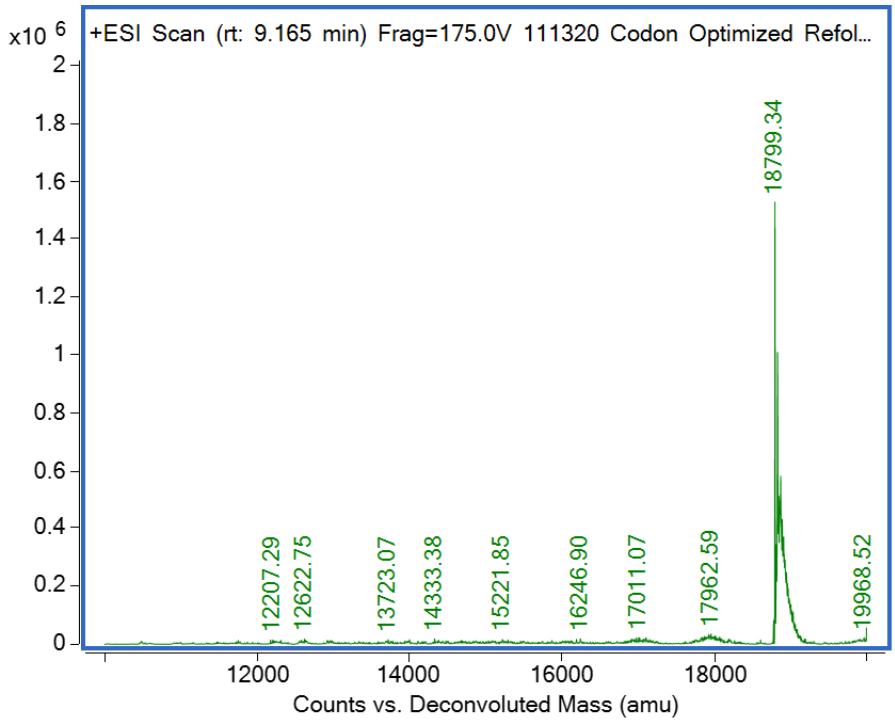

Figure 5.5.2. Intact mass spectrum of untagged G-CSF after purification and refolding.

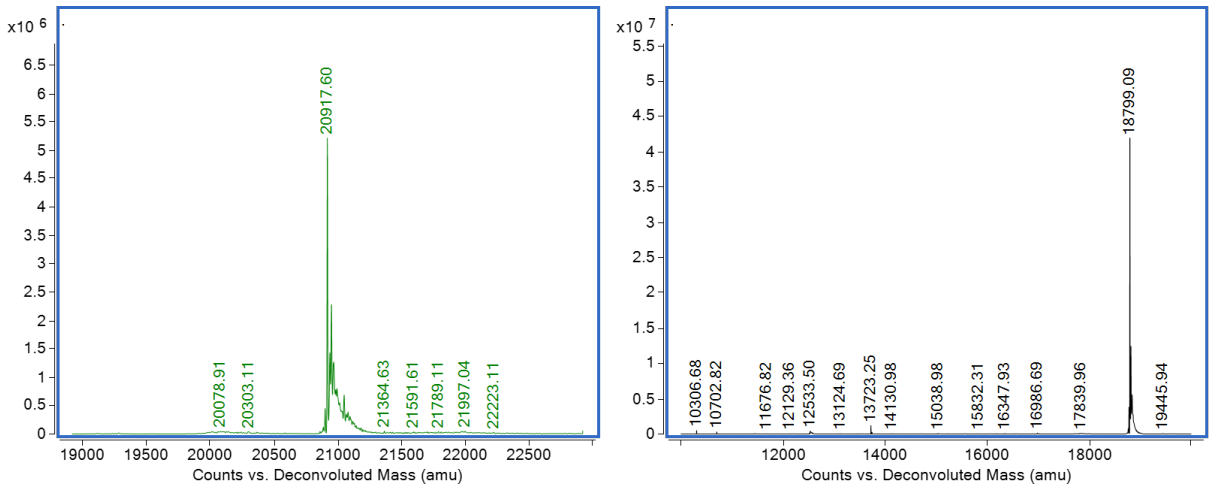

Figure 5.5.3. Intact mass spectrum of His-tagged protein (left) and TEV-cleaved G-CSF (right).